ESA Climate Change Initiative "Plus" (CCI+)

Product Validation and Intercomparison Report (PVIR) for data set CRDP9

for the Essential Climate Variable (ECV)

Greenhouse Gases (GHG):

XCO_2 and/or XCH_4 from

OCO-2, Sentinel-5-Precursor and GOSAT-2

Written by: GHG-CCI+ Phase 2 project team

Lead author: Michael Buchwitz, Institute of Environmental Physics (IUP), University of Bremen, Germany

Co-authors:

Bart Dils (BIRA-IASB, Belgium, Brussels)

Maximilian Reuter, Oliver Schneising-Weigel, Michael Hilker (IUP, Univ. Bremen, Germany)

Andrew Barr, Tobias Borsdorff, (SRON, Leiden, The Netherlands)

Change log:

Version Nr.	Date	Status	Reason for change
Version 1.1	13-Mar-2020	Approved	New document for CRDP5
Version 2.0	10-Feb-2021	Approved	Update for CRDP6
Version 2.1	19-Mar-2021	Approved	Content for Sect. 4.2.2 added on request of ESA.
Version 3.0	16-Feb-2022	Approved	Update for CRDP7
Version 4.0	29-Aug-2023	Approved	Update for CRDP8
Version 5.0	28-Jan-2025	Submitted	Update for CRDP9
Version 5.0	20-Feb-2025	Approved	Update for CRDP9; typos corrected

Table of Contents

1 Executive Summary

This document is the Product Validation and Intercomparison Report (PVIR) version 5, which is a deliverable of the ESA project GHG-CCI+ (https://climate.esa.int/en/projects/ghgs/) Phase 2.

Phase 2 of the GHG-CCI+ project started in September 2022 and is carrying out research and development (R&D) as needed to generate new and/or improve existing Greenhouse Gas (GHG) Essential Climate Variable (ECV) satellite-derived CO_2 and CH_4 data products.

These products are column-averaged dry-air mole fractions of carbon dioxide (CO_2), denoted XCO_2, and methane (CH_4), denoted XCH_4, from these satellites / satellite sensors using European scientific retrieval algorithms:

- XCO_2 from OCO-2 using the University of Bremen FOCAL algorithm (product **CO2_OC2_FOCA**),
- XCH_4 from Sentinel-5 Precursor (S5P) using University of Bremen's WFM-DOAS (or WFMD) algorithm (product **CH4_S5P_WFMD**),
- XCO_2 and XCH_4 from GOSAT-2 using SRON's RemoTeC algorithm (products **CO2_GO2_SRFP, CH4_GO2_SRFP, CH4_GO2_SRPR**)

This project aims to generate GHG ECV data products in-line with GCOS (Global Climate Observing System) requirements. GCOS defines the ECV GHG as follows (see Sect. 2 for comments related to the recent update of the GCOS requirements): "Retrievals of greenhouse gases, such as CO_2 and CH_4, of sufficient quality to estimate regional sources and sinks". Within the GHG-CCI+ project satellite-derived XCO_2 (in ppm) and XCH_4 (in ppb) data products are retrieved from satellite radiance observations in the Short-Wave-Infra-Red (SWIR) spectral region. These instruments are used because their measurements are sensitive also to the lowest atmospheric layer and therefore provide information on the regional surface sources and sinks of CO_2 and CH_4. All products are generated with independent retrieval algorithms developed to convert GOSAT-2, OCO-2 and TROPOMI/S5P radiance spectra into Level 2 (L2) XCO_2 and/or XCH_4 data products.

In this document the validation and intercomparison results are presented. The validation is based on comparisons with TCCON (Total Carbon Column Observation Network) ground-based XCO_2 and XCH_4 retrievals. The validation has been carried out by the GHG-CCI+ independent Validation Team (VALT) and by the data provider (DP) of a given product.

For each data product and each assessment method the following validation summary "figures of merit" have been determined and are reported in this document: (i) Single measurement precision, (ii) mean bias (global offset), (iii) relative systematic error (or relative accuracy), (iv) stability (linear bias drift or trend). Furthermore, also the reported XCO_2 and XCH_4 uncertainties have been validated by computing a quantity called "Uncertainty ratio", which is the ratio of the (mean value of the) reported uncertainty and the standard deviation of satellite minus TCCON differences. The results are summarized in **Table 1-1** for the XCO_2 products and **Table 1-2** for the XCH_4 product.

Table 1-1: *Summary of the validation of XCO_2 products CO2_OC2_FOCA and CO2_GO2_SRFP of data set Climate Research Data Package No. 9 (CRDP#9, to be released in February 2025) via comparison with TCCON ground-based XCO_2 retrievals. VALT refers to the assessment results of the GHG-CCI+ independent validation team and DP refers to the assessment results of the data provider. (*) Excluding a possible global offset, which is reported separately in this document. The range reported for VALT results in square brackets […] correspond with the upper and lower 95% confidence bound on the parameter. "n.a." means "not applicable" and "n.e." means "not evaluated (e.g., because time series too short).*

Summary validation results GHG-CCI+ CRDP#9 XCO_2 products by comparisons with TCCON			
Product CO2_OC2_FOCA (v11, global, 9.2014 – 2.2024)			
Parameter	**Achieved**	**Required**	**Comments**
Random error (single obs., 1σ) [ppm]	VALT: 1.37 [1.23,1.44] DP: 1.57	T:<8; B:<3; G:<1	T=threshold; B=breakthrough; G=goal
Systematic error [ppm]	VALT: 0.42 [0.28, 0.63] / 0.53 [0.40, 0.66] DP: 0.45 / 0.51	< 0.5	"Relative accuracy" (*) Spatial / spatio-temp.
Stability: Linear bias trend [ppm/year]	VALT: 0.02 [-0.02, 0.05] DP: 0.04 ± 0.19	< 0.5	1σ uncertainty

Product CO2_GO2_SRFP (v02.0.3, global, 2.2019 – 1.2024)			
Parameter	**Achieved**	**Required**	**Comments**
Random error (single obs., 1σ) [ppm]	VALT: 2.16 [2.08, 2.36] DP: 2.14	T:<8; B:<3; G:<1	T=threshold; B=breakthrough; G=goal
Systematic error [ppm]	VALT: 0.39 [-0.01, 0.57] / 0.86 [0.64, 1.09] DP: 0.57 / 0.89	< 0.5	"Relative accuracy" (*) Spatial / spatio-temp.
Stability: Linear bias trend [ppm/year]	VALT: 0.0 [-0.07, 0.06] DP: 0.48	< 0.5	1σ uncertainty Only short time period

Table 1-2: *Summary of the validation of XCH_4 products CH4_S5P_WFMD of data set Climate Research Data Package No. 9 (CRDP#9, to be released in February 2025) via comparison with TCCON ground-based XCH_4 retrievals. VALT refers to the assessment results of the GHG-CCI+ independent validation team and DP refers to the assessment results of the data provider. (*) Excluding a possible global offset, which is reported separately in this document. The range reported for VALT results in square brackets […] correspond with the upper and lower 95% confidence bound on the parameter. "n.a." means "not applicable" and "n.e." means "not evaluated (e.g., because time series is too short).*

Summary validation results GHG-CCI+ CRDP#9 XCH_4 products by comparisons with TCCON			
Product CH4_S5P_WFMD (v1.8, global, 11.2017– 6.2024)			
Parameter	**Achieved**	**Required**	**Comments**
Random error (single obs., 1σ) [ppb]	VALT: 13.7 [12.9, 15.0] DP: 12.4	T:<34; B:<17; G:<9	T=threshold; B=breakthrough; G=goal
Systematic error [ppb]	VALT: 3.4 [0.5, 4.7] / 5.6 [4.5, 6.9] DP: 5.1 / 5.2	< 10	"Relative accuracy" (*) Spatial / spatio-temp.
Stability: Linear bias trend [ppb/year]	VALT: -0.2 [-0.7, 0.2] DP: 0.01	< 3	1σ uncertainty

Product CH4_GO2_SRFP (v02.0.3, global, 2.2019– 12.2021)			
Parameter	**Achieved**	**Required**	**Comments**
Random error (single obs., 1σ) [ppb]	VALT: 13.9 [13.2, 15.2] DP: 15.2	T:<34; B:<17; G:<9	T=threshold; B=breakthrough; G=goal
Systematic error [ppb]	VALT: 3.1 [1.1, 4.7] / 5.7 [3.9, 7.2] DP: 4.8 / 6.0	< 10	"Relative accuracy" (*) Spatial / spatio-temp.
Stability: Linear bias trend [ppb/year]	VALT: 1.7 [1.0, 2.0] DP: 0.77	< 3	1σ uncertainty

Table is continued on the following page …

Table 1-2: *Continued from previous page.*

Product CH4_GO2_SRPR (v02.0.3, global, 2.2019– 12.2023)			
Parameter	**Achieved**	**Required**	**Comments**
Random error (single obs., 1σ) [ppb]	VALT: 15.1 [13.9, 15.8] DP: 15.7	T:<34; B:<17; G:<9	T=threshold; B=breakthrough; G=goal
Systematic error [ppb]	VALT: 2.6 [0.0, 3.8] / 5.8 [4.3, 7.1] DP: 5.2 / 5.6	< 10	"Relative accuracy" (*) Spatial / spatio-temp.
Stability: Linear bias trend [ppb/year]	VALT: 0.6 [-0.3, 1.2] DP: 1.2	< 3	1σ uncertainty

2 Introduction

This document is the Product Validation and Intercomparison Report (PVIR) version 5, which is a deliverable of the ESA project GHG-CCI+ (https://climate.esa.int/en/projects/ghgs/) Phase 2.

GHG-CCI+ Phase 2 started in September 2022 and is carrying out the R&D needed to generate new or improve existing Greenhouse Gas (GHG) Essential Climate Variable (ECV) satellite-derived CO_2 and CH_4 data products.

These products are column-averaged dry-air mole fractions of carbon dioxide (CO_2), denoted XCO_2, and methane (CH_4), denoted XCH_4, from these satellites / satellite sensors using European scientific retrieval algorithms:

- XCO_2 from OCO-2,
- XCO_2 and XCH_4 from GOSAT-2 and
- XCH_4 from S5P

This project aims to generate GHG ECV data products in-line with GCOS (Global Climate Observing System) requirements **/GCOS-154/ /GCOS-195/ /GCOS-200/**. GCOS defines the ECV GHG as follows: "Retrievals of greenhouse gases, such as CO_2 and CH_4, of sufficient quality to estimate regional sources and sinks".

Note that GCOS has recently (in 2022) published updated requirements **/GCOS-245/**. These requirements are on one hand more appropriate for our data products as "CO_2 column average dry air mixing ratio", i.e., XCO_2, and "CH_4 column average dry air mixing ratio", i.e., XCH_4, are now listed as ECV products (in contrast to earlier GCOS documents referring to products not generated by us (for good reasons) such as tropospheric columns, etc.) but on the other hand the requirements are less appropriate as they partially refer to future missions or cannot be met for the existing satellites we are using. For example, the XCO_2 threshold requirements for temporal resolution (72 hours; neither OCO-2 nor GOSAT-2 meet this requirement) and uncertainty (0.8 ppm, 1-sigma) refer to CO2M (launch 2026). The threshold stability requirement is 0.3 ppm per decade (0.03 ppm/year) which is according to our experience significantly smaller that the uncertainty of methods used to establish stability (taking into account "noise" due to sampling aspects, stability of the reference data, etc.). Similar for XCH_4: The required minimum (threshold) uncertainty is 10 ppb (1-sigma), which (for many locations on Earth) cannot be met by S5P. For the breakthrough requirement of 5 ppb, it is argued that this is based on "Expert judgement based on expected improvement of TROPOMI/S5P". Typical TROPOMI/S5P XCH_4 uncertainty is on the order of 15 ppb and this is mainly due to instrument noise and no improvement can change this (except by limiting retrievals to highly reflecting scenes). Furthermore, the arguably most important requirement for users who use our data products for inverse modelling of sources and sinks is related to systematic errors (high accuracy or low biases) but this is not addressed in **/GCOS-245/** as the uncertainty requirement is essentially a random error (dispersion, scatter) related requirement.

ECV GHG requirements for satellite-derived XCO_2 and XCH_4 products avoiding these limitations have been formulated by the GHG-CCI+ project Climate Research Group (CRG) and are document in the GHG-CCI+ User Requirements Document (URD) **/URDv4.0/**. In the past we assessed the achieved quality of our products in detail considering these URD requirements and we follow this approach also during GHG-CCI+ Phase 2.

Once the products are of sufficient quality for a climate service and cover a long enough time period, it is expected that the data will become part of the Copernicus Climate Change Service (C3S, https://climate.copernicus.eu/) as done for earlier products initially developed by GHG-CCI, see Copernicus Climate Data Store (CDS, https://cds.climate.copernicus.eu/):

- CO_2 products: https://cds.climate.copernicus.eu/cdsapp#!/dataset/satellite-carbon-dioxide?tab=overview
- CH_4 products: https://cds.climate.copernicus.eu/cdsapp#!/dataset/satellite-methane?tab=overview

Within GHG-CCI+ satellite-derived XCO_2 (in ppm) and XCH_4 (in ppb) data products are retrieved from satellite radiance observations in the Short-Wave-Infra-Red (SWIR) spectral region. These instruments are used because their measurements are sensitive also to the lowest atmospheric layer and therefore provide information on the regional surface sources and sinks of CO_2 and CH_4.

This document provides validation and intercomparison results for the XCO_2 and XCH_4 datasets as listed in **Table 2-1** for XCO_2 and **Table 2-2** for XCH_4.

All products are generated with independent retrieval algorithms developed to convert GOSAT-2, OCO-2 and/or TROPOMI/S5P radiance spectra into Level 2 (L2) XCO_2 and/or XCH_4 data products.

For more information on these products see also **Table 2-3**.

Table 2-1: *Overview GHG-CCI+ algorithms for XCO_2 retrieval.*

XCO_2 Product Identifier	Algorithm (version)	Institute	Technique	Reference
CO2_OC2_FOCA	FOCAL (v11)	IUP, Univ. Bremen, Germany	Optimal Estimation; approximation for an optically thin scattering layer	Reuter et al., 2017a, b
CO2_GO2_SRFP	SRFP or RemoTeC (v2.0.3)	SRON, Netherlands	Phillips-Tikhonov regularization	Butz et al., 2009, 2010

Table 2-2: *Overview GHG-CCI+ algorithms for XCH_4 retrieval.*

XCH_4 Product Identifier	Algorithm (version)	Institute	Technique	Reference
CH4_S5P_WFMD	WFM-DOAS (v1.8)	IUP, Univ. Bremen, Germany	Weighted least squares	Schneising et al., 2023
CH4_GO2_SRPR	SRPR or RemoTeC (v2.0.3)	SRON, Netherlands	Proxy (PR) retrieval method	Frankenberg et al., 2005
CH4_GO2_SRFP	SRFP or RemoTeC (v2.0.3)	SRON, Netherlands	Phillips-Tikhonov regularization; Full Physics (FP) method	Butz et al., 2009, 2010

Table 2-3: *Overview of (other) GHG-CCI+ product related documents. ATBD = Algorithm Theoretical Basis Document, PUG = Product User Guide, E3UB = End-to-End ECV Uncertainty Budget document.*

Product ID	Document	Link
CO2_OC2_FOCA	ATBD	Available from: https://www.iup.uni-bremen.de/carbon_ghg/cg_data.html#GHG-CCI and https://climate.esa.int/de/projekte/ghgs/key-documents/
-"-	PUG	- " -
-"-	E3UB	- " -
CH4_S5P_WFMD	ATBD	- " -
-"-	PUG	- " -
-"-	E3UB	- " -
CO2_GO2_SRFP	ATBD	- " -
-"-	PUG	- " -
-"-	E3UB	- " -
CH4_GO2_SRFP	ATBD	- " -
-"-	PUG	- " -
-"-	E3UB	- " -
CH4_GO2_SRPR	ATBD	- " -
-"-	PUG	- " -
-"-	E3UB	- " -

3 General description of the processing system

A schematic overview of the GHG-CCI+ processing system is given in **Figure 3-1**.

The processing system consists of the different algorithms (see **Tables 2-1 and 2-2**), running at the different responsible institutes. The different institutes have their own access to the required input data (satellite data, ECMWF meteorological data, model data for priors, spectroscopic databases, etc.), and their own computational facilities in the form of multi-CPU Unix/Linux systems. The Level-2 (L2) output data (XCO_2 and XCH_4) generated by the algorithms at the different institutes are available via the CCI Open Data Portal (*https://climate.esa.int/en/odp/#/dashboard*) and additional information is given at the GHG-CCI+ website (https://climate.esa.int/en/projects/ghgs/). The different parts of the GHG-CCI+ processing systems running at the different institutes are described in more detail in the System Specification Document (SSD) document **/Aben et al., 2019/**.

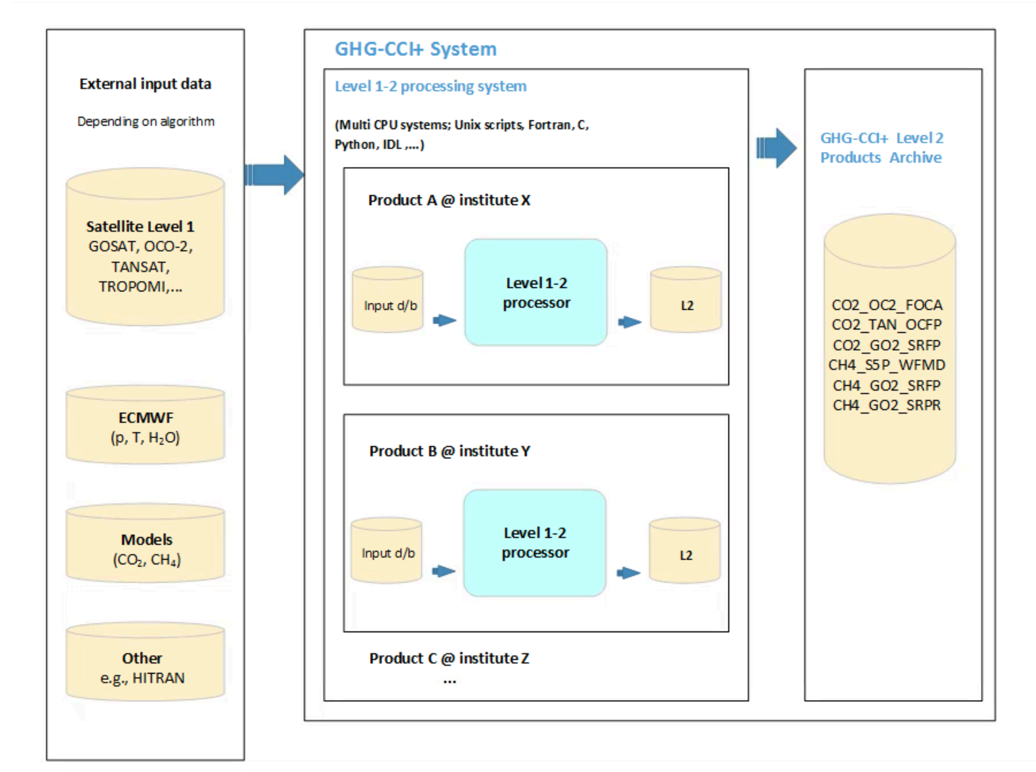

Figure 3-1: *Overview of the GHG-CCI+ processing system. Note that the GHG-CCI+ Level 2 product data archive is the CCI Open Data Portal (https://climate.esa.int/en/odp/#/dashboard). Note that product CO2_TAN_OCFP (XCO_2 from TanSat) has been generated (only) in Phase 1 of the GHG-CCI+ project.*

4 Independent validation by validation team

This chapter deals with the validation of the GHG-CCI+ retrieval products using ground-based FTIR remote sensing measurements from the Total Carbon Column Observing Network (TCCON) **/Wunch et al.2011/** and, in the case of XCH_4, the Network for the Detection of Atmospheric Composition Change (NDACC) **/De Mazière et al. 2018/**. Take note that NDACC's data protocol is less harmonized as compared to TCCON's. For instance, it allows the use of 2 retrieval algorithms (SFIT4 and PROFFIT9). However, analysis between the two algorithms showed no bias between them **/Hase et al. 2004/**). It also features more stations in what we may call 'challenging environments', that being high altitude sites (Zugspitze, Jungfraujoch, Izaña, Mauna Loa and Reunion (Maido), near major urban sites (Xianghe) and high latitude sites (Eureka, Ny Alesund, Arrival Heights). It also relies on the surface pressure to derive the dry air mole fraction (see equation 1 in **/Deutscher et al., 2010/**) as it cannot rely on a retrieved CH_4/O_2 ratio to reduce errors in the retrieval process.

TCCON also benefits from an extensive calibration campaign, which results in a calibration factor to reduce its systematic bias **/Wunch et al., 2011/**. TCCON's network accuracy can be determined by the uncertainty on this calibration factor, which have been improved in the GGG2020 retrieval version used here (a list of the main 2014-2020 feature differences, including a new way to calculate the *a priori* profiles **/Laughner et al., 2023/**, can be found here: https://tccon-wiki.caltech.edu/Main/DataDescriptionGGG2020). and amounts to 0.05% for XCO_2, and 0.1% for XCH_4. The random uncertainty of TCCON is about 0.5% for XCH_4 and 0.25% for XCO_2. **/Wunch et al. 2015/.**

For NDACC, the systematic and random uncertainties of CH_4 total columns are estimated to be 3.0% and 1.5%, respectively. The first is mainly coming from the uncertainty of the spectroscopy.

Comparisons between TCCON and NDACC XCH_4 measurements **/Ostler et al., 2014/** do demonstrated that there is no overall bias between both TCCON and NDACC XCH_4 retrieval methods. Therefore, we feel confident to include NDACC in our analysis, as it may provide some insight into regions that are not sampled by TCCON (Latin America being a prime example). An added benefit of the NDACC data is that it does not use a profile scaling retrieval method, but uses optimal estimation instead, retrieving profiles with ~2.5 degrees of freedom. This should, in principle, reduce the smoothing error, when we apply the satellite averaging kernels as it does not rely on the assumption that the real profile conforms to a pre-determined shape. Nor is the data used in post-retrieval bias-correction methods, that are employed by various satellite algorithms, to reduce the effect of residual systematic error components. While this approach is certainly valid, it also results in retrieval data that is optimized in some sense to the TCCON retrieval sites.

That said, the summary numbers in the tables, are still based on the TCCON analysis only. Mainly due to the much higher prevalence of high altitude/ high latitude sites and higher interstation biases in the NDACC network.

Here we used public TCCON GGG2020 data as available on the TCCON Data Archive (https://tccondata.org/) as well as all publicly available data on the NDACC archive (https://www-air.larc.nasa.gov/missions/ndacc/data.html) on the 1st of July 2024. We also included data from Garmisch, Sodankylä and Xianghe, which are currently not officially part of NDACC but perform observations and data analysis fully compatible with NDACC guidelines.

Table 4.1: TCCON station coordinates and references.

STATION	Lat	Lon	Alt (km)	Ref
EUREKA	80.05 N	86.42 W	0.61	/Strong et al., 2022/
NY ALESUND	78.92 N	11.92 E	0.02	/Buschmann et al., 2022/
SODANKYLA	67.37N	26.62E	0.19	/Kivi et al., 2022/
EASTTROUTLAKE	54.35 N	104.99 W	0.50	/Wunch et al., 2022/
BREMEN	53.10 N	8.85 E	0.03	/Notholt et al., 2022/
HARWELL	51.57 N	1.32 W	0.14	/Wiedmann et al., 2023/
KARLSRUHE	49.10 N	8.44 E	0.12	/Hase et al., 2023/
PARIS	48.85 N	2.36 E	0.06	/Té et al., 2022/
ORLEANS	47.97 N	2.11 E	0.13	/Warneke et al., 2022/
GARMISCH	47.48 N	11.06 E	0.74	/Sussmann et al., 2023/
PARKFALLS	45.95 N	90.27 W	0.44	/Wennberg et al., 2022/
RIKUBETSU	43.46 N	143.77 E	0.38	/Morino et al., 2022a/
XIANGHE	39.80 N	116.69 E	0.04	/Zhou et al., 2022/
LAMONT	36.60 N	97.49 W	0.32	/Wennberg et al., 2022b/
TSUKUBA	36.05 N	140.12 E	0.03	/Morino et al., 2022b/
NICOSIA	35.14 N	33.38 E	0.18	/Petri et al., 2022/
EDWARDS	34.96 N	117.88 W	0.70	/Iraci et al., 2022/
JPL	34.20 N	118.18 W	0.39	/Wennberg et al. 2022b/
PASADENA	34.14 N	118.13 W	0.23	/Wennberg et al. 2022c/
SAGA	33.24 N	130.29 E	0.01	/Shiomi et al. 2022/
HEFEI	31.91 N	117.17 E	0.03	/Liu et al. 2022/
IZAÑA	28.30 N	16.50 W	2.37	/Garcia et al., 2022/
BURGOS	18.53 N	120.65 E	0.04	/Morino et al., 2022c/
REUNION	20.90 S	55.49 E	0.09	/De Mazière et al., 2022/
WOLLONGONG	34.41 S	150.88 E	0.03	/Deutscher et al. 2023/
LAUDER	45.04 S	169.68 E	0.37	/Sherlock et al., 2022/

Table 4-2: NDACC station coordinates and institutes/references.

STATION	Lat	Lon	Alt (km)	Institutes
EUREKA	80.05 N	86.42 W	0.61	**U. of Toronto, /Batchelor et al., 2009/,/Strong 2021/**
NY ALESUND	78.92 N	11.93 E	0.01	**U. of Bremen, /Notholt et al., 2021a/**
KIRUNA	67.84 N	20.40 E	0.2	**KIT-ASF, IRF Kiruna /Blumenstock et al., 2020/**
SODANKYLA	67.37 N	26.65 E	0.18	**FMI, BIRA-IASB**
HARESTUA	60.20 N	10.80 E	0.60	**Chalmers, /Mellqvist et al., 2021/**
St. PETERSBURG	59.88 N	29.83 E	0.02	**SPbU, /Marakova et al., 2017/**
BREMEN	53.11 N	8.85 E	0.03	**U. of Bremen, /Notholt et al., 2021b/**
GARMISCH	47.48 N	11.06 E	0.74	**KIT-IFU**
ZUGSPITZE	47.42 N	10.98 E	2.96	**KIT-IFU, /Sussmann et al., 2018/**
JUNGFRAUJOCH	46.55 N	7.98 E	3.58	**U. of Liège, /Mahieu, 2017/**
RIKUBETSU	43,46 N	143.77 E	0.38	**Nagoya U, NIES**
BOULDER	40.04 N	105.24 W	1.61	**NCAR, /Ortega et al. 2019/**
XIANGHE	39.75 N	116.96 E	0.04	**IAP-CAS**
TSUKUBA	36.05 N	140.13 E	0.03	**NIES**
IZAÑA	28.30 N	16.50 E	2.37	**AEMET, KIT-ASF**
MAUNA LOA	19.54 N	155.57 W	3.40	**NCAR**
REUNION (MAÏDO)	21.08 S	55.38 E	2.16	**BIRA-IASB**
WOLLONGONG	34.41 S	150.88 E	0.03	**U. of Wollongong**
LAUDER	45.04 S	169.68 E	0.37	**NIWA**
ARRIVAL HEIGHTS	77.82 S	166.65	0.20	**NIWA**

As before, the key concept behind this validation is to apply an as uniform as possible validation strategy for all the involved algorithms. We uphold the same methodology as in the previous PVIR (see **/PVIR GHG-CCI+ v4.0, 2023**/ for details) analysis.

Choosing collocation criteria is a balance between minimizing the potential collocation error and still retaining a large enough sample so as to be able to derive adequate statistics. Also of note is that some of the current available algorithms have processed data for a limited time span only, which hampers certain aspects of the analysis.

Concerning the Figures of Merit (FoM), we did not employ any pre-analysis averaging and looked at individual satellite-TCCON pairs. This was done mainly to have statistical parameters that relate to the quality of the original data. Users of the data however should keep in mind that some algorithms opt to have a high-density dataset with a larger random error component versus a much stricter quality-flagged low density dataset with a smaller random error component. After averaging (in space or time) the first might outperform the latter.

4.1 Validation method

Each individual satellite measurement is paired, if the criteria are met, with an individual FTS measurement (from TCCON or NDACC). This particular, FTS measurements needs to be taken within 2 hours and within 500 km of the satellite measurement. Only for CH4_S5P_WFMD is the collocation criteria tightened to within 100 km and within 1 hour (TCCON) or 2 hours (NDACC) due to its high data density. If more than one FTS measurement fits the above criteria, the FTS measurement that has been measured closest (in time) to the satellite coordinates will be the one paired with said satellite measurement. This creates a collocated dataset with unique individual satellite-FTS pairs.

Prior to the FoM analysis we try to limit the impact of differences in *a priori* and vertical sensitivity between FTS and the satellite product (**/Rodgers, 2000/**). To limit the impact of the former we adjust the satellite dry air mole fraction using the FTS *a priori* as in

$$\hat{c}_{S,adj} = \hat{c}_S + \sum_l pw_l\,(1 - A_l)\left(x_{F,a}^l - x_{S,a}^l\right)$$

where, $\hat{c}_S$ represents the originally retrieved satellite column-averaged dry air mole fraction, l is the index of the vertical layer, A_l the corresponding column averaging kernel of the satellite algorithm, $x_{S,a}$ and $x_{F,a}$ are the satellite and FTS *a priori* dry air mole fraction profiles respectively. pw_l is the pressure weight associated with level or layer l.

Likewise, to address the latter we apply the satellite averaging kernel onto the FTS data.

Unlike NDACC which directly yields retrieved profiles ($x_{F,r}$), TCCON provides total column dry air mole fractions only. So here we apply this smoothing onto the scaled TCCON *a priori,* where the scaling factor takes into account the actual retrieval (which is based on a scaling an *a priori* profile) as well as the post retrieval correction to bring TCCON in line with in situ measurements. Thus, the scaled TCCON profile ($x_{F,r}$) corresponds with

$$x_{F,r} = x_{F,a} \times \hat{c}_{F,r}/\hat{c}_{F,a}$$

where$x_{F,a}$ is the TCCON *a priori* profile. $\hat{c}_{F,r} \wedge \hat{c}_{F,a}$ are the TCCON retrieved and *a priori* column-averaged dry air mole fractions.

The adjusted FTS dry air mole fraction then corresponds with

$$\hat{c}_{F,adj} = \sum_l pw_l\left(x_{F,a}^l + \left(x_{F,r}^l - x_{F,a}^l\right)A_l\right)$$

where, pw_l again represents the pressure weight associated with the level or vertical layer with index l and A_l the corresponding column averaging kernel of the satellite algorithm. $x_{F,a}$ and $x_{F,r}$ are the FTS *a priori* and scaled dry air mole fraction profiles respectively.

Prior to these adjustments, the FTS *a priori* needs to be interpolated onto the satellite product vertical grid. This is done using a regridding method that preserves mass (**/Langerock et al.,**

2015/) and in case the satellite pixel surface altitude is below that of the FTS site, the regridded FTS profile is extrapolated towards the surface assuming a constant dry air molefraction.

This approach should minimize the differences between satellite and ground-based retrievals, regardless of the algorithm and target species involved.

The bias is defined as the median difference between the individual satellite and FTS pairs

$$\tilde{X}_{bias} = median\left(\hat{c}\right| \quad \left|S, adj - \hat{c}_{T,adj}\right)$$

This is done for each station after which the overall Bias FoM is defined as the median of all calculated station biases. One could also group all individual measurements, regardless of station, into one sample onto which we calculate the bias, but this would increase the impact of stations where the data density is high. Since having a high data density, does not necessarily correspond with the highest quality data (or best collocation environment), we deem our median of station biases approach more accurate.

The scatter at each station corresponds with the median absolute deviation (mad) scaled by 1.4826 which is a statistically more robust proxy for the standard deviation (std) of said difference as in:

$$scatter = 1.4826 \times median(|X_{bias} - \tilde{X}_{bias}|)$$

where $X_{bias} = \hat{c}_{S,adj} - \hat{c}_{F,adj}$

Again for the overall assessment of the scatter we take the median of all individual station scatter values.

Both parameters, bias and scatter, are presented with their 95% confidence interval in the validation summary tables (see **Tables 4-4, 4-6, 4-8, 4-11, 4-14, 4-17**). These confidence bands have been determined using a bootstrap methodology (**/Lunneborg, 2020/**), where the 95% confidence limits around the median $\tilde{X}$ corresponds with

- (97.5%tile - $\tilde{X}$), $\tilde{X}$ + ($\tilde{X}$- 0.25%tile)]

Using medians and scaled median absolute deviations instead of means and standard deviations makes for a more robust assessment as it is far less impacted by outliers. These outliers could be haphazard single outliers (in the satellite data as well as for the FTS measurements, due to cloud interference etc.) when calculation the station bias and scatter values, but also caused by far from ideal collocation circumstances, limited data, etc. at various FTS sites when calculating the overall FoMs.

Other FoM are the Relative Accuracy (RA) and Seasonal Relative Accuracy (SRA), which give an indication of the spatial and spatio-temporal accuracy of the algorithm. We define RA as the scaled median absolute deviation on the overall median biases (derived from individual data) obtained at each station. The "Seasonal Relative Accuracy" (SRA), differs from the relative accuracy in that it uses the seasonal bias medians at each station, instead of the overall biases obtained at each station, it is thus the scaled median absolute deviation over all station seasonal median bias results. The seasonal bias results are constructed, for each FTS station, from all data pairs which fall within the months of January till March (JFM), April till June (AMJ), July till September (JAS) or October till December (OND), regardless of the year the measurements are taken. Some stations feature only limited data during certain seasons, which sometimes results in erratic (seasonal) bias results. To avoid the inclusion of these results into the RA and SRA calculation, we do not include those results which are derived from less than 4 individual SAT-FTS pairs. This may seem as a low threshold, but combined with the fact that we draw upon median values, we deem this sufficient.

To verify the stability of the algorithm over time we fit a linear trend and seasonal cycle through the bias timeseries:

$$X = i + s.t + A.sin\big(2\pi.(t + ph)\big)$$

Here, *X* represents the satellite minus FTS difference, *i* the intercept, *s* the slope which corresponds with the linear drift, *A* the amplitude of the seasonal cycle and *ph* the phase shift. While the slope yields information on any potential drift, the amplitude in the above fit results gives us information on the potential mismatch between Satellite and FTS seasonal cycles. Ideally there should be no difference between these cycles which would yield a slope and amplitude=0 in the bias timeseries. This is done for all stations provided that the overlapping station satellite timeseries covers a timespan of at least 2 years. The overall long-term stability then corresponds with the median slope over all these stations as we expect the linear drift to be consistent for the entire dataset.

Figures 4-8, 4-13, 4-17, 4-27 4-28, 4-35, 4-36, 4-43 and 4-44 show the monthly medians of all data within certain latitude bands. To determine the seasonal cycle, as with the determination of the long-term stability, a fit as outlined above is performed on the (now monthly median instead of individual) data. For the seasonal cycle representation, we then subtract the linear part from the medians and calculate the mean of all medians for each given month.

Another Figure of Merit is the so-called Uncertainty Ratio, which is defined as the ratio between the algorithm's reported uncertainty and the above mentioned scatter. If the reported uncertainty is correctly assessed, the uncertainty ratio should approach unity. However, this baseline number ignores any aspect of temporal, spatial or FTS variability embedded in the scatter.

We therefore also calculate an improved Uncertainty Ratio, which is the ratio between the reported uncertainty and the uncertainty on the Satellite (σ_{SAT}) as determined from the scatter using the method outlined below. Both are reported in the summary tables of each algorithm (see **Tables 4-4, 4-6, 4-8, 4-11, 4-14, 4-17**), where the improved uncertainty ratio is marked by an *.

Taking into account the variability of the FTS reference data and the collocation error, when assuming independence, the scatter can be written down as:

$$\text{scatter}=\sqrt{\left(\sigma_{SAT}^2+\sigma_{FTS}^2+\sigma_{Collocation}^2\right)}$$

where σ_{SAT} is the standard deviation due to variability of the satellite product, σ_{FTS} due to variability within the FTS measurements and $\sigma_{Collocation}$ due to variability in time and space. σ_{SAT} as derived from our comparison between the satellite and FTS measurements is thus:

$$\sigma_{SAT}=\sqrt{\left(scatter^2-\sigma_{FTS}^2-\sigma_{Collocation}^2\right)}$$

The standard deviation on the ground-based FTS measurements can be readily calculated from the average variability of the FTIR measurements within the collocation timeframe (4 hours).

The Collocation uncertainty is harder to define and consists of a spatial and temporal component. The latter can be ignored since it is already embedded in our calculation of the FTS uncertainty (which is based on the actual variability of the FTS measurements in time and thus also contains the temporal natural variability).

Unfortunately, we have no solid information on the spatial collocation uncertainty. One method to at least visualize potential collocation biases is to take the satellite data and calculate the bias of all measurements within a satellite overpass with respect to the satellite data point that precisely targets the FTIR site location. After which the obtained biases can be averaged within certain predefined grid cells. This yields plots as in **Figure 4-1**, wherein WFMD XCH_4 was used to visualize spatial biases within WFMD XCH_4 around the Edwards (Dryden) and Pasadena (Caltech) sites. While located relatively close to one another, they nevertheless operate from very different environments. The Pasadena site is located in the Los Angeles basin, while Edwards is located in the Mojave Desert. As a result, we expect most of the measurements that are taken outside of the Los Angeles basin to have a negative bias towards the data taken at Pasadena, with the exception of data taken over the California Central Valley which features strong emissions from agriculture and petroleum extraction. Inversely, the Edwards site is surrounded by many areas that have a positive bias. While this certainly gives us insight into collocation aspects, it depends on relatively wide-swath high density satellite products and is thus currently restricted to S5P WFMD XCH_4 only. Furthermore, the obtained gridded biases should be averaged to such an extent that no temporal/random noise error component is in play. This can potentially be achieved by lowering the spatial resolution, at least for those stations where the data density is high enough. However, at some point this will certainly remove real spatial collocation features.

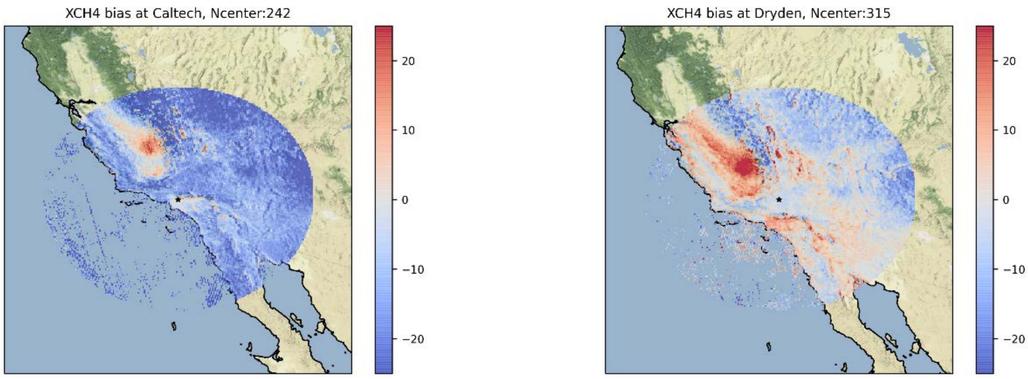

Figure 4-1: Average bias seen by WFMD XCH_4 within the same overpass, with respect to WFMD XCH4 data taken over the TCCON site location at Pasadena (left) and Edwards (right).

Another method, similar to the one above but potentially applicable to all satellite data is to spatially map all collocated satellite-FTS data pairs, grid them into a 0.1° by 0.1° (or 0.05°x0.05° in the case of S5P data) lat-lon grid (based on the location of the satellite measurement) and take the median bias of all biases within each individual grid. To add information we also mapped the number of pairs and the standard deviation of the biases observed in each grid. Additionally we also looked at the difference in observed surface pressures. As an example **Figure 4-2** explores the observed differences of the algorithm products in this study for Karlsruhe. Unlike the analysis above, the numbers here do include information of the ground-based FTS measurements. This is important as certain biases, certainly for grids where the number of collocated data is low, are (in part) due to the variability within the FTS data. Also note that the color scales are not fixed between figures. It is immediately clear (and expected) that we observe large differences between the different satellite instruments in terms of spatial coverage. In the OCO-2 (FOCAL) and TanSAT (OCFP) data we clearly see their relatively narrow cross track trajectories. Somewhat concerning is the fact that for FOCAL there appear to be consistent along track biases between adjacent tracks. However, these could very well be biases in time (and thus tied to the variability within the FTS measurements) instead of space given the limited averaging in some of these grid points. Overall coverage at Karlsruhe is good for WFMD S5P, but we can clearly see that in the 100km radius sampling is not uniform, with most of the data taken in the lower altitude (higher pressure) regions that corresponds with the Rhine valley. We also see that the observed biases (even where sampling is good) is not uniform and thus that additional uncertainty due to collocation is still present. For the GOSAT-2 products, due to its sparse spatial distribution, it is very difficult to interpret potential biases with respect to station location. To visualize information on the spatial distribution we have added gridded spatial bias plots for the FOCAL, OCFP and WFMD algorithms at all stations in **Figures 4-7, 4-12, 4-25 and 4-26**. We did not include these figures for the GOSAT-2 retrieval products as it is very difficult to discern any spatial bias information from them due to their limited spatial coverage.

For several sites/ algorithms this provides useful information on the collocation aspect. However due to low data density at some sites, this also proved difficult to apply systematically. While we certainly want to explore this further in more detail (either to have a better idea of the collocation bias or as a method to better select collocation areas), we currently maintain the method as described in the previous PVIR analysis.

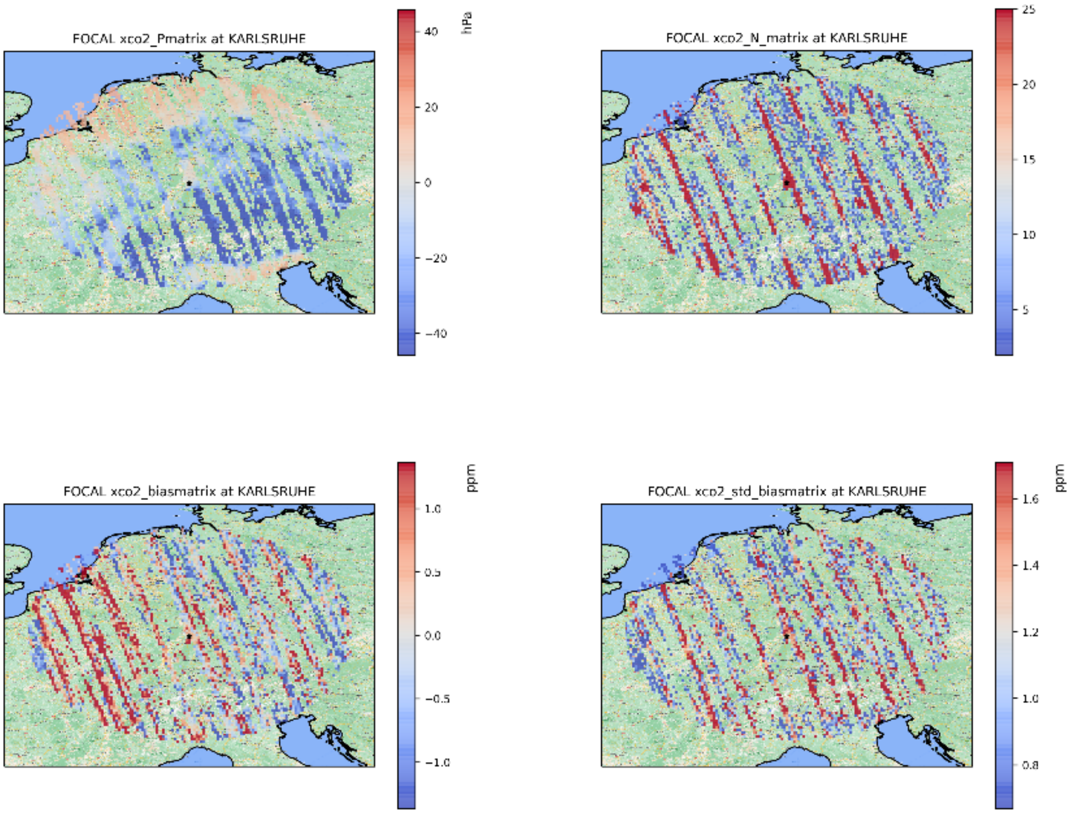

Figure 4-2a: median FOCAL - FTS surface pressure difference (top left), number of collocated XCO_2 measurements in each 0.1 by 0.1° grid cell (top right), median FOCAL-FTS XCO_2 difference (bottom left) and standard deviation on the FOCAL-FTS XCO_2 biases in each grid cell.

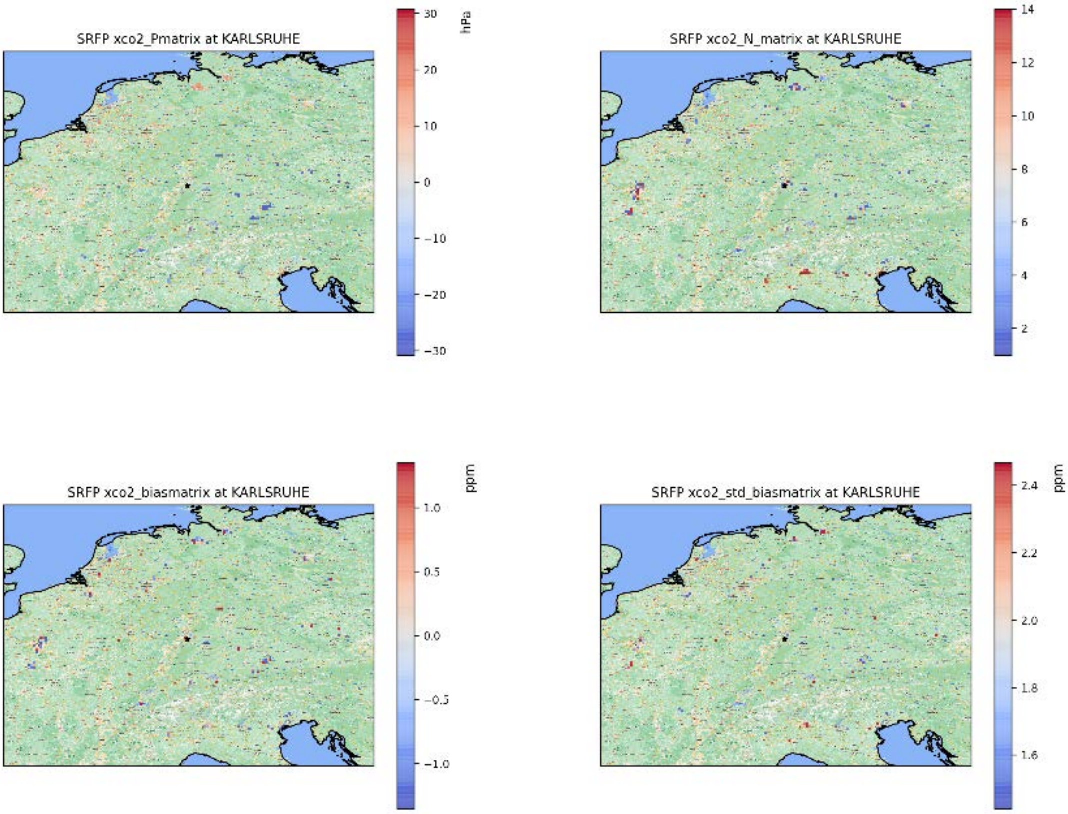

Figure 4-2b: median SRFP - FTS surface pressure difference (top left), number of collocated XCO_2 measurements in each 0.1 by 0.1° grid cell (top right), median SRFP-FTS XCO_2 difference (bottom left) and standard deviation on the SRFP-FTS XCO_2 biases in each grid cell.

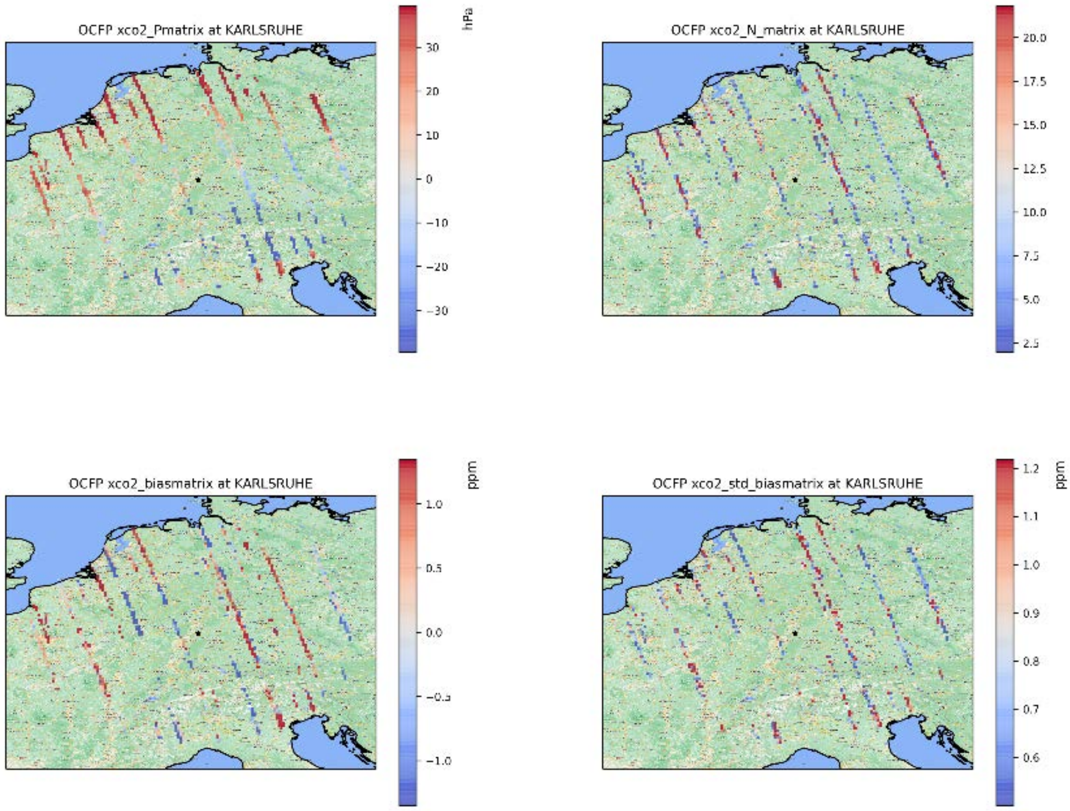

Figure 4-2c: median OCFP - FTS surface pressure difference (top left), number of collocated XCO_2 measurements in each 0.1 by 0.1° grid cell (top right), median OCFP-FTS XCO_2 difference (bottom left) and standard deviation on the OCFP-FTS XCO_2 biases in each grid cell.

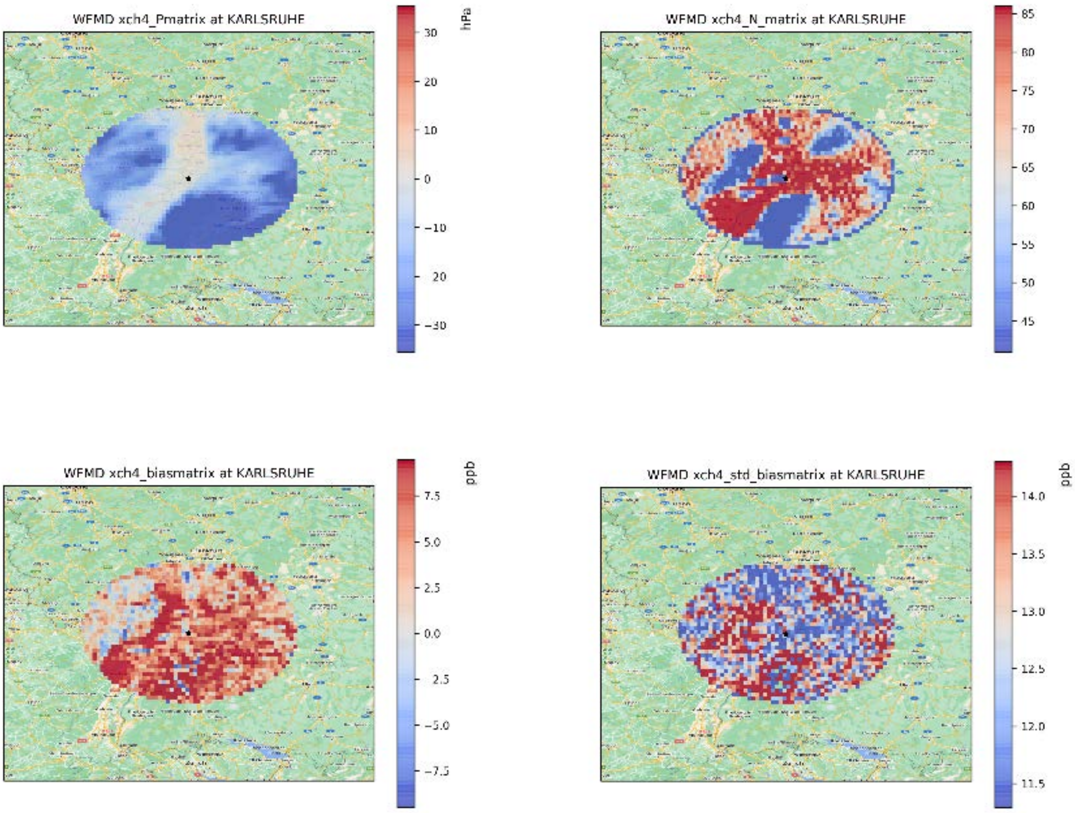

Figure 4-2d: median WFMD - FTS surface pressure difference (top left), number of collocated XCH_4 measurements in each 0.05 by 0.05° grid cell (top right), median WFMD-FTS XCH_4 difference (bottom left) and standard deviation on the WFMD-FTS XCH_4 biases in each grid cell.

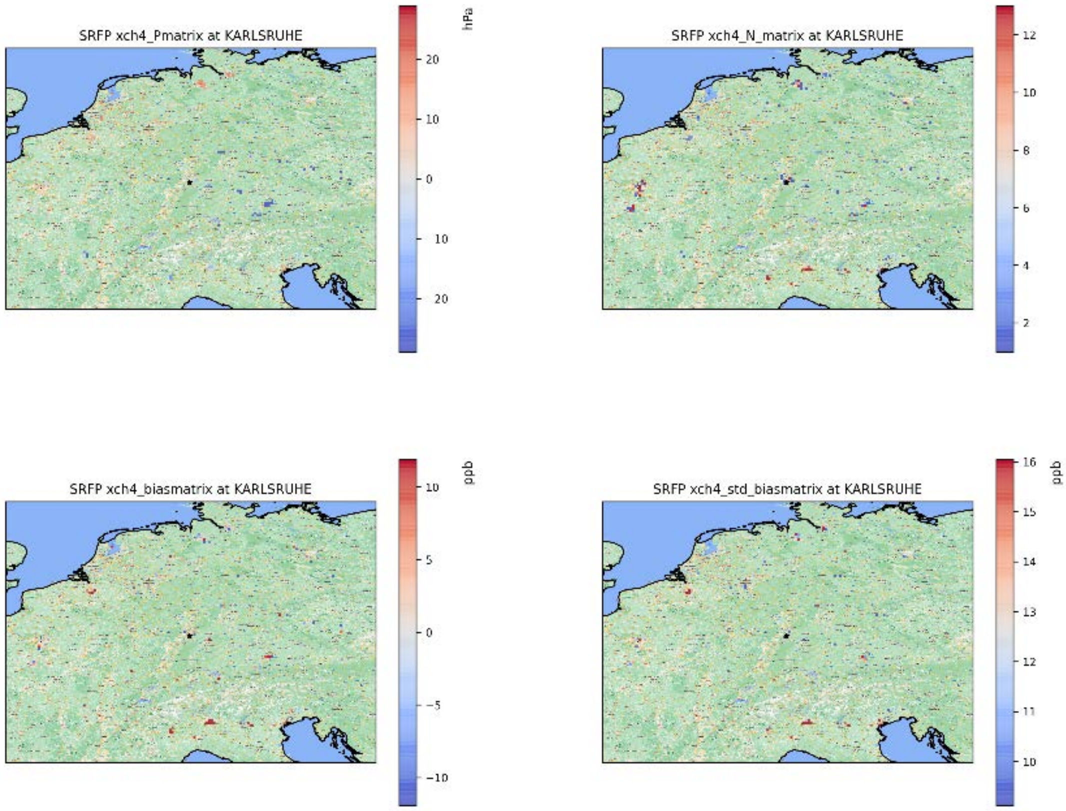

Figure 4-2e: median SRFP - FTS surface pressure difference (top left), number of collocated XCH_4 measurements in each 0.1 by 0.1° grid cell (top right), median SRFP-FTS XCH_4 difference (bottom left) and standard deviation on the SRFP-FTS XCH_4 biases in each grid cell.

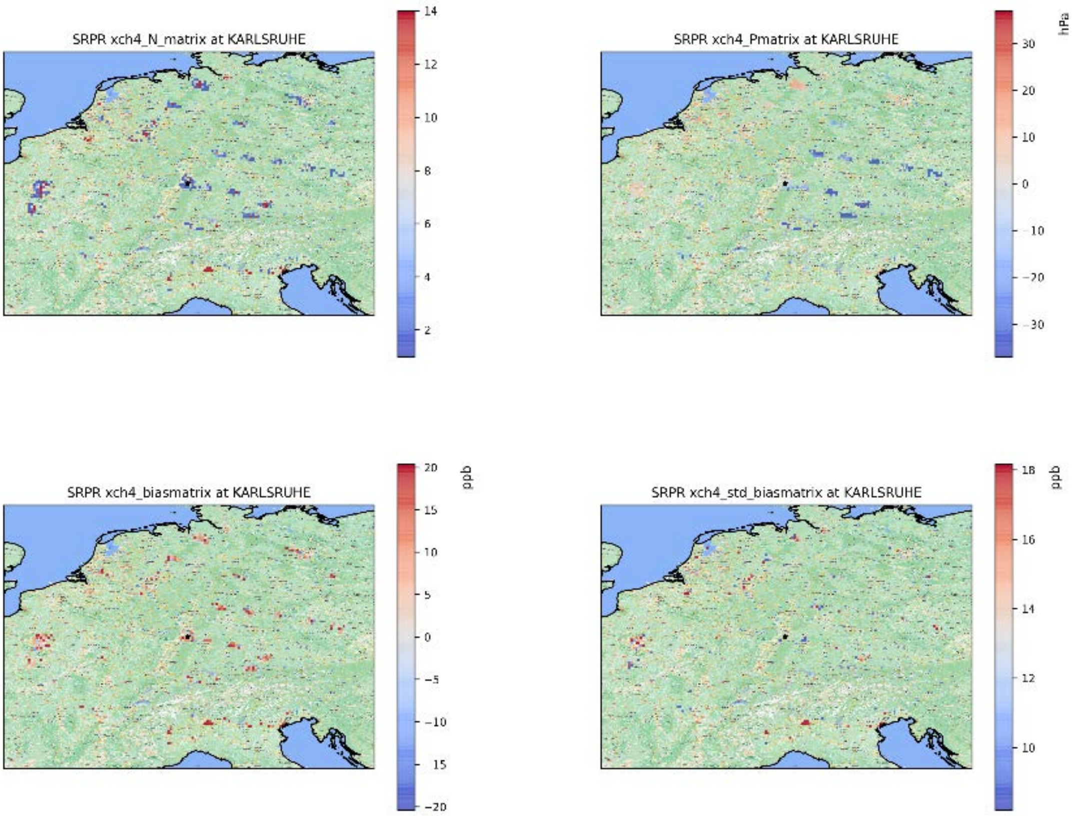

Figure 4-2f: median SRPR - FTS surface pressure difference (top left), number of collocated XCH_4 measurements in each 0.1 by 0.1° grid cell (top right), median SRPR-FTS XCH_4 difference (bottom left) and standard deviation on the SRPR-FTS XCH_4 biases in each grid cell.

Therefore, our current best, universally applicable, but flawed, estimate of this factor can be derived from fitting a linear equation through the sat-TCCON residuals as a function of distance between the FTS site and the satellite pixel center points (we do this for all satellite FTS pairs drawn from all stations, see **Figure 4-3**). From the obtained slope a, we can then estimate the uncertainty associated with the collocation by simply taking the standard deviation of points along the slope (a×dist(i)), where dist(i) is the distance between the FTS station and satellite centre point for a given sat-FTS pair with index i. Note that we here use the normal standard deviation as, by default, there are no outliers in the points that constitute the slope.

As already mentioned, this is a mere estimate and corresponds more with a lower bound threshold, as station to station bias results can differ profoundly. Most noticeable is to look at bias value differences between sites where the collocation areas overlap to a large degree, such as Pasadena and Edwards (see **Tables 4-3, 4-5, 4-7, 4-9, 4-12, 4-15**).

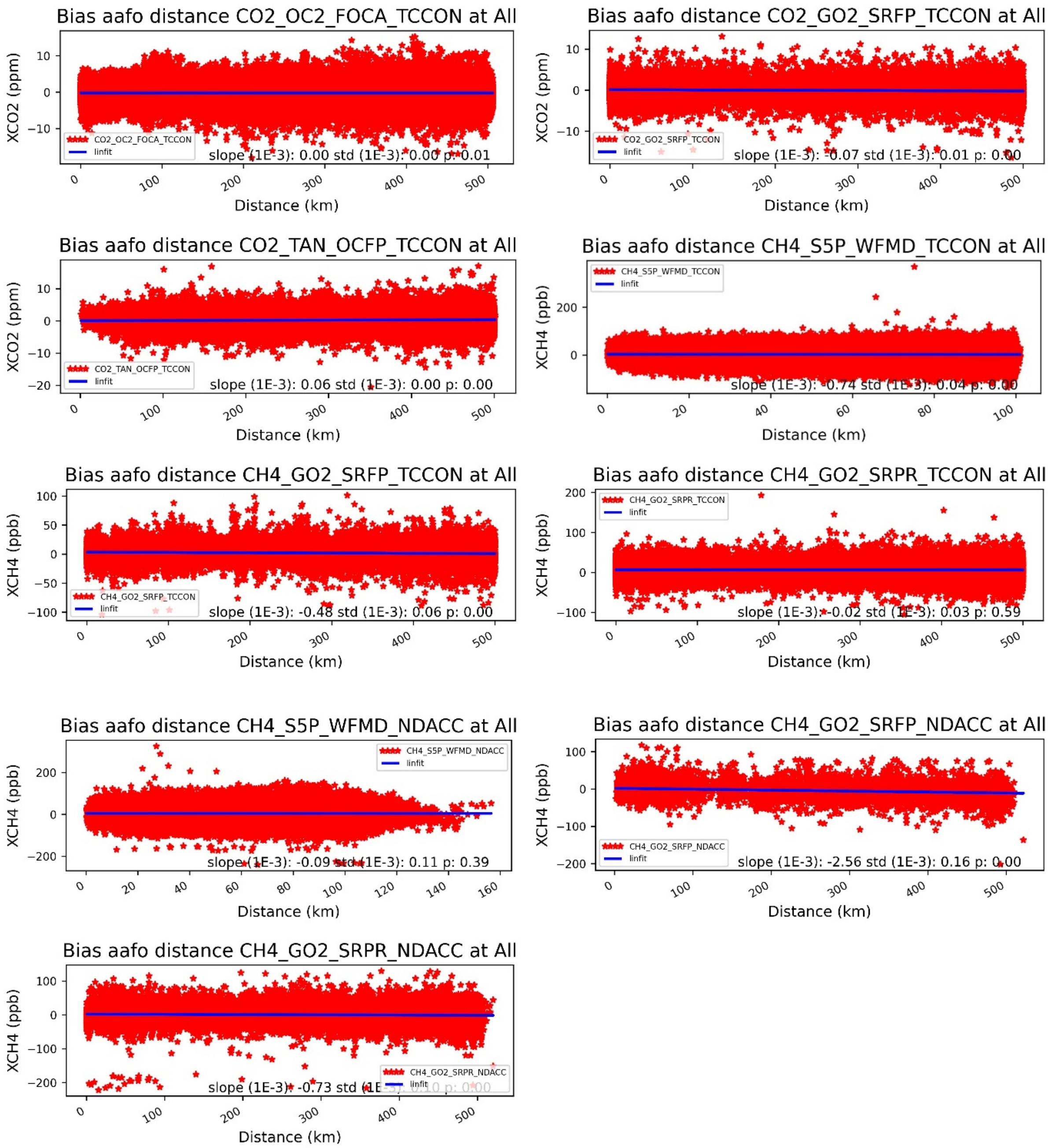

Figure 4-3: Satellite-TCCON or NDACC bias as a function of (aafo) distance between the satellite and TCCON/NDACC sampling point, for all algorithms in this study. Slope in ppm/100 km for XCO_2 and ppb/100 km for XCH_4.

As can be seen in **Figure 4-3**, which shows all the 'bias as a function of distance' plots, the effect is fairly limited. For XCO_2, values range between -0.07 and 0.06 ppm/100 km, for XCH_4 we see values between -0.74 and -0.02 ppb/100km for TCCON and between -2.56 and -0.09ppb/100km for NDACC.

4.2 Validation results

This section lists all validation results for the algorithms presently available in this study. First we show, for each algorithm, a general overview of the collocated data.

This comprises of a Taylor plot and a mosaic overview of the obtained timeseries.

The Taylor plot shows the correlation between the various FTS sites and the retrieval algorithm (straight lines), the standard deviation of the FTS data at each site, relative to the standard deviation of the satellite (normalized to 1) (light grey arches) and the root mean square error of the sat-fts difference (dark grey arches).

After this we discuss the different statistical parameters as obtained on a per station level.

Then the temporal variability is discussed, showing all the station timeseries as well as a more broad 'latitudinal band' based discussion on the long-term trend (if any) and seasonality.

After this we discuss the overall FoM, obtained from the analysis of individual data, and their statistical reliability.

Thus, in each section, we show:

1) A Taylor and Mosaic overview plot.
2) A table listing all Bias, Scatter, correlation (R), number of collocated data pairs (N) for all stations, and, if the timeseries allows, the slopes and amplitudes of the trend fits.
3) Example timeseries of individual data.
4) Monthly averaged timeseries and seasonal plots for broader latitude bands.
5) A Summary table of the Figures of Merit drawn from the values, drawn from individual measurements, at all stations.

4.2.1 Validation results for product CO2_OC2_FOCA

Below we show the validation results of the XCO_2 concentrations as derived by the CO2_OC2_FOCA v11 algorithm using OCO-2 spectra. Data was available from September 2014 until mid February 2024. The FOCAL algorithm provides *a priori* and column averaging kernel data on a 5-layer profile. Compared to the last PVIR iteration little has changed in terms of its comparisons with TCCON. There are slight changes in the FoM but never abruptly and always within the previously established confidence bounds.

4.2.1.1 Detailed results

The Taylor diagram below in **Figure 4-4** yields a concise overview of the capabilities of the CO2_OC2_FOCA algorithm. Most TCCON sites cluster between the 0.9 and 0.99 correlation line. Also, the normalized standard deviation of most sites is close to 1, indicating that the variability of both datasets (due to natural variability and random error) is comparable. The normalized standard deviation of the bias (std(sat-fts)/std(sat)) sits (for most sites) at and even below 0.4, which is very encouraging as it indicates that a large fraction of the variability (we can only assume it is the natural variability part) within the TCCON time series is also captured by the satellite.

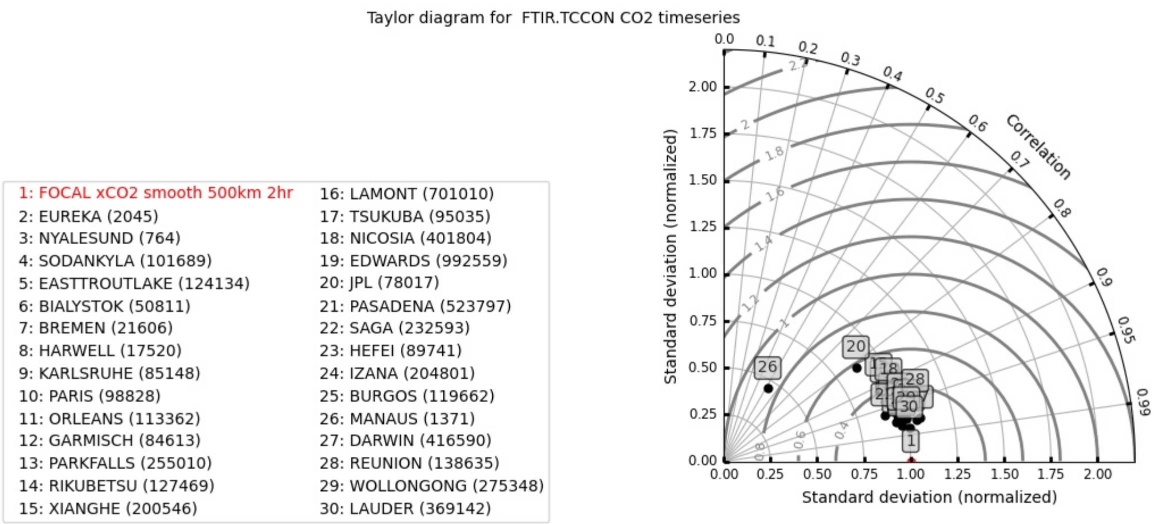

Figure 4-4: Tayor plot of XCO_2 TCCON values relative to CO2_OC2_FOCA . Straight lines correspond with the correlation, light grey lines yield the variability of the TCCON data relative to the satellite variability and the dark grey lines correspond with the variability of the Satellite -TCCON bias relative to the satellite variability.

Notable outlier is Manaus with lower correlations ~0.5) but this dataset only cover a limited fraction of the sampled time period (see **Figure 4-5**)

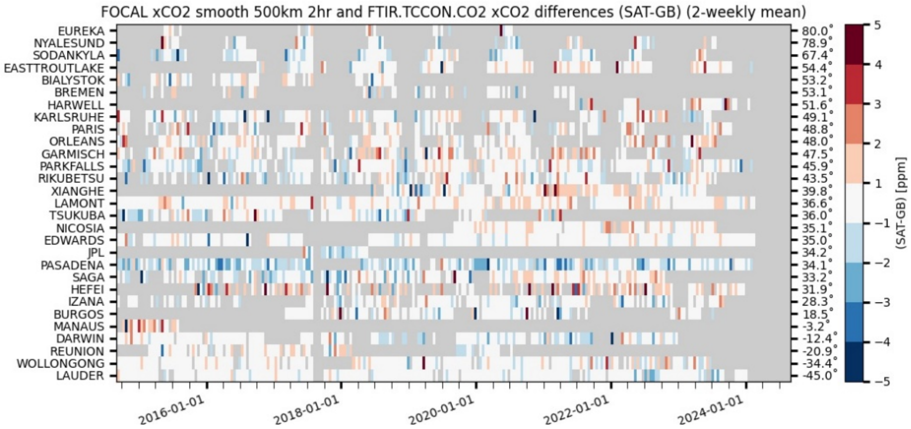

Figure 4-5: Mosaic plot of bi-weekly mean CO2_OC2_FOCA-TCCON XCO_2 biases as a function of time and TCCON station.

It is hard to discern a pattern in the above mosaic plot (**Figure 4-5**), which shows the mean bi-weekly bias between the satellite and TCCON measurement pairs. One can see the seasonal unavailability of data during winter (not visible for the Southern hemisphere as Lauder (New Zealand) still sits at a modest 45°S). Pasadena has consistent negative biases (see also **Table 4-3**) in line withthe previous analysis (v10.1). This is not surprising as it is located within the Los Angeles basin and typically measures larger concentrations than what is present outside the basin. The nearby Edwards site which to a large degree has an overlapping collocation area (see **Figure 4-1 and 4-7**) features much different bias values -0.21 ppm compared to -1.18 ppm at Pasadena). The algorithm produces on average ~120000 data pairs per station. Which roughly corresponds with around 13000 data pairs per station per year. Of the stations, only 2 out of 29 have a correlation coefficient under 0.90. These two are Manaus and JPL which feature very limited temporal coverage. The correlation of all data (regardless of station) equals 0.97. The bias ranges between -1.30 ppm (JPL) and 1.34 ppm (Manaus) and the scatter between 2.08 ppm (Xianghe) and 0.94 ppm (Lauder). Long term trends on the bias (the so-called drift) range between -0.21 ppm/year (Ny Alesund) and 0.29 ppm/year (Bialystok). Note that we only calculated long-term trends for stations whose collocated dataset spans at least 3 years. The amplitude on the other hand ranges between 0.08ppm at Edwards and Izaña and 4 ppm at Eureka. Excluding Eureka (which features significant seasonal gaps which affects the quality of the seasonal amplitude fit), the highest amplitude is absorved at Burgos (1.05 ppm)

Table 4-3: Number of collocated data pairs (N), Correlation (R), Bias, Scatter, long term trend difference (ltt) and uncertainty thereon (ltt_err), seasonal amplitude difference (A) and uncertainty thereon (A_err) as well as the latitude of the TCCON station. The last row lists the median values over all stations. Product: CO2_OC2_FOCA.

STATION	N	R	Bias	Scat	ltt	ltt_err	A	A_err	Lat
EUREKA	2045	0.94	0.11	1.59	0.03	0.13	4	2.37	80
NYALESUND	764	0.96	-0.4	1.5	-0.21	0.07	1.38	0.87	78.9
SODANKYLA	101689	0.97	-0.57	1.29	0.08	0.04	0.94	0.3	67.4
EASTTROUTLAKE	124134	0.96	0.19	1.41	0.14	0.05	0.26	0.13	54.4
BIALYSTOK	50811	0.93	0.21	1.29	0.29	0.14	0.16	0.24	53.2
BREMEN	21606	0.98	0.19	1.29	-0.06	0.08	0.29	0.35	53.1
HARWELL	17520	0.91	-0.11	1.14	-	-	-	-	51.6
KARLSRUHE	85148	0.97	0.12	1.39	0	0.04	1.07	0.17	49.1
PARIS	98828	0.97	0.25	1.3	0.02	0.04	0.71	0.19	48.8
ORLEANS	113362	0.97	0.49	1.2	0.07	0.03	0.57	0.15	48
GARMISCH	84613	0.97	0.56	1.52	0.09	0.06	0.75	0.15	47.5
PARKFALLS	255010	0.97	-0.24	1.42	0.09	0.03	0.48	0.11	45.9
RIKUBETSU	127469	0.98	0.07	1.38	0.05	0.04	1.04	0.15	43.5
XIANGHE	200546	0.9	0.42	2.08	0.38	0.1	0.56	0.15	39.8
LAMONT	701010	0.97	0.3	1.36	0.04	0.02	0.33	0.07	36.6
TSUKUBA	95035	0.95	-0.36	1.5	0.12	0.08	0.24	0.16	36
NICOSIA	401804	0.92	0.38	1.37	-0.01	0.06	0.21	0.09	35.1
EDWARDS	992559	0.98	-0.21	1.32	0.01	0.02	0.08	0.07	35
JPL	78017	0.82	-1.3	1.66	-	-	-	-	34.2
PASADENA	523797	0.96	-1.18	1.69	0.02	0.03	0.13	0.1	34.1
SAGA	232593	0.96	-0.03	1.5	0.3	0.04	0.13	0.12	33.2
HEFEI	89741	0.95	1.05	1.72	-0.05	0.04	0.23	0.2	31.9
IZANA	204801	0.97	-0.35	1.15	-0.01	0.04	0.08	0.11	28.3
BURGOS	119662	0.96	-0.03	0.98	0	0.07	1.05	0.19	18.5
MANAUS	1371	0.52	1.34	1.67	-	-	-	-	-3.2
DARWIN	416590	0.98	-0.34	1.29	-0.16	0.02	0.13	0.08	-12.4
REUNION	138635	0.95	0.29	1.09	-0.19	0.06	0.23	0.14	-20.9
WOLLONGONG	275348	0.97	-0.09	1.19	0	0.03	0.25	0.1	-34.4
LAUDER	369142	0.98	0.02	0.94	-0.07	0.02	0.35	0.06	-45
MEDIAN	119662	0.96	0.07	1.37	0.02	0.04	0.31	0.15	

The timeseries below in **Figure 4-6** show individual satellite and ground-based fts measurements. The capture of the seasonal cycle and long term trend is similar to that of TCCON. Some (mostly low concentration) outliers are still present in the data (for instance in the Rikubetsu, Tsukuba or Sagaplots) but overall most measurements yield good comparison results.

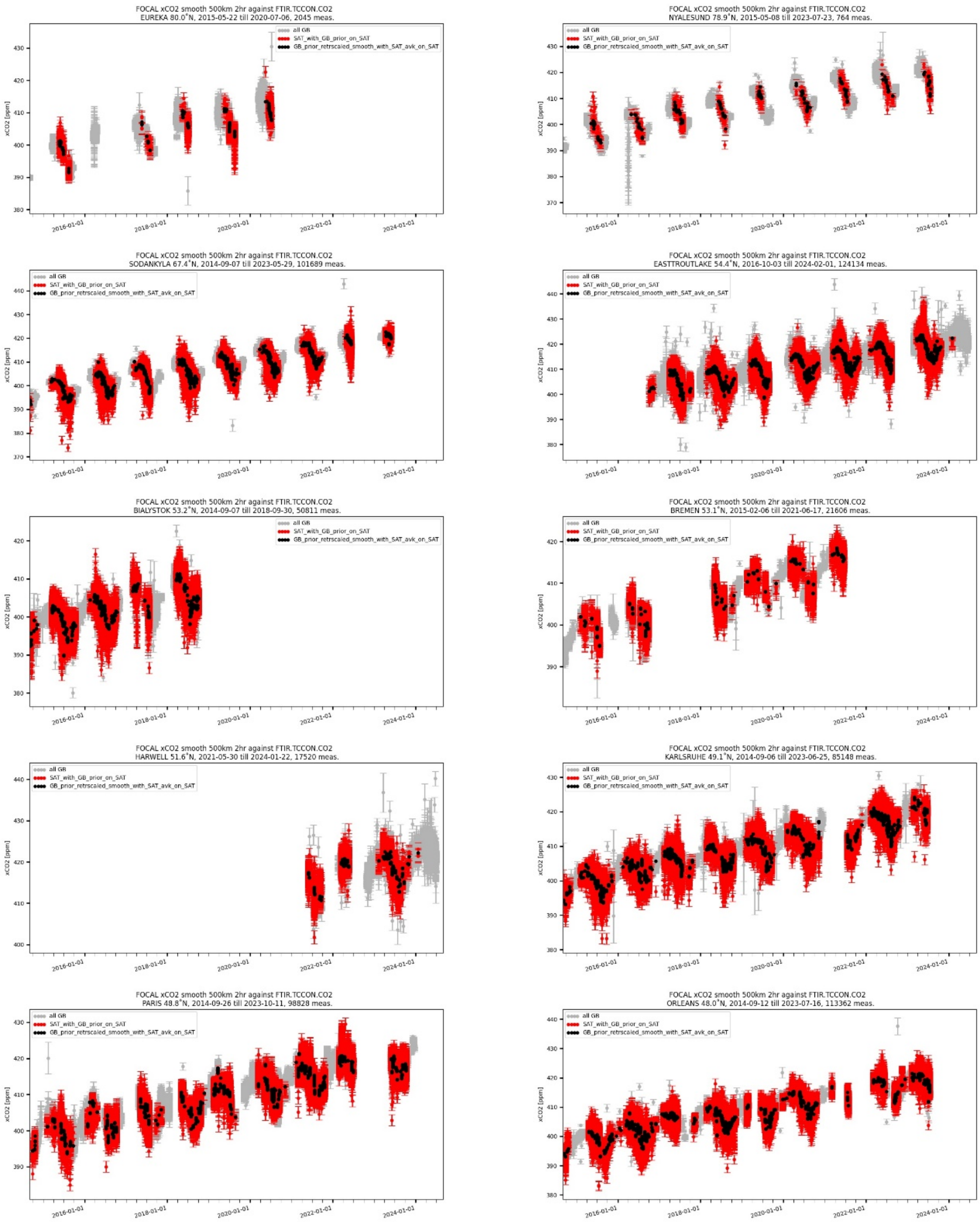
FOCAL xCO2 smooth 500km 2hr against FTIR.TCCON.CO2
EUREKA 80.0°N, 2015-05-22 till 2020-07-06, 2045 meas.
FOCAL xCO2 smooth 500km 2hr against FTIR.TCCON.CO2
NYALESUND 78.9°N, 2015-05-08 till 2023-07-23, 764 meas.
FOCAL xCO2 smooth 500km 2hr against FTIR.TCCON.CO2
SODANKYLA 67.4°N, 2014-09-07 till 2023-05-29, 101689 meas.
FOCAL xCO2 smooth 500km 2hr against FTIR.TCCON.CO2
EASTTROUTLAKE 54.4°N, 2016-10-03 till 2024-02-01, 124134 meas.
FOCAL xCO2 smooth 500km 2hr against FTIR.TCCON.CO2
BIALYSTOK 53.2°N, 2014-09-07 till 2018-09-30, 50811 meas.
FOCAL xCO2 smooth 500km 2hr against FTIR.TCCON.CO2
BREMEN 53.1°N, 2015-02-06 till 2021-06-17, 21606 meas.
FOCAL xCO2 smooth 500km 2hr against FTIR.TCCON.CO2
HARWELL 51.6°N, 2021-05-30 till 2024-01-22, 17520 meas.
FOCAL xCO2 smooth 500km 2hr against FTIR.TCCON.CO2
KARLSRUHE 49.1°N, 2014-09-06 till 2023-06-25, 85148 meas.
FOCAL xCO2 smooth 500km 2hr against FTIR.TCCON.CO2
PARIS 48.8°N, 2014-09-26 till 2023-10-11, 98828 meas.
FOCAL xCO2 smooth 500km 2hr against FTIR.TCCON.CO2
ORLEANS 48.0°N, 2014-09-12 till 2023-07-16, 113362 meas.
all GB
SAT_with_GB_prior_on_SAT
GB_prior_retrscaled_smooth_with_SAT_avk_on_SAT
xCO2 [ppm]
2016-01-01
2018-01-01
2020-01-01
2022-01-01
2024-01-01

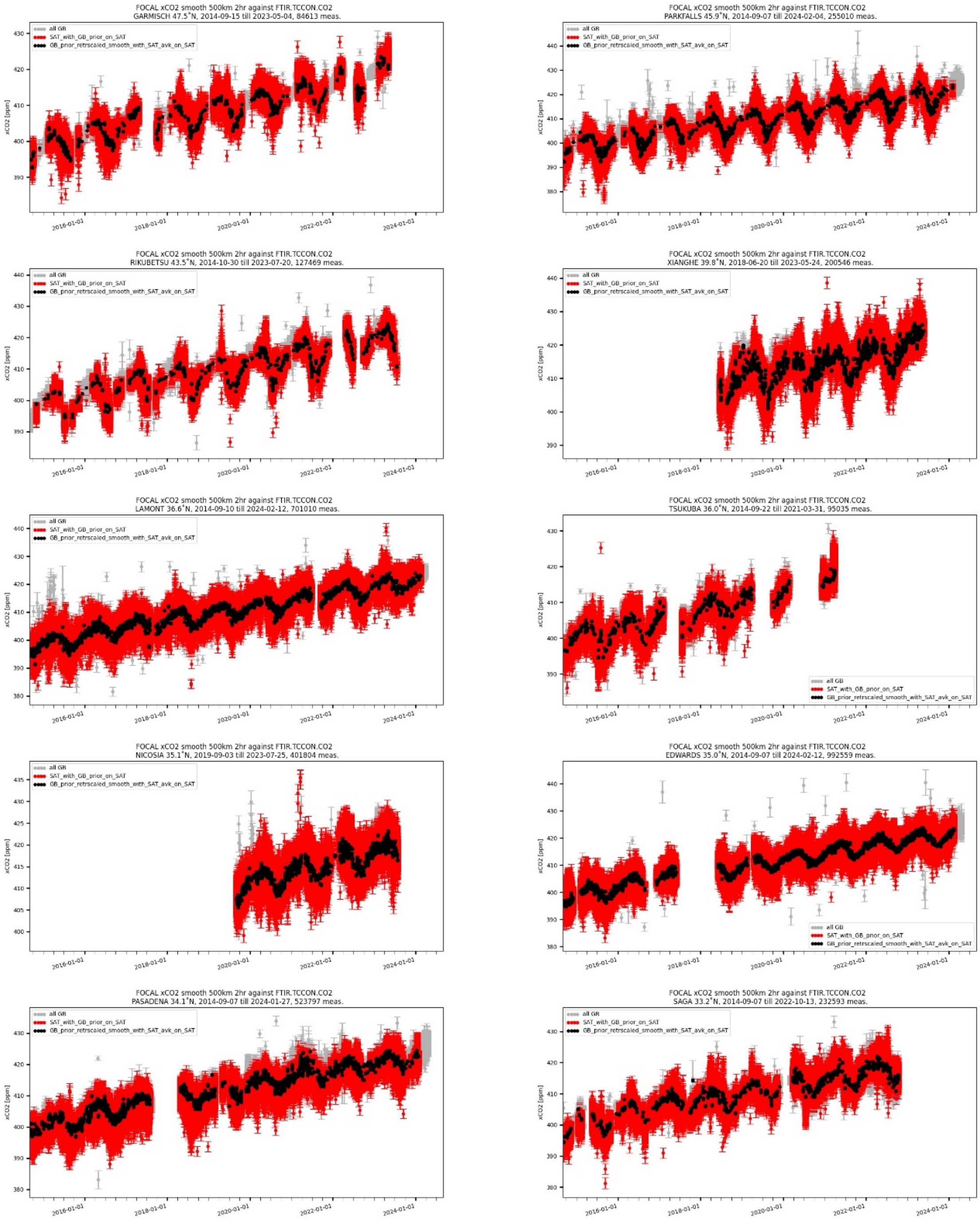

FOCAL xCO2 smooth 500km 2hr against FTIR.TCCON.CO2
GARMISCH 47.5°N, 2014-09-15 till 2023-05-04, 84613 meas.
FOCAL xCO2 smooth 500km 2hr against FTIR.TCCON.CO2
PARKFALLS 45.9°N, 2014-09-07 till 2024-02-04, 255010 meas.
FOCAL xCO2 smooth 500km 2hr against FTIR.TCCON.CO2
RIKUBETSU 43.5°N, 2014-10-30 till 2023-07-20, 127469 meas.
FOCAL xCO2 smooth 500km 2hr against FTIR.TCCON.CO2
XIANGHE 39.8°N, 2018-06-20 till 2023-05-24, 200546 meas.
FOCAL xCO2 smooth 500km 2hr against FTIR.TCCON.CO2
LAMONT 36.6°N, 2014-09-10 till 2024-02-12, 701010 meas.
FOCAL xCO2 smooth 500km 2hr against FTIR.TCCON.CO2
TSUKUBA 36.0°N, 2014-09-22 till 2021-03-31, 95035 meas.
FOCAL xCO2 smooth 500km 2hr against FTIR.TCCON.CO2
NICOSIA 35.1°N, 2019-09-03 till 2023-07-25, 401804 meas.
FOCAL xCO2 smooth 500km 2hr against FTIR.TCCON.CO2
EDWARDS 35.0°N, 2014-09-07 till 2024-02-12, 992559 meas.
FOCAL xCO2 smooth 500km 2hr against FTIR.TCCON.CO2
PASADENA 34.1°N, 2014-09-07 till 2024-01-27, 523797 meas.
FOCAL xCO2 smooth 500km 2hr against FTIR.TCCON.CO2
SAGA 33.2°N, 2014-09-07 till 2022-10-13, 232593 meas.
all GB
SAT_with_GB_prior_on_SAT
GB_prior_retrscaled_smooth_with_SAT_avk_on_SAT
xCO2 [ppm]

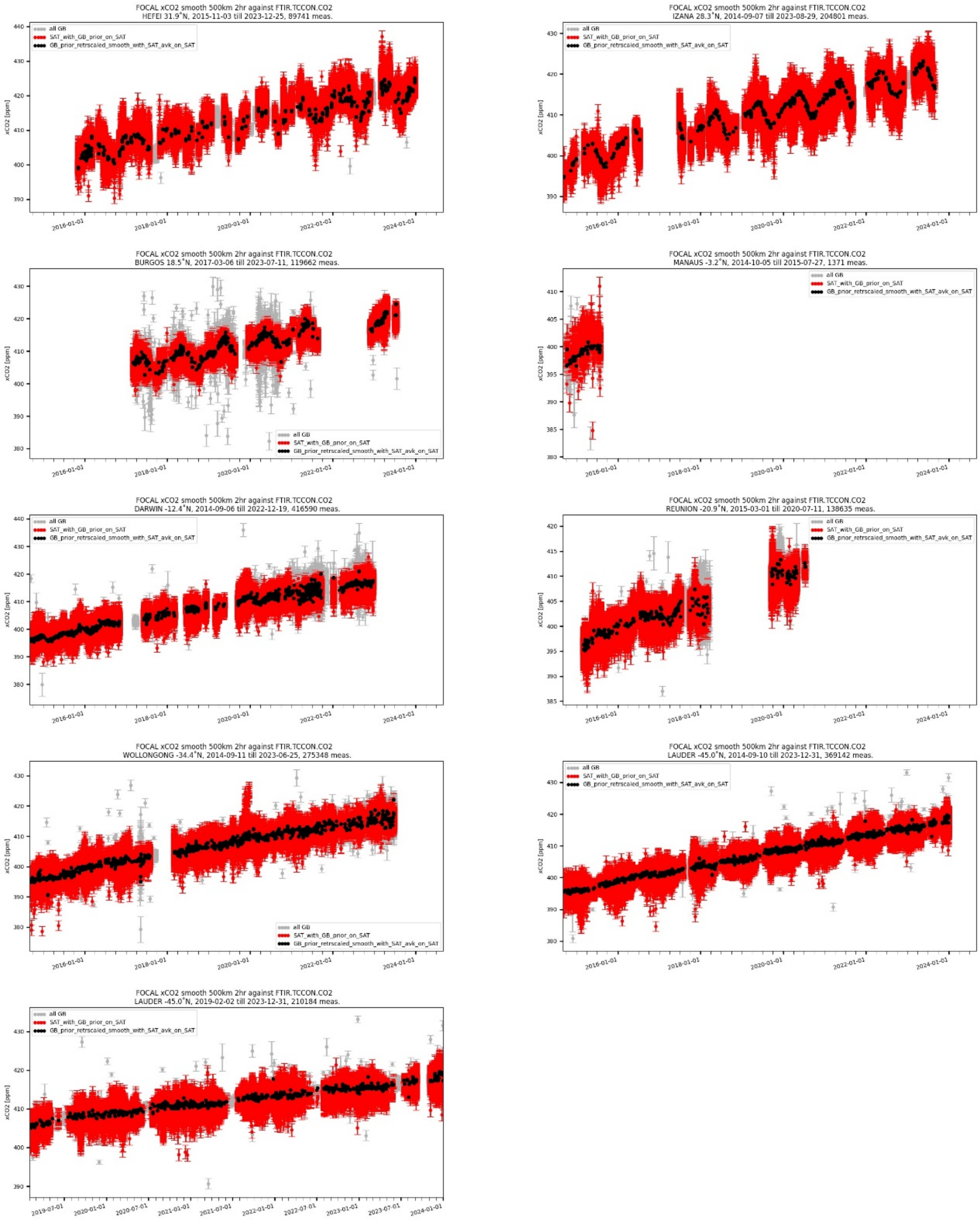

Figure 4-6: XCO_2 timeseries at all TCCON sites (red= CO2_OC2_FOCA data, black is collocated TCCON data and grey are the uncollocated TCCON data).

Figure 4-7 below shows the spatial distribution of the observed biases. Note that the colorbar range has been set to the positive and negative largest absolute value between the 20% and 80% quartile of observed biases and can differ between stations. For most stations, the colorbar range sits close to +1 and -1 ppm. The largest range is observed at Pasadena. Some sites show clear signs of spatial biases. For instance with Park Falls we see a difference between measurements taken over the great lakes and those inland. The same seems to hold true (land-sea bias) for Tsukuba. For other near-water sites the picture is even less clear. Other spatial features are for instance visible in the Edwards plot, where we see high biases over the Los Angeles area as well as the San Joaquin Valley. For other sites, the identification of spatial bias features due to terrain etc. is complicated by the observation of significant striping in the bias plots. A good example here is the Lamont site which features a pronounced positive and negative bias striping pattern. To what extent this is a feature of the algorithm or due to sampling (even though it has over 700000 colocated data pairs) and FTS variability needs to be further investigated.

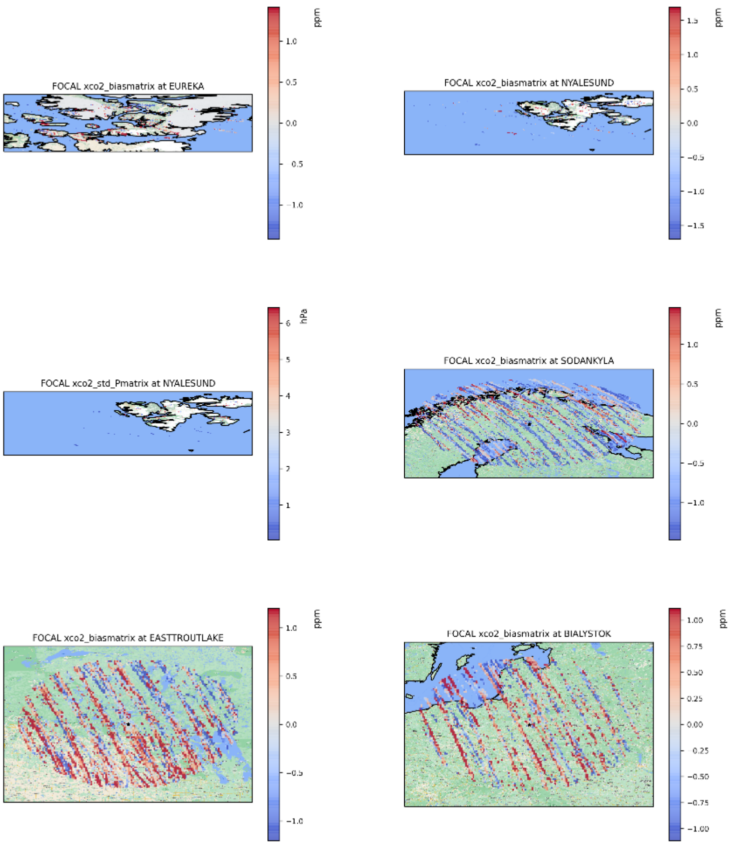

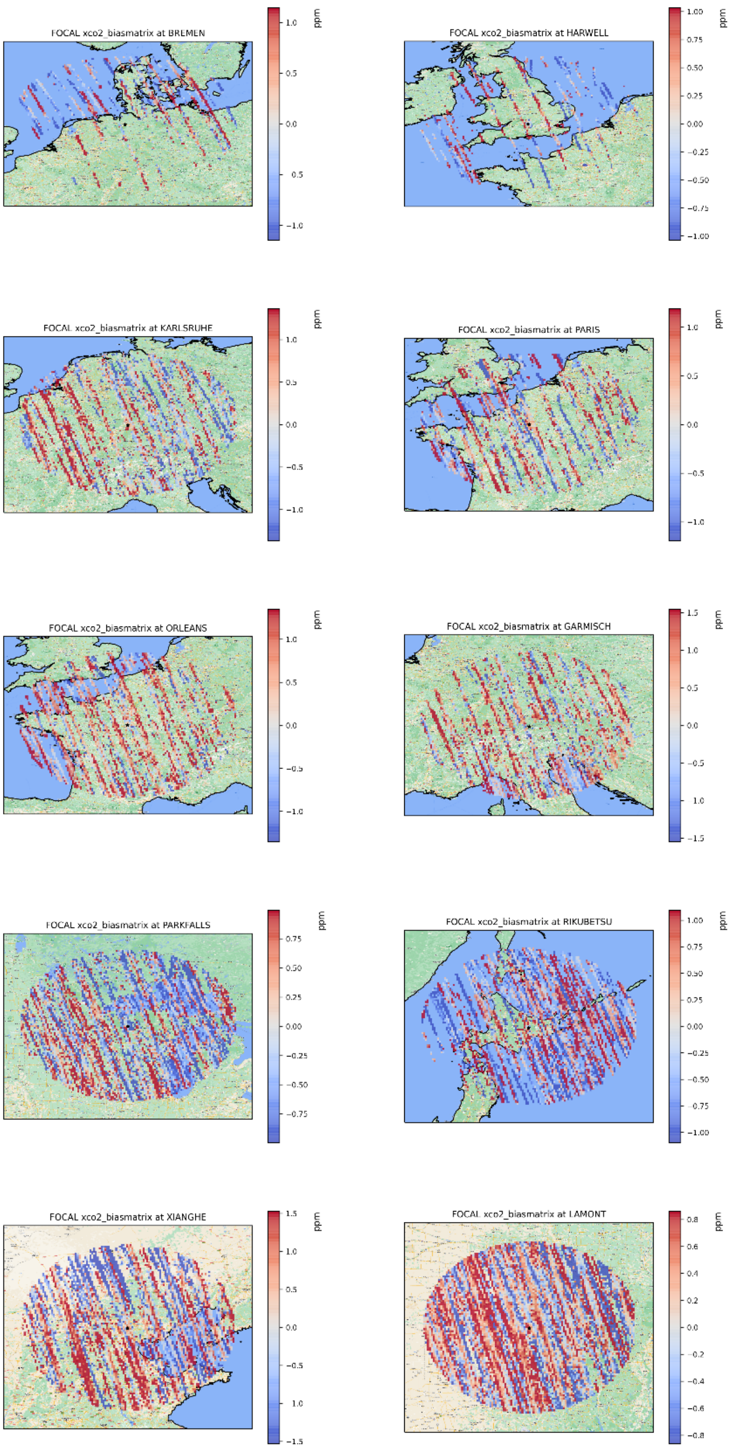
FOCAL xco2_biasmatrix at BREMEN
FOCAL xco2_biasmatrix at HARWELL
FOCAL xco2_biasmatrix at KARLSRUHE
FOCAL xco2_biasmatrix at PARIS
FOCAL xco2_biasmatrix at ORLEANS
FOCAL xco2_biasmatrix at GARMISCH
FOCAL xco2_biasmatrix at PARKFALLS
FOCAL xco2_biasmatrix at RIKUBETSU
FOCAL xco2_biasmatrix at XIANGHE
FOCAL xco2_biasmatrix at LAMONT
ppm

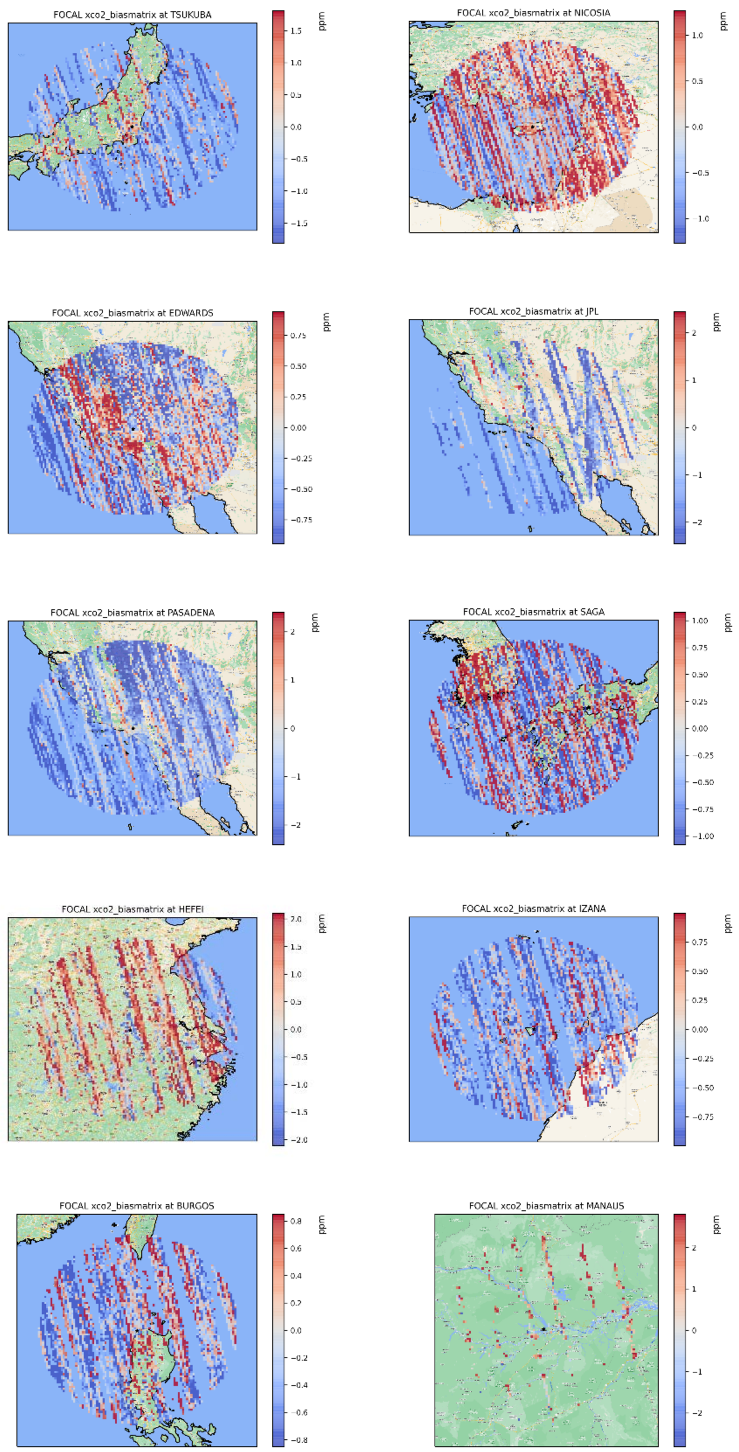

FOCAL xco2_biasmatrix at TSUKUBA
FOCAL xco2_biasmatrix at NICOSIA
FOCAL xco2_biasmatrix at EDWARDS
FOCAL xco2_biasmatrix at JPL
FOCAL xco2_biasmatrix at PASADENA
FOCAL xco2_biasmatrix at SAGA
FOCAL xco2_biasmatrix at HEFEI
FOCAL xco2_biasmatrix at IZANA
FOCAL xco2_biasmatrix at BURGOS
FOCAL xco2_biasmatrix at MANAUS
ppm

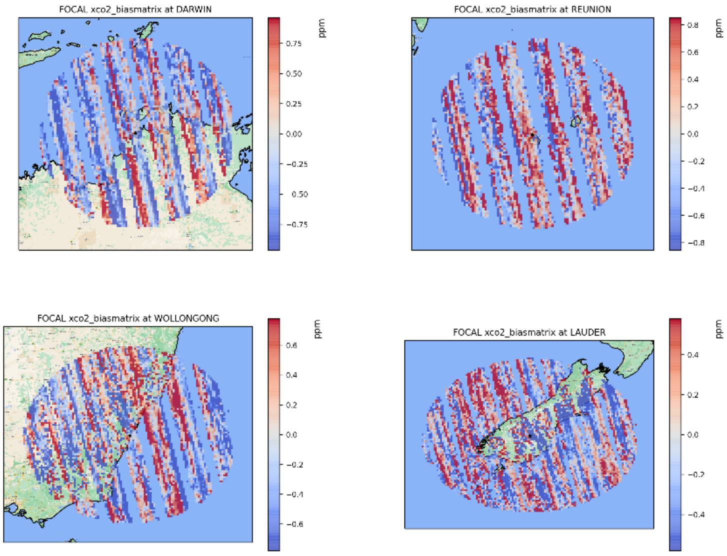

Figure 4-7: Spatial representation of the observed FOCAL-FTS XCO2 biases for each of the TCCON stations. Shown is the median of all biases within each 0.1 by 0.1° latitude-longitude grid.

Figure 4-8 shows monthly median timeseries for TCCON and FOCAL XCO_2 for all data that fall within certain latitude bands, namely all sites north of 40°N latitude (top), all sites between 40°N and the equator (mid) and all sites in the Southern hemisphere (bottom). Again, note that the Southern Hemisphere is only covered by Reunion and Lauder. As can be seen, for all bands, the TCCON and FOCAL data feature long term trends that differ by maximum 0.1 ppm/year only which is well within its uncertainty bounds. On the right hand side of each figure is the detrended monthly median values as a function of month. Again, this clearly shows that FOCAL accurately captures the seasonal cycle. The median amplitude derived from seasonal fits through the individual bias data at each station amounts to 0.31 [0.02, 0.38] ppm.

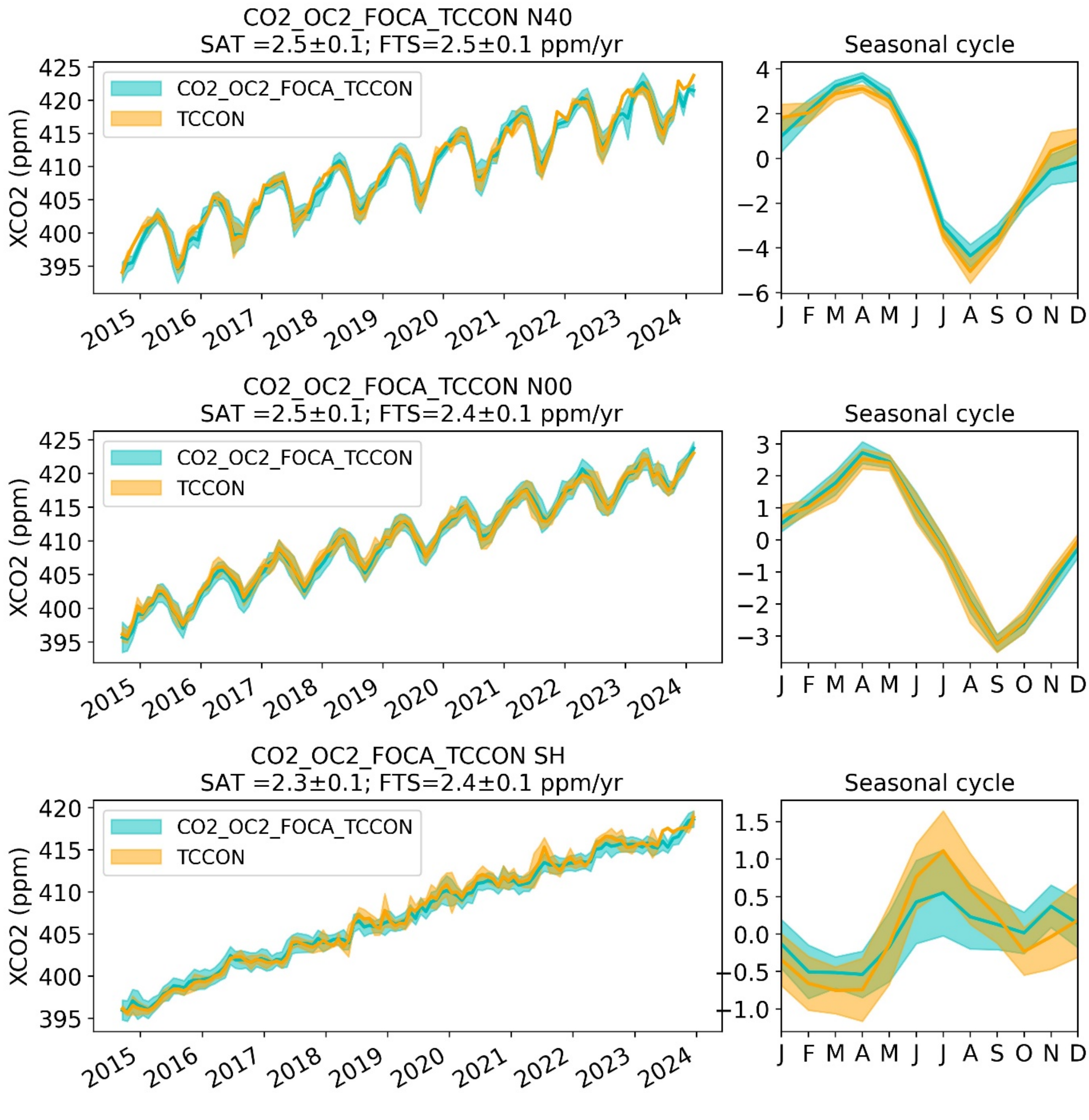

Figure 4-8: Monthly median collocated Sat and TCCON XCO_2 concentrations as a function of time and the detrended monthly medians as a function of season. The shaded areas correspond with the scaled median absolute deviation.

4.2.1.2 Summary

Listed in the table below (**Table 4-4**) are the Figure of Merit parameters as derived from the individual data pairs at the different TCCON stations. Values in square brackets [ ] correspond with the upper and lower 95% confidence bound on the parameter. The uncertainty ratio features 2 numbers as outlined in the validation method.

Overall, the CO2_OC2_FOCA product delivers data that matches very well with that of TCCON. This is apparent in the Taylor diagram time series plots as well as the Figures of Merit. However, the observed features in the spatial bias patterns show room for improvement.

The differences between the Figures of Merit in our previous assessment **/PVIR GHG-CCI+ v4.0, 2023**/ and this analysis are extremely small and fall wel between the confidence bands. The determined Relative Accuracy changed from 0.35 [0.12, 0.50] ppm to 0.42 [0.28, 0.63] ppm already below, both below the <0.5 ppm accuracy requirements. The Seasonal Relative Accuracy (SRA at 0.54 [0.43, 0.67] ppm in the previous analysis) now sits at 0.53 [0.40, 0.67] ppm, only slightly above the threshold but with overlapping confidence bands with the target. Take note that the accuracy requirements of < 0.5 ppm, assumes the abolishment of any collocation influence, nor any station-to-station differences within the TCCON network (its network accuracy is estimated to be within 0.4 ppm), all of which do contribute to the obtained RA and SRA values.

The reported uncertainty is, when compared to the scatter, very accurate (1.13 or 1.23) and even slightly too high. The scatter itself (1.37 ppm) has reached the so-called breakthrough levels (< 3 ppm). From the timeseries plots and Taylor diagram we in fact see that the variability closely matches this of TCCON. The overall bias is essentially zero 0.07 [-0.06, 0.25]). And finally the dataset shows no significant long term drift.

Table 4-4: presents an overview of the estimated data quality of CO2_OC2_FOCA, as obtained by the VALT team, from comparisons with TCCON ground-based reference observations. Values in square brackets [ ] correspond with the upper and lower 95% confidence bound on the parameter. The uncertainty ratio features 2 numbers as outlined in the validation method.

Product Quality Summary Table for Product: CO2_OC2_FOCA Level: 2, Version: v11, Time period covered: 9.2014 – 9.2024 Assessment: Validation Team (VALT)			
Parameter [unit]	**Achieved performance**	**Requirement**	**Comments**
Single measurement precision (1-sigma) in [ppm]	1.37 [1.23, 1.44]	< 8 (T) < 3 (B) < 1 (G)	Computed as the median over all station scaled median absolute differences to TCCON
Uncertainty ratio [-]: Ratio reported uncertainty to standard deviation of satellite-TCCON difference	1.13, 1.23*	-	No requirement but value close to unity expected for a high quality data product with reliable reported uncertainty.
Median bias (global offset) [ppm]	0.07 [-0.06, 0.26]	-	No requirement but value close to zero expected for a high quality data product.
Accuracy: Relative systematic error [ppm]	Spatial: 0.42 [0.28, 0.63] Spatio-temporal: 0.53 [0.40, 0.66]	< 0.5	Spatial: Computed as standard deviation of the biases at the various TCCON sites. Spatio-temporal: As "Spatial" but also considering seasonal biases.
Stability: Drift [ppm/year]	0.02 [-0.02, 0.05]	< 0.5	Linear drift

4.2.2 Validation results for product CO2_TAN_OCFP

Here we present the VALT validation results for the CO2_TAN_OCFP product. The analysis is identical to the one in the previous PVIR (no changes of product), apart from the addition of a representation of the spatial biases in **Figure 4-12**. The analysis pertains to the global v1.2 dataset, which is exactly the same algorithm as used in the previous study. Data is available from March 2017 up to and including May 2018 (again no change). The OCFP algorithm provides *a priori* and column averaging kernel information on a 20 level profile. Given the very limited time period that is covered by this product, these validation results will be rather preliminary in nature, nor can we make useful statements about long term trends.

4.2.2.1 Detailed results

The Taylor diagram below in **Figure 4-9** shows a short overview of the capabilities of the CO2_TAN_OCFP product. Most TCCON sites are clustered between the 0.6 and 0.9 0.75 correlation value, but with negative correlation values for Bremen, likely due its extremely limited collocated dataset. Other stations with low correlation values (<0.2) are Izaña, Burgos and Reunion(all featuring very limited temporal overlap). The normalized standard deviation ranges between 0.5 and 1.25 with most sites clustering around the 0.75 mark, indicating that the variability of the TCCON data is (in most cases) smaller. The normalized standard deviation of the bias sits (for most sites) between 1 and 0.6. All this indicates that while OCFP data features a stronger variability (random error and/or seasonal variability) than the TCCON data, the biases still harbors less variability then either of them, an indication of OCFP capturing the natural variability.

There is no real discernible pattern in the mosaic plot (**Figure 4-10**), which shows the mean bi-weekly bias between the satellite and TCCON measurement pairs. August seems to exhibit some more outspoken biases (negative and positive), but since the period covered by the plot is very limited, it is hard to tell if this is indeed a systematic feature or merely coincidence.

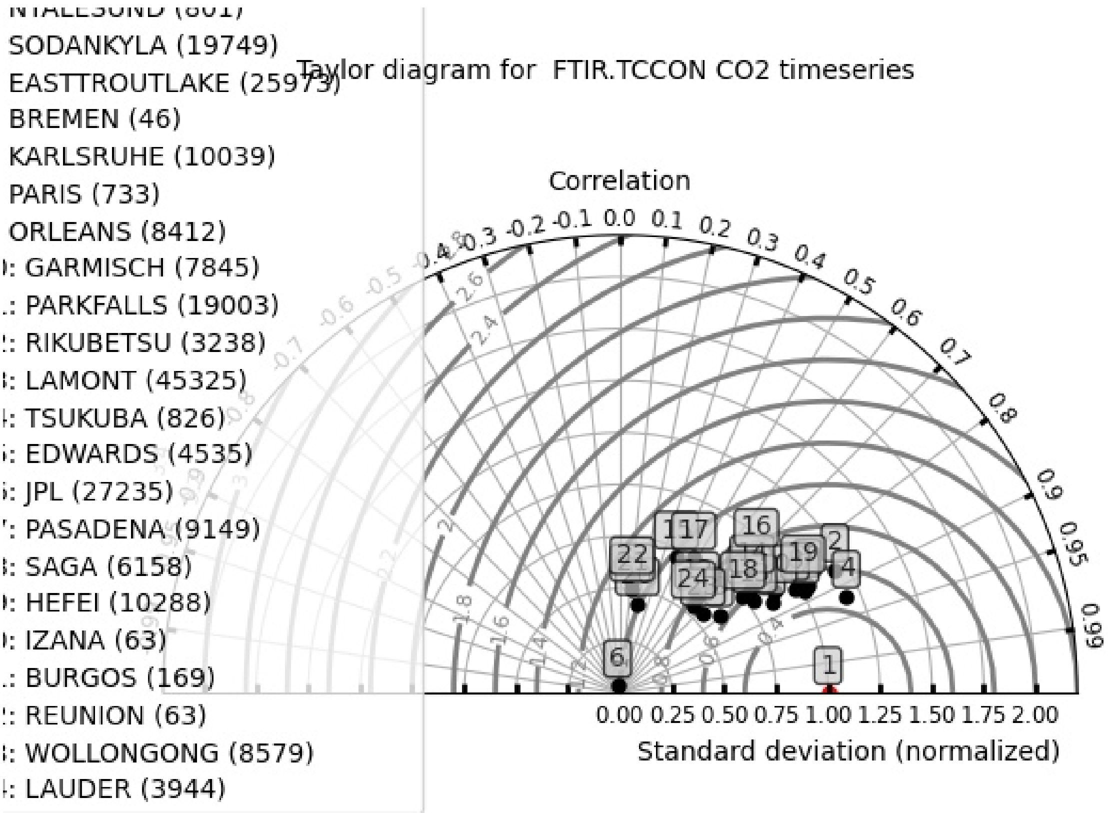

Figure 4-9: Taylor plot of daily averaged XCO_2 TCCON values relative to product CO2_TAN_OCFP. Straight lines correspond with the correlation, light grey lines yield the variability of the TCCON data relative to the satellite variability and the dark grey lines correspond with the variability of the Satellite - TCCON bias relative to the satellite variability.

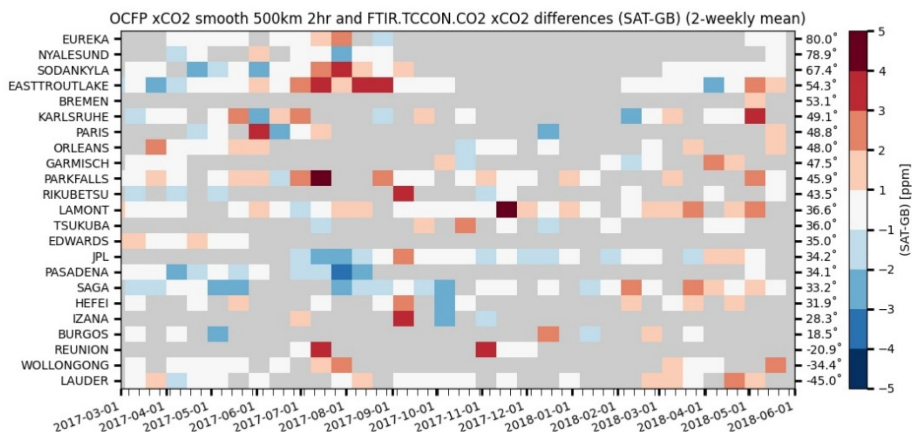

Figure 4-10: Mosaic plot of bi-weekly mean CO2_TAN_OCFP-TCCON XCO_2 biases as a function of time and TCCON station.

Table 4-5 lists all bias and scatter results derived from individual data pairs at all TCCON stations. The algorithm produces on average ~6150 data pairs per station which corresponds with ~4900 pairs per station per year. The observed median bias ranges between -0.95 (Rikubetsu) and 1.95 ppm (Bremen), while the scatter ranges between 3.15 ppm (Izaña) and 0.63 ppm (Wollongong). Note that large bias results are observed at stations that are quite close to one another. One in the Los Angeles basin (Pasadena) and the other just outside on the other side of the San Gabriel Mountain range (Edwards), which separates the basin from the Mojave Desert. Correlation values range between -0.33 (Bremen) and 0.92 (Sodankyla), with the median over all stations equal to 0.79. The correlation using all data regardless of station equals 0.83. Given the limited timespan covered by the product, we did not calculate any long term trend. But as can be seen in **Figures 4-11 and 4-13** no clear-cut drift is observable.

Table 4-5: Number of collocated data pairs (N), Correlation (R), Bias, Scatter, long term trend difference (ltt) and uncertainty thereon (ltt_err), seasonal amplitude difference (A) and uncertainty thereon (A_err) as well as the latitude of the TCCON station. The last row lists the median values over all stations. Product: CO2_TAN_OCFP.

STATION	N	R	Bias	Scat	ltt	ltt_err	A	A_err	lat
EUREKA	928	0.87	1.01	1.56	-	-	-	-	80
NYALESUND	801	0.86	-0.57	1.12	-	-	-	-	78.9
SODANKYLA	19749	0.92	0.35	1.27	-	-	-	-	67.4
EASTTROUTLAKE	25973	0.87	0.56	1.71	-	-	-	-	54.3
BREMEN	46	-0.33	1.95	0.91	-	-	-	-	53.1
KARLSRUHE	10039	0.88	0.27	1.42	-	-	-	-	49.1
PARIS	733	0.86	1.21	1.05	-	-	-	-	48.8
ORLEANS	8412	0.79	0.49	1.05	-	-	-	-	48
GARMISCH	7845	0.84	0.22	1.72	-	-	-	-	47.5
PARKFALLS	19003	0.79	0	1.66	-	-	-	-	45.9
RIKUBETSU	3238	0.63	-0.95	1.7	-	-	-	-	43.5
LAMONT	45325	0.83	0.56	1.42	-	-	-	-	36.6
TSUKUBA	826	0.76	-0.44	1.69	-	-	-	-	36
EDWARDS	4535	0.38	0.79	1.18	-	-	-	-	35
JPL	27235	0.7	-0.52	1.86	-	-	-	-	34.2
PASADENA	9149	0.48	-0.59	1.69	-	-	-	-	34.1
SAGA	6158	0.79	-0.2	1.69	-	-	-	-	33.2
HEFEI	10288	0.85	1.16	1.61	-	-	-	-	31.9
IZANA	63	0.19	-0.24	3.15	-	-	-	-	28.3
BURGOS	169	0.12	0.72	1.29	-	-	-	-	18.5
REUNION	63	0.11	0.83	0.84	-	-	-	-	-20.9
WOLLONGONG	8579	0.73	0.63	1.59	-	-	-	-	-34.4
LAUDER	3944	0.65	0.77	1.28	-	-	-	-	-45
MEDIAN	**6158**	**0.79**	**0.49**	**1.56**	**-**	**-**	**-**	**-**	**36.6**

The timeseries below in **Figure 4-11** show individual satellite and ground-based fts measurements. As can be seen, and was already apparent from the Taylor diagram, OCFP XCO_2 features a somewhat higher scatter than TCCON, but overall the seasonality is well captured. An occasional outlier is still noticeable (both in the TCCON and OCFP dataset).

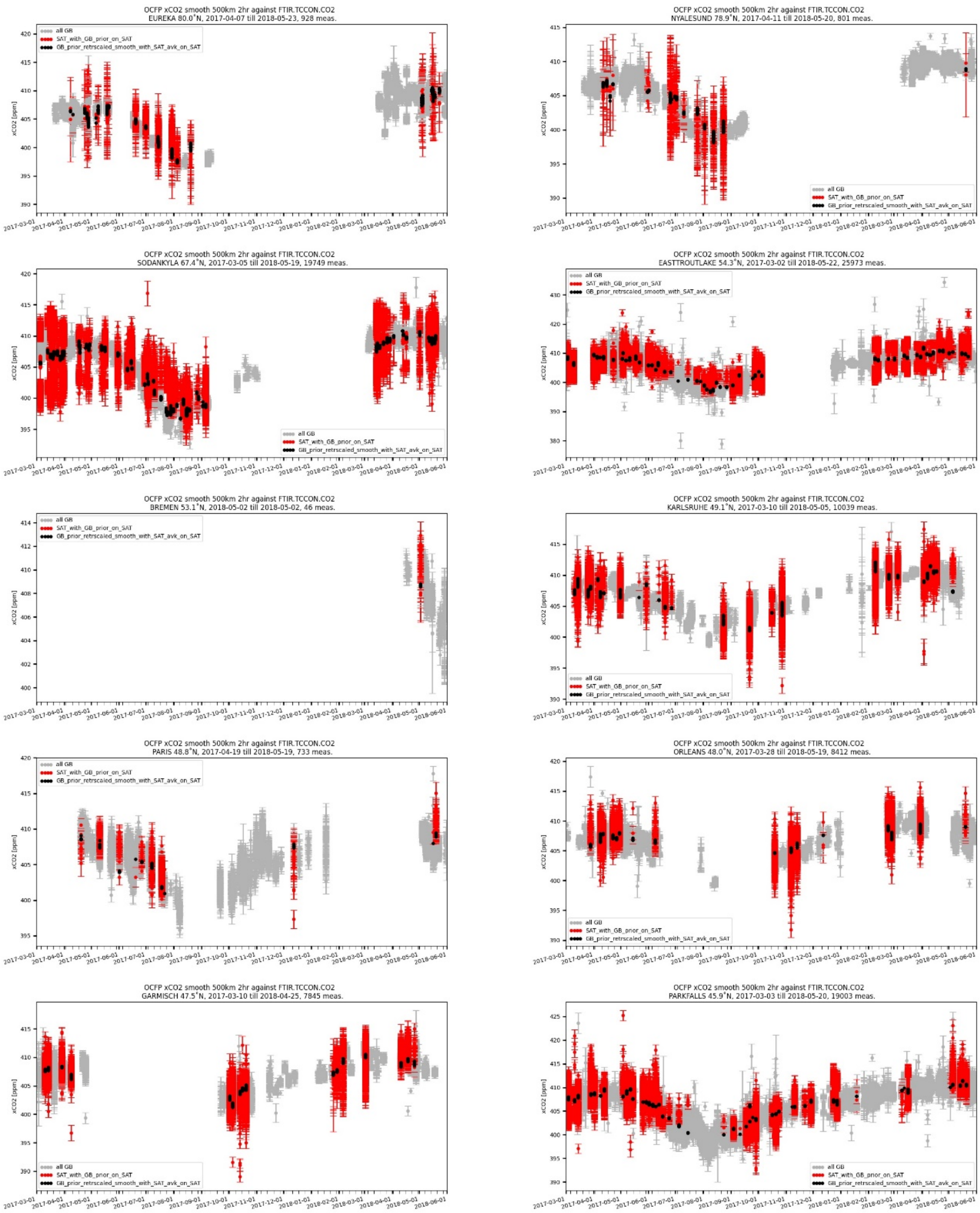

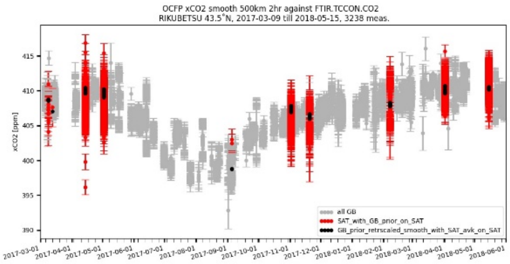

OCFP xCO2 smooth 500km 2hr against FTIR.TCCON.CO2
RIKUBETSU 43.5°N, 2017-03-09 till 2018-05-15, 3238 meas.
xCO2 [ppm]
all GB
SAT_with_GB_prior_on_SAT
GB_prior_retrscaled_smooth_with_SAT_avk_on_SAT

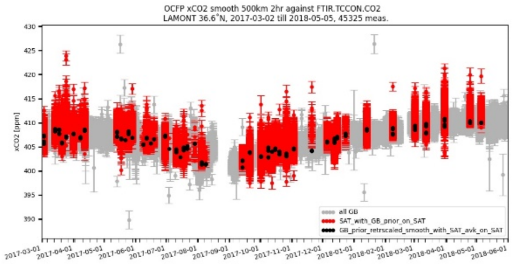

OCFP xCO2 smooth 500km 2hr against FTIR.TCCON.CO2
LAMONT 36.6°N, 2017-03-02 till 2018-05-05, 45325 meas.
xCO2 [ppm]
all GB
SAT_with_GB_prior_on_SAT
GB_prior_retrscaled_smooth_with_SAT_avk_on_SAT

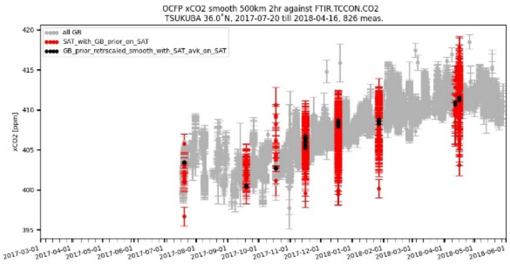

OCFP xCO2 smooth 500km 2hr against FTIR.TCCON.CO2
TSUKUBA 36.0°N, 2017-07-20 till 2018-04-16, 826 meas.
xCO2 [ppm]
all GB
SAT_with_GB_prior_on_SAT
GB_prior_retrscaled_smooth_with_SAT_avk_on_SAT

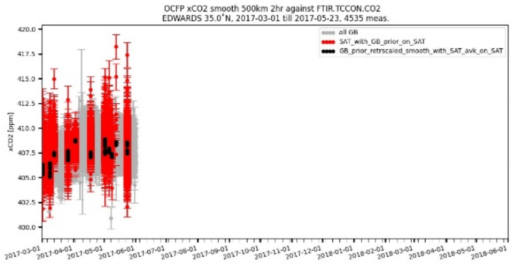

OCFP xCO2 smooth 500km 2hr against FTIR.TCCON.CO2
EDWARDS 35.0°N, 2017-03-01 till 2017-05-23, 4535 meas.
xCO2 [ppm]
all GB
SAT_with_GB_prior_on_SAT
GB_prior_retrscaled_smooth_with_SAT_avk_on_SAT

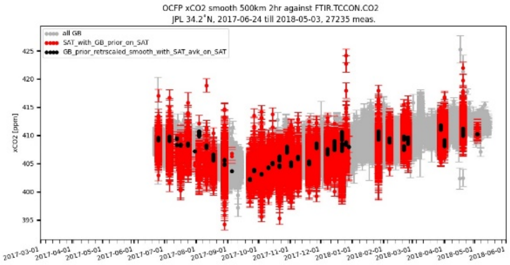

OCFP xCO2 smooth 500km 2hr against FTIR.TCCON.CO2
JPL 34.2°N, 2017-06-24 till 2018-05-03, 27235 meas.
xCO2 [ppm]
all GB
SAT_with_GB_prior_on_SAT
GB_prior_retrscaled_smooth_with_SAT_avk_on_SAT

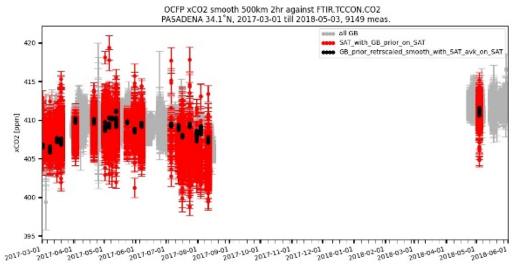

OCFP xCO2 smooth 500km 2hr against FTIR.TCCON.CO2
PASADENA 34.1°N, 2017-03-01 till 2018-05-03, 9149 meas.
xCO2 [ppm]
all GB
SAT_with_GB_prior_on_SAT
GB_prior_retrscaled_smooth_with_SAT_avk_on_SAT

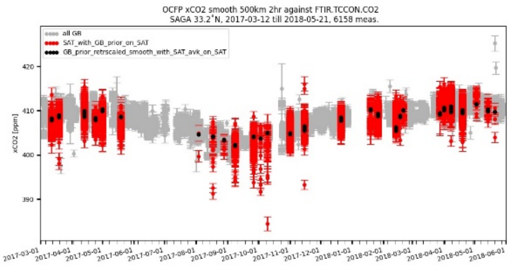

OCFP xCO2 smooth 500km 2hr against FTIR.TCCON.CO2
SAGA 33.2°N, 2017-03-12 till 2018-05-21, 6158 meas.
xCO2 [ppm]
all GB
SAT_with_GB_prior_on_SAT
GB_prior_retrscaled_smooth_with_SAT_avk_on_SAT

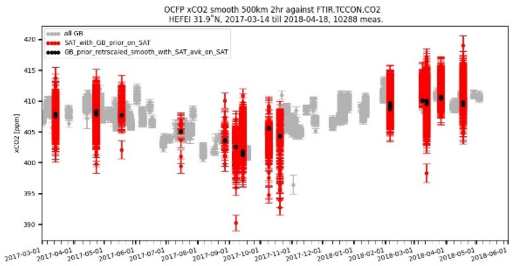

OCFP xCO2 smooth 500km 2hr against FTIR.TCCON.CO2
HEFEI 31.9°N, 2017-03-14 till 2018-04-18, 10288 meas.
xCO2 [ppm]
all GB
SAT_with_GB_prior_on_SAT
GB_prior_retrscaled_smooth_with_SAT_avk_on_SAT

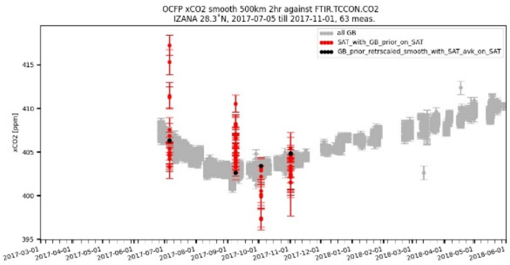

OCFP xCO2 smooth 500km 2hr against FTIR.TCCON.CO2
IZANA 28.3°N, 2017-07-05 till 2017-11-01, 63 meas.
xCO2 [ppm]
all GB
SAT_with_GB_prior_on_SAT
GB_prior_retrscaled_smooth_with_SAT_avk_on_SAT

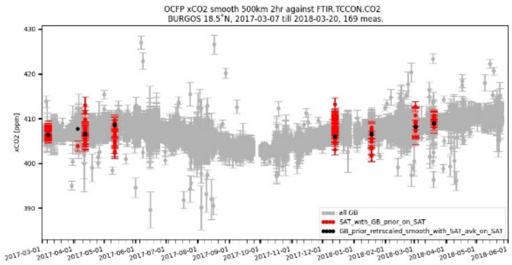

OCFP xCO2 smooth 500km 2hr against FTIR.TCCON.CO2
BURGOS 18.5°N, 2017-03-07 till 2018-03-20, 169 meas.
xCO2 [ppm]
all GB
SAT_with_GB_prior_on_SAT
GB_prior_retrscaled_smooth_with_SAT_avk_on_SAT

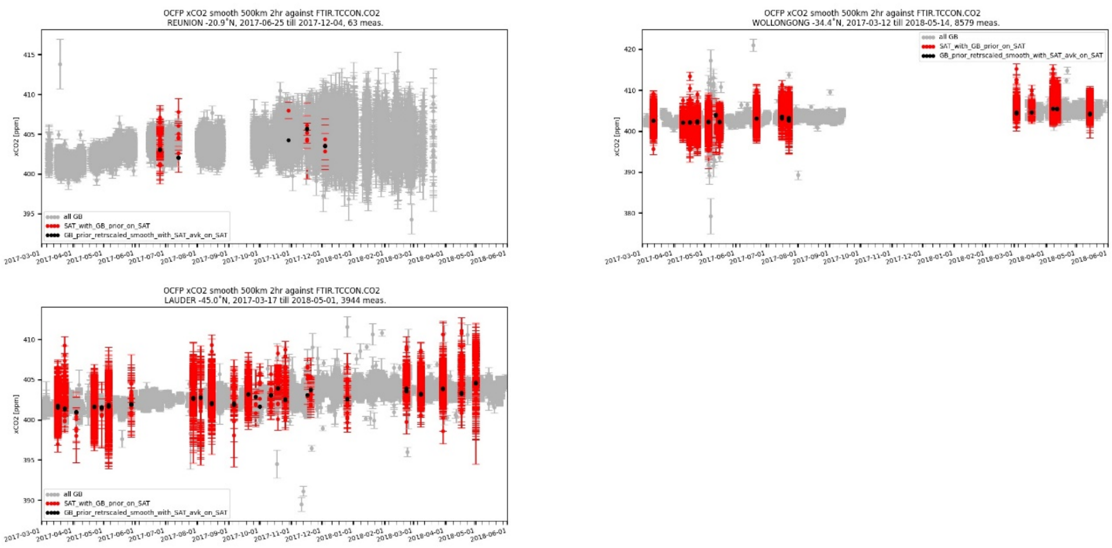

Figure 4-11: XCO_2 timeseries at all TCCON sites (red= CO2_TAN_OCFP data, black is collocated TCCON data and grey are the uncollocated TCCON data).

Figure 4-12 below shows the OCFP-FTS XCO_2 biases as a function of the satellite sampling location. It is obvious that OCFP's limited temporal range (and thus limited amount of data) results in limited coverage. As with FOCAL, biases appear not to be tied to the surface as much as they are tied to the satellite's track. However, due to the limited sampling, biases in time may very well present themselves as biases in space.

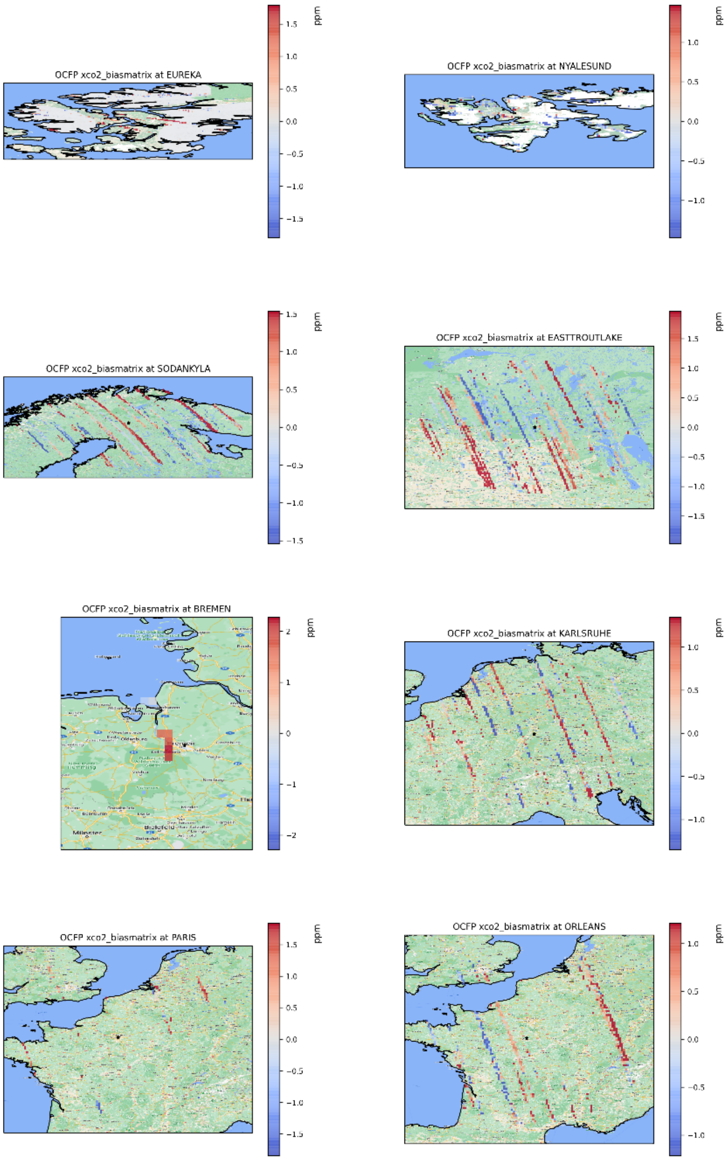

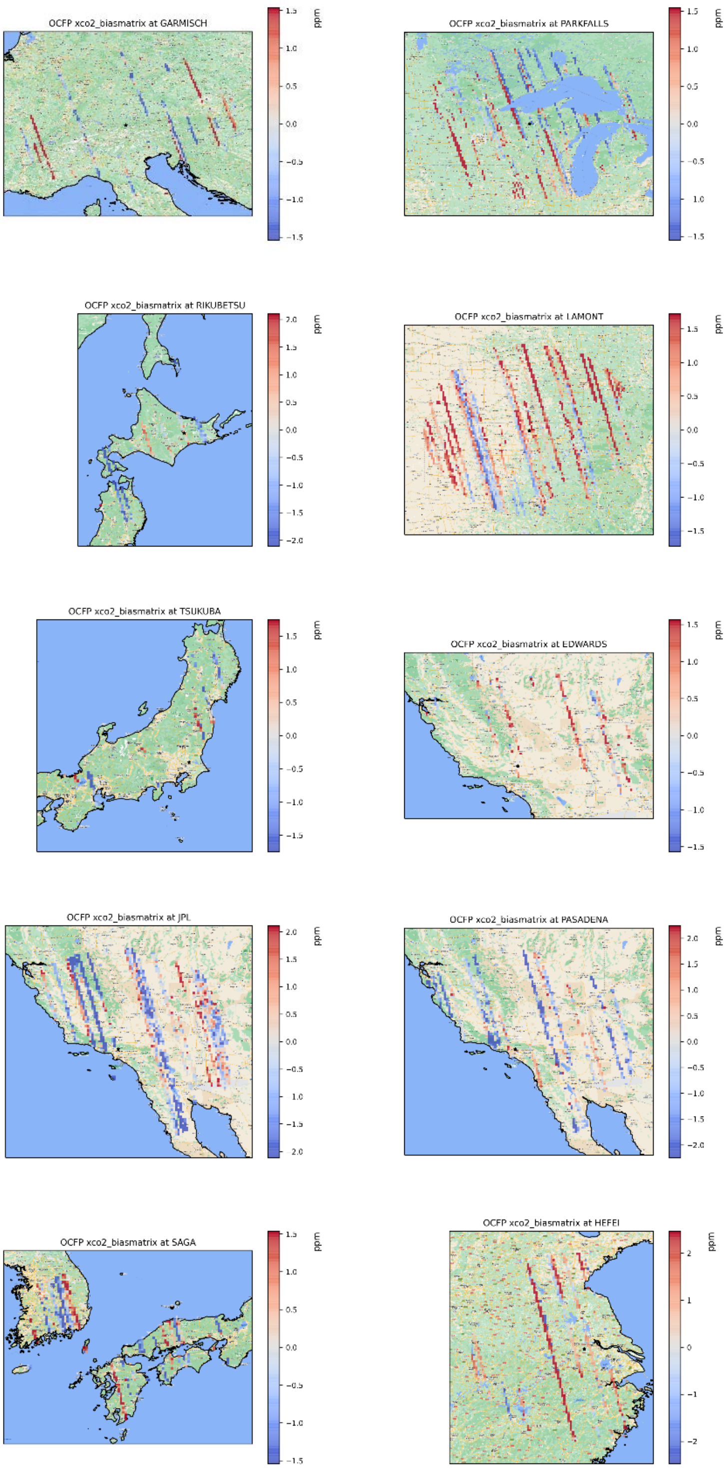

OCFP xco2_biasmatrix at GARMISCH
OCFP xco2_biasmatrix at PARKFALLS
OCFP xco2_biasmatrix at RIKUBETSU
OCFP xco2_biasmatrix at LAMONT
OCFP xco2_biasmatrix at TSUKUBA
OCFP xco2_biasmatrix at EDWARDS
OCFP xco2_biasmatrix at JPL
OCFP xco2_biasmatrix at PASADENA
OCFP xco2_biasmatrix at SAGA
OCFP xco2_biasmatrix at HEFEI
ppm

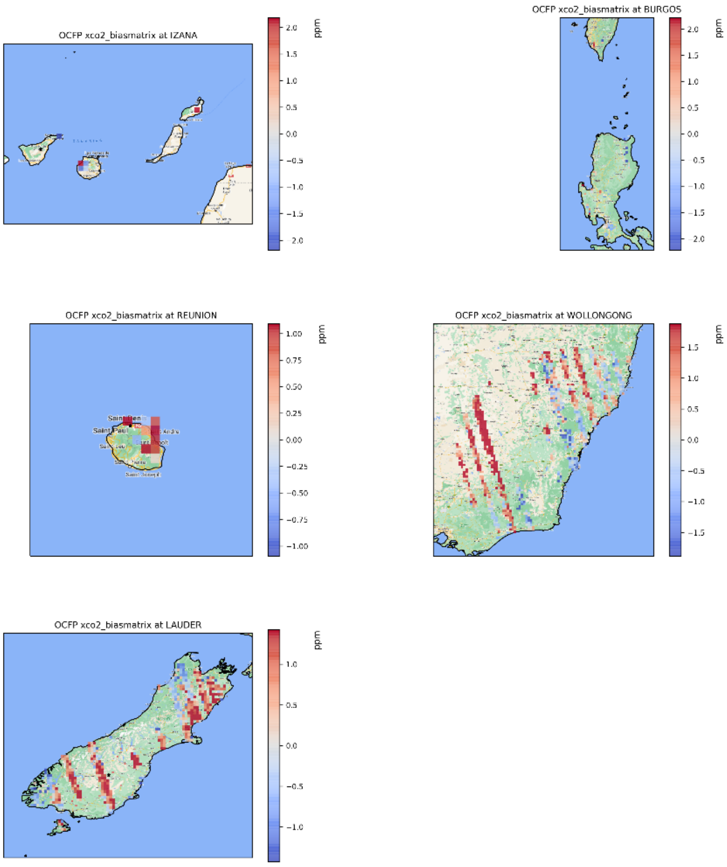

Figure 4-12: Spatial representation of the observed OCFP-FTS XCO2 biases for each of the TCCON stations. Shown is the median of all biases within each 0.1 by 0.1° latitude-longitude grid.

Figure 4-13 shows monthly median timeseries for TCCON and OCFP XCO_2 for all data that falls within certain latitude bands, namely all sites North of 40°N latitude (top), all sites between 40°N and the equator (mid) and all sites in the Southern hemisphere (bottom). It also features the values for a trend+seasonal fit through both datasets. The obtained long term trends have overlapping standard deviations apart from the Southern hemisphere analysis. Also both FTIR and OCFP XCO_2 seem to follow the same seasonal cycle in the Northern Hemisphere but again not for the Southern hemisphere. However, the observed trend values are, given the short timeframe covered, and limited Southern Hemisphere data, not robust. Combined with the limited seasonal variability in the Southern hemisphere it is not surprising that we see differences in the fitting parameters.

All in all, we can state that OCFP clearly captures the overall seasonality.

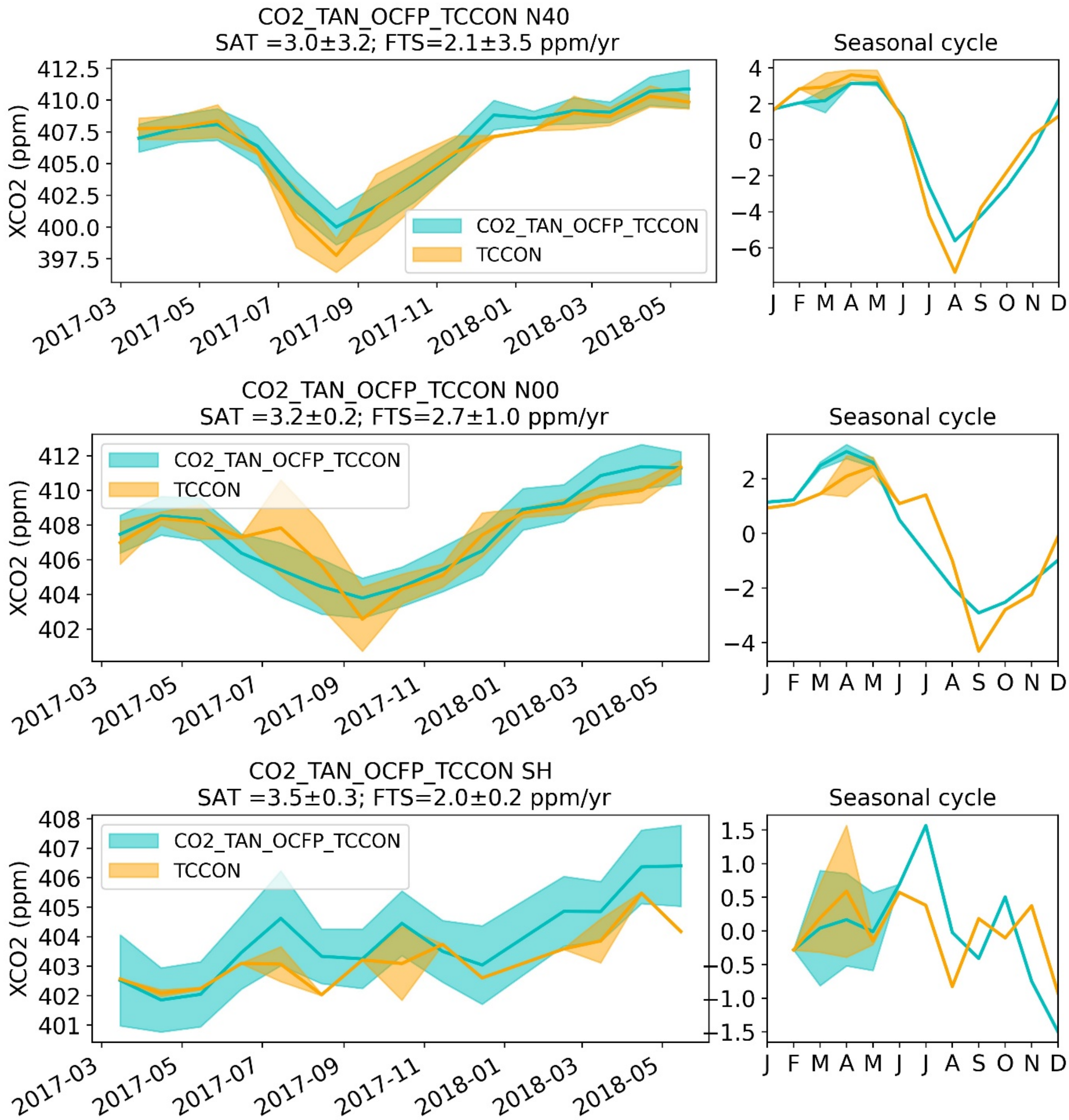

Figure 4-13: Monthly median collocated Sat and TCCON XCO_2 concentrations as a function of time. The shaded areas correspond with the scaled median absolute deviation.

4.2.2.2 Summary

Despite the limited amount of collocated data and the relatively small time period covered, we can already state that we see no obvious defects embedded within the CO2_TAN_OCFP product.

The OCFP reported uncertainty is underestimated by roughly 15% (Uncertainty ratio = 0.85) and the overall bias equals 0.49 ppm and the scatter equals 1.56 ppm. The spatial relative accuracy (RA), and the spatio-temporal relative accuracy (SRA) are 0.72 and 1.01 respectively.
The confidence bands for RA still overlap with the stated goal requirement of (>0.5 ppm) but not those of the SRA. As already mentioned in the analysis of FOCAL XCO2, these numbers ignore TCCON network and collocation errors. Due to the limited temporal coverage, no Stability parameter has been calculated, but we did not see any apparent problems in this area.

Table 4-6 presents an overview of the estimated data quality of CO2_TAN_OCFP, as obtained by the VALT team, from comparisons with TCCON ground-based reference observations. Values in square brackets [ ] correspond with the upper and lower 95% confidence bound on the parameter. The uncertainty ratio features 2 numbers as outlined in the validation method.

Product Quality Summary Table for Product: CO2_TAN_OCFP Level: 2, Version: v01.2.0, Time period covered: 03.2017 – 05.2018 Assessment: Validation Team (VALT)			
Parameter [unit]	**Achieved performance**	**Requirement**	**Comments**
Single measurement precision (1-sigma) in [ppm]	1.56 [1.42, 1.85]	< 8 (T) < 3 (B) < 1 (G)	Computed as the median over all station scaled median absolute differences to TCCON
Uncertainty ratio [-]: Ratio reported uncertainty to standard deviation of satellite-TCCON difference	0.76, 0.85*	-	No requirement but value close to unity expected for a high quality data product with reliable reported uncertainty.
Mean bias (global offset) [ppm]	0.49 [0.21,0.97]	-	No requirement but value close to zero expected for a high quality data product.
Accuracy: Relative systematic error [ppm]	Spatial: 0.72 [0.35, 1.13] Spatio-temporal: 1.01 [0.76, 1.28]	< 0.5	Spatial: Computed as standard deviation of the biases at the various TCCON sites. Spatio-temporal: As "Spatial" but also considering seasonal biases.
Stability: Drift [ppm/year]	-	< 0.5	Linear drift

4.2.3 Validation results for product CO2_GO2_SRFP

Below we show the validation results of the XCO_2 concentrations as derived by the CO2_GO2_SRFP v2.0.3 algorithm using GOSAT-2 spectra. Data was available from February 2019 up to and including December 2023. The SRFP algorithm provides *a priori* and column averaging kernel information on a 12 layers profile. The covered time period has thus been expanded by one year

4.2.3.1 Detailed results

The Taylor diagram below in **Figure 4-14** shows a short overview of the capabilities of the CO2_GO2_SRFP product. Most TCCON sites cluster around the intercept of the 0.8 correlation line and a normalized standard deviation of ~0.85, with Reunion and Eureka notable exceptions. However, both of these outlier stations have limited collocated data. The normalized standard deviation of most sites range between 0.75 and 1.0, indicating that on average the variability of the TCCON data is smaller. The normalized standard deviation of the bias sits (for most sites) around 0.6. All this indicates that while SRFP data features a slightly stronger variability (random error and/or seasonal variability) than the TCCON data, the biases still harbors less variability then either of them, an indication of SRFP capturing the natural variability.

There is no strong discernible pattern in the mosaic plot (**Figure 4-15**), which shows the mean bi-weekly bias between the satellite and TCCON measurement pairs. Stronger biases (negative and positive) at high latitude stations tend to appear in early spring, right after the end of the winter period when TCCON measurements are unavailable. In the previous analysis (v 2.0.2) a period with lower biases across all latitudes featured between 10-2019 and 7-2020 was observed. No such general pattern can be observed now..

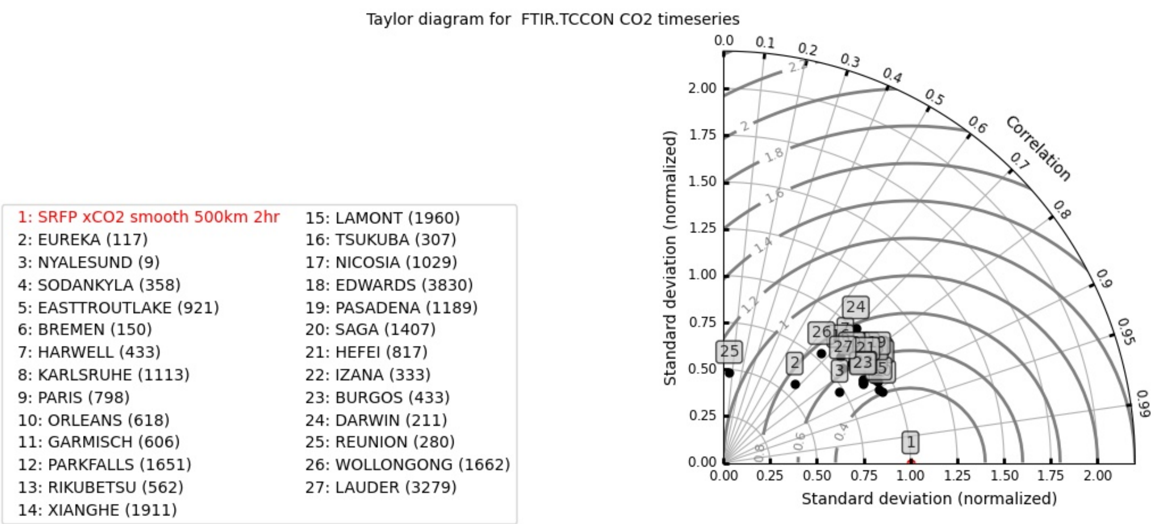

Figure 4-14: Taylor plot of daily averaged XCO_2 TCCON values relative to product CO2_GO2_SRFP. Straight lines correspond with the correlation, light grey lines yield the variability of the TCCON data relative to the satellite variability and the dark grey lines correspond with the variability of the Satellite - TCCON bias relative to the satellite variability.

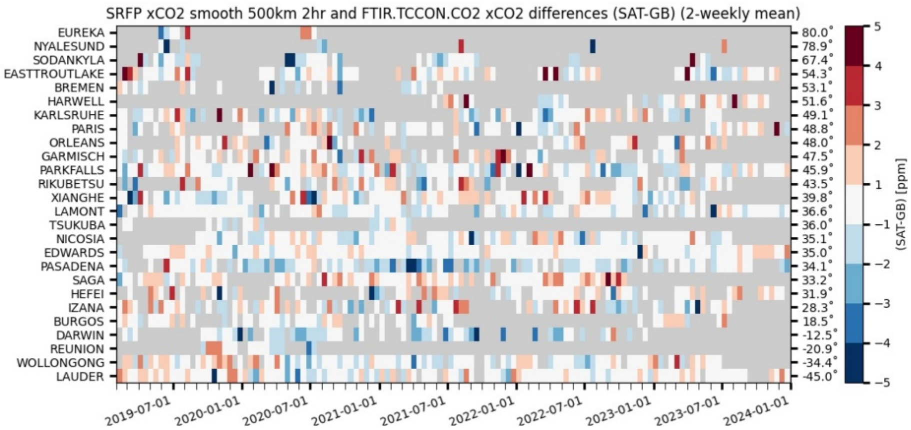

Figure 4-15: Mosaic plot of bi-weekly mean CO2_GO2_SRFP-TCCON XCO_2 biases as a function of time and TCCON station.

Table 4-7 lists all bias and scatter results derived from individual data pairs at all TCCON stations. The algorithm produces on average ~708 data pairs per station which corresponds with ~140 pairs per station per year. The observed median bias ranges between -1.32 ppm (Pasadena) and 0.86 ppm (Saga), while the scatter ranges between 1.56 ppm (Darwin) and 3.28 (Ny Alesund). Correlation values range between 0.67 (Eureka and Wollongong) and 0.91 (Orleans), with most correlation values sitting around 0.8. Of course the limited dataset hampers the correlation values at certain stations. The correlation using all data regardless of station equals 0.86. The median long term trend equals -0.005 ppm/year with values ranging between –0.22 (Park Falls) and 0.18 (Sodankyla). In **Figures 4-16 and 4-17** no clear-cut drift is observable.

Table 4-7: Number of collocated data pairs (N), Correlation (R), Bias, Scatter, long term trend difference (ltt) and uncertainty thereon (ltt_err), seasonal amplitude difference (A) and uncertainty thereon (A_err) as well as the latitude of the TCCON station. The last row lists the median values over all stations. Product: CO2_GO2_SRFP.

STATION	N	R	Bias	Scat	ltt	ltt_err	A	A_err	Lat
EUREKA	117	0.67	0.16	2.98	-	-	-	-	80
NYALESUND	9	0.85	-1.18	3.28	-	-	-	-	78.9
SODANKYLA	358	0.88	-1.28	2.04	0.18	0.24	1.99	0.85	67.4
EASTTROUTLAKE	921	0.86	0.11	2.37	-0.21	0.11	0.51	0.28	54.3
BREMEN	150	0.86	-0.7	2.05	-	-	-	-	53.1
HARWELL	433	0.73	0.46	2.18	-	-	-	-	51.6
KARLSRUHE	1113	0.83	-0.22	2.18	-0.07	0.14	0.91	0.19	49.1
PARIS	798	0.81	0.06	2.26	-0.1	0.12	0.91	0.23	48.8
ORLEANS	618	0.91	0.36	1.91	0.02	0.14	0.7	0.23	48
GARMISCH	606	0.85	0.45	2.27	0.07	0.29	0.21	0.27	47.5
PARKFALLS	1651	0.86	-0.02	2.22	-0.22	0.1	0.19	0.18	45.9
RIKUBETSU	562	0.87	-0.04	1.9	-0.1	0.11	0.89	0.28	43.5
XIANGHE	1911	0.87	-0.01	2.29	0.3	0.11	0.73	0.17	39.8
LAMONT	1960	0.9	-0.11	1.78	-0.01	0.07	0.42	0.12	36.6
TSUKUBA	307	0.74	-1.01	1.95	-	-	-	-	36
NICOSIA	1029	0.86	-0.24	1.94	0.06	0.09	0.58	0.14	35.1
EDWARDS	3830	0.85	0.09	1.79	0.04	0.05	0.38	0.09	35
PASADENA	1189	0.84	-1.32	2.13	-0.05	0.13	0.63	0.14	34.1
SAGA	1407	0.79	0.86	2.32	0.17	0.11	0.63	0.18	33.2
HEFEI	817	0.84	0.35	2.07	0.11	0.11	0.7	0.23	31.9
IZANA	333	0.87	0.03	2.23	-0.04	0.13	0.85	0.34	28.3
BURGOS	433	0.87	0.25	1.83	0.19	0.13	0.72	0.27	18.5
DARWIN	211	0.7	-1.17	1.56	-0.06	0.26	0.45	0.25	-12.5
REUNION	280	0.07	-0.51	2.48	-	-	-	-	-20.9
WOLLONGONG	1662	0.67	-0.27	2.2	-0.2	0.08	0.79	0.15	-34.4
LAUDER	3279	0.78	0.24	1.9	0	0.08	0.27	0.15	-45
MEDIAN	708	0.85	-0.015	2.155	-0.005	0.11	0.665	0.21	

The timeseries below in **Figure 4-16** show individual satellite and ground-based fts measurements. As can be seen, and was already apparent from the Taylor diagram, SRFP XCO_2 features at most stations a somewhat higher scatter than TCCON, but overall the seasonality is well captured.

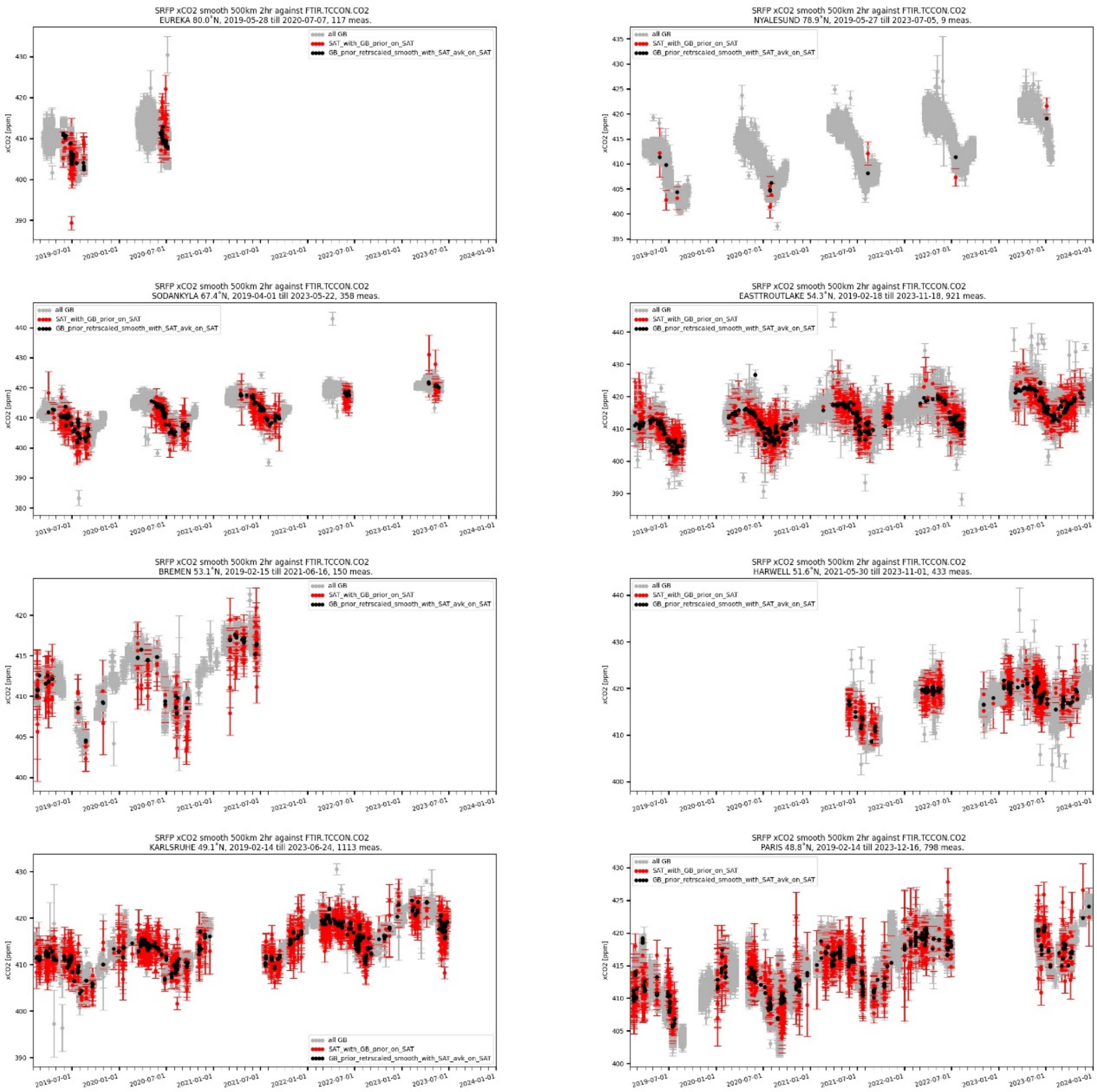

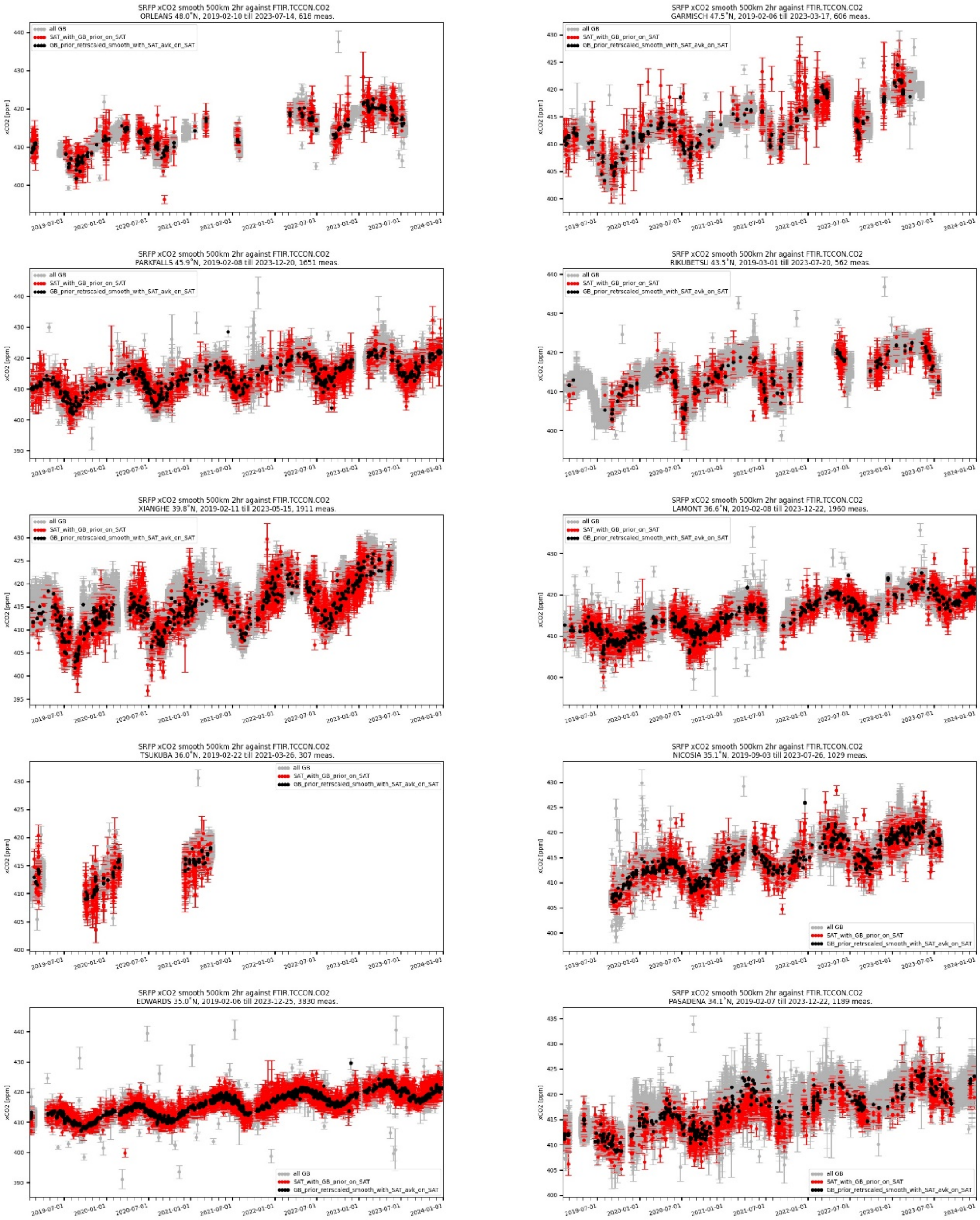

SRFP xCO2 smooth 500km 2hr against FTIR.TCCON.CO2
ORLEANS 48.0°N, 2019-02-10 till 2023-07-14, 618 meas.
SRFP xCO2 smooth 500km 2hr against FTIR.TCCON.CO2
GARMISCH 47.5°N, 2019-02-06 till 2023-03-17, 606 meas.
SRFP xCO2 smooth 500km 2hr against FTIR.TCCON.CO2
PARKFALLS 45.9°N, 2019-02-08 till 2023-12-20, 1651 meas.
SRFP xCO2 smooth 500km 2hr against FTIR.TCCON.CO2
RIKUBETSU 43.5°N, 2019-03-01 till 2023-07-20, 562 meas.
SRFP xCO2 smooth 500km 2hr against FTIR.TCCON.CO2
XIANGHE 39.8°N, 2019-02-11 till 2023-05-15, 1911 meas.
SRFP xCO2 smooth 500km 2hr against FTIR.TCCON.CO2
LAMONT 36.6°N, 2019-02-08 till 2023-12-22, 1960 meas.
SRFP xCO2 smooth 500km 2hr against FTIR.TCCON.CO2
TSUKUBA 36.0°N, 2019-02-22 till 2021-03-26, 307 meas.
SRFP xCO2 smooth 500km 2hr against FTIR.TCCON.CO2
NICOSIA 35.1°N, 2019-09-03 till 2023-07-26, 1029 meas.
SRFP xCO2 smooth 500km 2hr against FTIR.TCCON.CO2
EDWARDS 35.0°N, 2019-02-06 till 2023-12-25, 3830 meas.
SRFP xCO2 smooth 500km 2hr against FTIR.TCCON.CO2
PASADENA 34.1°N, 2019-02-07 till 2023-12-22, 1189 meas.
all GB
SAT_with_GB_prior_on_SAT
GB_prior_retrscaled_smooth_with_SAT_avk_on_SAT
xCO2 [ppm]

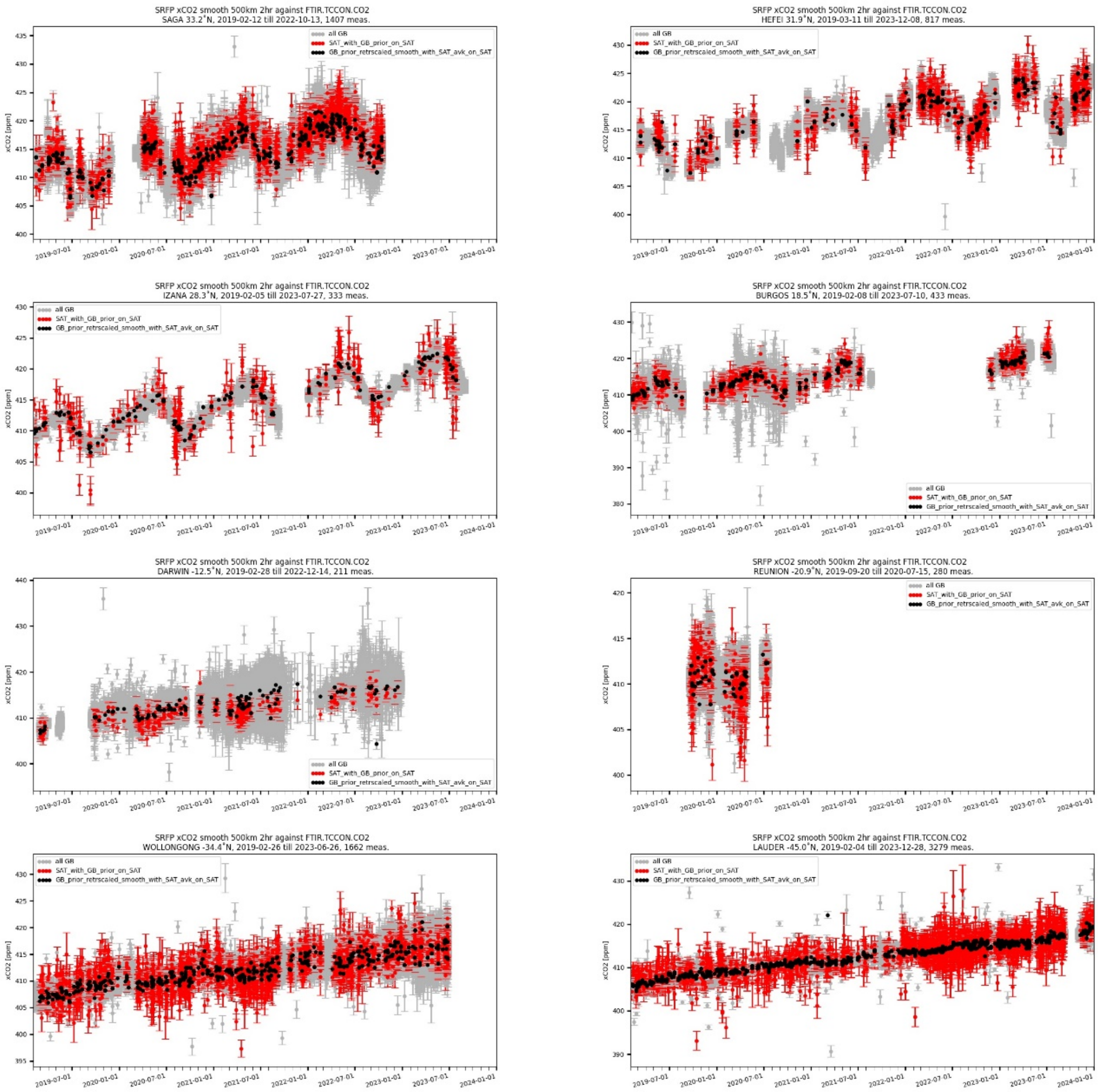

Figure 4-16: XCO_2 timeseries at all TCCON sites (red= CO2_GO2_SRFP data, black is collocated TCCON data and grey are the uncollocated TCCON data).

Figure 4-17 shows monthly median timeseries for TCCON and SRFP XCO_2 for all data that falls within certain latitude bands, namely all sites North of 40°N latitude (top), all sites between 40°N and the equator (mid) and all sites in the Southern hemisphere (bottom). It also features the values for a trend+seasonal fit through both datasets. For all bands , the differences in the obtained long term trends are very small (0.1 ppm/year or less) and can be covered by their respective standard deviations.

All in all, we can state that SRFP clearly captures the overall seasonality.

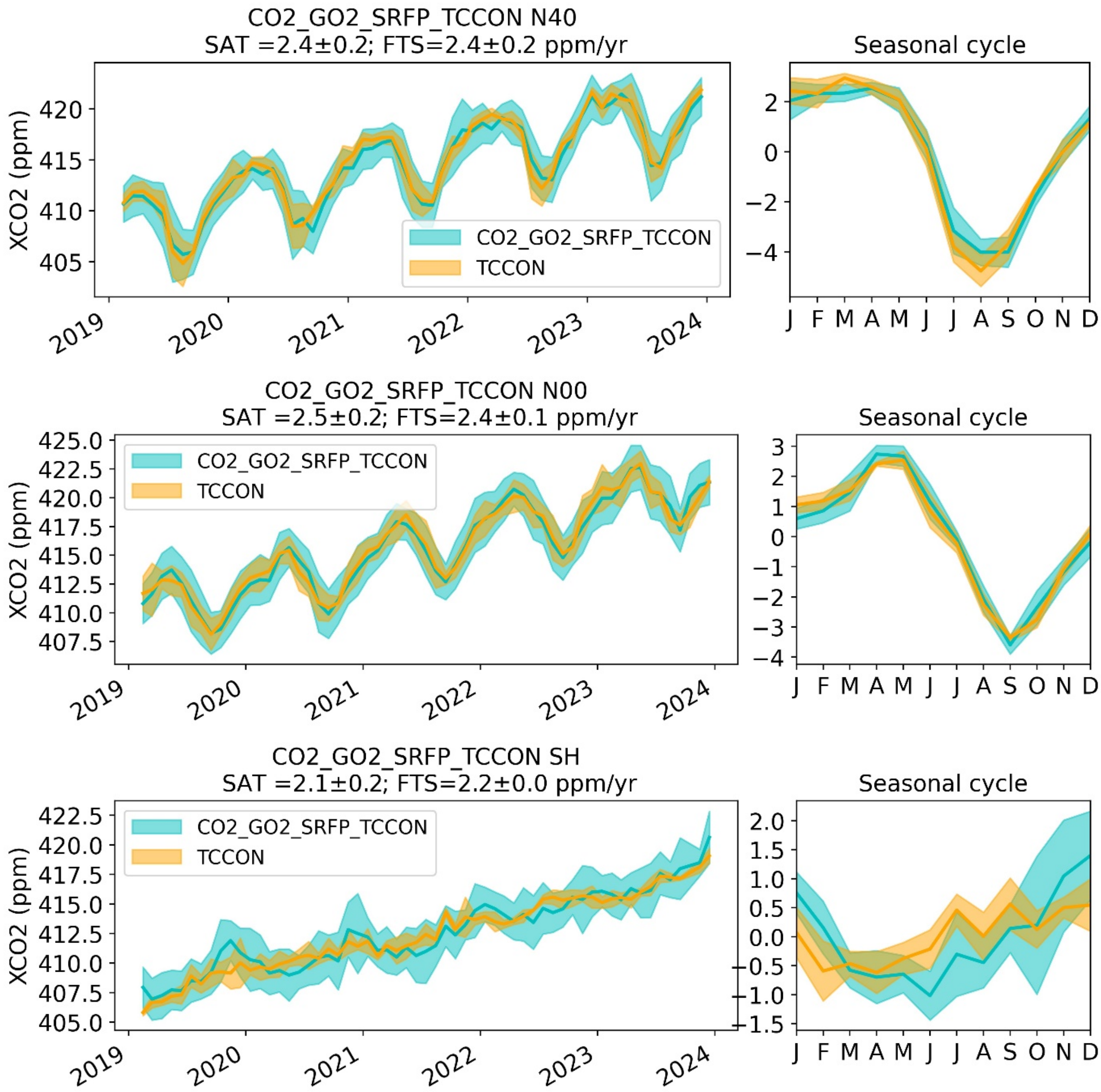

Figure 4-17: Monthly median collocated Sat and TCCON XCO_2 concentrations as a function of time. The shaded areas correspond with the scaled median absolute deviation.

4.2.3.2 Summary

With this updated product and the extension of the timeseries we can confidently state that there are no obvious defects embedded within the CO2_GO2_SRFP product. The SRFP reported uncertainty corresponds closely with our analysis (Uncertainty ratio = 0.82). The spatial (RA), 0.39 ppm has met the stated goal requirement of (>0.5 ppm), but the spatio-temporal relative accuracy (SRA) has not, nor do its confidence interval overlap [0.64, 1.09]. The long term stability (-0.005 ppm/year) meets the linear drift requirements (<0.5 ppm/year).

Table 4-8 presents an overview of the estimated data quality of CO2_GO2_SRFP, as obtained by the VALT team, from comparisons with TCCON ground-based reference observations. Values in square brackets [ ] correspond with the upper and lower 95% confidence bound on the parameter. The uncertainty ratio features 2 numbers as outlined in the validation method.

Product Quality Summary Table for Product: CO2_GO2_SRFP Level: 2, Version: v02.0.3, Time period covered: 2.2019 – 1.2024 Assessment: Validation Team (VALT)			
Parameter [unit]	**Achieved performance**	**Requirement**	**Comments**
Single measurement precision (1-sigma) in [ppm]	2.16 [2,08,2.36]	< 8 (T) < 3 (B) < 1 (G)	Computed as the median over all station scaled median absolute differences to TCCON
Uncertainty ratio [-]: Ratio reported uncertainty to standard deviation of satellite-TCCON difference	0.79, 0.82*	-	No requirement but value close to unity expected for a high quality data product with reliable reported uncertainty.
Mean bias (global offset) [ppm]	-0,02 [-0.16, 0.22]	-	No requirement but value close to zero expected for a high quality data product.
Accuracy: Relative systematic error [ppm]	Spatial: 0.39 [-0,01, 0.57] Spatio-temporal: 0.86 [0.64, 1.09]	< 0.5	Spatial: Computed as standard deviation of the biases at the various TCCON sites. Spatio-temporal: As "Spatial" but also considering seasonal biases.
Stability: Drift [ppm/year]	-0,00 [-0.07, 0.06]	< 0.5	Linear drift

4.2.4 Validation results for product CH4_S5P_WFMD

Below we show the validation results of the XCH_4 concentrations as derived by the CH4_S5P_WFMD v1.8 algorithm using S5P spectra. Compared to the previous analysis, the algorithm has remained the same, only the timeseries has been extended. Data was available from November 2017 up to and including May 2024. The WFMD algorithm provides *a priori* and column averaging kernel data on a 20 layers vertical profile. We have made comparisons with data from both the TCCON and NDACC networks. Note that instead of ‘within 500 km and 2 hour’ collocation criteria, we here have used ‘within 100km and 1 hours’ for TCCON and ‘within 100km and 2 hours’ for NDACC. In the plots and tables below, the TCCON figure/table is always shown first. The obtained Figures of Merit in the summary table (**table 4-11**) pertain to the TCCON analysis only, partly to ensure continuity with previous assessments, but also due to the higher systematic uncertainty and high prevalence of high-latitude and mountain sites in the NDACC network, which might distort our analysis.

4.2.4.1 Detailed results

The Taylor plot for product CH4_S5P_WFMD is shown in **Figure 4-18**. Most FTIR sites are clustered between the 0.6 and 0.9 correlation line, with the standard deviation of the differences sitting between 0.75 and 1 times the standard deviation of the satellite data itself. The variability on the TCCON data is consistently smaller than that of WFMD apart from the Reunion station. In fact the Reunion site, together with Eureka, Bialystok and JPL are the only stations that stands out. Other stations are fairly well grouped together. This indicates a good consistency of both Satellite product and station network. Note that the Reunion site is an island site with the lowest collocation pair density.

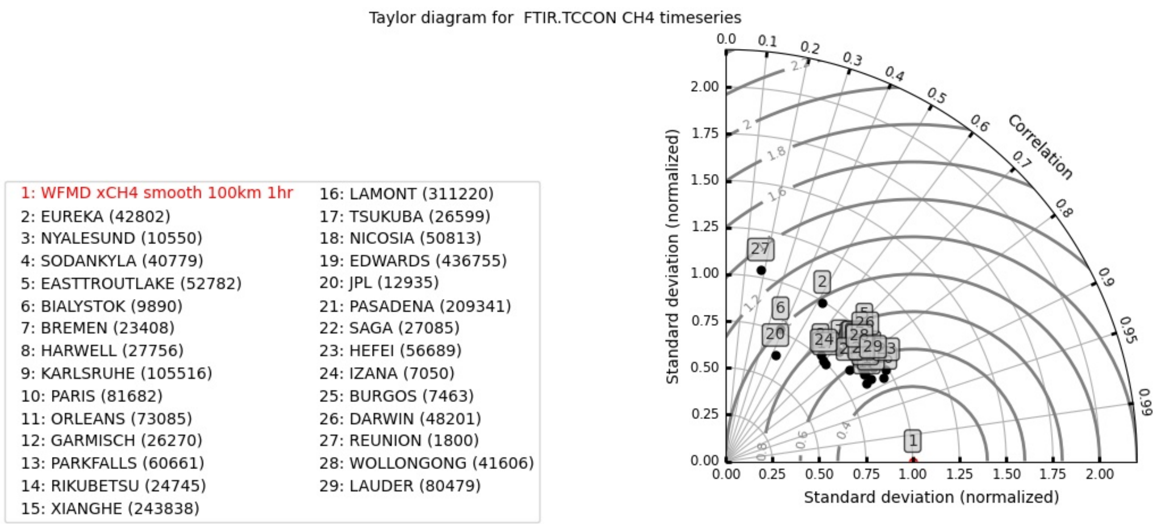

Figure 4-18: Tayor plot of daily averaged XCH4 TCCON values relative to CH4_S5P_WFMD. Straight lines correspond with the correlation, light grey lines yield the variability of the TCCON data relative to the satellite variability and the dark grey lines correspond with the variability of the Satellite -TCCON bias relative to the satellite variability.

The NDACC Taylorplot shows way more dispersion, indicating either less consistency within the network, less ideal collocation circumstances or a satellite product that is less attuned to the NDACC network. Also the correlation, standard deviation of the difference and standard deviation of the satellite data relative to NDACC yields poorer results. Correlations, on average with a lot of leeway, sits around 0.7, while the standard deviation on the Satellite data has a wide range relative to the NDACC data with some stations showing lower and other higher scatter than NDACC. The scatter on the SAT-NDACC difference, relative to the scatter of the NDACC data itself sits around 0.8 but with many outliers. Notable outliers are Eureka, Porto Velho, Toronto, Harestua and La Reunion Maïdo, with much lower correlation values. Toronto and Bremen also feature very high scatter values with respect to the satellite data.

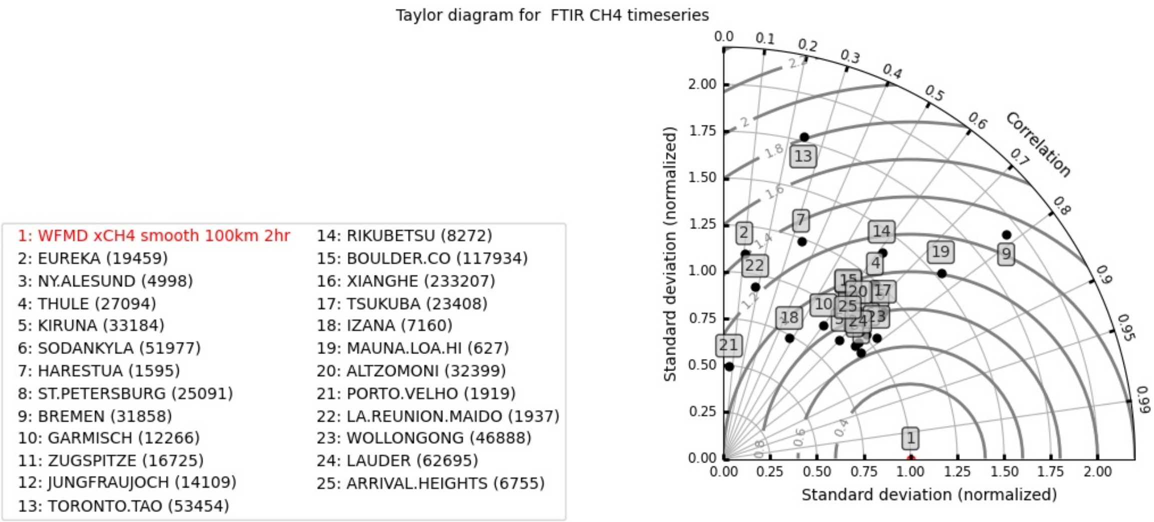

Figure 4-19: Tayor plot of daily averaged XCH4 NDACC values relative to CH4_S5P_WFMD. Straight lines correspond with the correlation, light grey lines yield the variability of the NDACC data relative to the satellite variability and the dark grey lines correspond with the variability of the Satellite -NDACC bias relative to the satellite variability.

The mosaic overview of bi-weekly sat-TCCON biases (**Figure 4-20**) does not reveal any systematic trend over time, nor any as a function of latitude. There are some very pronounced biases (negative in Parkfalls and positive in Izaña, the latter, being a high altitude stations).

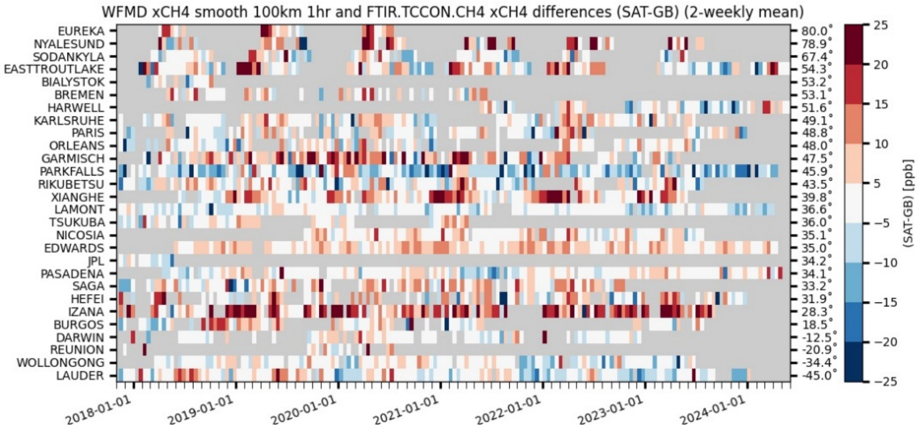

Figure 4-20: Mosaic plot of bi-weekly mean CH4_S5P_WFMD - TCCON XCH_4 biases as a function of time and TCCON station.

For NDACC we see more pronounced differences with strong positive biases at Thule, Altzomoni and Arrival Heights and negative ones at Jungfraujoch, Wollongong and Lauder. For Toronto we even see a shifting bias, with lower values at the start and higher values at the end of the observed timeframe. This corresponds with a significant increase in the Toronto FTIR scatter (see **Figure 4-21**). Paramaribo (only 2 collocation data pairs!) and Porto Velho cover only a tiny fraction of the retrieved timeseries, while Altzomoni's bias is probably tied to its high altitude location, next to a megacity (see **Figure 4-22**). Due to all these issues, Altzomoni, Toronto, Thule, Paramaribo and Porto Velho are excluded from **Tables 4-10, 4-13 and 4-16**.

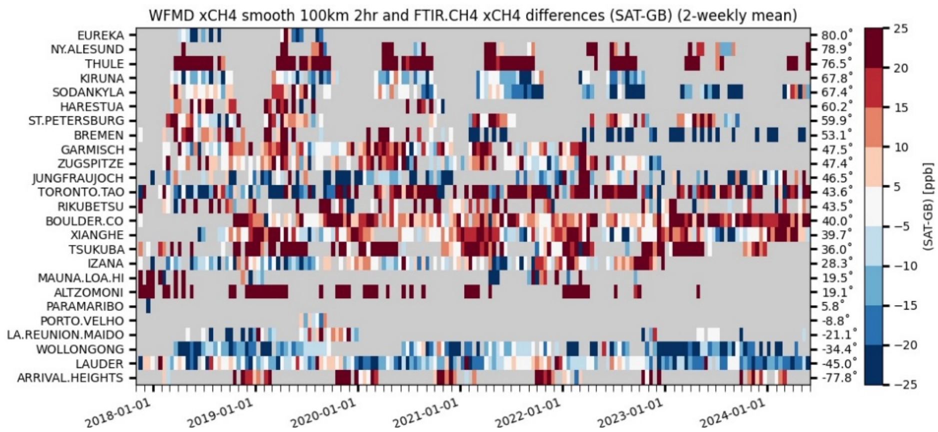

Figure 4-21: Mosaic plot of bi-weekly mean CH4_S5P_WFMD - NDACC XCH_4 biases as a function of time and NDACC station.

Tables 4-9 and 4-10 lists all bias and scatter results derived from individual data pairs at all TCCON and NDACC stations respectively. For TCCON, the algorithm produces on average ~42200 data pairs per station which corresponds with ~6000 pairs per station per year. Also keep in mind that the collocation criteria are substantially stricter. The observed median bias ranges between -7.16 ppb (Parkfalls) and 17.21 ppb (Eureka), while the scatter ranges between 11.12 ppb (Lamont) and 21.64 ppb (Easttroutlake). Correlation values range between 0.18 (Reunion) and 0.88 (Lamont), with most correlation values sitting between 0.6 and 0. 96. The correlation of all data, regardless of station, equals 0.88. The long term trend on the bias ranges between -1.99 ppb/year at Lauder and 1.81 ppb/year at Tsukuba. Finally, the seasonal amplitude present in the sat-TCCON bias ranges between 1.14 ppb (Lamont) and 10.22 ppb (Xianghe).

For NDACC (**Table 4-11**), the overall corrolation (0.88) is identical to the one with TCCON, while the median correlation is a little lower (0.70). Biases range from -12.9 ppb (Wollongong) to 38.9 ppb (Ny Alesund). Scatter numbers range from 13.2 (Reunion) to 38.7 ppb (Bremen). Long term trends range between -12.7 ppb/year (Bremen) and 4.5 ppb/year (Izana).

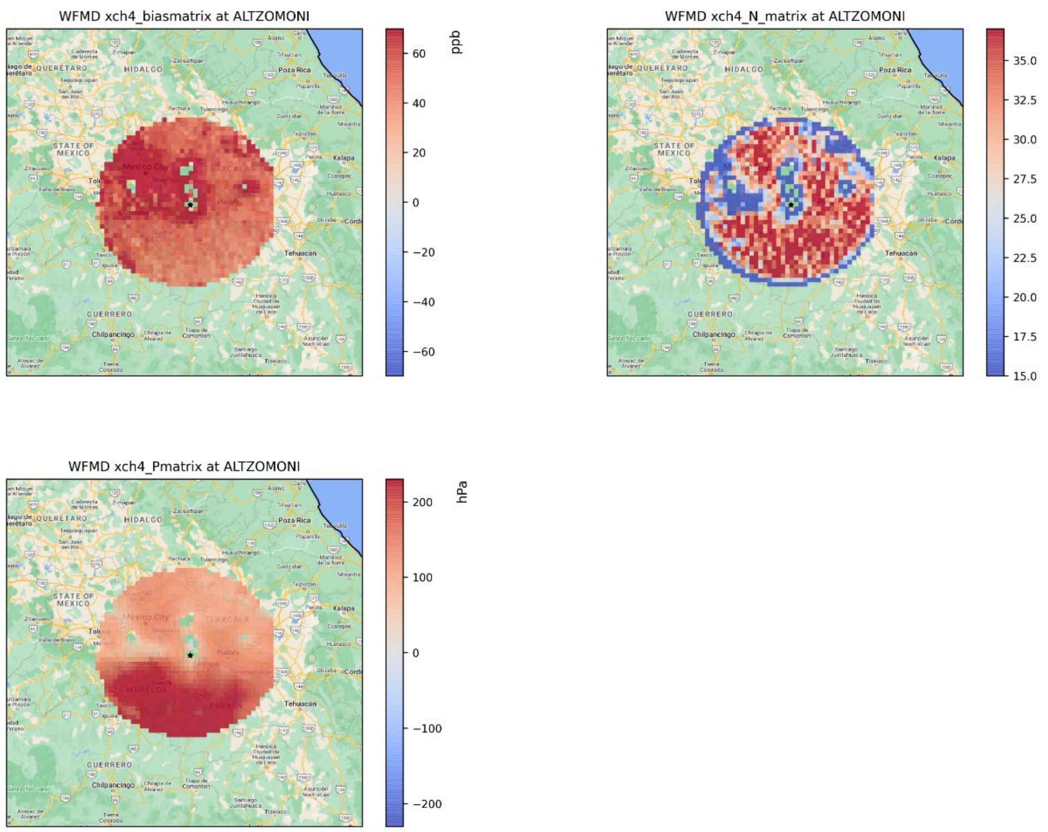

Figure 4-22: XCH_4 Bias, number of collocated data and pressure difference between WFMD and FTS around and at the Altzomoni site

Table 4-9: Number of collocated data pairs (N), Correlation (R), Bias, Scatter, long term trend difference (ltt) and uncertainty thereon (ltt_err), seasonal amplitude difference (A) and uncertainty thereon (A_err) as well as the latitude of the TCCON station. The last row lists the median values over all stations. Product: CH4_S5P_WFMD.

STATION	N	R	Bias	Scat	ltt	ltt_err	A	A_err	lat
EUREKA	42802	0.52	17.21	18.78	-	-	-	-	80
NYALESUND	10550	0.85	12.71	19.31	0.39	1.31	7.52	4.55	78.9
SODANKYLA	40779	0.75	1.84	16.08	-0.64	0.79	3.79	1.62	67.4
EASTTROUTLAKE	52782	0.74	6.19	21.64	-0.56	0.54	4.33	0.95	54.3
BIALYSTOK	9890	0.38	3.1	12.21	-	-	-	-	53.2
BREMEN	23408	0.72	6.03	11.75	0.3	0.79	5.79	1.44	53.1
HARWELL	27756	0.67	3.74	13.24	-	-	-	-	51.6
KARLSRUHE	105516	0.83	5.81	12.53	-0.15	0.33	4.88	0.64	49.1
PARIS	81682	0.83	3.63	12.46	0.48	0.41	3.45	0.81	48.8
ORLEANS	73085	0.87	4.47	12.09	0.42	0.42	3.18	0.82	48
GARMISCH	26270	0.76	10.62	14.06	-1.12	0.82	3.98	0.94	47.5
PARKFALLS	60661	0.82	-7.16	14.24	-0.51	0.44	5.71	0.75	45.9
RIKUBETSU	24745	0.8	1.64	15.88	0.44	0.52	3.31	0.83	43.5
XIANGHE	243838	0.77	8.33	17.46	1	0.45	10.22	0.71	39.8
LAMONT	311220	0.88	-2.24	11.12	-0.41	0.22	1.04	0.43	36.6
TSUKUBA	26599	0.72	4.02	12.28	1.81	0.9	3.25	1.09	36
NICOSIA	50813	0.78	3.21	12.12	-0.92	0.52	1.62	0.52	35.1
EDWARDS	436755	0.87	5.91	11.29	-0.21	0.18	3.1	0.33	35
JPL	12935	0.43	-2.31	14.66	-	-	-	-	34.2
PASADENA	209341	0.85	0.18	13.51	0.02	0.25	3.19	0.39	34.1
SAGA	27085	0.8	8.06	15.41	0.96	0.55	4.17	0.87	33.2
HEFEI	56689	0.87	5.6	13.9	-0.97	0.6	5.62	0.98	31.9
IZANA	7050	0.7	8.32	19.37	0.9	0.66	3.23	1.23	28.3
BURGOS	7463	0.83	5.25	12.91	-0.18	0.67	4.79	1.21	18.5
DARWIN	48201	0.76	-0.11	11.16	-0.97	0.4	5.02	0.88	-12.5
REUNION	1800	0.18	3.82	14.42	-	-	-	-	-20.9
WOLLONGONG	41606	0.79	0.96	14.53	-0.19	0.33	2.1	0.66	-34.4
LAUDER	80479	0.84	-1.99	13.58	-1.93	0.25	6.61	0.51	-45
MEDIAN	42204	0.785	3.92	13.74	-0.18	0.52	3.98	0.83	38.2

Table 4-10: Number of collocated data pairs (N), Correlation (R), Bias, Scatter, long term trend difference (ltt) and uncertainty thereon (ltt_err), seasonal amplitude difference (A) and uncertainty thereon (A_err) as well as the latitude of the NDACC station. The last row lists the median values over all stations. Product: CH4_S5P_WFMD.

STATION	N	R	Bias	Scat	ltt	ltt_err	A	A_err	lat
STATION	N	R	Bias	Std	ltt	ltt_err	A	A_err	lat
EUREKA	19459	0.1	-1.9	24.68	-	-	-	-	79.8
NY.ALESUND	4998	0.79	38.89	20.92	-0.38	1.99	22.93	5.49	78.9
KIRUNA	33184	0.7	-6.67	18.06	-0.5	1.2	3.42	1.25	67.7
SODANKYLA	51977	0.74	0.31	22.71	-4.28	0.69	8.61	1.62	67.2
HARESTUA	1595	0.34	20.58	20.89	-	-	-	-	60.1
ST.PETERSBURG	25091	0.76	12.16	18.32	1.37	0.69	9.44	1.67	59.7
BREMEN	31858	0.78	5.41	38.67	-12.69	3.86	4.46	3.21	52.9
GARMISCH	12266	0.6	8.28	18.52	0.3	1.19	10.75	1.43	47.4
ZUGSPITZE	16725	0.68	8.87	18.04	-0.71	0.71	11.9	1.36	47.3
JUNGFRAUJOCH	14109	0.62	-10.93	23.53	2.3	2.06	11.83	2.11	46.4
RIKUBETSU	8272	0.61	13.82	26.2	-3.18	3.36	25.96	4.34	43.3
BOULDER.CO	117934	0.62	12.31	17.16	2.46	0.58	2.06	1.02	39.9
XIANGHE	233207	0.75	9.6	19.81	-1.58	0.5	17.56	0.77	39.7
TSUKUBA	23408	0.74	22.66	20.08	-1.21	1.04	7.32	2.44	36
IZANA	7160	0.48	-10.59	23.97	4.5	1.24	6.09	1.49	28.2
MAUNA.LOA.HI	627	0.76	23.73	23.51	-3.84	4.16	10.46	10.29	19.5
LA.REUNION.MAIDO	3485	0.69	-4.89	13.24	-0.64	2.33	5.9	4.13	-21
WOLLONGONG	46888	0.78	-12.92	18.08	-0.74	0.6	10.05	1.22	-34.4
LAUDER	63006	0.76	-8.48	16.66	-1.23	0.47	5.68	0.94	-45
ARRIVAL.HEIGHTS	6755	0.69	21.82	20.57	-2.38	0.83	18.8	5.14	-77.7
MEDIAN	18092	0.70	8.58	20.33	-0.725	1.12	9.745	1.65	44.85

Figure 4-20 shows all collocated WFMD and TCCON data time series. From these figures, it is clear that the variability of WFMD XCH_4 is substantially stronger. Also a fair amount of, particularly negative, outliers is present at many stations.

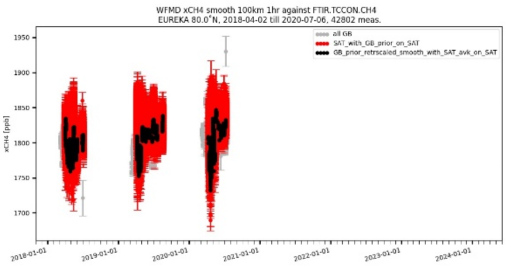
WFMD xCH4 smooth 100km 1hr against FTIR.TCCON.CH4
EUREKA 80.0˚N, 2018-04-02 till 2020-07-06, 42802 meas.
all GB
SAT_with_GB_prior_on_SAT
GB_prior_retrscaled_smooth_with_SAT_avk_on_SAT

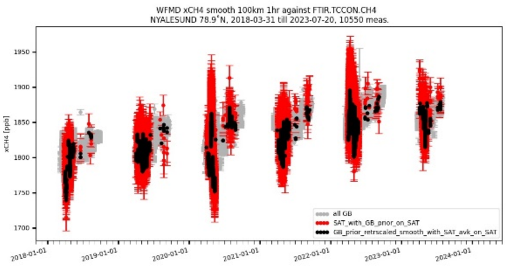
WFMD xCH4 smooth 100km 1hr against FTIR.TCCON.CH4
NYALESUND 78.9˚N, 2018-03-31 till 2023-07-20, 10550 meas.
all GB
SAT_with_GB_prior_on_SAT
GB_prior_retrscaled_smooth_with_SAT_avk_on_SAT

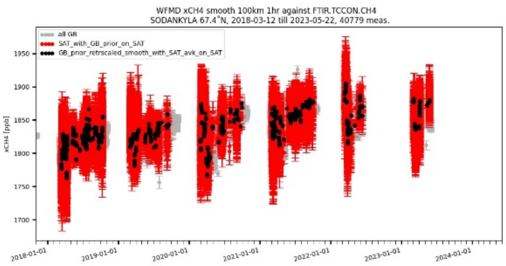
WFMD xCH4 smooth 100km 1hr against FTIR.TCCON.CH4
SODANKYLA 67.4˚N, 2018-03-12 till 2023-05-22, 40779 meas.
all GB
SAT_with_GB_prior_on_SAT
GB_prior_retrscaled_smooth_with_SAT_avk_on_SAT

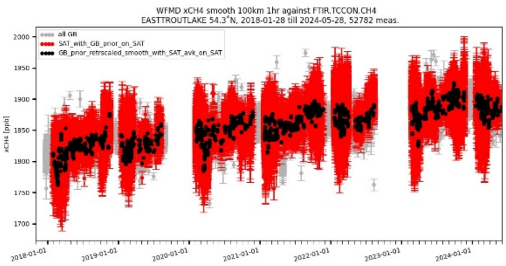
WFMD xCH4 smooth 100km 1hr against FTIR.TCCON.CH4
EASTTROUTLAKE 54.3˚N, 2018-01-28 till 2024-05-28, 52782 meas.
all GB
SAT_with_GB_prior_on_SAT
GB_prior_retrscaled_smooth_with_SAT_avk_on_SAT

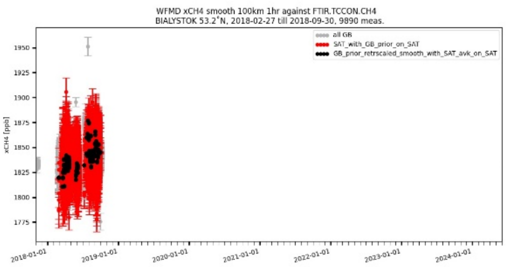
WFMD xCH4 smooth 100km 1hr against FTIR.TCCON.CH4
BIALYSTOK 53.2˚N, 2018-02-27 till 2018-09-30, 9890 meas.
all GB
SAT_with_GB_prior_on_SAT
GB_prior_retrscaled_smooth_with_SAT_avk_on_SAT

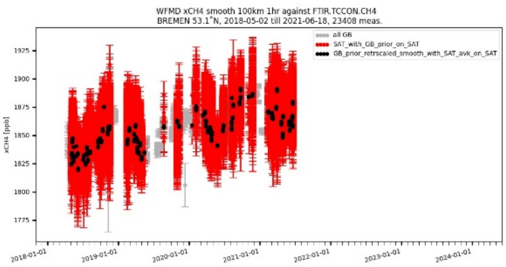
WFMD xCH4 smooth 100km 1hr against FTIR.TCCON.CH4
BREMEN 53.1˚N, 2018-05-02 till 2021-06-18, 23408 meas.
all GB
SAT_with_GB_prior_on_SAT
GB_prior_retrscaled_smooth_with_SAT_avk_on_SAT

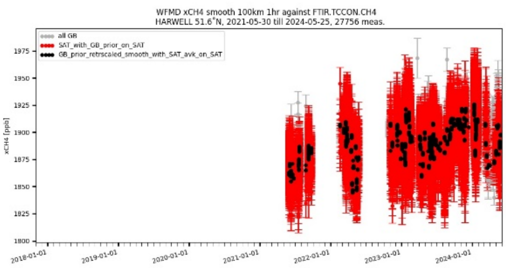
WFMD xCH4 smooth 100km 1hr against FTIR.TCCON.CH4
HARWELL 51.6˚N, 2021-05-30 till 2024-05-25, 27756 meas.
all GB
SAT_with_GB_prior_on_SAT
GB_prior_retrscaled_smooth_with_SAT_avk_on_SAT

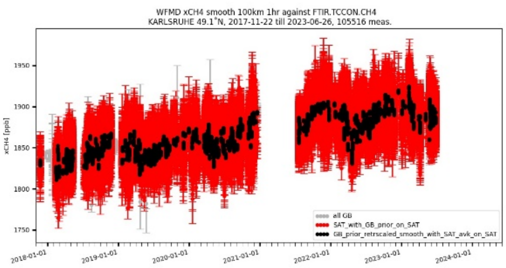
WFMD xCH4 smooth 100km 1hr against FTIR.TCCON.CH4
KARLSRUHE 49.1˚N, 2017-11-22 till 2023-06-26, 105516 meas.
all GB
SAT_with_GB_prior_on_SAT
GB_prior_retrscaled_smooth_with_SAT_avk_on_SAT

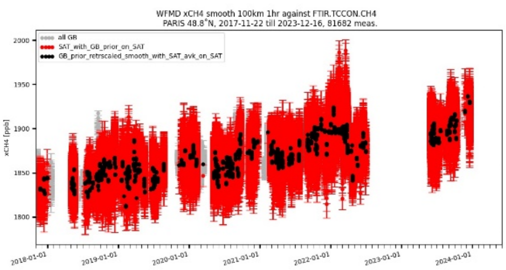
WFMD xCH4 smooth 100km 1hr against FTIR.TCCON.CH4
PARIS 48.8˚N, 2017-11-22 till 2023-12-16, 81682 meas.
all GB
SAT_with_GB_prior_on_SAT
GB_prior_retrscaled_smooth_with_SAT_avk_on_SAT

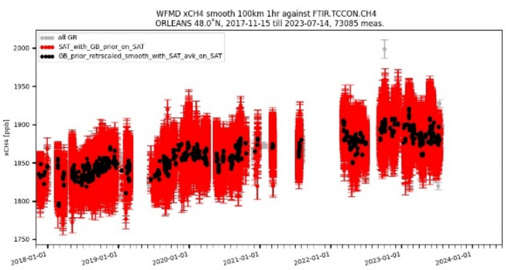
WFMD xCH4 smooth 100km 1hr against FTIR.TCCON.CH4
ORLEANS 48.0˚N, 2017-11-15 till 2023-07-14, 73085 meas.
all GB
SAT_with_GB_prior_on_SAT
GB_prior_retrscaled_smooth_with_SAT_avk_on_SAT

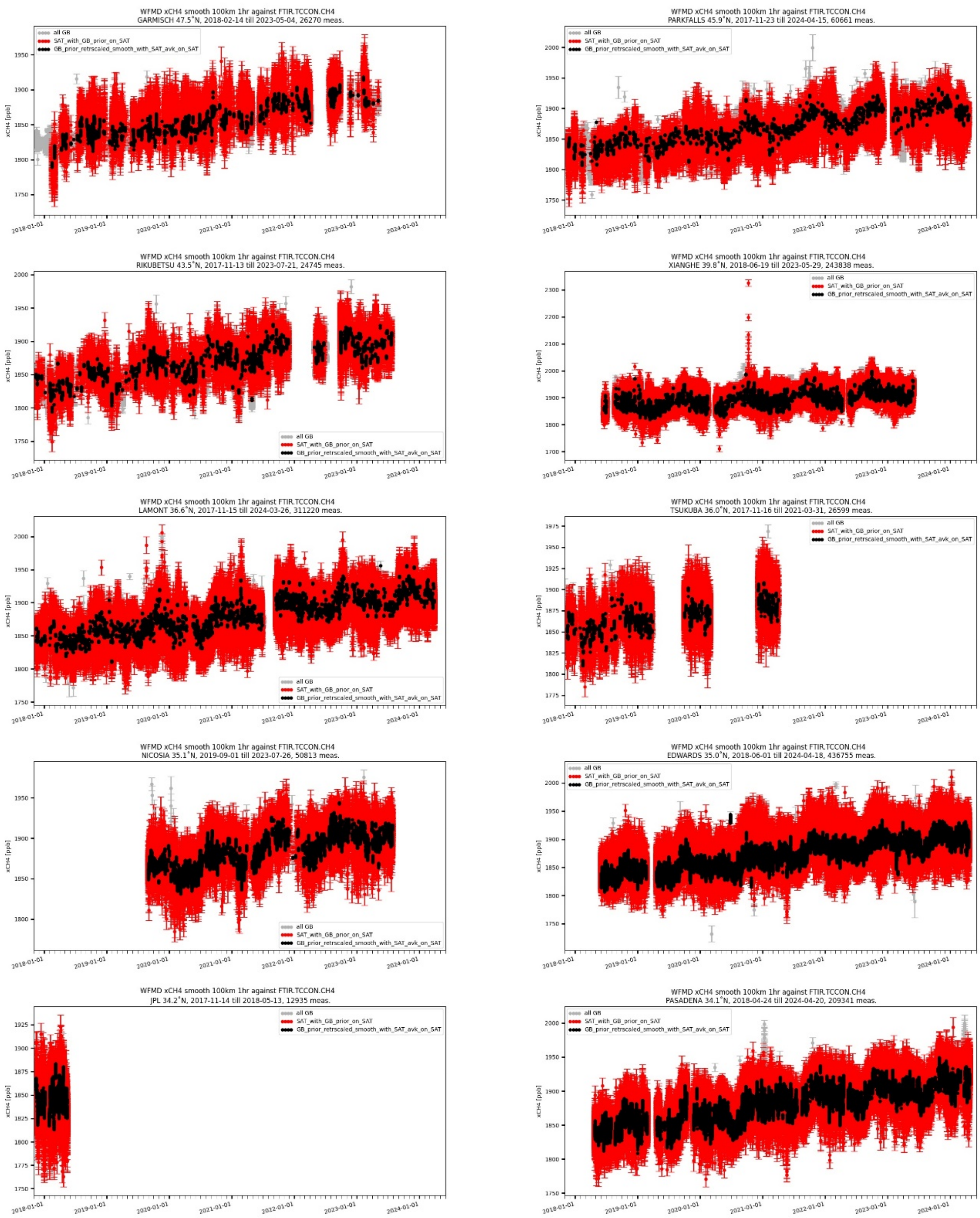

WFMD xCH4 smooth 100km 1hr against FTIR.TCCON.CH4
GARMISCH 47.5°N, 2018-02-14 till 2023-05-04, 26270 meas.
WFMD xCH4 smooth 100km 1hr against FTIR.TCCON.CH4
PARKFALLS 45.9°N, 2017-11-23 till 2024-04-15, 60661 meas.
WFMD xCH4 smooth 100km 1hr against FTIR.TCCON.CH4
RIKUBETSU 43.5°N, 2017-11-13 till 2023-07-21, 24745 meas.
WFMD xCH4 smooth 100km 1hr against FTIR.TCCON.CH4
XIANGHE 39.8°N, 2018-06-19 till 2023-05-29, 243838 meas.
WFMD xCH4 smooth 100km 1hr against FTIR.TCCON.CH4
LAMONT 36.6°N, 2017-11-15 till 2024-03-26, 311220 meas.
WFMD xCH4 smooth 100km 1hr against FTIR.TCCON.CH4
TSUKUBA 36.0°N, 2017-11-16 till 2021-03-31, 26599 meas.
WFMD xCH4 smooth 100km 1hr against FTIR.TCCON.CH4
NICOSIA 35.1°N, 2019-09-01 till 2023-07-26, 50813 meas.
WFMD xCH4 smooth 100km 1hr against FTIR.TCCON.CH4
EDWARDS 35.0°N, 2018-06-01 till 2024-04-18, 436755 meas.
WFMD xCH4 smooth 100km 1hr against FTIR.TCCON.CH4
JPL 34.2°N, 2017-11-14 till 2018-05-13, 12935 meas.
WFMD xCH4 smooth 100km 1hr against FTIR.TCCON.CH4
PASADENA 34.1°N, 2018-04-24 till 2024-04-20, 209341 meas.
all GB
SAT_with_GB_prior_on_SAT
GB_prior_retrscaled_smooth_with_SAT_avk_on_SAT
xCH4 [ppb]

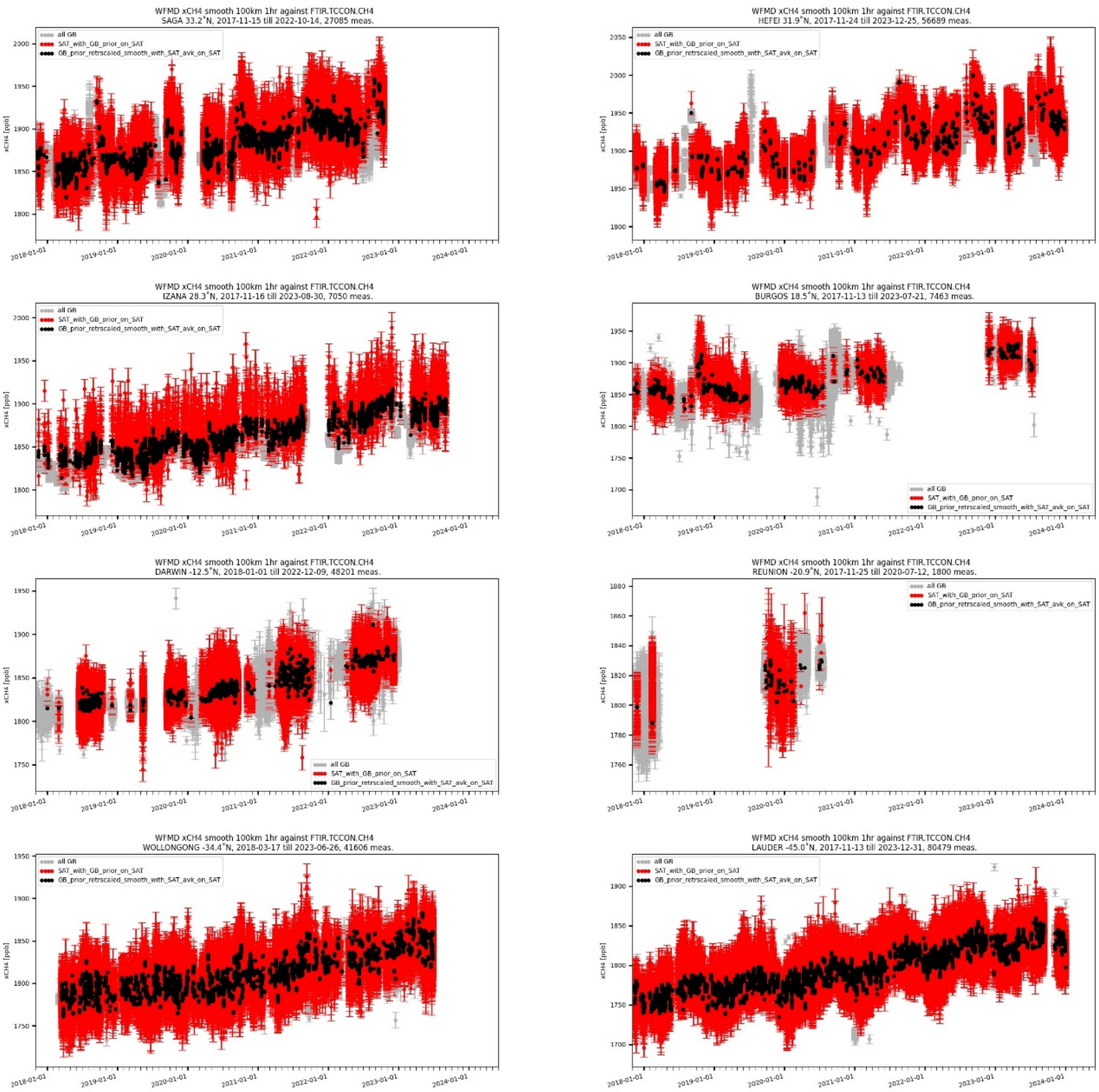

Figure 4-23: Timeseries of XCH_4 TCCON (collocated=black, all=grey) and CH4_S5P_WFMD (red) data at selected TCCON sites.

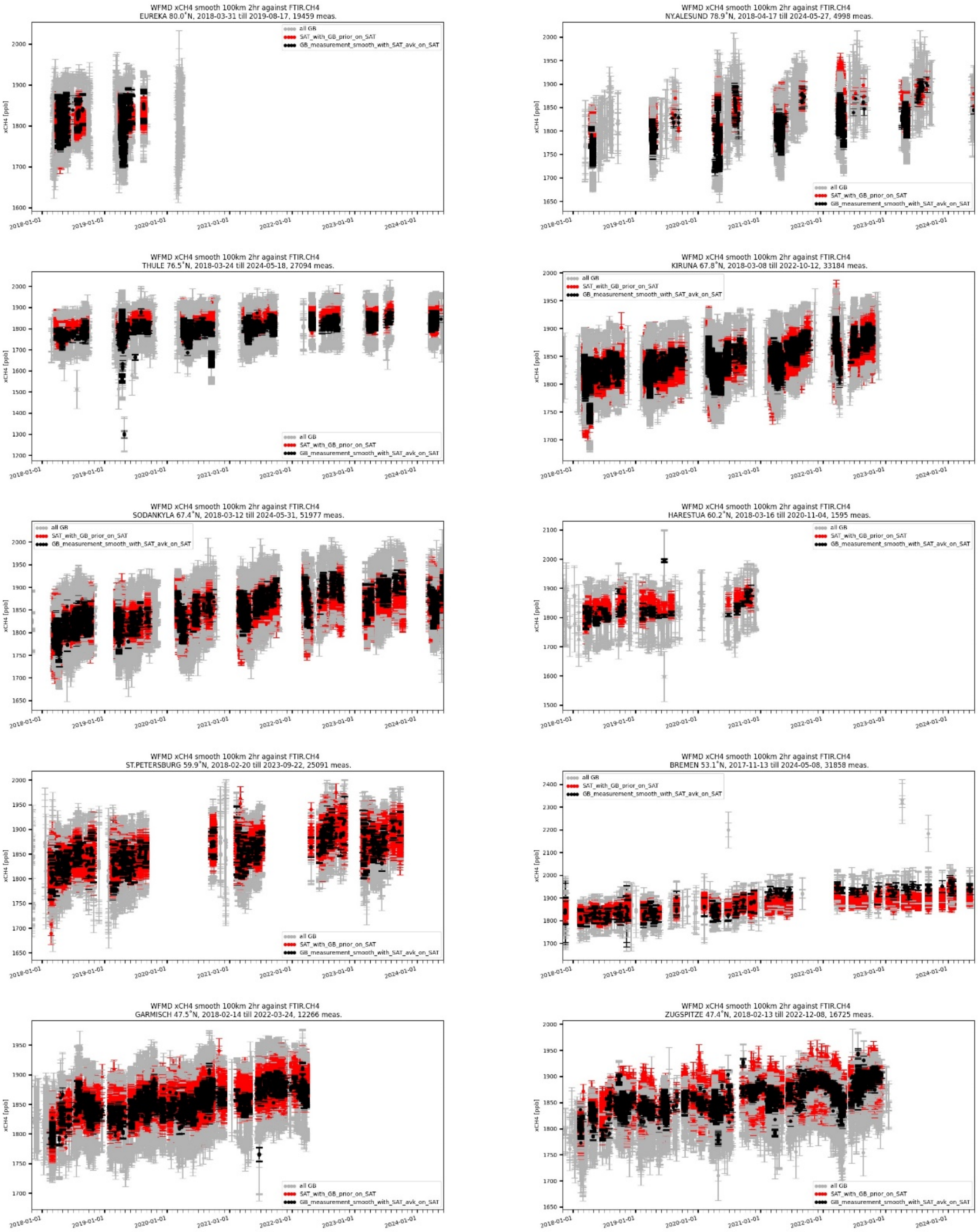
WFMD xCH4 smooth 100km 2hr against FTIR.CH4
EUREKA 80.0°N, 2018-03-31 till 2019-08-17, 19459 meas.
WFMD xCH4 smooth 100km 2hr against FTIR.CH4
NY.ALESUND 78.9°N, 2018-04-17 till 2024-05-27, 4998 meas.
WFMD xCH4 smooth 100km 2hr against FTIR.CH4
THULE 76.5°N, 2018-03-24 till 2024-05-18, 27094 meas.
WFMD xCH4 smooth 100km 2hr against FTIR.CH4
KIRUNA 67.8°N, 2018-03-08 till 2022-10-12, 33184 meas.
WFMD xCH4 smooth 100km 2hr against FTIR.CH4
SODANKYLA 67.4°N, 2018-03-12 till 2024-05-31, 51977 meas.
WFMD xCH4 smooth 100km 2hr against FTIR.CH4
HARESTUA 60.2°N, 2018-03-16 till 2020-11-04, 1595 meas.
WFMD xCH4 smooth 100km 2hr against FTIR.CH4
ST.PETERSBURG 59.9°N, 2018-02-20 till 2023-09-22, 25091 meas.
WFMD xCH4 smooth 100km 2hr against FTIR.CH4
BREMEN 53.1°N, 2017-11-13 till 2024-05-08, 31858 meas.
WFMD xCH4 smooth 100km 2hr against FTIR.CH4
GARMISCH 47.5°N, 2018-02-14 till 2022-03-24, 12266 meas.
WFMD xCH4 smooth 100km 2hr against FTIR.CH4
ZUGSPITZE 47.4°N, 2018-02-13 till 2022-12-08, 16725 meas.
all GB
SAT_with_GB_prior_on_SAT
GB_measurement_smooth_with_SAT_avk_on_SAT
xCH4 [ppb]

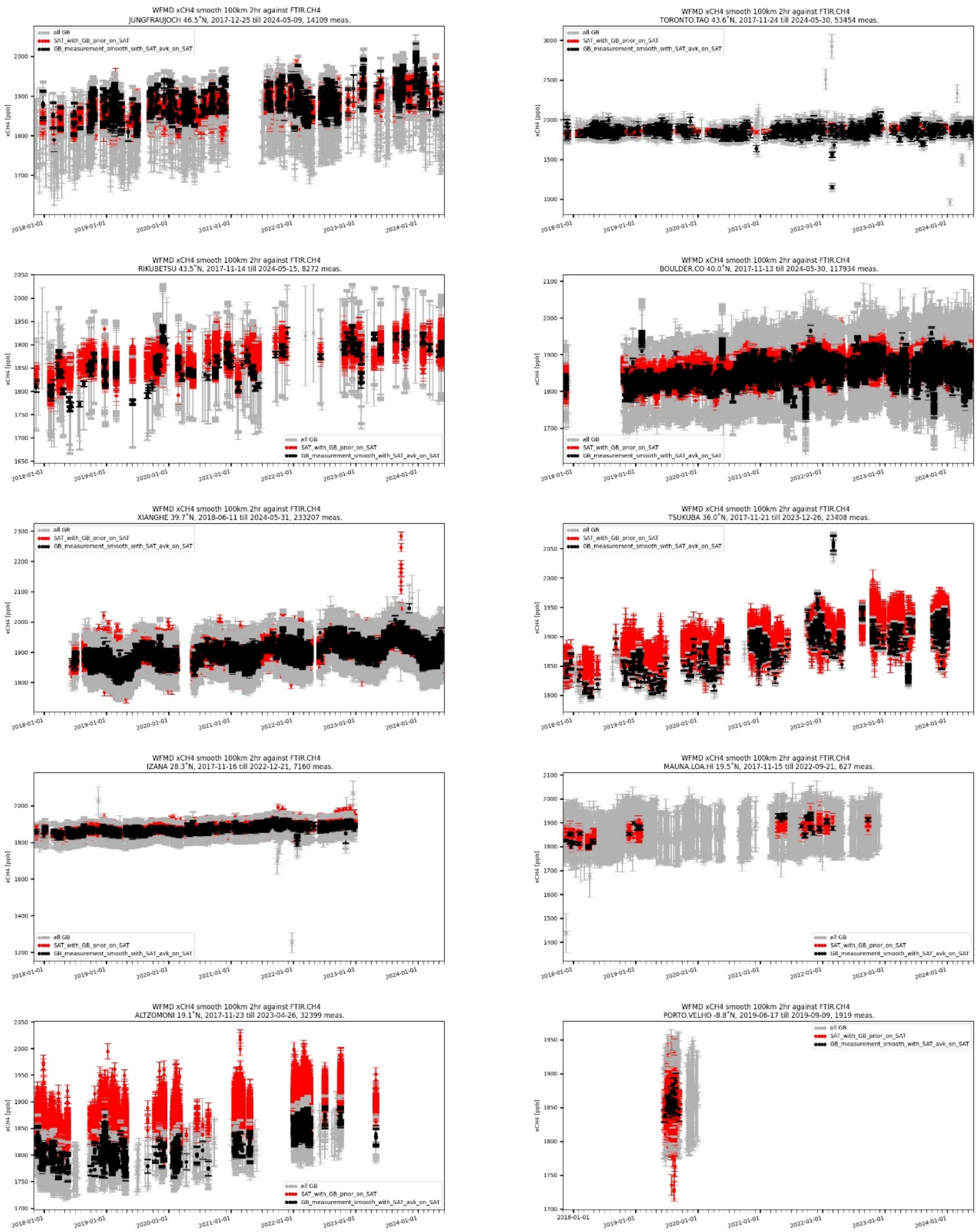
WFMD xCH4 smooth 100km 2hr against FTIR.CH4
JUNGFRAUJOCH 46.5°N, 2017-12-25 till 2024-05-09, 14109 meas.
WFMD xCH4 smooth 100km 2hr against FTIR.CH4
TORONTO.TAO 43.6°N, 2017-11-24 till 2024-05-30, 53454 meas.
WFMD xCH4 smooth 100km 2hr against FTIR.CH4
RIKUBETSU 43.5°N, 2017-11-14 till 2024-05-15, 8272 meas.
WFMD xCH4 smooth 100km 2hr against FTIR.CH4
BOULDER.CO 40.0°N, 2017-11-13 till 2024-05-30, 117934 meas.
WFMD xCH4 smooth 100km 2hr against FTIR.CH4
XIANGHE 39.7°N, 2018-06-11 till 2024-05-31, 233207 meas.
WFMD xCH4 smooth 100km 2hr against FTIR.CH4
TSUKUBA 36.0°N, 2017-11-21 till 2023-12-26, 23408 meas.
WFMD xCH4 smooth 100km 2hr against FTIR.CH4
IZANA 28.3°N, 2017-11-16 till 2022-12-21, 7160 meas.
WFMD xCH4 smooth 100km 2hr against FTIR.CH4
MAUNA.LOA.HI 19.5°N, 2017-11-15 till 2022-09-21, 627 meas.
WFMD xCH4 smooth 100km 2hr against FTIR.CH4
ALTZOMONI 19.1°N, 2017-11-23 till 2023-04-26, 32399 meas.
WFMD xCH4 smooth 100km 2hr against FTIR.CH4
PORTO.VELHO -8.8°N, 2019-06-17 till 2019-09-09, 1919 meas.
all GB
SAT_with_GB_prior_on_SAT
GB_measurement_smooth_with_SAT_avk_on_SAT

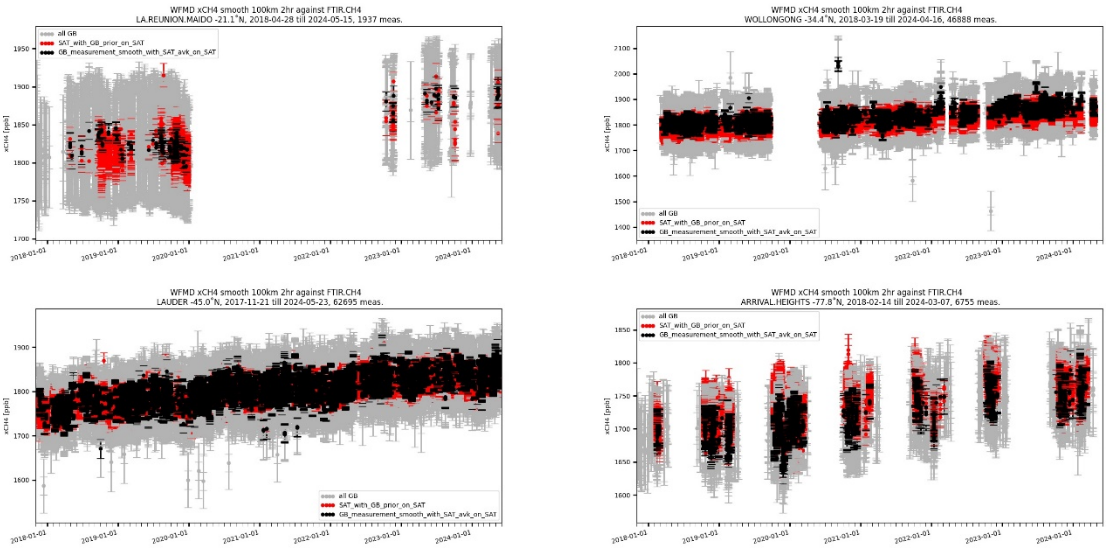

Figure 4-24: Timeseries of XCH_4 NDACC (collocated=black, all=grey) and CH4_S5P_WFMD (red) data at selected NDACC sites.

Figures 4-25 and 4-26 show the median spatial distribution of the observed WFMD-FTS XCH4 biases for all TCCON and NDACC stations respectively. If location isn't a contributing parameter to the observed biases one would expect to see little to no features in these plots apart from a degree of random variability. For most stations however spatial features can be clearly observed. Some tied to land-sea, urban vs. rural or differences in altitude which (even though we apply a correction) influence the observed biases. In the future, therefore smarter (but less universal and thus limiting algorithm intercomparisons) colocation methods may need to be applied to get a more accurate assessment of the biases. This in itself is not trivial as several sites show marked spatial bias difference in close proximity to the actual FTIR site.

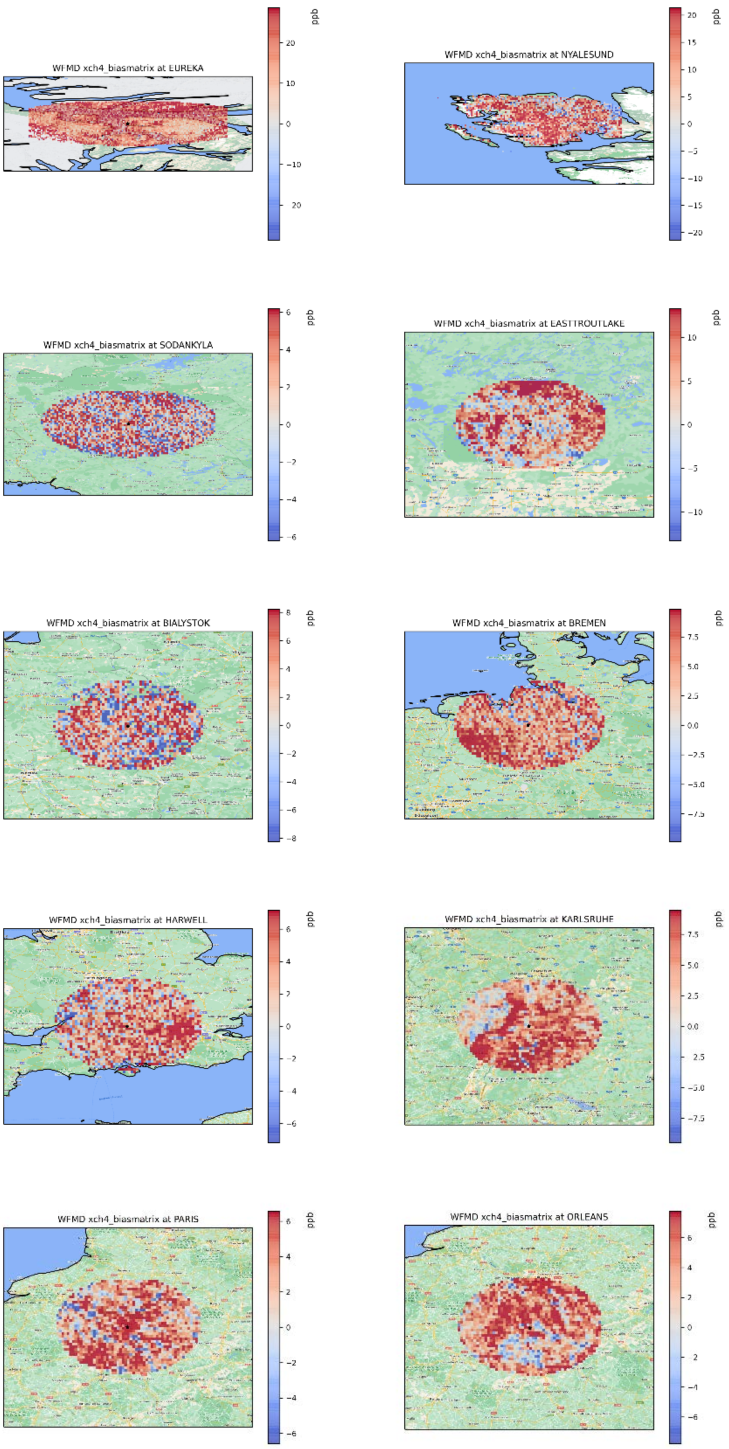
WFMD xch4_biasmatrix at EUREKA
WFMD xch4_biasmatrix at NYALESUND
WFMD xch4_biasmatrix at SODANKYLA
WFMD xch4_biasmatrix at EASTTROUTLAKE
WFMD xch4_biasmatrix at BIALYSTOK
WFMD xch4_biasmatrix at BREMEN
WFMD xch4_biasmatrix at HARWELL
WFMD xch4_biasmatrix at KARLSRUHE
WFMD xch4_biasmatrix at PARIS
WFMD xch4_biasmatrix at ORLEANS
ppb

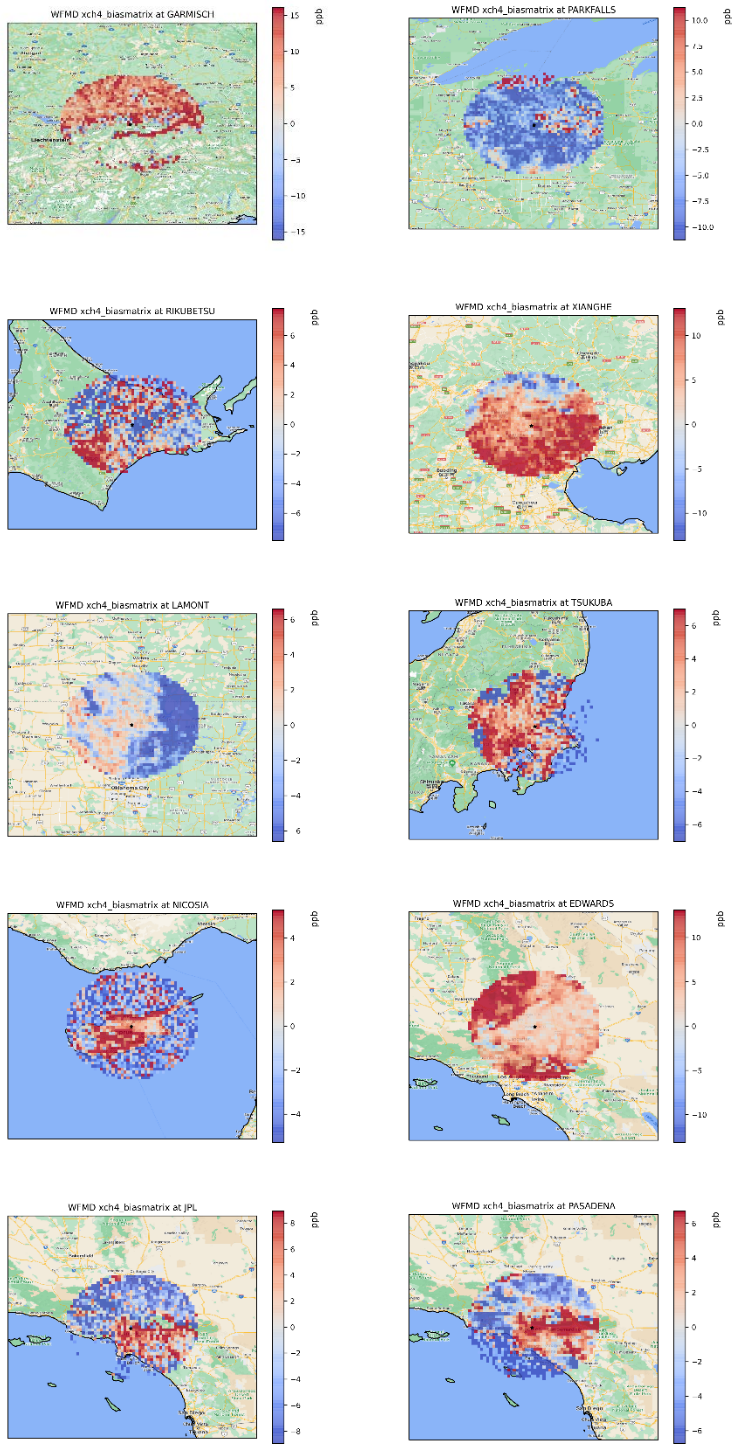

WFMD xch4_biasmatrix at GARMISCH
ppb
WFMD xch4_biasmatrix at PARKFALLS
ppb
WFMD xch4_biasmatrix at RIKUBETSU
ppb
WFMD xch4_biasmatrix at XIANGHE
ppb
WFMD xch4_biasmatrix at LAMONT
ppb
WFMD xch4_biasmatrix at TSUKUBA
ppb
WFMD xch4_biasmatrix at NICOSIA
ppb
WFMD xch4_biasmatrix at EDWARDS
ppb
WFMD xch4_biasmatrix at JPL
ppb
WFMD xch4_biasmatrix at PASADENA
ppb

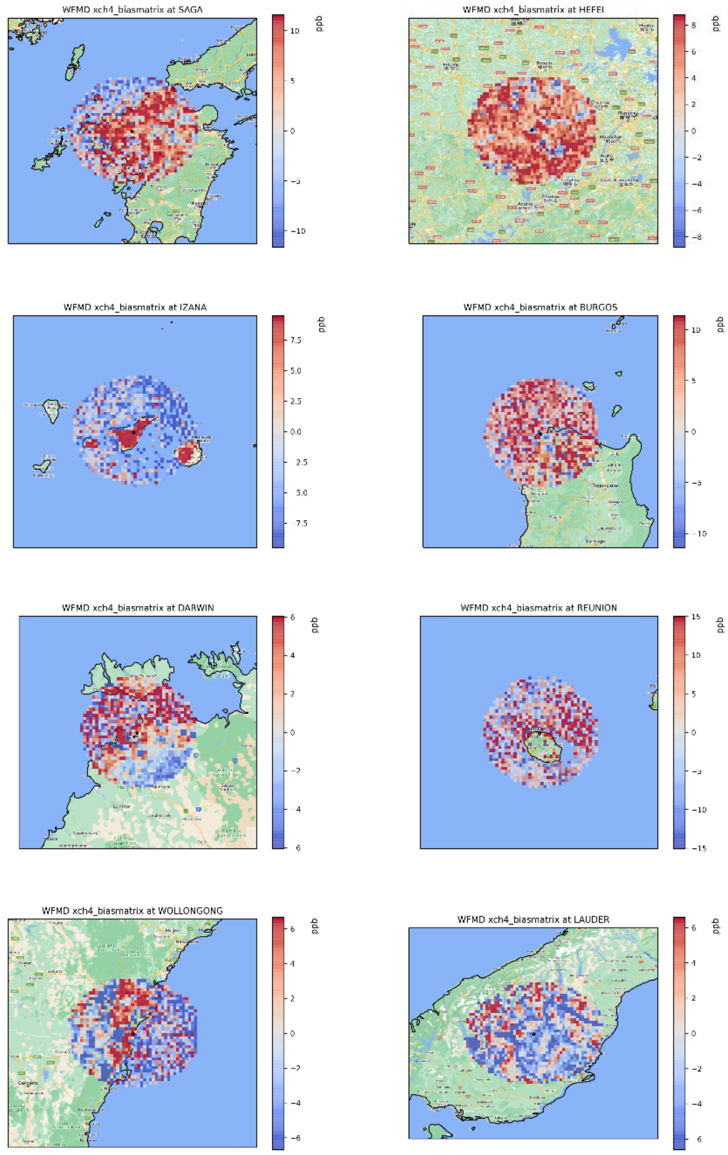

Figure 4-25: Spatial representation of the observed WFMD-FTS XCH4 biases for each of the TCCON stations. Shown is the median of all biases within each 0.05 by 0.05° latitude-longitude grid.

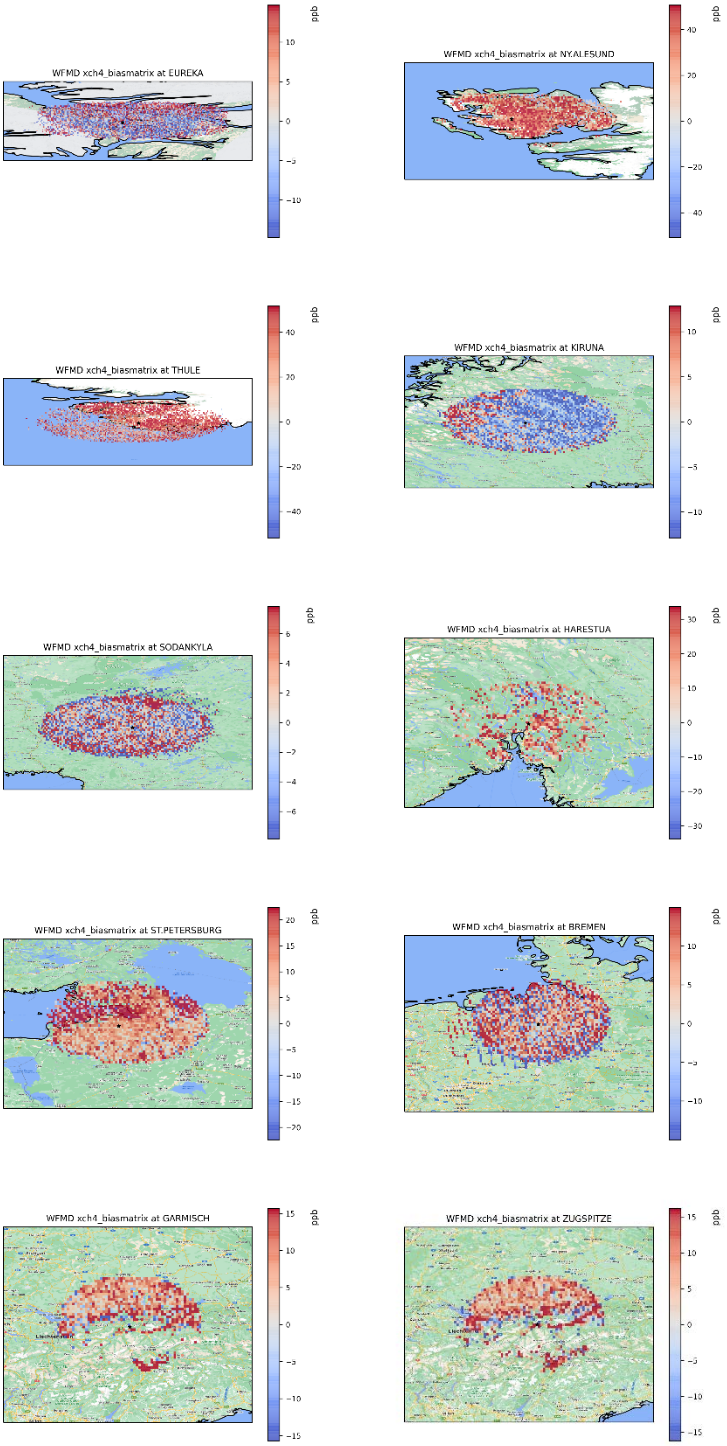
WFMD xch4_biasmatrix at EUREKA
WFMD xch4_biasmatrix at NY.ALESUND
WFMD xch4_biasmatrix at THULE
WFMD xch4_biasmatrix at KIRUNA
WFMD xch4_biasmatrix at SODANKYLA
WFMD xch4_biasmatrix at HARESTUA
WFMD xch4_biasmatrix at ST.PETERSBURG
WFMD xch4_biasmatrix at BREMEN
WFMD xch4_biasmatrix at GARMISCH
WFMD xch4_biasmatrix at ZUGSPITZE
ppb

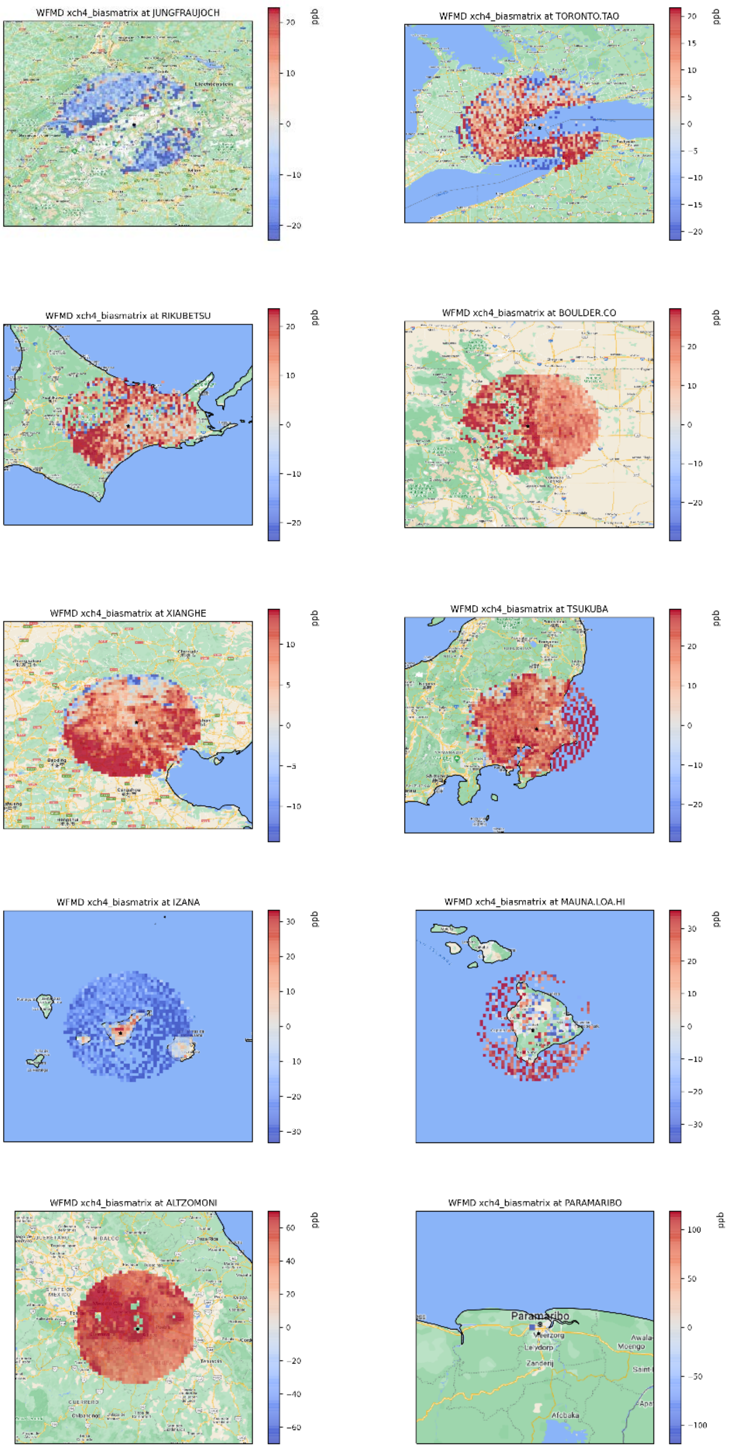

WFMD xch4_biasmatrix at JUNGFRAUJOCH
WFMD xch4_biasmatrix at TORONTO.TAO
WFMD xch4_biasmatrix at RIKUBETSU
WFMD xch4_biasmatrix at BOULDER.CO
WFMD xch4_biasmatrix at XIANGHE
WFMD xch4_biasmatrix at TSUKUBA
WFMD xch4_biasmatrix at IZANA
WFMD xch4_biasmatrix at MAUNA.LOA.HI
WFMD xch4_biasmatrix at ALTZOMONI
WFMD xch4_biasmatrix at PARAMARIBO
ppb

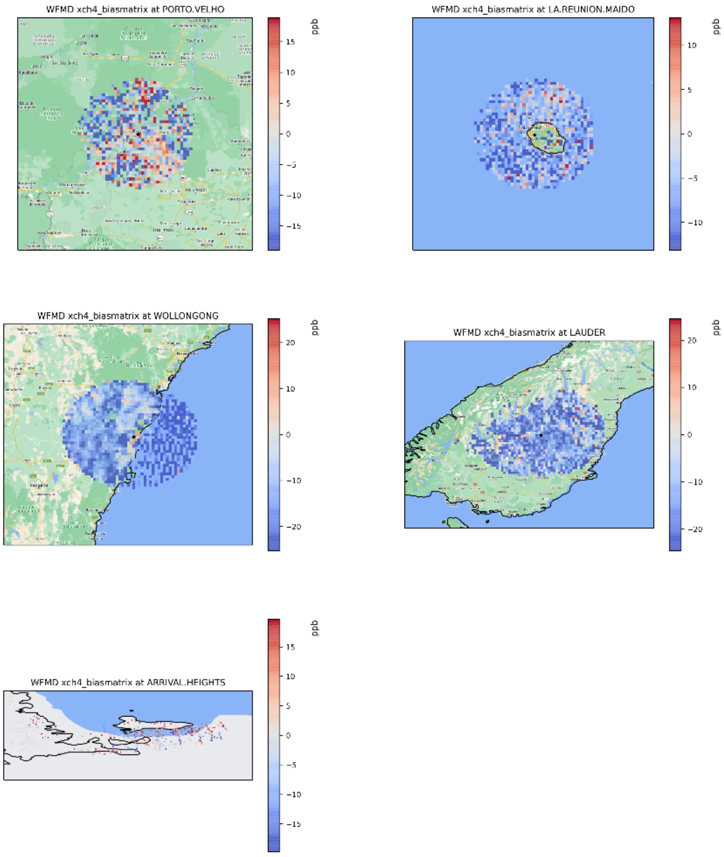

Figure 4-26: Spatial representation of the observed WFMD-FTS XCH4 biases for each of the NDACC stations. Shown is the median of all biases within each 0.05 by 0.05° latitude-longitude grid.

Figure 4-27 shows monthly median timeseries for TCCON and WFMD XCH_4 for all data that fall within certain latitude bands, namely all sites North of 40°N latitude (top), all sites between 40°N and the equator (mid) and all sites in the Southern hemisphere (bottom). The figures clearly show that WFMD is capable of capturing the larger scale temporal evolution of XCH_4 as well as seasonal variability.

Figure 4-28 shows the same for NDACC with high altitude stations and the Toronto site removed from the data pool. Here we see good agreement for all latitude bands, with the largest difference in slope being 1.1 (well within the combined uncertainty bounds) at high latitudes. Also no strong deviations in the seasonality are observed.

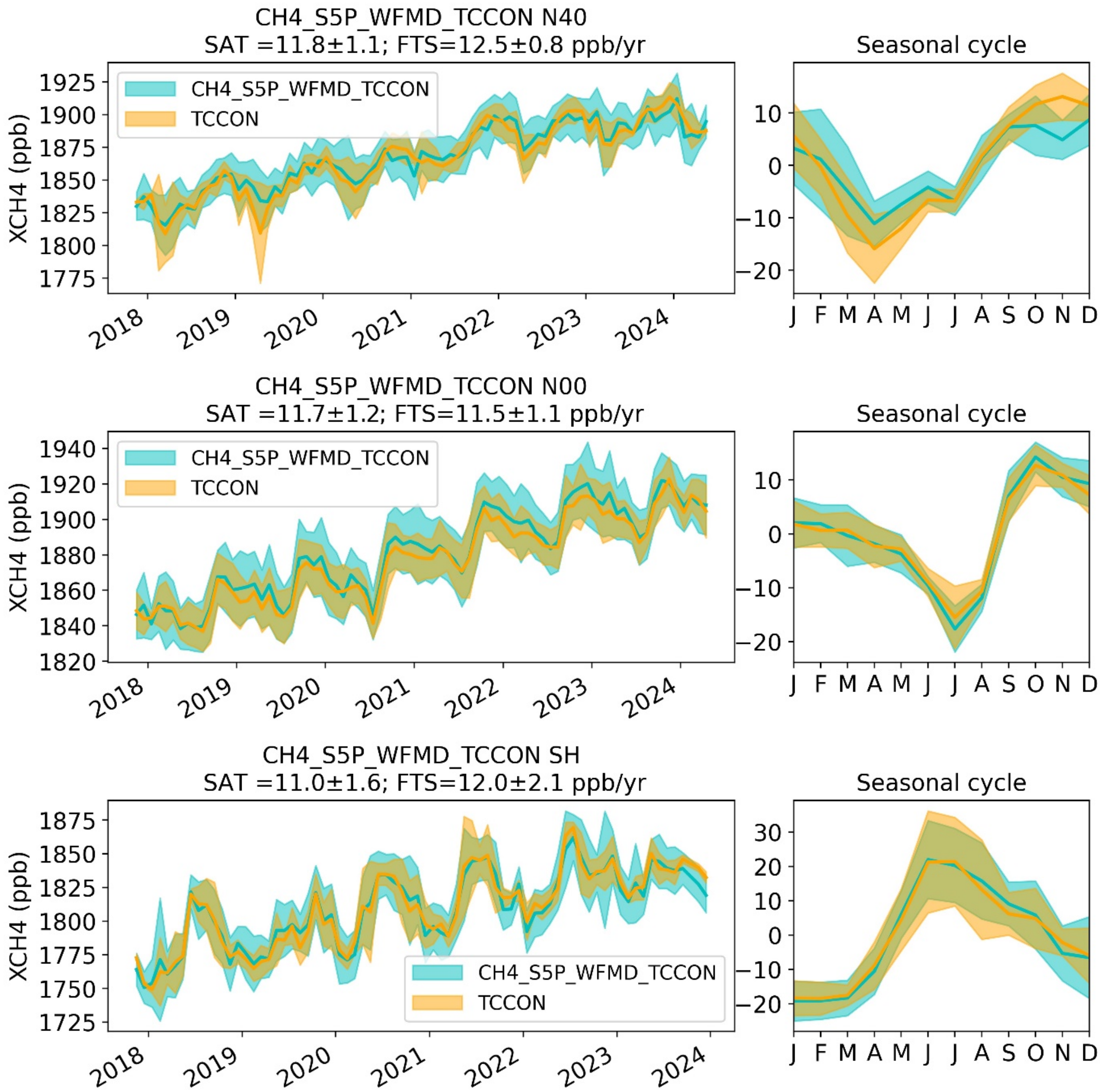

Figure 4-27: Monthly median collocated Sat and TCCON XCH_4 concentrations as a function of time and the detrended monthly medians as a function of season. The shaded areas correspond with the scaled median absolute deviation.

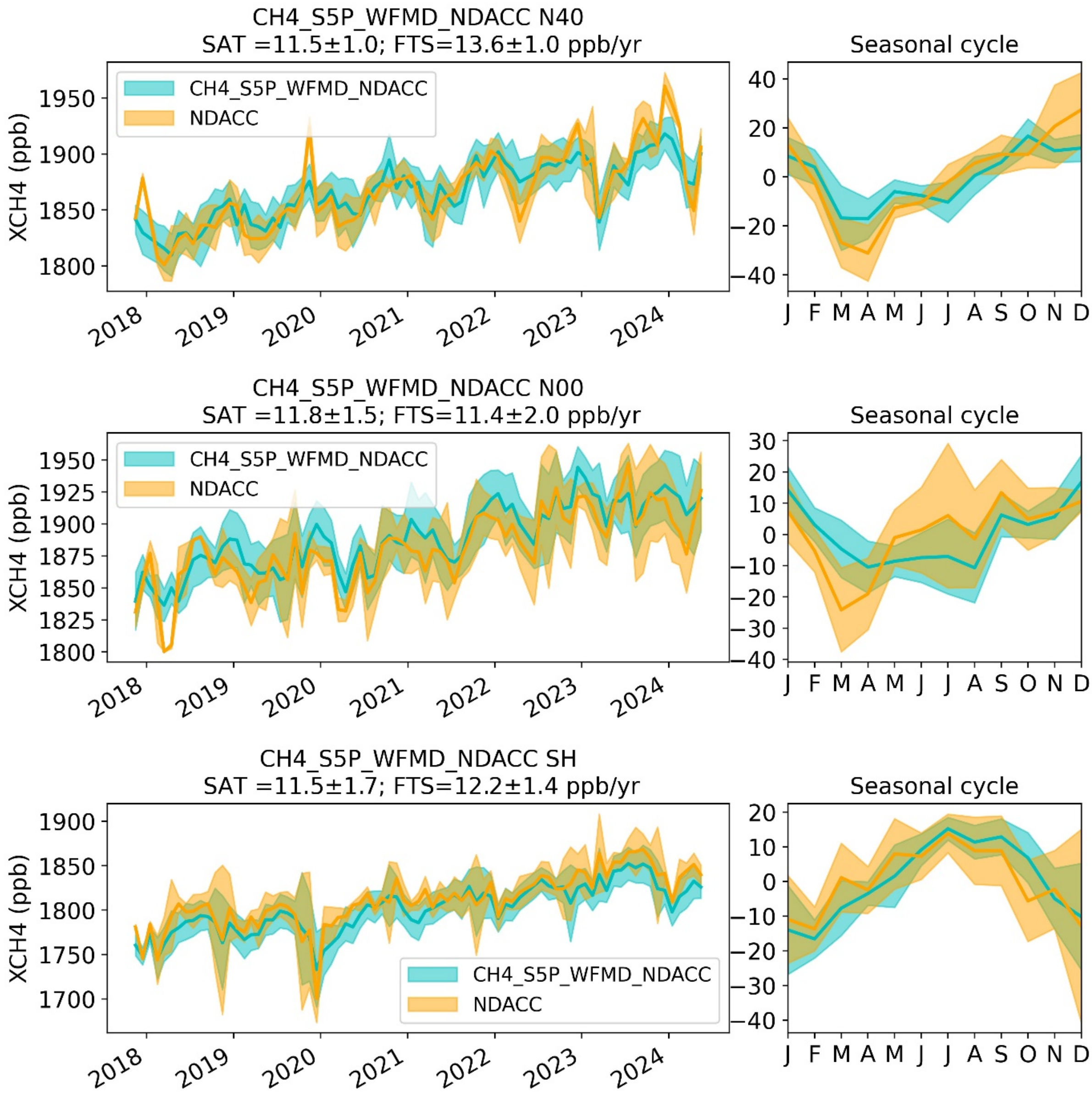

Figure 4-28: Monthly median collocated Sat and NDACC XCH_4 concentrations as a function of time and the detrended monthly medians as a function of season. The shaded areas correspond with the scaled median absolute deviation.

4.2.4.2 Summary

As with our previous assessment the current CH4_S5P_WFMD data contains little noticeable outliers (it is the same product after all). The seasonal cycles and long-term trends seem well captured. The obtained Stability equals -0.2 ppb/year with confidence bands that overlap 0. The single measurement precision equals 13.7 , thus reaching the breakthrough < 17 ppb target value. The reported uncertainty sits at 0.90 times what we find in our analysis. The overall bias sits at 3.9 ppb. The Relative and Seasonal relative accuracies equal 3.4 and 5.6 ppb respectively, thus reaching the <10 ppb target.

For NDACC, limiting our analysis to the stations featured in **Table 4-11**,- we obtain a single measurement precision 20.3 [17.5,22.4] ppb, an overall bias of 7.1 [0.5,13.7] ppb and relative accuracy values: RA 14.7 [10.7, 20.6] and SRA 16.7 [14.2,19.7]. The confidence bands for NDACC are significantly wider indicating larger inter-station differences. This naturally also manifests itself in the relative accuracy numbers. It is however safe to say that inter-station biases (even after removing high altitude and low sampling sites) between the NDACC stations still contribute to this number.

Table 4-11 presents an overview of the estimated data quality of CH4_S5P_WFMD, as obtained by the VALT team, from comparisons with TCCON ground-based reference observations. Values in square brackets [ ] correspond with the upper and lower 95% confidence bound on the parameter. The uncertainty ratio features 2 numbers as outlined in the validation method.

Product Quality Summary Table for Product: CH4_S5P_WFMD Level: 2, Version: v1.8, Time period covered: 11.2017 – 06.2024 Assessment: Validation Team (VALT)			
Parameter [unit]	**Achieved performance**	**Requirement**	**Comments**
Single measurement precision (1-sigma) in [ppb]	13.7 [12.9,15.0]	< 34 (T) < 17 (B) < 9 (G)	Computed as the median over all station scaled median absolute differences to TCCON
Uncertainty ratio [-]: Ratio reported uncertainty to standard deviation of satellite-TCCON difference	0.89, 0.90*	-	No requirement but value close to unity expected for a high quality data product with reliable reported uncertainty.
Mean bias (global offset) [ppb]	3.9 [2.0, 5.4]	-	No requirement but value close to zero expected for a high quality data product.
Accuracy: Relative systematic error [ppb]	Spatial: 3.4 [0.5, 4.7] Spatio-temporal: 5.6 [4.5, 6.9]	< 10	Spatial: Computed as standard deviation of the biases at the various TCCON sites. Spatio-temporal: As "Spatial" but also considering seasonal biases.
Stability: Drift [ppb/year]	-0.2 [-0.7,0.2]	< 3	Linear drift

4.2.5 Validation results for product CH4_GO2_SRFP

Below we show the validation results of the XCH_4 concentrations as derived by the CH4_GO2_SRFP v2.0.3 algorithm using GOSAT-2 spectra, FP standing for the Full Physics version of the algorithm developed at SRON. Data was available from February 2019 up to and including December 2023. The SRFP algorithm provides *a priori* and column averaging kernel information on a 12 layer profile.

4.2.5.1 Detailed results

The Taylor diagram above in **Figure 4-29** yields a concise overview of the capabilities of the CH4_GO2_SRFP algorithm with respect to the TCCON network. Most TCCON sites are nicely clustered apart from Eureka which exhibits a limited seasonal cycle (only FTIR measurements in spring-summer) and data pair availability, and Reunion (an island site). Both have lower correlation and relative standard deviations. All other sites cluster around the 0.8 correlation line. TCCON yields standard deviations that are 0.7 to 0.9 times that of the algorithm and the relative standard deviation of the bias sits around 0.7.

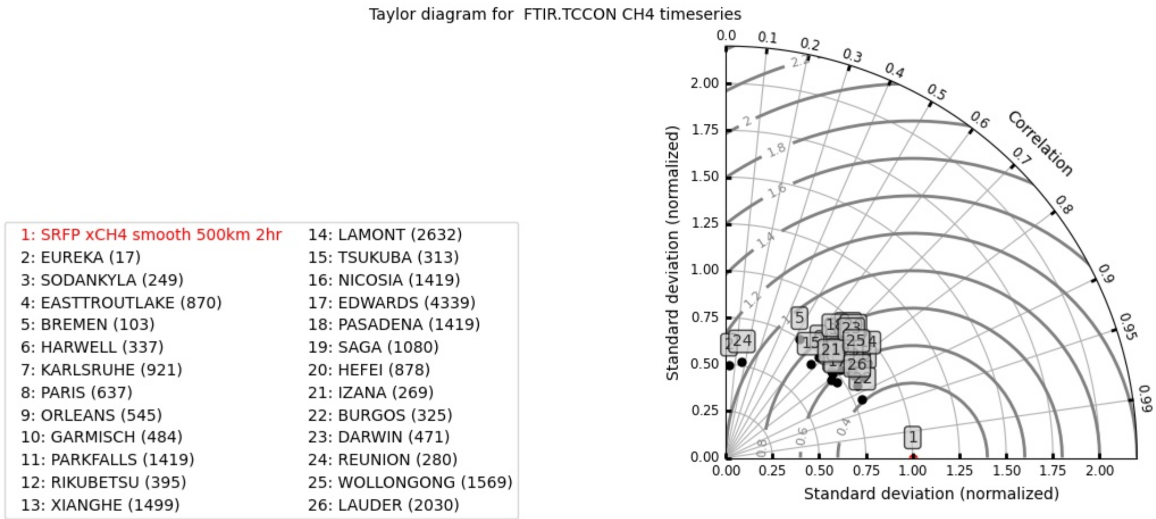

Figure 4-29: Tayor plot of XCH_4 TCCON values relative to CH4_GO2_SRFP. Straight lines correspond with the correlation, light grey lines yield the variability of the TCCON data relative to the satellite variability and the dark grey lines correspond with the variability of the Satellite -TCCON bias relative to the satellite variability.

For NDACC (**Figure 4-30**) we again see much more dispersion with strong outliers at Paramaribo, Mauna Loa and Toronto. Correlations are generally weaker compared to TCCON, whereas its variability relative to the FTIR measurements is lower (indicating higher variability in NDACC). As with WFMD, we have excluded Altzomoni, Toronto, Thule, Paramaribo and Porto Velho from **Table 4-13** and the calculation of the overall FoMs.

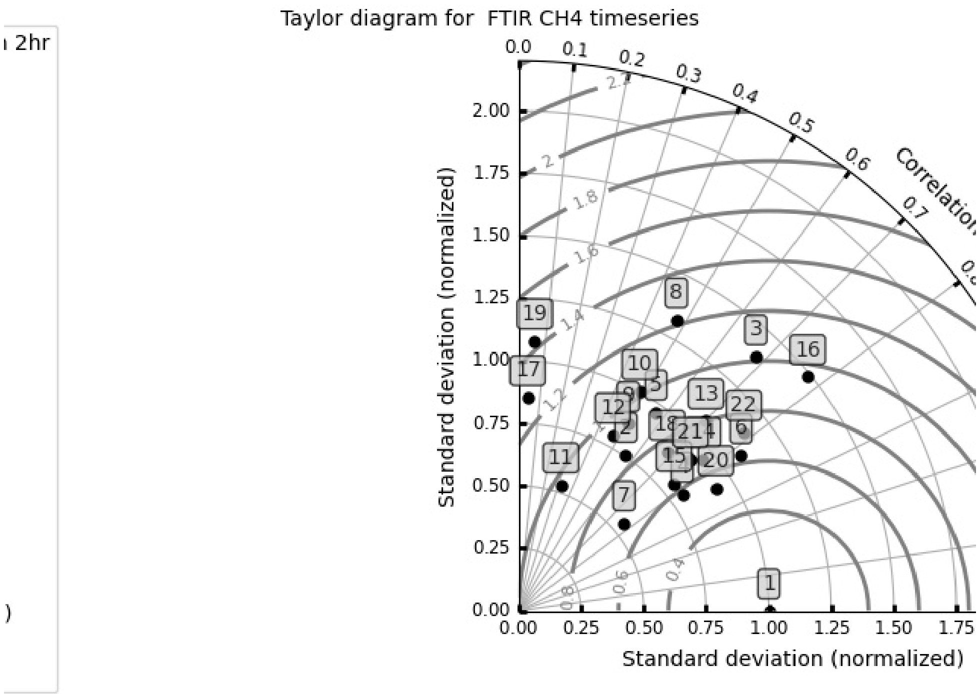

Figure 4-30: Tayor plot of XCH_4 NDACC values relative to CH4_GO2_SRFP. Straight lines correspond with the correlation, light grey lines yield the variability of the NDACC data relative to the satellite variability and the dark grey lines correspond with the variability of the Satellite -NDACC bias relative to the satellite variability.

Looking at **Figure 4-31**, which shows the mean bi-weekly bias between the satellite and TCCON measurement pairs. Unlike other TCCON comparison mosaic plots which do show relatively stable station to station biases, here we observe a temporal component in the bias as well, with lower and even negative biases observed up to mid 2021, after which we see a sudden increase in the bias observed at many stations. There also seems to be a small seasonal component with higher biases in the first half of each year (particularly in the post mid-2021 period). The picture for NDACC (**Figure 4-32**) is far less clear with its many datagaps and far more outspoken biases.

At this point it is too early to say that these are clear indications of any issues with the algorithm. However, they do point to areas of interest for further investigation.

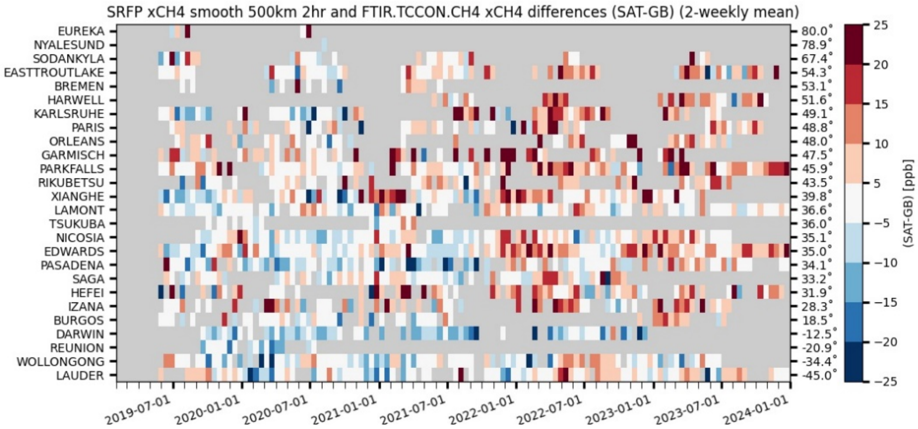

Figure 4-31. Mosaic plot of bi-weekly mean CH4_GO2_SRFP – TCCON XCH_4 biases as a function of time and TCCON station.

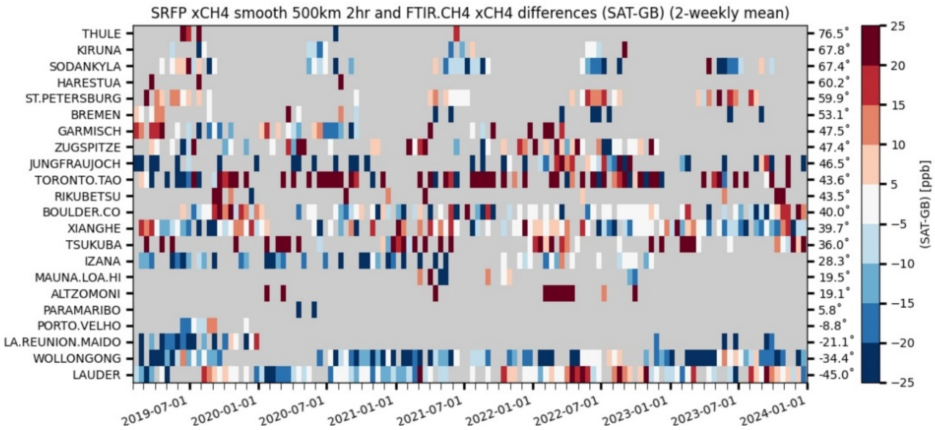

Figure 4-32. Mosaic plot of bi-weekly mean CH4_GO2_SRFP – NDACC XCH_4 biases as a function of time and NDACC station.

Table 4-12 lists all bias and scatter results derived from individual data pairs at all TCCON stations. The algorithm produces on average 590 data pairs per station, which corresponds with ~125 pairs per station per year. Several stations however have far less collocated measurements (Ny Alesund has only 1 data pair, and Eureka only 17) hampering an accurate assessment of the data quality at these sites. The observed median bias ranges between -8.26 (Darwin) and 8.42 (Harwell), while the scatter ranges between 7.1 ppb (Eureka) and 18.34 ppb (Xianghe). The long term trend ranges between -0.49 ppb/year (Orleans) and 3.64 ppb/year (Karlsruhe). Only one station features a negative bias (Orleans). The overall correlation using all collocated data regardless of station equals 0.79.

Table 4-12: Number of collocated data pairs (N), Correlation (R), Bias, Scatter, long term trend difference (ltt) and uncertainty thereon (ltt_err), seasonal amplitude difference (A) and uncertainty thereon (A_err) as well as the latitude of the TCCON station. The last row lists the median values over all stations. Product: CH4_GO2_SRFP.

STATION	N	R	Bias	Scat	ltt	ltt_err	A	A_err	lat
EUREKA	17	0.04	1.56	7.1	-	-	-	-	80
NYALESUND	1	nan	-5.03	0	-	-	-	-	78.9
SODANKYLA	249	0.71	3.63	11.48	1.47	1.93	14.36	9.23	67.4
EASTTROUTLAKE	870	0.82	4.98	14.88	2.15	0.85	2.55	1.8	54.3
BREMEN	103	0.53	1.55	14.55	-	-	-	-	53.1
HARWELL	337	0.68	8.42	13.33	-	-	-	-	51.6
KARLSRUHE	921	0.81	5.21	15.18	3.64	1.33	2.56	1.85	49.1
PARIS	637	0.84	3.06	12.6	2.24	0.96	2.47	1.96	48.8
ORLEANS	545	0.82	4.95	14.04	-0.49	0.9	2.5	1.91	48
GARMISCH	484	0.78	8.45	16.09	3.34	1.46	6.09	2.38	47.5
PARKFALLS	1419	0.81	6.25	14.25	1.53	0.74	3.02	1.44	45.9
RIKUBETSU	395	0.86	6.02	10.55	3.53	0.73	3.27	2.3	43.5
XIANGHE	1499	0.73	2.07	18.34	1.61	0.9	9.63	1.73	39.8
LAMONT	2632	0.83	0.81	13.15	0.69	0.47	2.48	0.83	36.6
TSUKUBA	313	0.67	-0.38	13.36	-	-	-	-	36
NICOSIA	1419	0.82	1.43	12.55	2.47	0.4	6.95	0.79	35.1
EDWARDS	4339	0.83	3.17	15.84	2.54	0.51	7.63	0.76	35
PASADENA	1419	0.7	-4.23	14.6	2.51	0.7	3.35	1.37	34.1
SAGA	1080	0.79	2.9	13.84	0.99	1.36	4.02	1.38	33.2
HEFEI	878	0.75	7.78	15.43	1.3	0.75	5.62	2.17	31.9
IZANA	269	0.77	3.84	15.89	1.4	0.78	8.17	2.04	28.3
BURGOS	325	0.92	1.9	11.49	3.23	0.71	2.97	1.54	18.5
DARWIN	471	0.76	-8.26	11.49	0.42	0.94	2.43	1.34	-12.5
REUNION	280	0.17	-7.58	14.4	-	-	-	-	-20.9
WOLLONGONG	1569	0.8	-0.4	13.88	1.79	0.59	7.02	0.96	-34.4
LAUDER	2030	0.88	2.17	11.32	1.7	0.59	6.57	0.97	-45
MEDIAN	591	0.79	2.535	13.86	1.745	0.765	3.685	1.635	38.2

Table 4-13: Number of collocated data pairs (N), Correlation (R), Bias, Scatter, long term trend difference (ltt) and uncertainty thereon (ltt_err), seasonal amplitude difference (A) and uncertainty thereon (A_err) as well as the latitude of the NDACC station. The last row lists the median values over all stations. Product: CH4_GO2_SRFP.

STATION	N	R	Bias	Scat	ltt	ltt_err	A	A_err	lat
KIRUNA	61	0.68	-10.5	11.04	5.11	4.53	43.55	29.75	67.8
SODANKYLA	301	0.81	-8.91	15.55	-4.52	1.18	9.95	8.08	67.3
HARESTUA	7	0.57	37.83	9.25	-	-	-	-	60.1
ST.PETERSBURG	479	0.82	8.39	12.56	1.55	1.27	6.74	2.25	59.8
BREMEN	165	0.77	-2.76	34.87	-12.8	11.95	7.15	10.51	53
GARMISCH	251	0.48	-1.73	24.06	4.59	3.96	14.15	3.37	47.4
ZUGSPITZE	414	0.51	4.92	21.43	2.11	2.42	14.31	3.41	47.4
JUNGFRAUJOCH	593	0.48	-10.52	32.58	7.38	4.47	7.63	5.17	46.5
RIKUBETSU	66	0.47	11.87	14.95	-1.62	5.52	29.27	13.53	43.4
BOULDER.CO	363	0.7	0.95	18.79	0.1	1.5	8.2	2.53	40
XIANGHE	1319	0.77	-6.73	18.54	-1.88	0.9	11.16	1.91	39.7
TSUKUBA	456	0.77	23.1	23.6	-1.91	2.57	5.32	6.24	36
IZANA	185	0.78	-12.37	13.96	5.35	1.77	1.18	2.37	28.3
MAUNA.LOA.HI	61	0.04	-13.81	22.54	-	-	-	-	19.5
LA.REUNION.MAIDO	339	0.84	-15.3	14.62	0.05	3.04	10.06	2.2	-21.1
WOLLONGONG	1357	0.75	-12.34	18.58	1.79	1.37	17.78	2.04	-34.4
LAUDER	1132	0.78	1.67	14.63	3.57	1.08	5.34	1.64	-45
MEDIAN	339	0.75	-2.76	18.54	1.55	2.42	9.95	3.37	43.4

Table 4-13 lists the same variables but now for the NDACC stations. Here again we sometimes have very little overlap between the ground-based and satellite measurements. Harestua only features 7 data pairs. The correlation coefficient ranges between 0.04 (Mauna Loa) and 0.84 (Reunion). The bias ranges between -13.81 ppb (Mauna Loa) and 37.83ppb (Harestua) while the scatter ranges between 9.25 ppb (Harestua) and 34.87 ppb (Bremen).

The timeseries below in **Figure 4-33** show individual satellite and ground-based TCCON measurements, while **Figure 4-34** does the same for NDACC. For TCCON we see that SRFP generally manages to capture the seasonal cycle. While the scatter is somewhat higher for SRFP XCH_4, compared to TCCON, it is relatively free of outliers. Looking at the timeseries the observed bias shift seen in the TCCON mosaic plot is far less obvious due to the scatter in both TCCON and SRFP data. However if we look closely at such stations as Edwards etc. we do see that the bias at the beginning of the timeseries is different from that at the end.

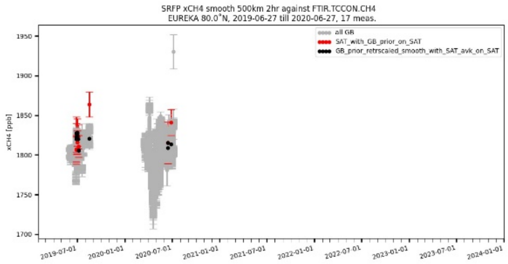
SRFP xCH4 smooth 500km 2hr against FTIR.TCCON.CH4
EUREKA 80.0°N, 2019-06-27 till 2020-06-27, 17 meas.

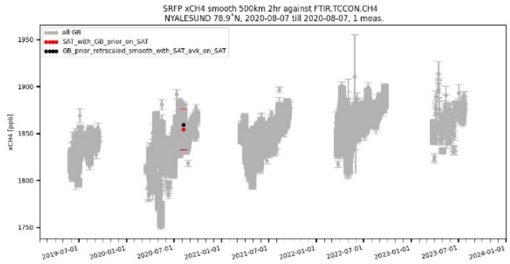
SRFP xCH4 smooth 500km 2hr against FTIR.TCCON.CH4
NYALESUND 78.9°N, 2020-08-07 till 2020-08-07, 1 meas.

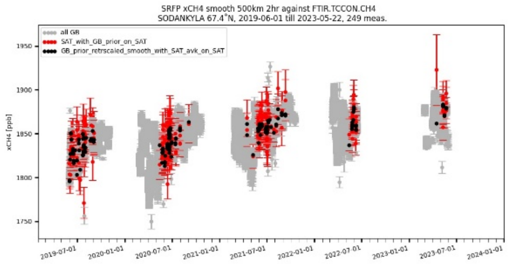
SRFP xCH4 smooth 500km 2hr against FTIR.TCCON.CH4
SODANKYLA 67.4°N, 2019-06-01 till 2023-05-22, 249 meas.

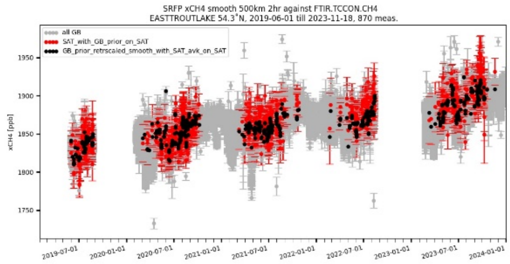
SRFP xCH4 smooth 500km 2hr against FTIR.TCCON.CH4
EASTTROUTLAKE 54.3°N, 2019-06-01 till 2023-11-18, 870 meas.

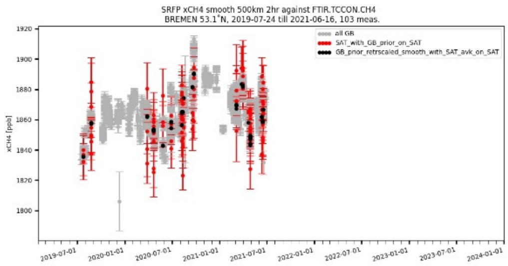
SRFP xCH4 smooth 500km 2hr against FTIR.TCCON.CH4
BREMEN 53.1°N, 2019-07-24 till 2021-06-16, 103 meas.

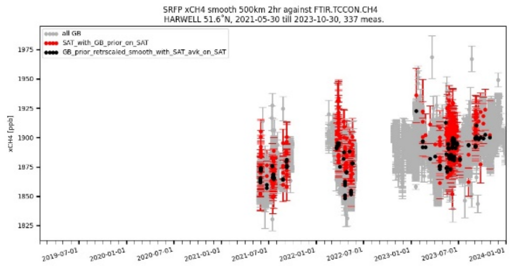
SRFP xCH4 smooth 500km 2hr against FTIR.TCCON.CH4
HARWELL 51.6°N, 2021-05-30 till 2023-10-30, 337 meas.

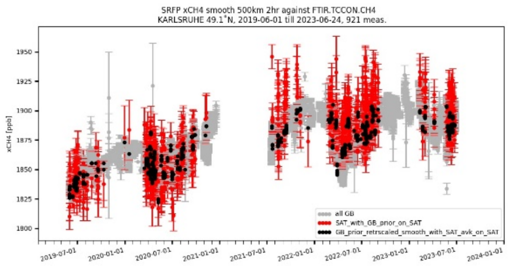
SRFP xCH4 smooth 500km 2hr against FTIR.TCCON.CH4
KARLSRUHE 49.1°N, 2019-06-01 till 2023-06-24, 921 meas.

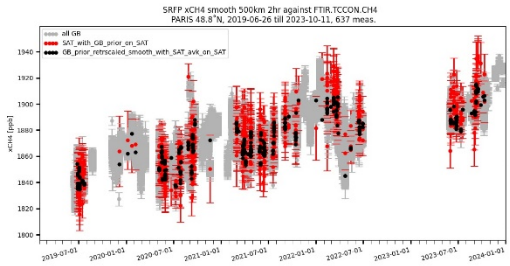
SRFP xCH4 smooth 500km 2hr against FTIR.TCCON.CH4
PARIS 48.8°N, 2019-06-26 till 2023-10-11, 637 meas.

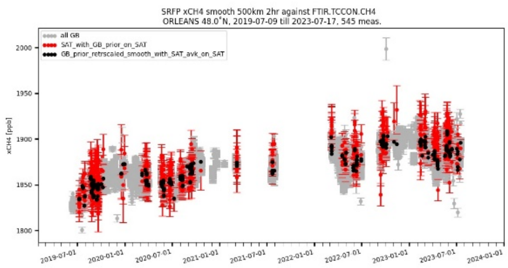
SRFP xCH4 smooth 500km 2hr against FTIR.TCCON.CH4
ORLEANS 48.0°N, 2019-07-09 till 2023-07-17, 545 meas.

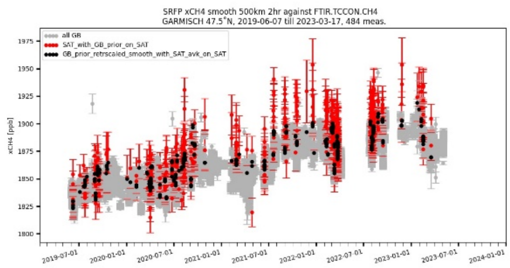
SRFP xCH4 smooth 500km 2hr against FTIR.TCCON.CH4
GARMISCH 47.5°N, 2019-06-07 till 2023-03-17, 484 meas.

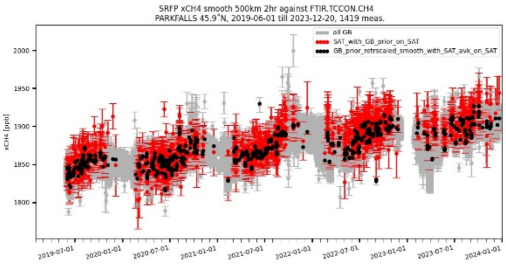
SRFP xCH4 smooth 500km 2hr against FTIR.TCCON.CH4
PARKFALLS 45.9°N, 2019-06-01 till 2023-12-20, 1419 meas.
all GB
SAT_with_GB_prior_on_SAT
GB_prior_retrscaled_smooth_with_SAT_avk_on_SAT
xCH4 [ppb]

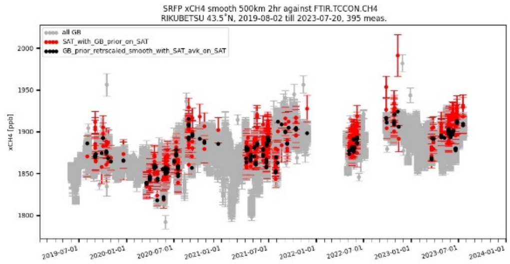
SRFP xCH4 smooth 500km 2hr against FTIR.TCCON.CH4
RIKUBETSU 43.5°N, 2019-08-02 till 2023-07-20, 395 meas.
all GB
SAT_with_GB_prior_on_SAT
GB_prior_retrscaled_smooth_with_SAT_avk_on_SAT
xCH4 [ppb]

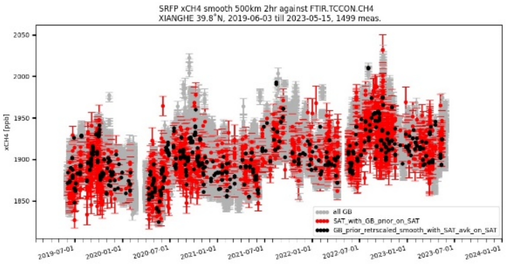
SRFP xCH4 smooth 500km 2hr against FTIR.TCCON.CH4
XIANGHE 39.8°N, 2019-06-03 till 2023-05-15, 1499 meas.
all GB
SAT_with_GB_prior_on_SAT
GB_prior_retrscaled_smooth_with_SAT_avk_on_SAT
xCH4 [ppb]

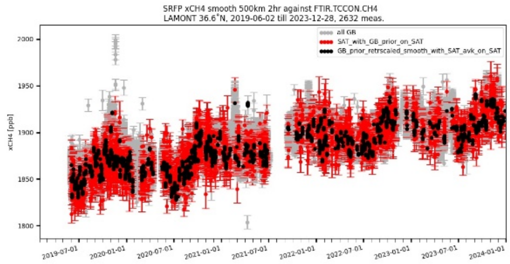
SRFP xCH4 smooth 500km 2hr against FTIR.TCCON.CH4
LAMONT 36.6°N, 2019-06-02 till 2023-12-28, 2632 meas.
all GB
SAT_with_GB_prior_on_SAT
GB_prior_retrscaled_smooth_with_SAT_avk_on_SAT
xCH4 [ppb]

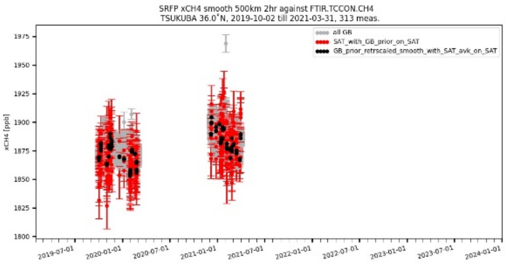
SRFP xCH4 smooth 500km 2hr against FTIR.TCCON.CH4
TSUKUBA 36.0°N, 2019-10-02 till 2021-03-31, 313 meas.
all GB
SAT_with_GB_prior_on_SAT
GB_prior_retrscaled_smooth_with_SAT_avk_on_SAT
xCH4 [ppb]

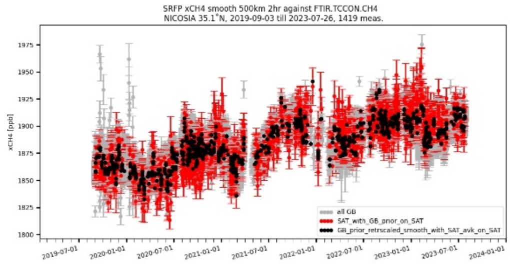
SRFP xCH4 smooth 500km 2hr against FTIR.TCCON.CH4
NICOSIA 35.1°N, 2019-09-03 till 2023-07-26, 1419 meas.
all GB
SAT_with_GB_prior_on_SAT
GB_prior_retrscaled_smooth_with_SAT_avk_on_SAT
xCH4 [ppb]

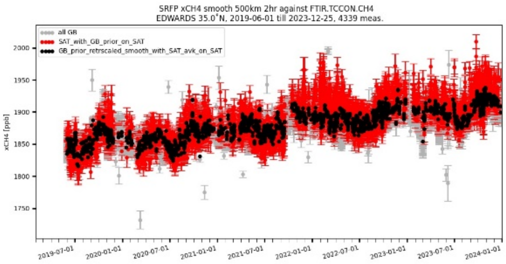
SRFP xCH4 smooth 500km 2hr against FTIR.TCCON.CH4
EDWARDS 35.0°N, 2019-06-01 till 2023-12-25, 4339 meas.
all GB
SAT_with_GB_prior_on_SAT
GB_prior_retrscaled_smooth_with_SAT_avk_on_SAT
xCH4 [ppb]

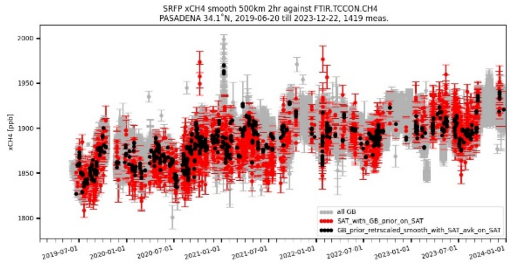
SRFP xCH4 smooth 500km 2hr against FTIR.TCCON.CH4
PASADENA 34.1°N, 2019-06-20 till 2023-12-22, 1419 meas.
all GB
SAT_with_GB_prior_on_SAT
GB_prior_retrscaled_smooth_with_SAT_avk_on_SAT
xCH4 [ppb]

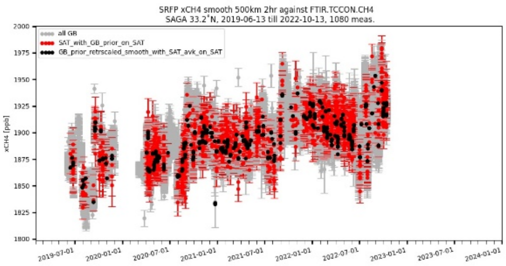
SRFP xCH4 smooth 500km 2hr against FTIR.TCCON.CH4
SAGA 33.2°N, 2019-06-13 till 2022-10-13, 1080 meas.
all GB
SAT_with_GB_prior_on_SAT
GB_prior_retrscaled_smooth_with_SAT_avk_on_SAT
xCH4 [ppb]

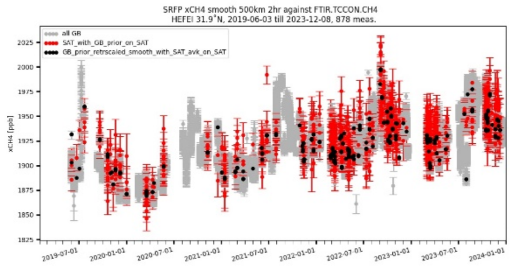
SRFP xCH4 smooth 500km 2hr against FTIR.TCCON.CH4
HEFEI 31.9°N, 2019-06-03 till 2023-12-08, 878 meas.
all GB
SAT_with_GB_prior_on_SAT
GB_prior_retrscaled_smooth_with_SAT_avk_on_SAT
xCH4 [ppb]

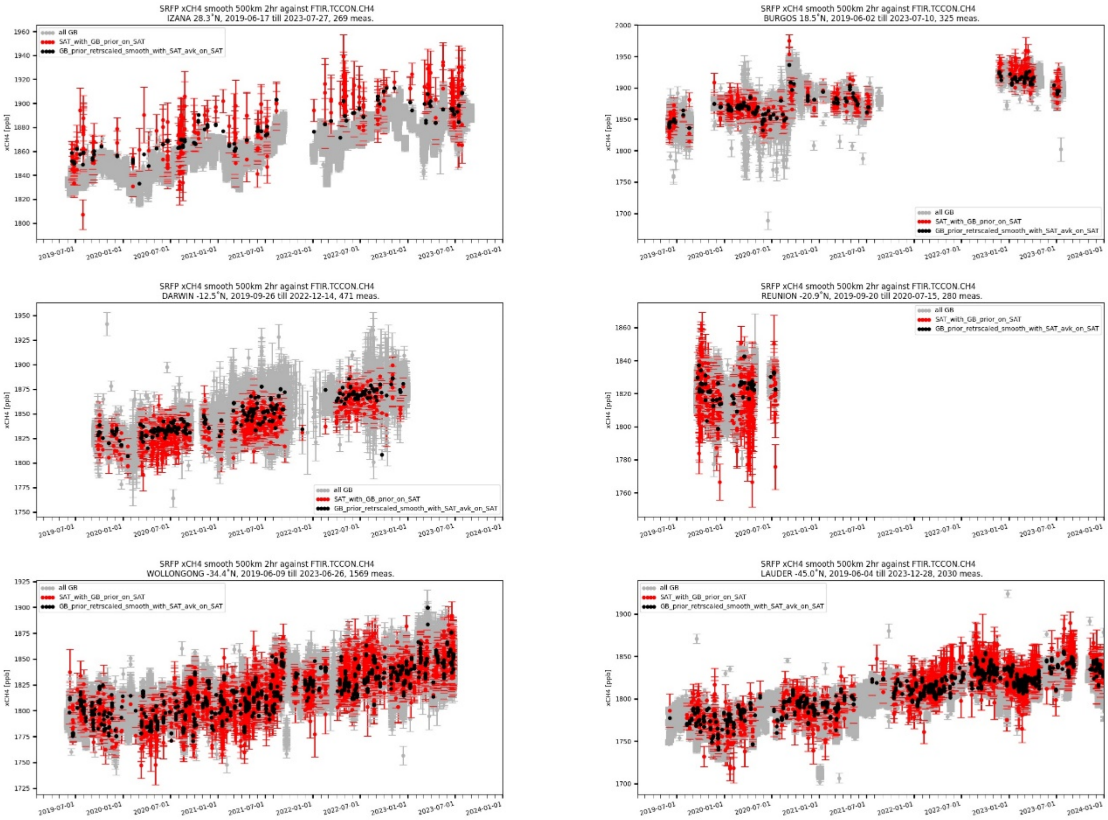

Figure 4-33: XCH_4 timeseries at all TCCON sites (red= CH4_GO2_SRFP data, black is collocated TCCON data and grey are the uncollocated TCCON data).

For NDACC it is clear that SRFP exhibits the same or at some stations even smaller temporal variability than NDACC. Also clearly visible is the sparsness of the dataset, with either little coverage at all, or significant datagaps in the timeseries. For stations where we do have consistent longer sampling, such as Garmisch, Boulder and Lauder, we see that NDACC and SRFP are in good agreement. For Toronto we clearly see the high variability in the NDACC data, worsening in the later stages of the time series, but as this is a consistent feature across all algorithms, it is most likely due to an issue with the NDACC data at this station.

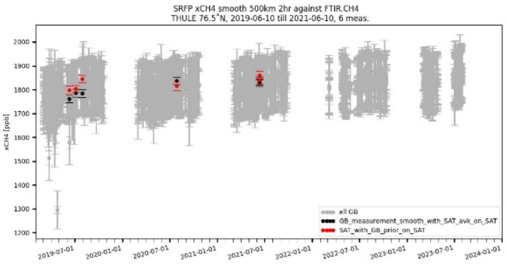
SRFP xCH4 smooth 500km 2hr against FTIR.CH4
THULE 76.5°N, 2019-06-10 till 2021-06-10, 6 meas.

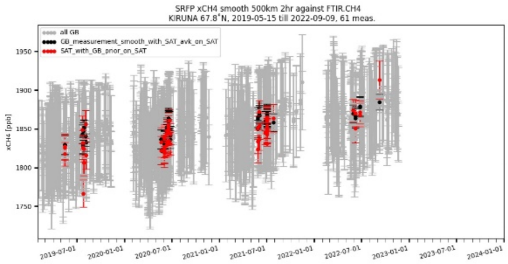
SRFP xCH4 smooth 500km 2hr against FTIR.CH4
KIRUNA 67.8°N, 2019-05-15 till 2022-09-09, 61 meas.

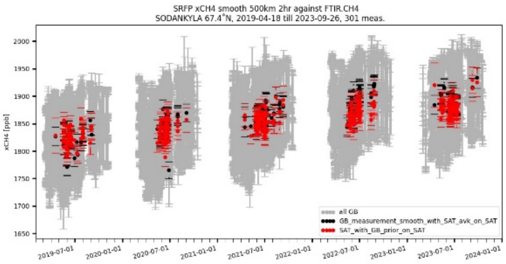
SRFP xCH4 smooth 500km 2hr against FTIR.CH4
SODANKYLA 67.4°N, 2019-04-18 till 2023-09-26, 301 meas.

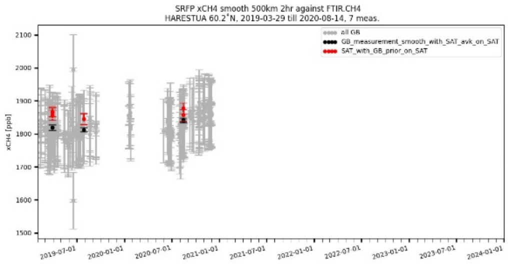
SRFP xCH4 smooth 500km 2hr against FTIR.CH4
HARESTUA 60.2°N, 2019-03-29 till 2020-08-14, 7 meas.

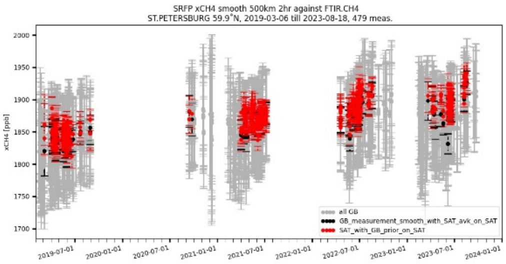
SRFP xCH4 smooth 500km 2hr against FTIR.CH4
ST.PETERSBURG 59.9°N, 2019-03-06 till 2023-08-18, 479 meas.

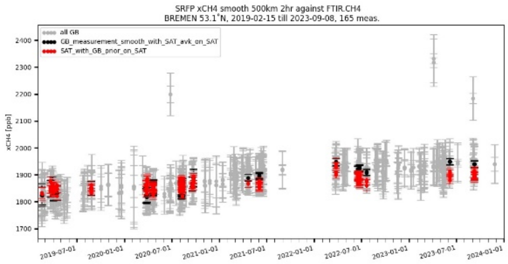
SRFP xCH4 smooth 500km 2hr against FTIR.CH4
BREMEN 53.1°N, 2019-02-15 till 2023-09-08, 165 meas.

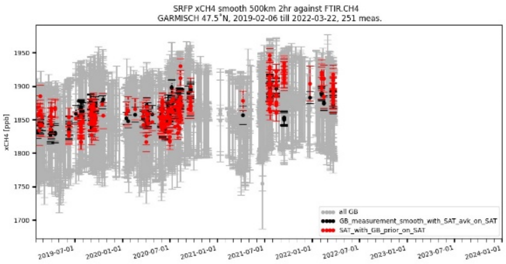
SRFP xCH4 smooth 500km 2hr against FTIR.CH4
GARMISCH 47.5°N, 2019-02-06 till 2022-03-22, 251 meas.

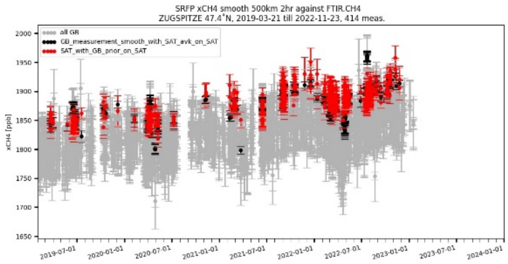
SRFP xCH4 smooth 500km 2hr against FTIR.CH4
ZUGSPITZE 47.4°N, 2019-03-21 till 2022-11-23, 414 meas.

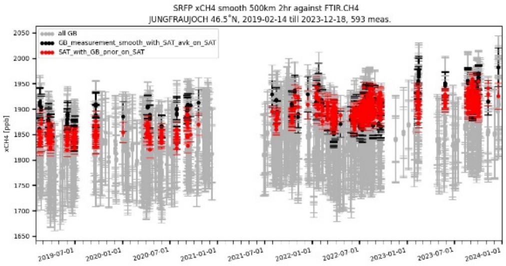
SRFP xCH4 smooth 500km 2hr against FTIR.CH4
JUNGFRAUJOCH 46.5°N, 2019-02-14 till 2023-12-18, 593 meas.

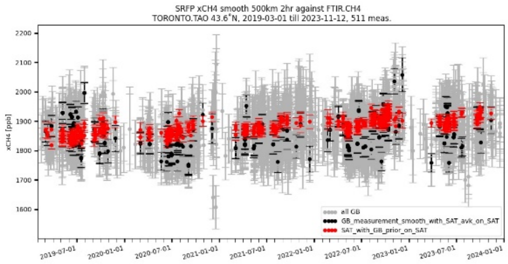
SRFP xCH4 smooth 500km 2hr against FTIR.CH4
TORONTO.TAO 43.6°N, 2019-03-01 till 2023-11-12, 511 meas.

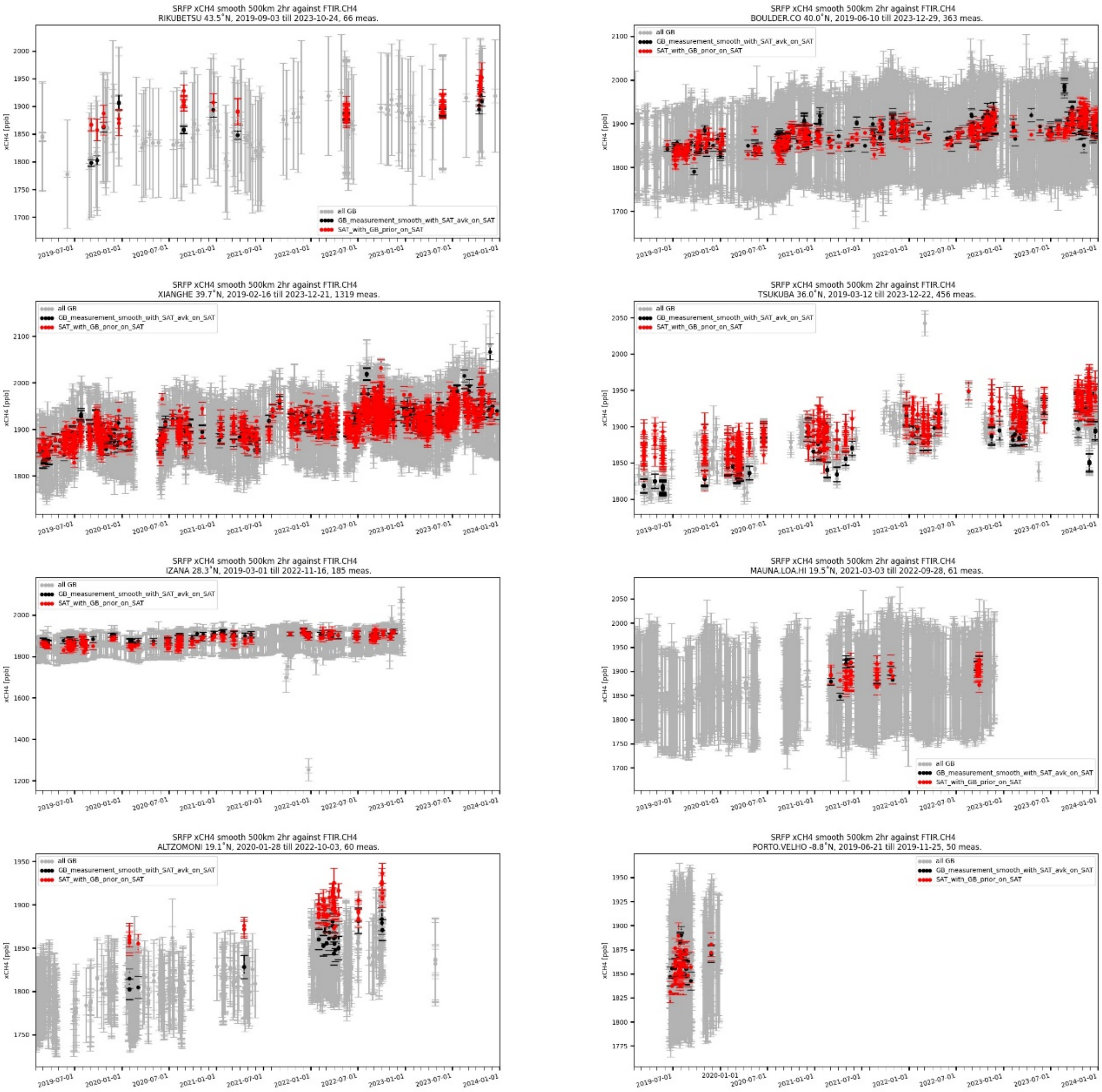

SRFP xCH4 smooth 500km 2hr against FTIR.CH4
RIKUBETSU 43.5°N, 2019-09-03 till 2023-10-24, 66 meas.
SRFP xCH4 smooth 500km 2hr against FTIR.CH4
BOULDER.CO 40.0°N, 2019-06-10 till 2023-12-29, 363 meas.
SRFP xCH4 smooth 500km 2hr against FTIR.CH4
XIANGHE 39.7°N, 2019-02-16 till 2023-12-21, 1319 meas.
SRFP xCH4 smooth 500km 2hr against FTIR.CH4
TSUKUBA 36.0°N, 2019-03-12 till 2023-12-22, 456 meas.
SRFP xCH4 smooth 500km 2hr against FTIR.CH4
IZANA 28.3°N, 2019-03-01 till 2022-11-16, 185 meas.
SRFP xCH4 smooth 500km 2hr against FTIR.CH4
MAUNA.LOA.HI 19.5°N, 2021-03-03 till 2022-09-28, 61 meas.
SRFP xCH4 smooth 500km 2hr against FTIR.CH4
ALTZOMONI 19.1°N, 2020-01-28 till 2022-10-03, 60 meas.
SRFP xCH4 smooth 500km 2hr against FTIR.CH4
PORTO.VELHO -8.8°N, 2019-06-21 till 2019-11-25, 50 meas.
all GB
GB_measurement_smooth_with_SAT_avk_on_SAT
SAT_with_GB_prior_on_SAT
xCH4 [ppb]

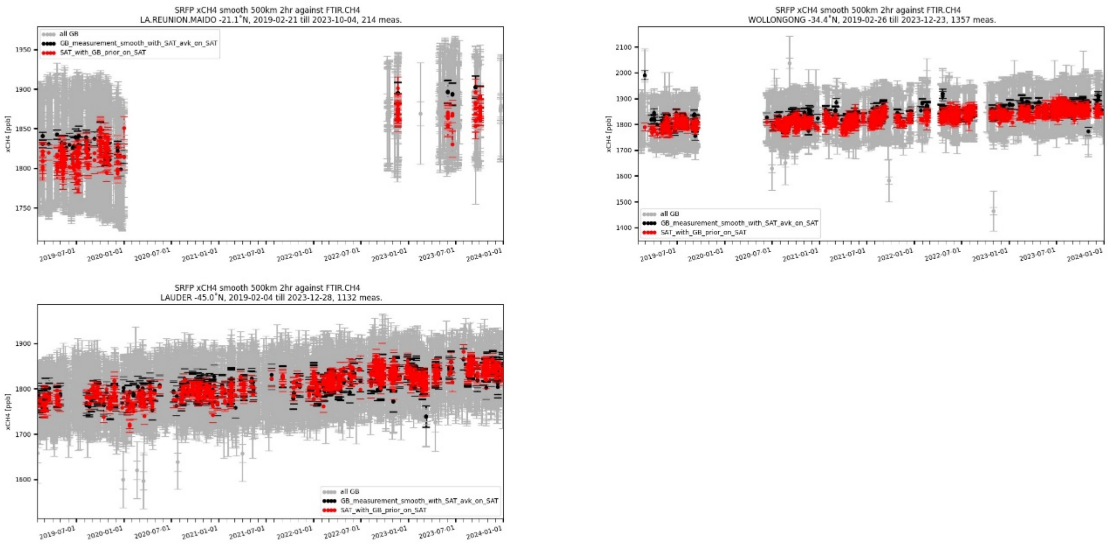

Figure 4-34: Timeseries of XCH_4 NDACC (collocated=black, all=grey) and CH4_GO2_SRFP (red) data at all NDACC sites.

Figure 4-35 shows monthly median timeseries for TCCON and SRFP XCH_4 for all data that fall within certain latitude bands, namely all sites North of 40°N latitude (top), all sites between 40°N and the equator (mid) and all sites in the Southern hemisphere (bottom). The plots also show the trend results of a trend+seasonality fit. Here we see a modest 1.9 ppb/year trend difference above 40°N, a stronger 2.8 ppb/year trend difference between 0° and 40°N and again a 2.7 ppb/year difference in the Southern hemisphere. However in all cases the combined uncertainty overlaps with these differences. Rather than a gradual trend mismath the plot seems to indicate a bias shift at the end of 2021 (particularly visible in the N40 plot). Since this plot comprises of all timeseries taken at all stations within certain latitude bands and signifact gaps in timeseries do occur on a station by station level this could simply be a feature caused by changes in the overall constellation. While the mosaic plot hinted at a seasonal component in the bias, this observation is far less evident here.

Figure 4-36 shows the same but for NDACC. Here we see a far more inconsistent picture with both stronger trends for the Satellite data (Southern hemisphere and >40°N) as well as weaker trends (N00). However the dataset used is extremely sparse with large gaps in the timeseries.

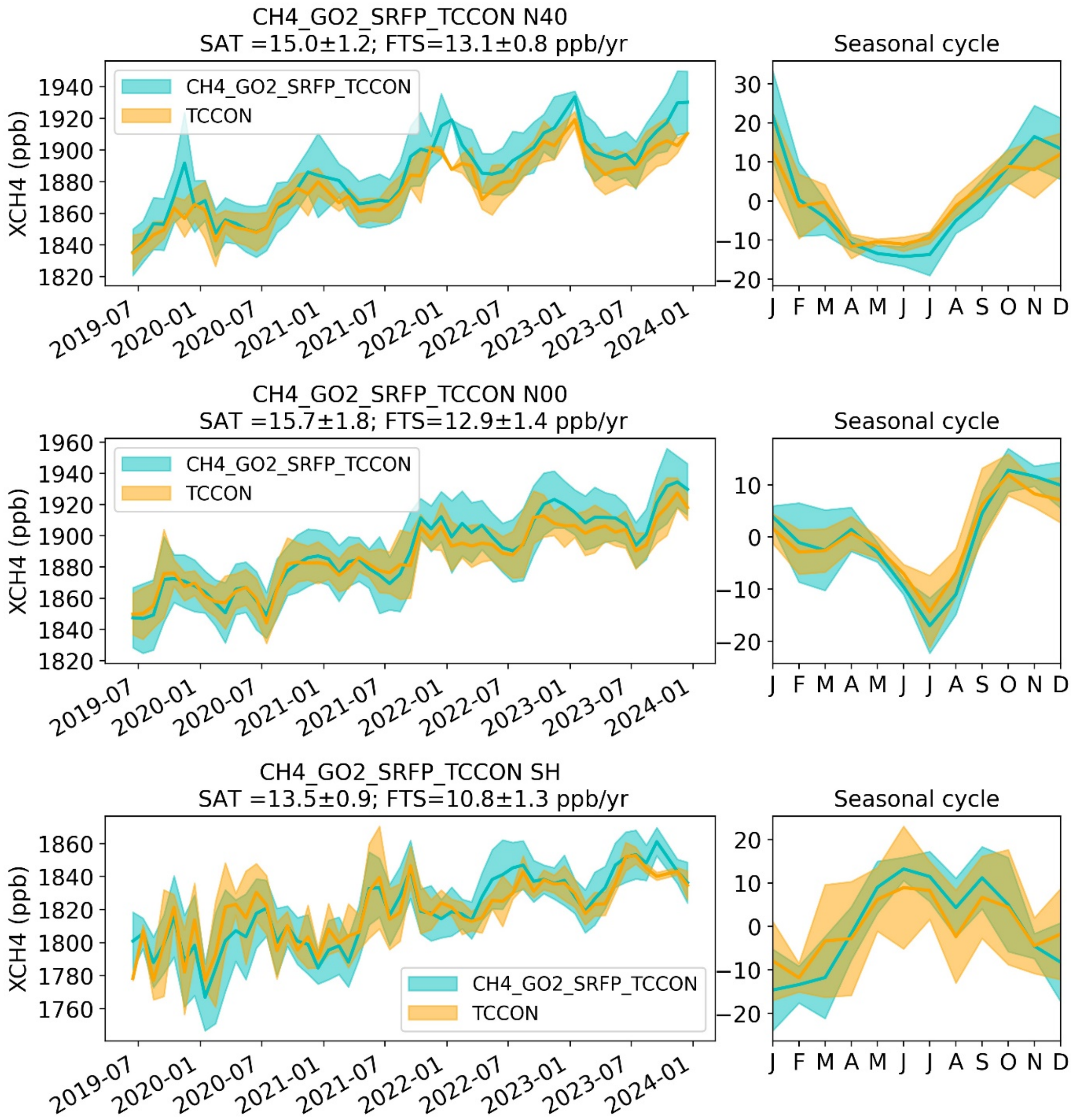

Figure 4-35: Monthly median collocated Sat and TCCON XCH_4 concentrations as a function of time. The shaded areas correspond with the scaled median absolute deviation.

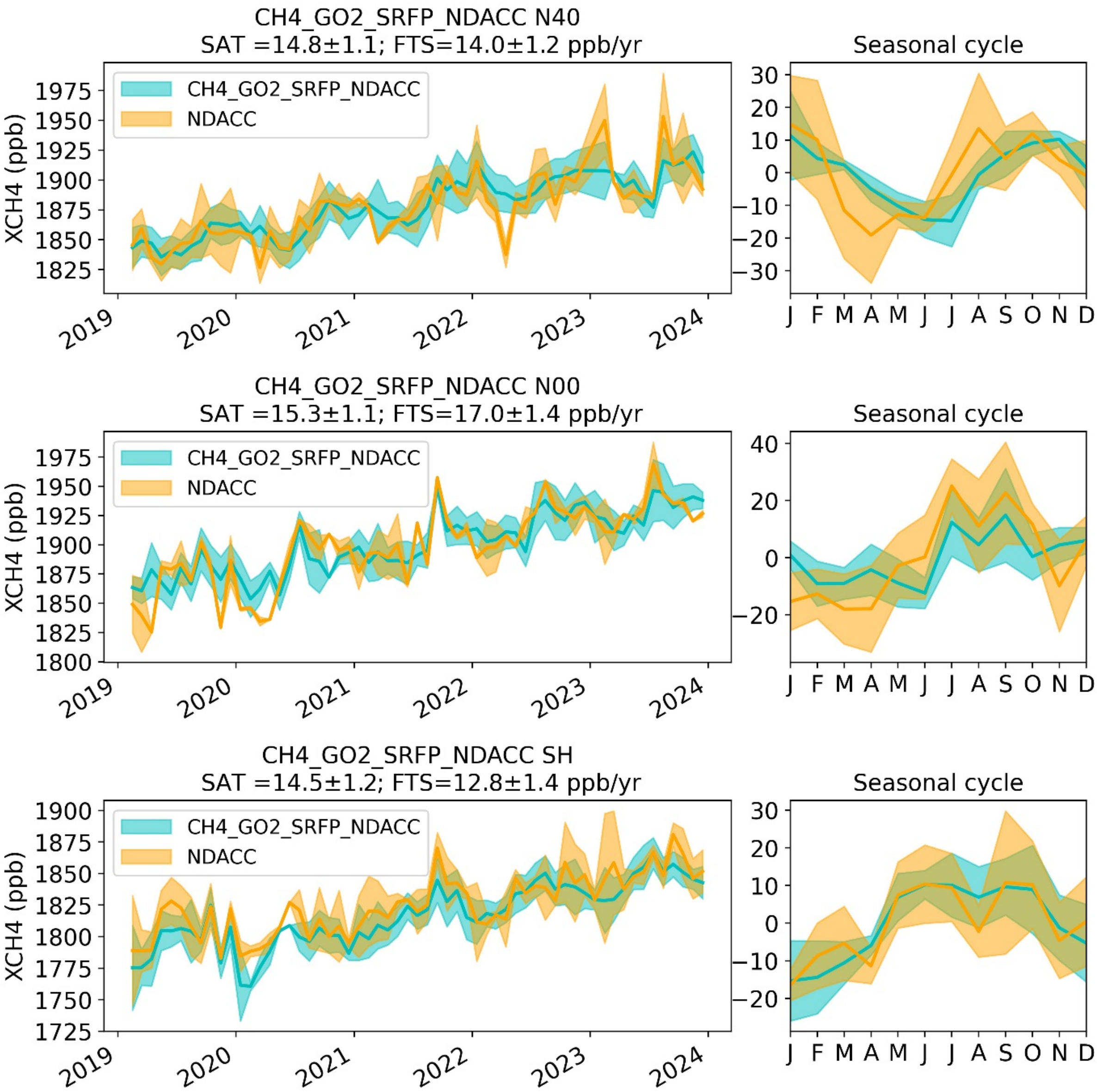

Figure 4-36: Monthly median collocated Sat and NDACC XCH_4 concentrations as a function of time. The shaded areas correspond with the scaled median absolute deviation.

4.2.5.2 Summary

Listed in the table below (**Table 4-14**) are the Figure of Merit parameters as derived from the individual collocated data pairs at each station.

SRFP XCH_4's single measurement precision equals 13.9 ppb, reaching the Breakthrough target of <17 ppb. The error assessment is slightly underestimated with an uncertainty ratio of 0.82. The median bias equals 2.9 ppb and is significant with confidence bands between 0.8 and 4.2 ppb. Both the spatial and spatio-temporal relative accuracies reach the <10 ppb target. A drift of 1.7 ppb/year is observed with confidence bands between 1.0 and 2.0 ppb/year. This is smaller than the <3 ppb/year requirement.

For NDACC, we obtain a single measurement precision of 20.7 [20.1, 22.2] ppb, a negative but not significant median bias of -2.8 [-10.4, 5.0] ppb. The median relative accuracy numbers do not meet the target but exhibit very large uncertainty bands (RA 11.5 [3.2, 19.8] ppb, SRA 14.9 [11.5, 19.2] ppb). Given these uncertainties, all obtained data overlap with our TCCON analysis.

Table 4-14 presents an overview of the estimated data quality of CH4_GO2_SRFP, as obtained by the VALT team, from comparisons with TCCON ground-based reference observations. Values in square brackets [ ] correspond with the upper and lower 95% confidence bound on the parameter. The uncertainty ratio features 2 numbers as outlined in the validation method.

Product Quality Summary Table for Product: CH4_GO2_SRFP Level: 2, Version: v02.0.3, Time period covered: 2.2019 – 1.2024 Assessment: Validation Team (VALT)			
Parameter [unit]	**Achieved performance**	**Requirement**	**Comments**
Single measurement precision (1-sigma) in [ppm]	13.9 [13.2,15.2]	< 34 (T) < 17 (B) < 9 (G)	Computed as the median over all station scaled median absolute differences to TCCON
Uncertainty ratio [-]: Ratio reported uncertainty to standard deviation of satellite-TCCON difference	0.81, 0.82*	-	No requirement but value close to unity expected for a high quality data product with reliable reported uncertainty.
Median bias (global offset) [ppm]	2.9 [0.8,4.2]	-	No requirement but value close to zero expected for a high quality data product.
Accuracy: Relative systematic error [ppm]	Spatial: 3.1 [1.1,4.7] Spatio-temporal: 5.7 [3.9,7.2]	< 10	Spatial: Computed as standard deviation of the biases at the various TCCON sites. Spatio-temporal: As "Spatial" but also considering seasonal biases.
Stability: Drift [ppm/year]	1.7 [1.0, 2.0]	< 3	Linear drift

4.2.6 Validation results for product CH4_GO2_SRPR

Below we show the validation results of the XCH_4 concentrations as derived by the CH4_GO2_SRPR v2.0.3 algorithm using GOSAT-2 spectra. 'PR' stands for the proxy version of the algorithm developed at SRON, whereby the retrieved CH_4 concentration is scaled by the modelled CO_2/retrieved CO_2 ratio. Data was available from February 2019 up to and including December 2023. The SRPR algorithm provides *a priori* and column averaging kernel data on a 3-layer vertical profile.

4.2.6.1 Detailed results

The Taylor diagram below in **Figure 4-37** yields a concise overview of the capabilities of the CH4_GO2_SRPR algorithm. Almost all TCCON sites cluster between the 0.6 and 0.8 correlation line. The TCCON scatter is smaller than that of SRPR while the variability of the bias roughly ranges between 0.6 and 0.8, relative to the SRPR variability. These results are very similar to the ones obtained from its Full Physics counterpart (see **Figure 4-24**).

Figure 4-38 yields the same information but for the NDACC comparisons. Again, we see more dispersion as compared to TCCON. Mauna Loa and Eureka even have negative correlation coefficients. At the same time there are manys stations where the NDACC scatter is higher than observed by SRPR.

In the mosaic plot analysis of the SRFP product (Figure 4-31) we saw a shift towards more positive biases at the end of 2021. Compared to SRFP, when looking at the mosaic plot for TCCON (**Figure 4-39**), we see more consistent positive biases across all latitudes and times. Again we see a significant shift towards more positive biases at the end of 2021. However unlike with SRFP, where this positive bias shift seemed to persist till the end of the measured period, for SRPR biases tend to return to pre-2022 levels from the start of 2023 onwards.

Figure 4-40 shows the same but for NDACC. Here we see more data gaps which hampers our ability to draw conclusions. Station to station biases are also (again) far more outspoken. Even so we also see hints of the 2022 bias increase in the NDACC comparison.

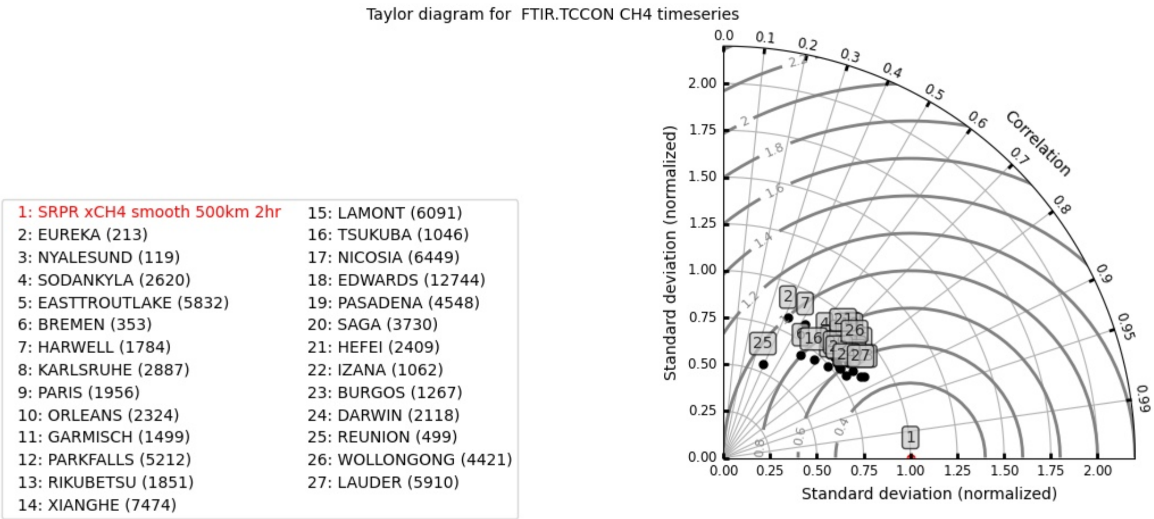

Figure 4-37: Tayor plot of XCH_4 TCCON values relative to CH4_GO2_SRPR. Straight lines correspond with the correlation, light grey lines yield the variability of the TCCON data relative to the satellite variability and the dark grey lines correspond with the variability of the Satellite -TCCON bias relative to the satellite variability.

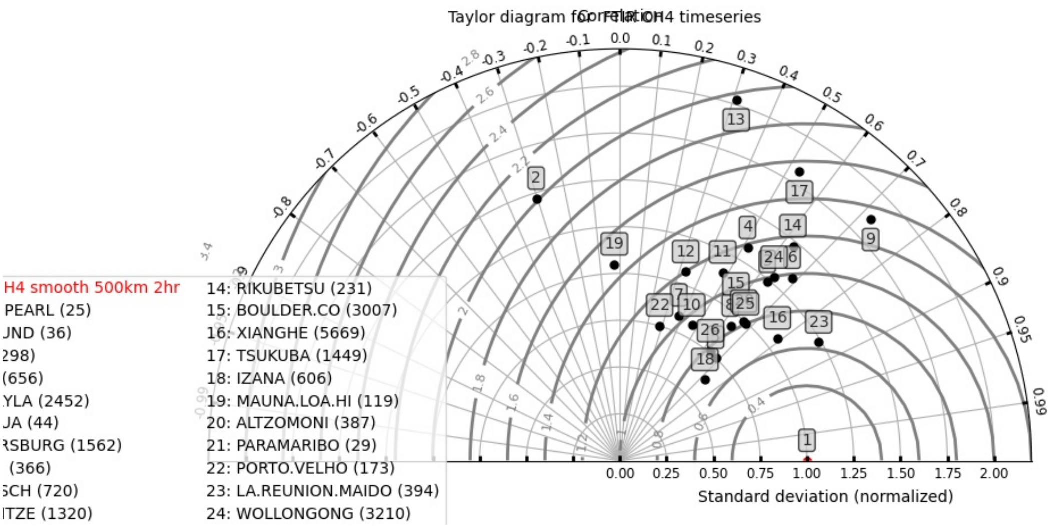

Figure 4-38: Tayor plot of XCH_4 NDACC values relative to CH4_GO2_SRPR. Straight lines correspond with the correlation, light grey lines yield the variability of the NDACC data relative to the satellite variability and the dark grey lines correspond with the variability of the Satellite –NDACC bias relative to the satellite variability.

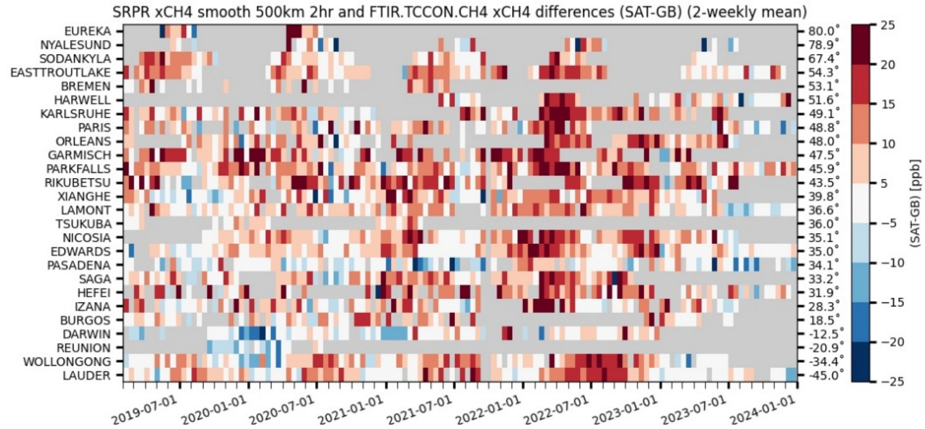

Figure 4-39. Mosaic plot of bi-weekly mean CH4_GO2_SRPR - TCCON XCH_4 biases as a function of time and TCCON station.

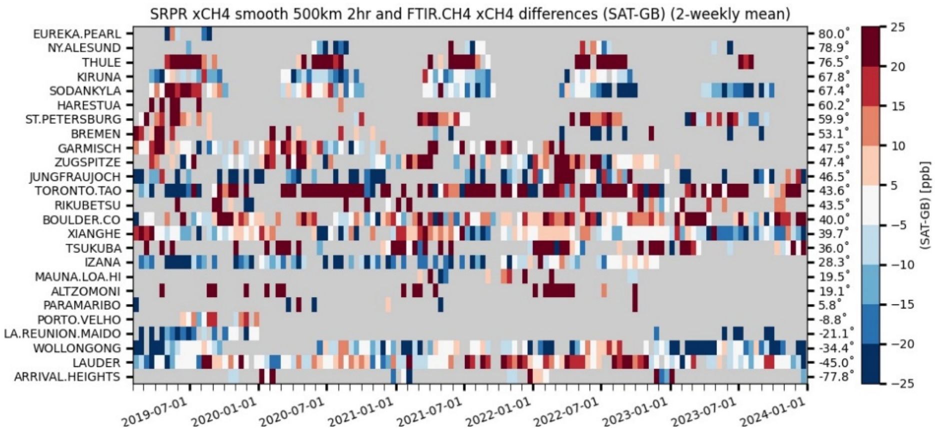

Figure 4-40. Mosaic plot of bi-weekly mean CH4_GO2_SRPR - NDACC XCH_4 biases as a function of time and NDACC station.

Table 4-15 lists all bias and scatter results derived from individual data pairs at all TCCON stations. The Proxy version of the algorithm produces roughly 4 times (note that in the previous PVIR iteration this was 2 times) as many collocated data pairs than its Full Physics counterpart, with on average ~2400 data pairs per station, which corresponds with ~480 pairs per station per year.. While the data density is higher, the single measurement precision is also somewhat higher (15.1 ppb for SRPR vs. 13.9 ppb for SRFP) with values ranging between 12.1 ppb (Darwin) and 18.11 ppb (Xianghe). This in turn impacts the median correlation values (0.79 for SRFP vs. 0.75 for SRPR). The correlation using all data regardless of station yields 0.89 which is only slightly below SRFP's 0.91.

Table 4-15: Number of collocated data pairs (N), Correlation (R), Bias, Scatter, long term trend difference (ltt) and uncertainty thereon (ltt_err), seasonal amplitude difference (A) and uncertainty thereon (A_err) as well as the latitude of the TCCON station. The last row lists the median values over all stations. Product: CH4_GO2_SRPR.

STATION	N	R	Bias	Scat	ltt	ltt_err	A	A_err	lat
EUREKA	213	0.42	10.75	17.21	-	-	-	-	80
NYALESUND	119	0.75	2.19	18.05	-0.81	1.83	3.07	7.33	78.9
SODANKYLA	2620	0.67	6.17	17.43	-2.62	0.97	3.55	1.07	67.4
EASTTROUTLAKE	5832	0.75	8.01	17.6	-0.55	0.43	4.11	0.74	54.3
BREMEN	353	0.6	7.21	15.96	-	-	-	-	53.1
HARWELL	1784	0.52	9.02	16.69	-	-	-	-	51.6
KARLSRUHE	2887	0.75	11.81	16.87	2.58	0.55	5.23	1.03	49.1
PARIS	1956	0.75	6.77	16	0.82	0.67	7.55	1.17	48.8
ORLEANS	2324	0.79	8.79	14.92	0.5	0.73	3.35	1.04	48
GARMISCH	1499	0.74	14.91	15.97	1.52	0.94	4.4	1.26	47.5
PARKFALLS	5212	0.76	8.5	16.19	0.11	0.5	4.83	0.78	45.9
RIKUBETSU	1851	0.79	14.24	14.73	1.6	0.96	3.12	1.32	43.5
XIANGHE	7474	0.78	6.86	18.11	1.46	0.69	6.39	1.05	39.8
LAMONT	6091	0.81	7.38	14.01	-0.31	0.49	3.23	0.7	36.6
TSUKUBA	1046	0.68	5.91	12.63	-	-	-	-	36
NICOSIA	6449	0.75	8.74	13.82	1.19	0.63	6.81	0.65	35.1
EDWARDS	12744	0.83	5.41	14.11	-0.05	0.4	5.33	0.56	35
PASADENA	4548	0.74	-2.21	14.45	0.51	0.61	3.21	0.8	34.1
SAGA	3730	0.77	10.17	14.75	2.43	0.99	5.28	1.03	33.2
HEFEI	2409	0.71	10.95	17.35	-0.94	0.73	1.14	1.93	31.9
IZANA	1062	0.79	2.78	14.98	0.58	0.62	8.12	0.96	28.3
BURGOS	1267	0.86	6.1	12.48	1.42	0.97	4.2	1.35	18.5
DARWIN	2118	0.83	1.13	12.14	3.42	0.79	3.59	0.81	-12.5
REUNION	499	0.39	-7.01	12.82	-	-	-	-	-20.9
WOLLONGONG	4421	0.78	6.46	15.24	1.61	0.56	7.82	0.78	-34.4
LAUDER	5910	0.86	5.8	13.12	-0.19	0.55	7.91	0.68	-45
MEDIAN	2366.5	0.75	7.035	15.11	0.58	0.67	4.4	1.03	38.2

Table 4-16 shows the same but for NDACC. Correlation numbers range between -0.3 (Eureka) and 0.85 (Reunion) and scatter ranges between 13.9 ppb (Reunion Maïdo again) and 34.3 ppb (Jungfraujoch). The median bias equals 1.6 ppb, but with much larger interstation variability compared to SRFP (from -18.1 ppb at Eureka to 33.3 ppb at Harestua). Note that we (again) have excluded Altzomoni, Toronto, Thule, Paramaribo and Porto Velho from the analysis. Long term trend values range between -11.8 ppb/year at Bremen and 7.4 ppb/year at Garmisch. Noting that many stations suffer from significant gaps in their data.

Table 4-16: Number of collocated data pairs (N), Correlation (R), Bias, Scatter, long term trend difference (ltt) and uncertainty thereon (ltt_err), seasonal amplitude difference (A) and uncertainty thereon (A_err) as well as the latitude of the NDACC station. The last row lists the median values over all stations. Product: CH4_GO2_SRPR.

STATION	N	R	Bias	Scat	ltt	ltt_err	A	A_err	lat
EUREKA.PEARL	25	-0.3	-18.14	28.39	-	-	-	-	80
NY.ALESUND	36	0.64	-8.9	27.1	0.77	4.79	18.91	17.09	78.8
KIRUNA	656	0.68	-6.74	17.22	2.53	1.89	7.46	3.57	67.7
SODANKYLA	2452	0.69	-5.53	23.95	-8.0	1.07	9.03	2.22	67.2
HARESTUA	44	0.38	33.27	14.97	-	-	-	-	60.1
ST.PETERSBURG	1562	0.63	15.25	18.96	-0.33	1.05	10.11	2.79	59.7
BREMEN	366	0.72	3.85	34.22	-11.77	7.42	16.36	6.3	53
GARMISCH	720	0.47	5.11	23.34	7.42	2.93	12.24	2.43	47.4
ZUGSPITZE	1320	0.48	10.01	23.51	2.89	2.06	15.4	2.61	47.4
JUNGFRAUJOCH	1369	0.33	-12.74	34.34	5.86	4.88	13.49	4.08	46.5
RIKUBETSU	231	0.63	20.33	19.78	-3.77	8.93	24.06	10.22	43.4
BOULDER.CO	3007	0.6	8.29	18.57	2.79	0.9	5.07	1.73	40
XIANGHE	5669	0.79	-0.23	20.1	-2.55	0.72	9.98	1.2	39.7
TSUKUBA	1449	0.53	21.44	27.08	-5.85	2.78	7.59	7.34	36
IZANA	606	0.72	-14.72	17.7	5.82	1.7	5.06	1.68	28.3
MAUNA.LOA.HI	119	-0.03	-7.68	25	-	-	-	-	19.5
LA.REUNION.MAIDO	577	0.85	-13.9	13.87	-0.53	3.93	9.24	2.8	-21.1
WOLLONGONG	3210	0.64	-7.37	20.62	0.19	1.62	17.38	2.08	-34.4
LAUDER	3054	0.68	3.88	17.86	1.06	1.18	6.91	1.62	-45
ARRIVAL.HEIGHTS	57	0.64	3.35	18.46	-0.03	2.71	23.01	35.92	-77.7
MEDIAN	688	0.635	1.56	20.36	0.19	2.06	10.11	2.79	44.95

The timeseries in **Figure 4-41** show individual satellite and ground-based TCCON measurements. While the scatter is even somewhat higher for SRPR XCH_4 with respect to both TCCON and SRFP, it is again relatively free of outliers and manages to capture (in most cases) TCCON's temporal variability.

Figure 4-42 shows the NDACC correlative data timeseries and here again it is obvious that NDACC in itself shows more variability (which affects single measurement precision and correlation numbers).

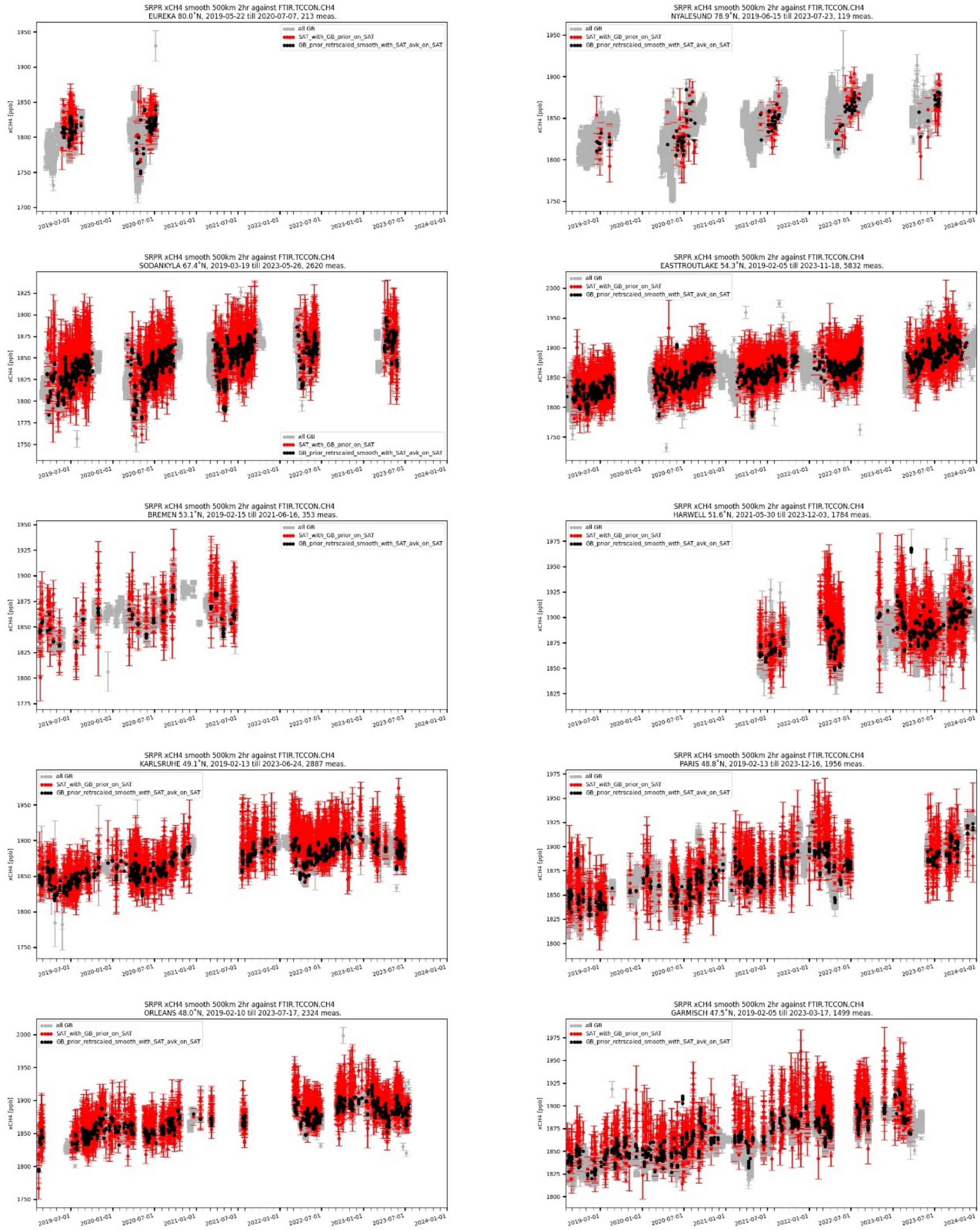

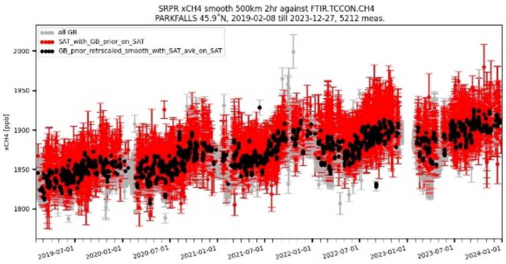

SRPR xCH4 smooth 500km 2hr against FTIR.TCCON.CH4
PARKFALLS 45.9°N, 2019-02-08 till 2023-12-27, 5212 meas.
all GB
SAT_with_GB_prior_on_SAT
GB_prior_retrscaled_smooth_with_SAT_avk_on_SAT
xCH4 [ppb]

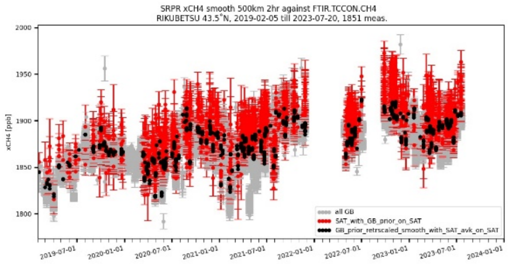

SRPR xCH4 smooth 500km 2hr against FTIR.TCCON.CH4
RIKUBETSU 43.5°N, 2019-02-05 till 2023-07-20, 1851 meas.
all GB
SAT_with_GB_prior_on_SAT
GB_prior_retrscaled_smooth_with_SAT_avk_on_SAT
xCH4 [ppb]

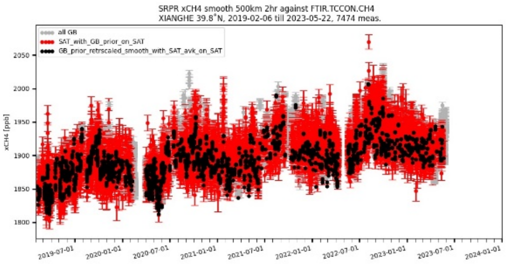

SRPR xCH4 smooth 500km 2hr against FTIR.TCCON.CH4
XIANGHE 39.8°N, 2019-02-06 till 2023-05-22, 7474 meas.
all GB
SAT_with_GB_prior_on_SAT
GB_prior_retrscaled_smooth_with_SAT_avk_on_SAT
xCH4 [ppb]

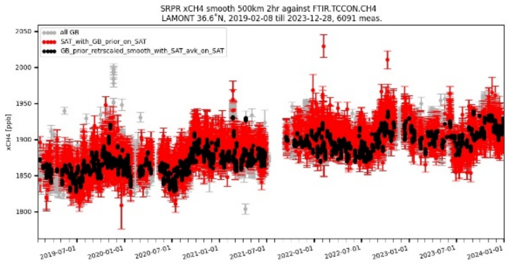

SRPR xCH4 smooth 500km 2hr against FTIR.TCCON.CH4
LAMONT 36.6°N, 2019-02-08 till 2023-12-28, 6091 meas.
all GB
SAT_with_GB_prior_on_SAT
GB_prior_retrscaled_smooth_with_SAT_avk_on_SAT
xCH4 [ppb]

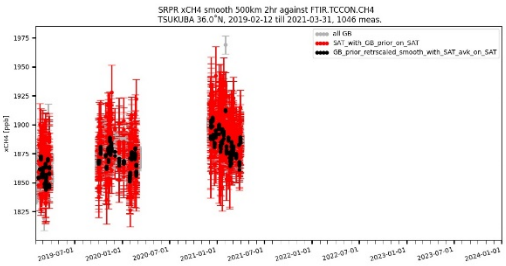

SRPR xCH4 smooth 500km 2hr against FTIR.TCCON.CH4
TSUKUBA 36.0°N, 2019-02-12 till 2021-03-31, 1046 meas.
all GB
SAT_with_GB_prior_on_SAT
GB_prior_retrscaled_smooth_with_SAT_avk_on_SAT
xCH4 [ppb]

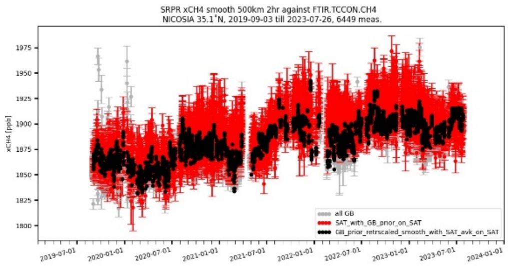

SRPR xCH4 smooth 500km 2hr against FTIR.TCCON.CH4
NICOSIA 35.1°N, 2019-09-03 till 2023-07-26, 6449 meas.
all GB
SAT_with_GB_prior_on_SAT
GB_prior_retrscaled_smooth_with_SAT_avk_on_SAT
xCH4 [ppb]

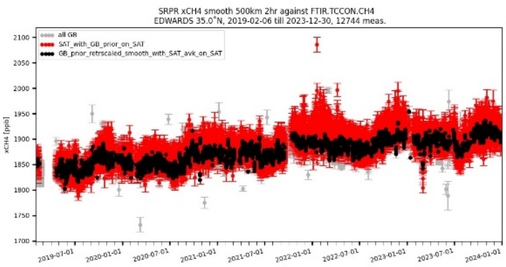

SRPR xCH4 smooth 500km 2hr against FTIR.TCCON.CH4
EDWARDS 35.0°N, 2019-02-06 till 2023-12-30, 12744 meas.
all GB
SAT_with_GB_prior_on_SAT
GB_prior_retrscaled_smooth_with_SAT_avk_on_SAT
xCH4 [ppb]

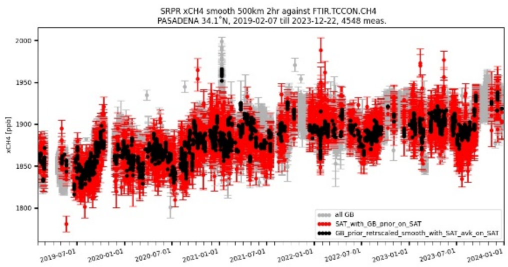

SRPR xCH4 smooth 500km 2hr against FTIR.TCCON.CH4
PASADENA 34.1°N, 2019-02-07 till 2023-12-22, 4548 meas.
all GB
SAT_with_GB_prior_on_SAT
GB_prior_retrscaled_smooth_with_SAT_avk_on_SAT
xCH4 [ppb]

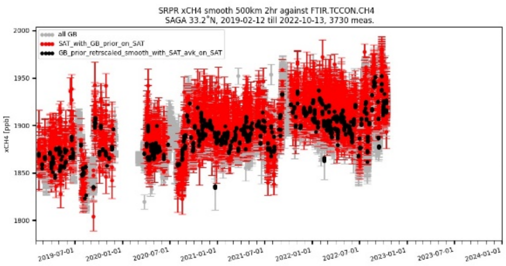

SRPR xCH4 smooth 500km 2hr against FTIR.TCCON.CH4
SAGA 33.2°N, 2019-02-12 till 2022-10-13, 3730 meas.
all GB
SAT_with_GB_prior_on_SAT
GB_prior_retrscaled_smooth_with_SAT_avk_on_SAT
xCH4 [ppb]

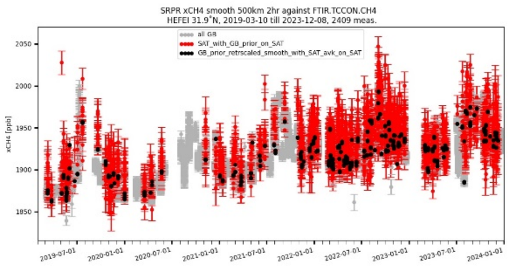

SRPR xCH4 smooth 500km 2hr against FTIR.TCCON.CH4
HEFEI 31.9°N, 2019-03-10 till 2023-12-08, 2409 meas.
all GB
SAT_with_GB_prior_on_SAT
GB_prior_retrscaled_smooth_with_SAT_avk_on_SAT
xCH4 [ppb]

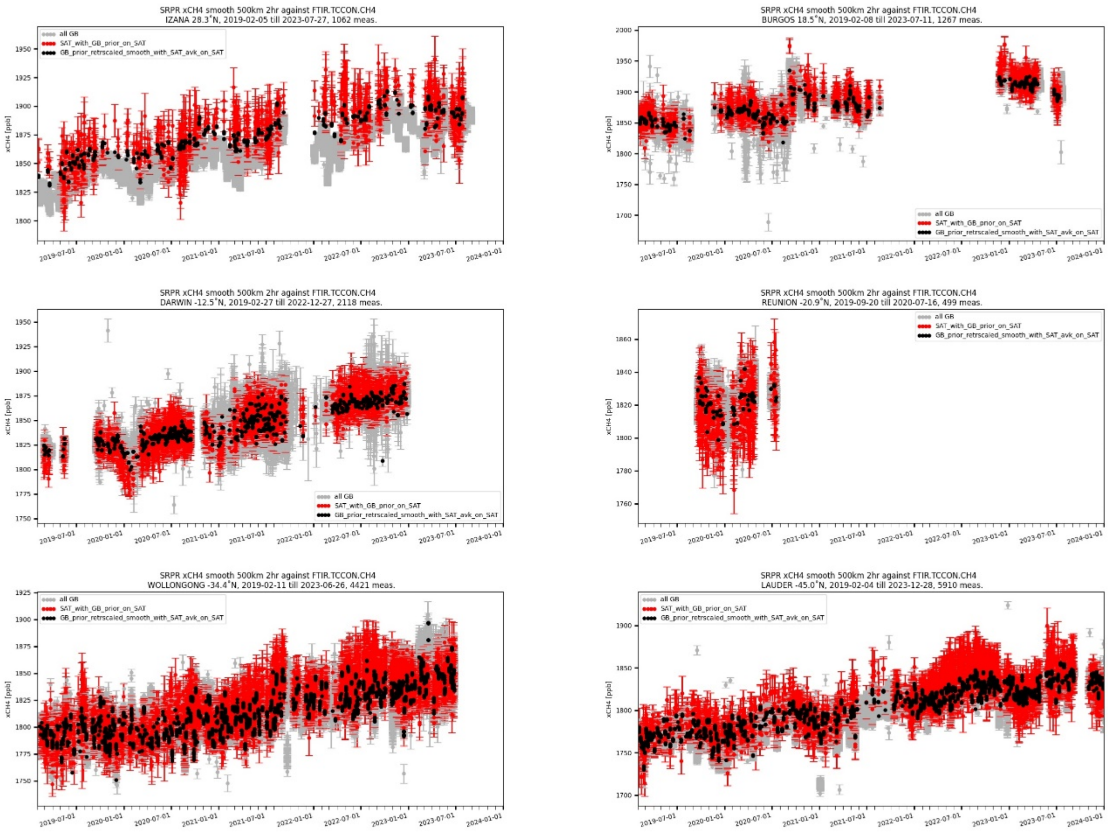

Figure 4-41: Timeseries of XCH_4 TCCON (collocated=black, all=grey) and CH4_GO2_SRPR (red) data at selected TCCON sites.

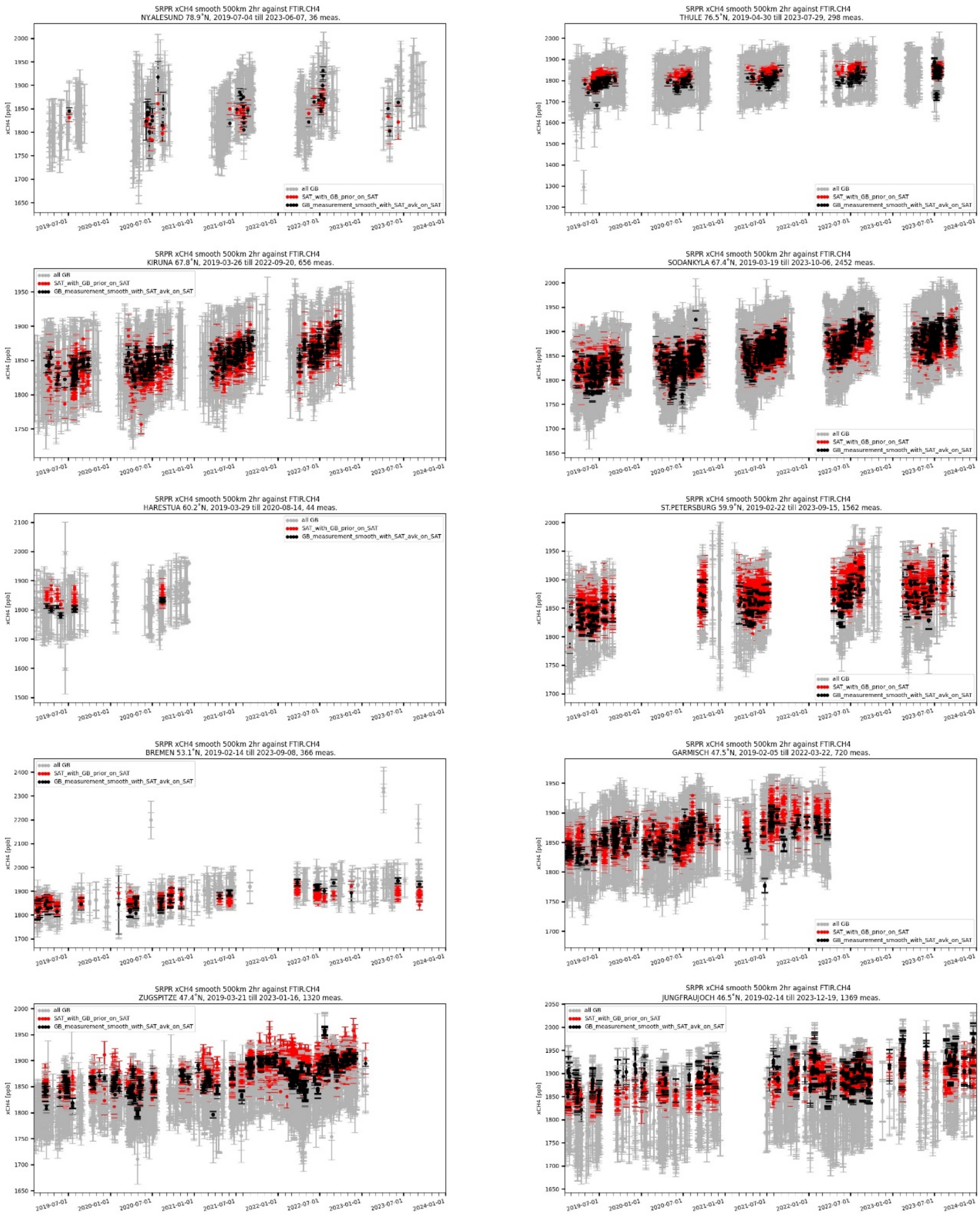

SRPR xCH4 smooth 500km 2hr against FTIR.CH4
NY.ALESUND 78.9°N, 2019-07-04 till 2023-06-07, 36 meas.
SRPR xCH4 smooth 500km 2hr against FTIR.CH4
THULE 76.5°N, 2019-04-30 till 2023-07-29, 298 meas.
SRPR xCH4 smooth 500km 2hr against FTIR.CH4
KIRUNA 67.8°N, 2019-03-26 till 2022-09-20, 656 meas.
SRPR xCH4 smooth 500km 2hr against FTIR.CH4
SODANKYLA 67.4°N, 2019-03-19 till 2023-10-06, 2452 meas.
SRPR xCH4 smooth 500km 2hr against FTIR.CH4
HARESTUA 60.2°N, 2019-03-29 till 2020-08-14, 44 meas.
SRPR xCH4 smooth 500km 2hr against FTIR.CH4
ST.PETERSBURG 59.9°N, 2019-02-22 till 2023-09-15, 1562 meas.
SRPR xCH4 smooth 500km 2hr against FTIR.CH4
BREMEN 53.1°N, 2019-02-14 till 2023-09-08, 366 meas.
SRPR xCH4 smooth 500km 2hr against FTIR.CH4
GARMISCH 47.5°N, 2019-02-05 till 2022-03-22, 720 meas.
SRPR xCH4 smooth 500km 2hr against FTIR.CH4
ZUGSPITZE 47.4°N, 2019-03-21 till 2023-01-16, 1320 meas.
SRPR xCH4 smooth 500km 2hr against FTIR.CH4
JUNGFRAUJOCH 46.5°N, 2019-02-14 till 2023-12-19, 1369 meas.
all GB
SAT_with_GB_prior_on_SAT
GB_measurement_smooth_with_SAT_avk_on_SAT
xCH4 [ppb]

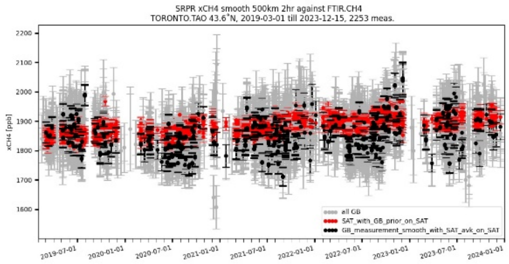
SRPR xCH4 smooth 500km 2hr against FTIR.CH4
TORONTO.TAO 43.6°N, 2019-03-01 till 2023-12-15, 2253 meas.

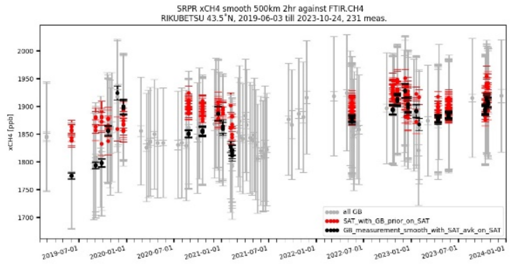
SRPR xCH4 smooth 500km 2hr against FTIR.CH4
RIKUBETSU 43.5°N, 2019-06-03 till 2023-10-24, 231 meas.

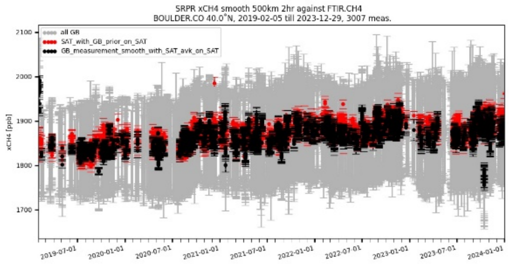
SRPR xCH4 smooth 500km 2hr against FTIR.CH4
BOULDER.CO 40.0°N, 2019-02-05 till 2023-12-29, 3007 meas.

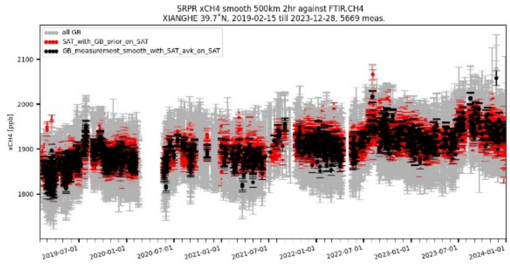
SRPR xCH4 smooth 500km 2hr against FTIR.CH4
XIANGHE 39.7°N, 2019-02-15 till 2023-12-28, 5669 meas.

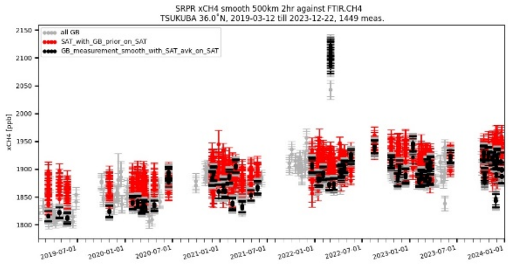
SRPR xCH4 smooth 500km 2hr against FTIR.CH4
TSUKUBA 36.0°N, 2019-03-12 till 2023-12-22, 1449 meas.

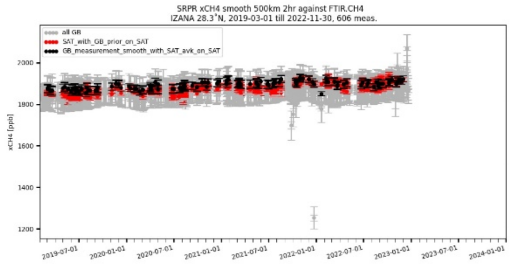
SRPR xCH4 smooth 500km 2hr against FTIR.CH4
IZANA 28.3°N, 2019-03-01 till 2022-11-30, 606 meas.

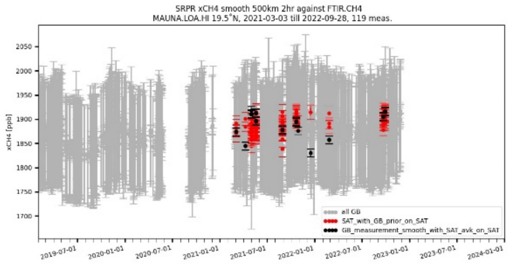
SRPR xCH4 smooth 500km 2hr against FTIR.CH4
MAUNA.LOA.HI 19.5°N, 2021-03-03 till 2022-09-28, 119 meas.

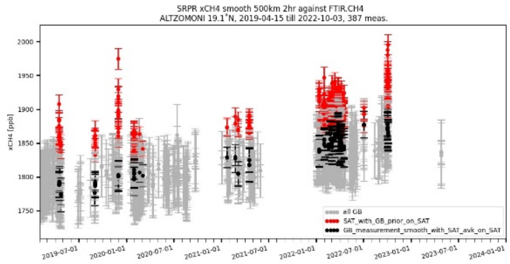
SRPR xCH4 smooth 500km 2hr against FTIR.CH4
ALTZOMONI 19.1°N, 2019-04-15 till 2022-10-03, 387 meas.

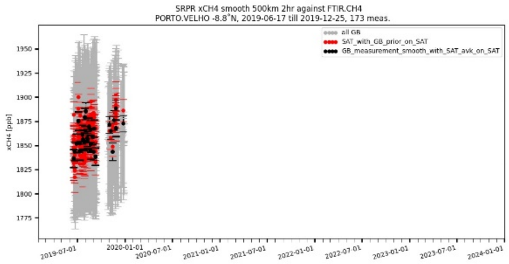
SRPR xCH4 smooth 500km 2hr against FTIR.CH4
PORTO.VELHO -8.8°N, 2019-06-17 till 2019-12-25, 173 meas.

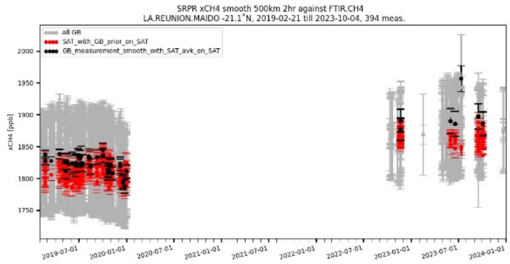
SRPR xCH4 smooth 500km 2hr against FTIR.CH4
LA.REUNION.MAIDO -21.1°N, 2019-02-21 till 2023-10-04, 394 meas.

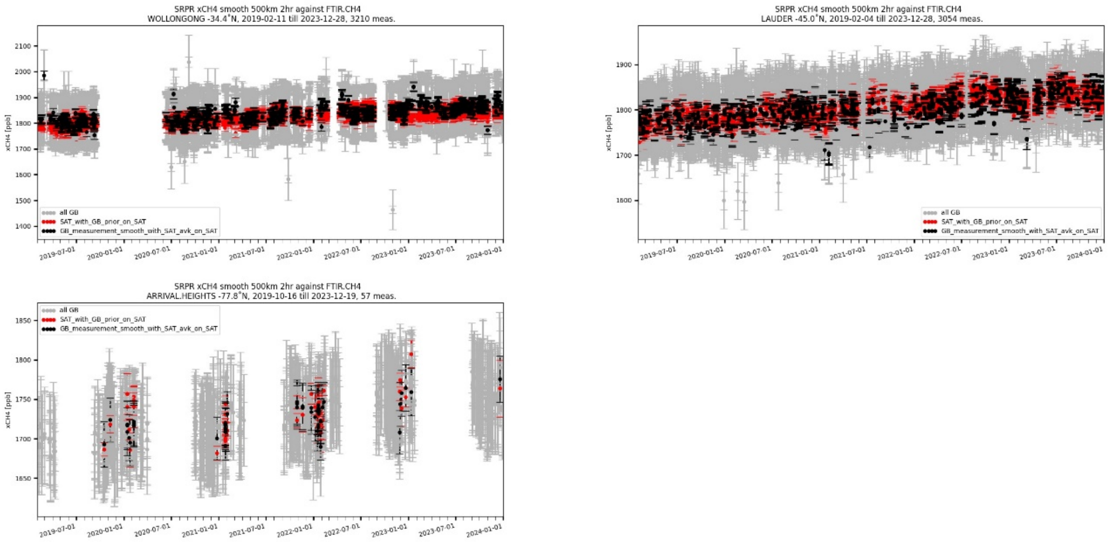

Figure 4-42: Timeseries of XCH_4 NDACC (collocated=black, all=grey) and CH4_GO2_SRPR (red) data at all NDACC sites.

Figure 4-43 shows monthly median timeseries for TCCON and SRPR XCH_4 for all data that fall within certain latitude bands, namely all sites North of 40°N latitude (top), all sites between 40°N and the equator (mid) and all sites in the Southern hemisphere (bottom). Here we see a picture that is consistent with that of SRFP in the sense that the bias increases around and 2021. However, by end 2023, this bias has disappeared again, which was not apparent in the SRFP product. As a result the overall trend over the entire timeperiod is very similar to that of TCCON (0.3 ppb/year difference for the Northern hemisphere, 1 ppb/year for the Southern Hemisphere, all with strong overlapping uncertainty bands. In our previous analysis of the v2.0.2 pruduct, the timeseries ended at the start of 2022, right when the an increase in the bias was observed, resulting in stronger long term trend differences. Concerning seasonality, there may be a difference in amplitude for the high latitude and Southern hemisphere, and a phase shift for the 0°-40°N latitude band. This was not apparent in the SRFP plots (**Figure 4-35**).

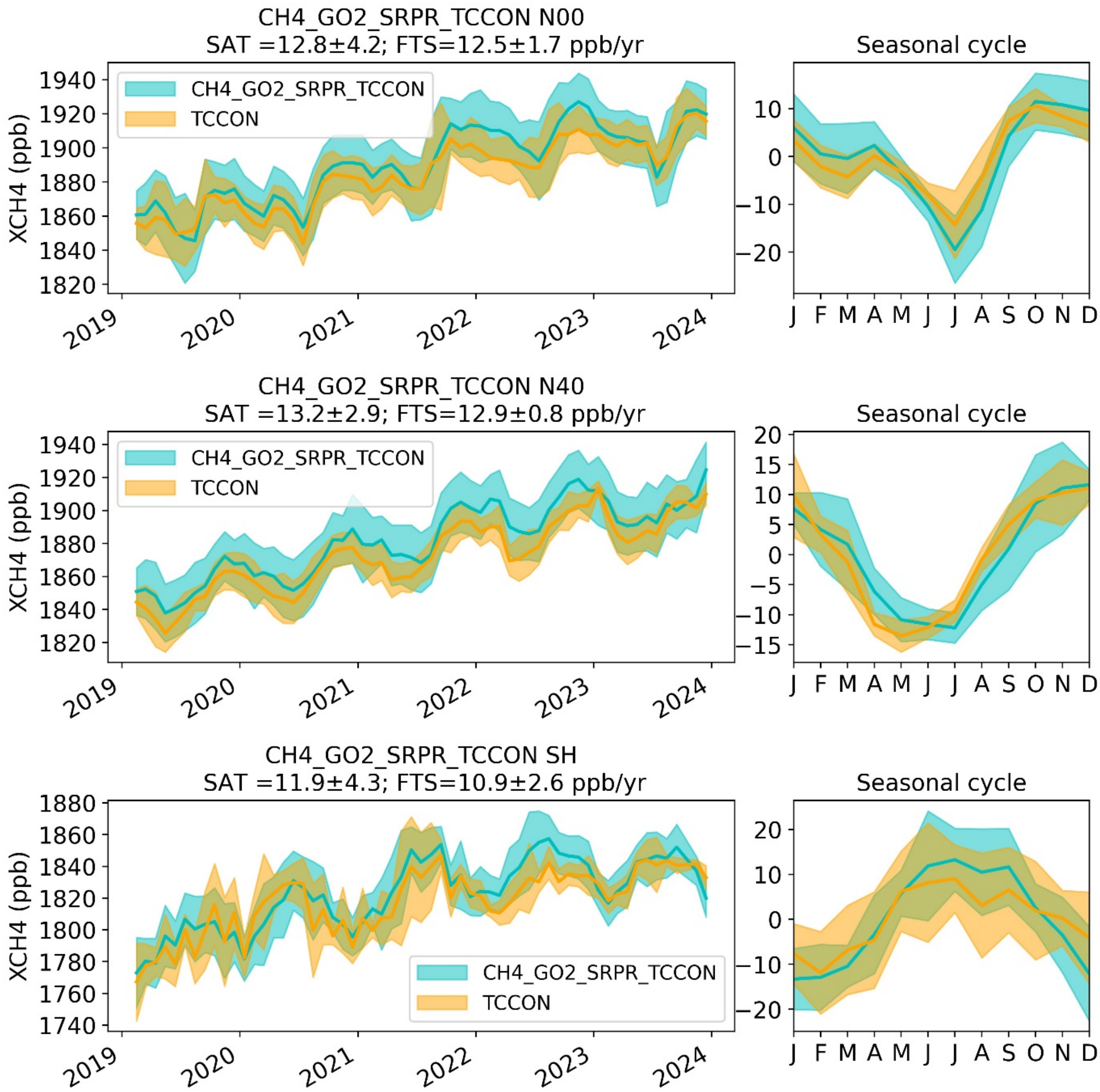

Figure 4-43: Monthly median collocated Sat and TCCON XCH_4 concentrations as a function of time. The shaded areas correspond with the scaled median absolute deviation.

Figure 4-44 shows the same but for NDACC (ignoring Altzomoni, Toronto, Thule, Paramaribo and Porto Velho). Due to the higher variability it is difficult to draw conclusions. Differences in long term trends are slightly more outspoken but well within the larger uncertainty bands. The 0°-40°N phase shift is equally present in the NDACC data. The differences in Amplitude for the other latitude bands are also present but far less obvious due to noise.

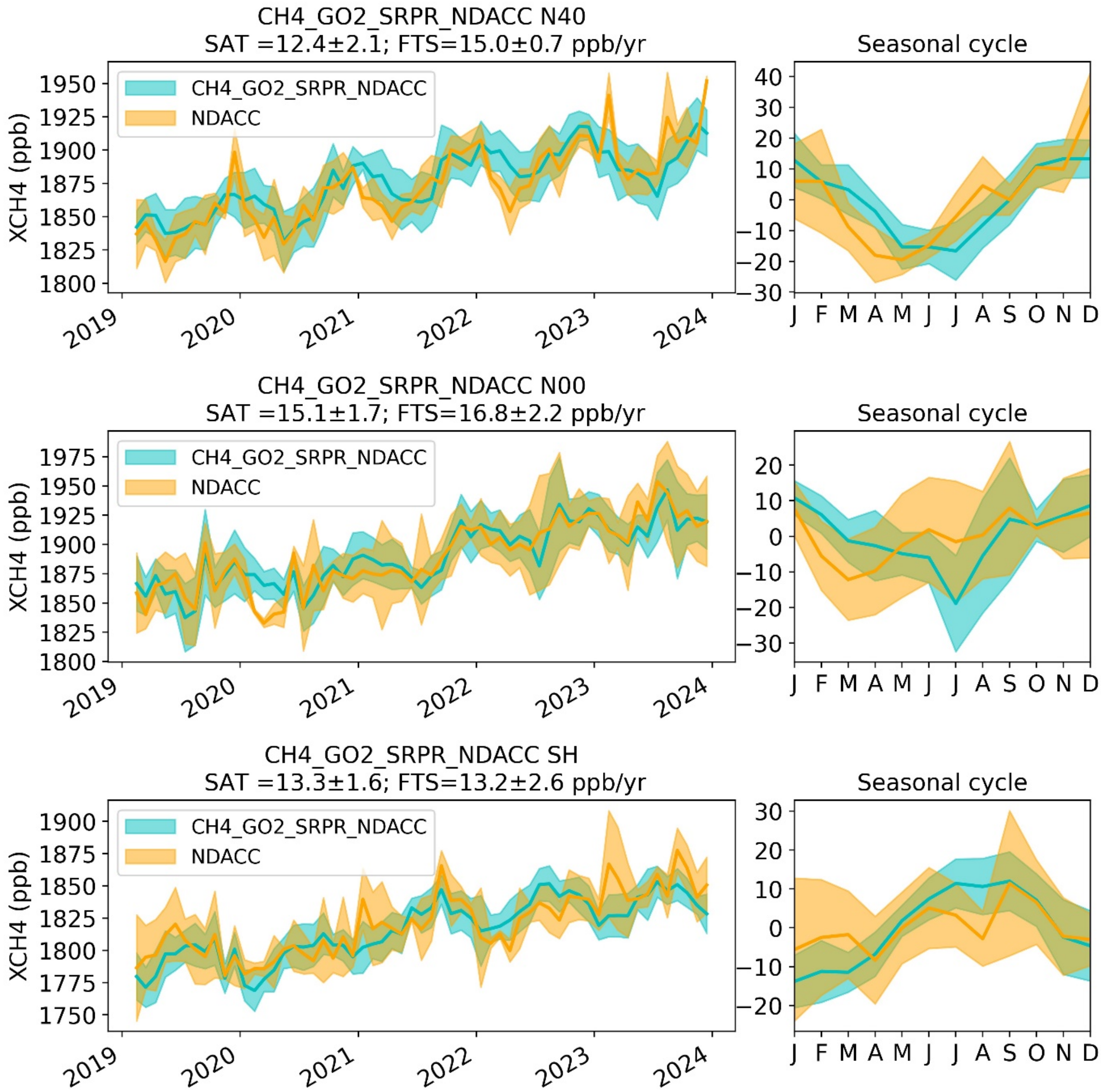

Figure 4-44: Monthly median collocated Sat and NDACC XCH_4 concentrations as a function of time. The shaded areas correspond with the scaled median absolute deviation.

4.2.6.2 Summary

Listed in the table below (**Table 4-17**) are the Figure of Merit parameters as derived from the individual collocated data pairs at each station.

SRPR XCH_4's single measurement precision equals 15.1 ppb, reaching the Breakthrough target of <17 ppb. The error assessment is somewhat underestimated with an uncertainty ratio of 0.79. The median bias is significant at 7.0 ppb with confidence bands between 5.3 and 8.0 ppb. Both the spatial and spatio-temporal relative accuracies reach the <10 ppb target (2.6 and 5.8 ppb for the RA and SRA respectively (an slight improvement compared to the previous analysis at 3.7 and 5.8), and well within the uncertainty bounds of, SRFP's RA and SRA (3.1 and 5.7 respectively).

Compared to NDACC we see a single measurement precision of 20.3 [16.2, 22.2] ppb, a likewise positive median bias of 1.6 [-3.6, 10.6] ppb, and relative accuracy values that do not meet the requirements (RA 13.5 [5.3, 20.4] ppb, SRA 17.4 [14.6, 23.1] ppb), although the confidence interval of the RA is so large it overlaps with the target of <10 ppb. The latter no doubt in part to the higher inter-station variability within the NDACC network itself.

Table 4-17 presents an overview of the estimated data quality of CH4_GO2_SRPR, as obtained by the VALT team, from comparisons with TCCON ground-based reference observations. Values in square brackets [ ] correspond with the upper and lower 95% confidence bound on the parameter. The uncertainty ratio features 2 numbers as outlined in the validation method.

Product Quality Summary Table for Product: CH4_GO2_SRPR Level: 2, Version: v02.0.3, Time period covered: 2.2019 – 12.2023 Assessment: Validation Team (VALT)			
Parameter [unit]	**Achieved performance**	**Requirement**	**Comments**
Single measurement precision (1-sigma) in [ppm]	15.1 [13.9,15.8]	< 34 (T) < 17 (B) < 9 (G)	Computed as the median over all station scaled median absolute differences to TCCON
Uncertainty ratio [-]: Ratio reported uncertainty to standard deviation of satellite-TCCON difference	0.78,0.79*	-	No requirement but value close to unity expected for a high quality data product with reliable reported uncertainty.
Median bias (global offset) [ppm]	7.0 [5.3,8.0]	-	No requirement but value close to zero expected for a high quality data product.
Accuracy: Relative systematic error [ppm]	Spatial: 2.6 [0, 3.8] Spatio-temporal: 5.8 [4.3, 7.1]	< 10	Spatial: Computed as standard deviation of the biases at the various TCCON sites. Spatio-temporal: As "Spatial" but also considering seasonal biases.
Stability: Drift [ppm/year]	0.6 [-0,3, 1.2]	< 3	Linear drift

5 Validation and intercomparisons results from data provider

5.1 Validation and intercomparison results for product CO2_OC2_FOCA

The validation results shown in this section are valid for FOCAL v11. The applied methods are similar to those described in BESD's comprehensive error characterization report **/CECRv3, 2017/** and also to those in the publication of **/Reuter et al., 2020/**. For all comparisons, averaging kernels have been applied and the influence of the smoothing error reduced as described in **Section 5.2** of ESA's GHG CCI+ product user guide version 5 (PUGv5) for the FOCAL XCO_2 OCO-2 data product CO2_OC2_FOCA **/PUGv5, 2025/**.

5.1.1 Co-location

FOCAL's XCO_2 has been validated with TCCON GGG2020 measurements **/Wunch et al., 2011; Laughner et al., 2022; TCCON GGG2020/**. The co-location criteria are defined by a maximum time difference of two hours, a maximum spatial distance of 500km, and a maximum surface elevation difference of 250m. Additionally, only TCCON sites with at least 1000 co-locations (4 in the case of daily, weekly, or monthly averages) covering a time period of at least two years are taken into account.

Figure 5.1 shows all 3741027 co-located FOCAL and TCCON XCO_2 retrieval results used for the validation study. One can see that the temporal sampling differs from site to site and that FOCAL captures the year-to-year increase and the seasonal features well.

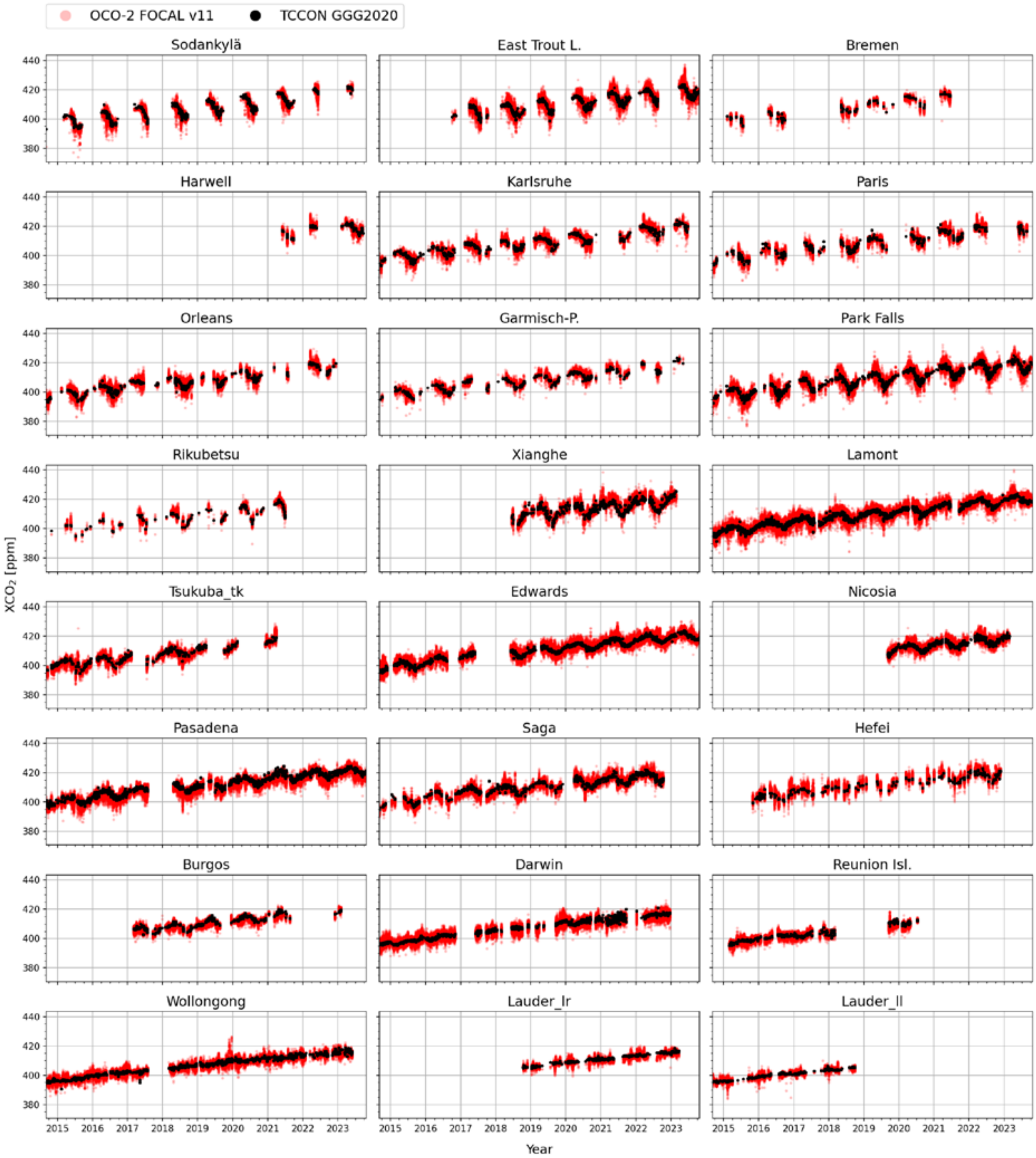

Figure 5.1: Co-located FOCAL and TCCON XCO2 retrieval results used for the validation study. The TCCON sites are order from top/left to bottom/right by average latitude of the co-located satellite soundings.

5.1.2 Daily, weekly, and monthly averages

For some applications, it is expected that FOCAL XCO_2 data will be aggregated to "super soundings" averaging, e.g., all soundings of an orbit in a surrounding of a target. Also, FOCAL XCO_2 data might be used to compute L3 (level 3) products, e.g., in the manner of gridded monthly averages. With such application in mind, we computed daily, weekly, and monthly averages of the FOCAL and TCCON co-locations at each TCCON site. In order to improve the robustness, daily, weekly, and monthly averages are only calculated when averaging at least 10, 30, or 50 individual soundings, respectively. As an example, **Figure 5.2** shows the daily, weekly, and monthly FOCAL XCO_2 averages for the Lamont and Wollongong TCCON sites. Due to OCO-2's data density, it is often the case that one overpass generates many co-colocations. This considerably reduces the scatter of the daily averages compared to the individual soundings.

Note that FOCAL reports only on the stochastic uncertainty of the individual soundings. In the case of daily, weekly, and monthly averages we computed the corresponding uncertainties by applying the rules of error propagation under the assumption of uncorrelated errors.

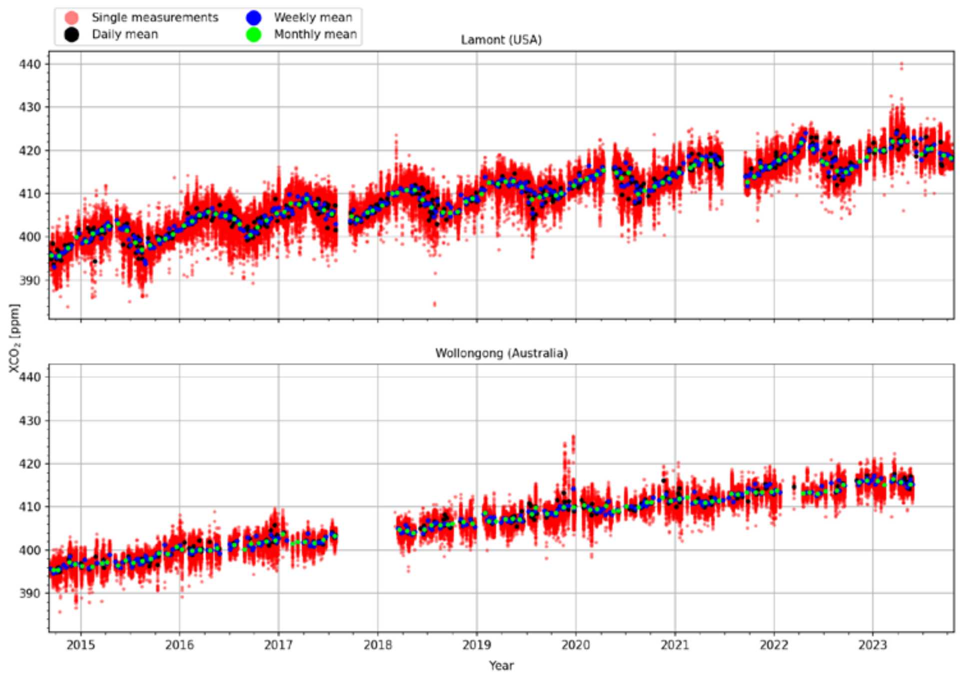

Figure 5.2: Co-located FOCAL XCO2 retrieval results and their daily, weekly, and monthly averages at the TCCON sites Lamont (top) and Wollongong (bottom) used for the validation study.

5.1.3 General overview

The overall agreement of the FOCAL data (and its averages) with TCCON data at all sites is illustrated in **Figure 5.3**. The histograms of the difference (FOCAL – TCCON) show in all cases a near Gaussian distribution with a center between 0.00ppm and 0.07ppm. The standard deviation of the difference reduces from 1.69ppm for individual soundings to 1.00ppm for monthly averages. The FOCAL vs. TCCON heat maps show a pronounced clustering along the one-to-one line for all cases. This is supported by a good agreement of the orthogonal distance regression with the one-to-one line and high Pearson correlation coefficients between 0.97 for individual soundings and 0.99 for monthly averages.

These results provide a first rough overview of FOCAL's agreement with TCCON. However, except for an average bias, they do not allow to separate systematic and stochastic error components.

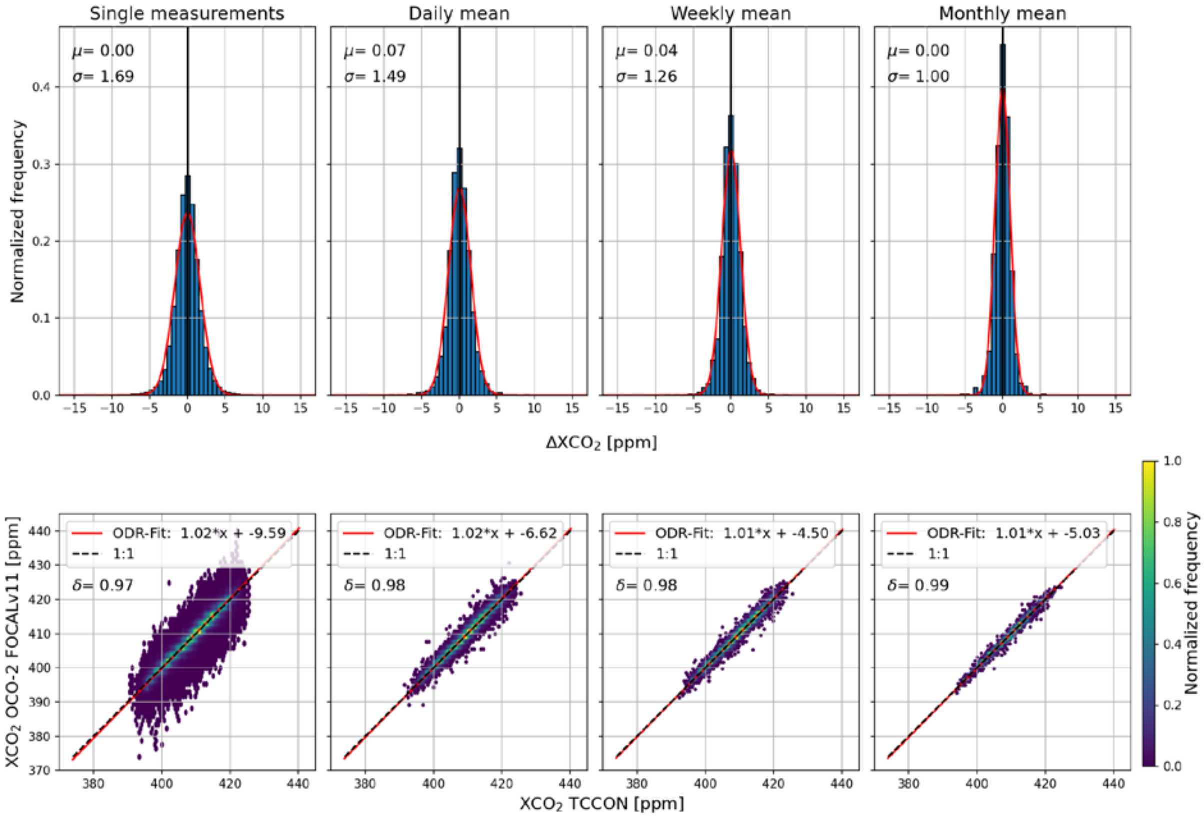

Figure 5.3: Overall overview on the agreement of the FOCAL data (and its averages) with TCCON data at all sites. Top: Normalized histograms of the difference FOCAL – TCCON. Bottom: Heat maps TCCON vs. FOCAL including one-to-one line, orthogonal distance regression (ODR), and Pearson correlation coefficient δ.

5.1.4 Stochastic and systematic error components

The method described in the following allows us to separate the stochastic errors from potential regional or seasonal biases as well as from a linear drift.

5.1.4.1 Per site performance statistics

For the co-locations of each site, we compute the FOCAL minus TCCON differences ΔX and fit the following bias model:

5-1 $$\Delta X = a_0 + a_1 t + a_2 sin(2\pi t + a_3) + \varepsilon$$

Here, t is the time of the measurements in fractional years, a_{0-3} the free fit parameters from which we compute the systematic error components, and ε the fit residuum. **Figure 5.4** shows at the example of the TCCON sites Lamont and Wollongong the fitted bias functions for the individual soundings, daily, weekly, and monthly averages.

We compute the station or regional bias Δ_{reg} from the average (ave) of the fit values:

5-2 $$\Delta_{reg} = \text{ave}[a_0 + a_1 t + a_2 sin(2\pi t + a_3)]$$

The seasonal bias Δ_{sea} is computed from the standard deviation (std) of the seasonal component of the fit:

5-3 $$\Delta_{sea} = \text{std}[a_2 sin(2\pi t + a_3)]$$

It shall be noted that the vector t consists only of the time of the measurements. This means, Δ_{sea} is only computed from those parts of the seasonal cycle actually covered by observations.

The linear drift corresponds to the fit parameter $\Delta_{dri} = a_1$, and the single sounding precision, i.e., the stochastic retrieval uncertainty σ, is computed from the standard deviation of the residuum.

5-4 $$\sigma = \text{std}[\varepsilon]$$

We define the spatiotemporal bias Δ_{spt} as combination of regional and seasonal bias.

5-5 $$\Delta_{spt} = \sqrt{\Delta_{reg}{}^2 + \Delta_{sea}{}^2}$$

The FOCAL retrieval algorithm reports on the XCO_2 stochastic uncertainty σ'_{rep} for each sounding. From these values, we compute the average reported uncertainty σ_{rep} per station by:

5-6 $$\sigma_{rep} = \sqrt{\mathrm{ave}\left({\sigma'_{rep}}^2\right)}$$

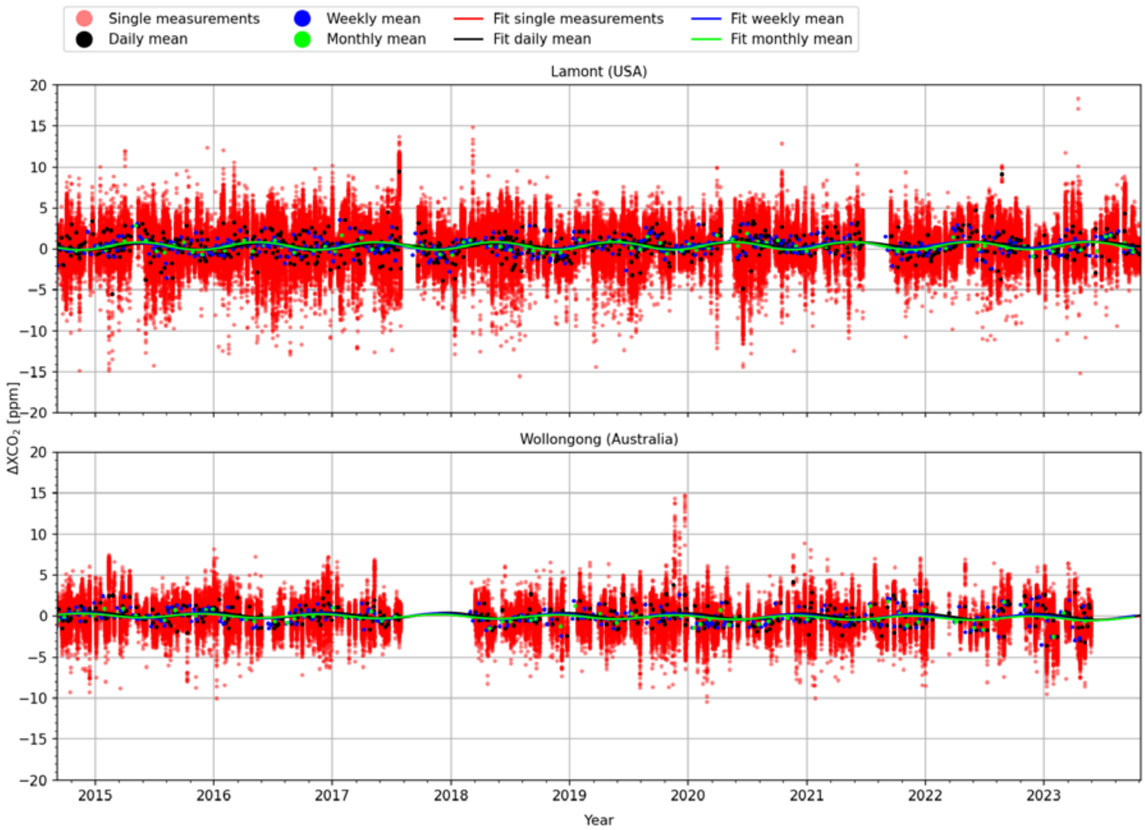

Figure 5.4: ΔXCO2 (FOCAL – TCCON) for the co-locations of the single measurements, daily, weekly, and monthly averages at the TCCON sites Lamont (top) and Wollongong (bottom). Additionally, the corresponding fits of the bias model (**Eq. 5-1**) are shown.

5.1.4.2 Summarizing performance statistics

Based on the per site statistics, the following summarizing performance statistics are calculated.

The average site bias $\overline{\Delta_{reg}}$ and the site-to-site variability is computed from the mean and the standard deviation of the individual site biases:

5-7 $$\overline{\Delta_{reg}} = \mathrm{ave}\left(\Delta_{reg}\right) \pm \mathrm{std}\left(\Delta_{reg}\right)$$

The average seasonal bias $\overline{\Delta_{sea}}$ is computed by:

5-8 $$\overline{\Delta_{sea}} = \mathrm{avg}(\Delta_{sea})$$

The overall spatiotemporal bias $\overline{\Delta_{spt}}$ is computed by:

5-9 $$\overline{\Delta_{spt}} = \sqrt{\overline{\Delta_{reg}}^2 + \overline{\Delta_{sea}}^2}$$

The average drift and the drift uncertainty is computed by:

5-10 $$\overline{\Delta_{dri}} = \mathrm{ave}(\Delta_{dri}) \pm \mathrm{std}(\Delta_{dri})$$

As the linear drift can be assumed to be globally constant, the station-to-station standard deviation of the linear drift can be considered a measure of its uncertainty. The overall single sounding precision and reported uncertainty are computed by:

5-11 $$\overline{\sigma} = \sqrt{\mathrm{ave}(\sigma^2)}$$

5-12 $$\overline{\sigma_{rep}} = \sqrt{\mathrm{ave}\left({\sigma_{rep}}^2\right)}$$

5.1.5 Results

The results of all site performance statistics as well as the summarizing performance statistics for individual soundings, daily, weekly, and monthly averages are illustrated in **Figure 5.5**. Based on this figure, it can first be noted that averaging does not have a substantial impact on the validation results for the systematic error components. This is especially the case for the summarizing performance statistics which are similar for individual soundings, daily, weekly, and monthly averages. Therefore, it is sufficient that we primarily concentrate on the results for individual soundings from now on and **Table 5.1** lists only values of the statistics for individual soundings.

However, the results for the stochastic error component show some important differences. The overall result for the stochastic error of the individual soundings amounts to 1.57ppm which agrees well with the corresponding reported uncertainty of 1.61ppm. This is no surprise, because FOCAL's uncertainty estimates have been empirically corrected **/ATBDv5, 2024/**. The actual stochastic error reduces for daily (1.30ppm), weekly (1.06ppm), and monthly (0.76ppm) averages, but the reduction is far less pronounced as for the reported uncertainty which has been computed under the assumption of uncorrelated errors. Therefore, it has to be expected that the separation of systematic and stochastic errors by **Eq. 5-1** is incomplete at least for the individual soundings. In other words, it can be expected that parts of the residuum ε of **Eq. 5-1** for the individual soundings are actually of systematic origin.

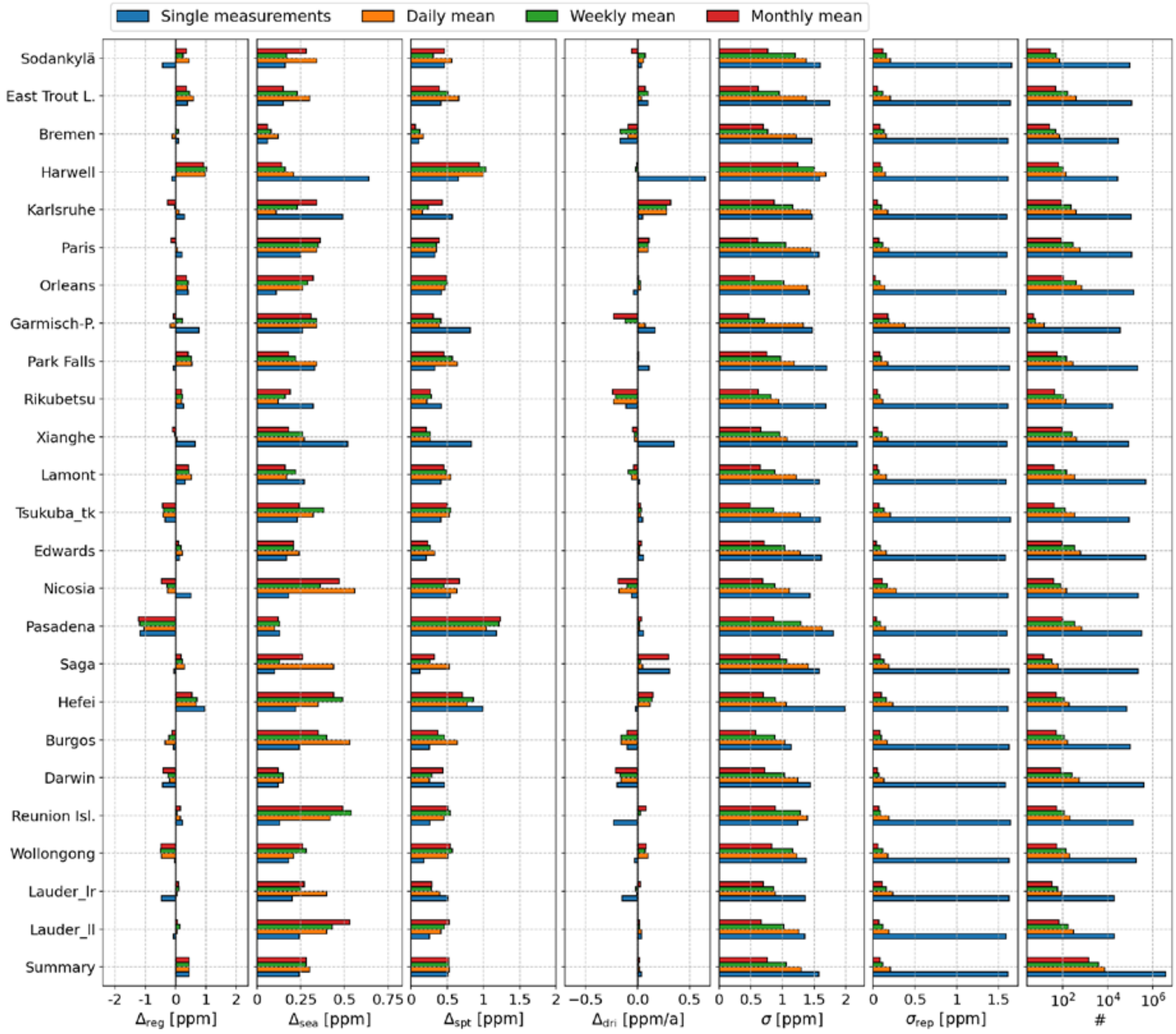

Figure 5.5: Validation results for FOCAL single measurements, daily, weekly, and monthly averages. From left to right, the figure shows the per site performance statistics (**Section 5.1.4.1**) regional (Δ_{reg}), seasonal (Δ_{sea}), and spatiotemporal bias (Δ_{spt}), the linear drift (Δ_{dri}), the actual (σ) and reported precision (σ_{rep}), and the number of soundings (#). TCCON sites are order from top to bottom by average latitude of the co-located satellite soundings. The last row includes the summarizing performance statistics as defined in **Section 5.1.4.2**.

For this reason, we grouped the residuum into bins consisting of $n = 1, 2, 3, \cdots$ elements and analyzed its standard deviation as function of the bin size. As the reported retrieval precision is usually relatively constant at one TCCON site, it should be expected that the standard deviation of the binned residuum scales approximately with $1/\sqrt{n}$. We performed this experiment for the TCCON site Lamont because of the large number of co-locations. As shown in **Figure 5.6** (top/left), the actual precision (standard deviation of the binned residuum) of the individual soundings does not follow the curve expected for uncorrelated errors. In contrast, the actual precision of daily (**Figure 5.6,** top/right), weekly (**Figure 5.6**, bottom/left), and monthly averages (**Figure 5.6**, bottom/right) agrees well with the expectation for uncorrelated errors. These results may differ in detail from TCCON site to TCCON site, but indicates that the errors of the individual soundings may have additional systematic components not covered by the seasonal component of Eq. 5-1.

Table 5.1: Validation results for FOCAL single measurements. From left to right, the table lists the per site performance statistics (**Section 5.1.4.1**) regional (Δ_{reg}), seasonal (Δ_{sea}), and spatiotemporal bias (Δ_{spt}), the linear drift (Δ_{dri}), the actual (σ) and reported precision (σ_{rep}), and the number of soundings (#). TCCON sites are order from top to bottom by average latitude of the co-located satellite soundings. The last row includes the summarizing performance statistics as defined in **Section 5.1.4.2**.

Station	Δ_{reg} [ppm]	Δ_{sea} [ppm]	Δ_{spt} [ppm]	Δ_{dri} [ppm/a]	σ [ppm]	σ_{rep} [ppm]	#
Sodankylä	-0.43	0.16	0.46	0.04	1.60	1.65	93234
East Trout L.	0.39	0.15	0.41	0.10	1.75	1.64	117415
Bremen	0.10	0.06	0.11	-0.17	1.46	1.61	29280
Harwell	-0.12	0.64	0.65	0.65	1.59	1.61	26985
Karlsruhe	0.29	0.49	0.57	0.05	1.47	1.60	108799
Paris	0.22	0.25	0.33	-0.00	1.57	1.60	116196
Orleans	0.41	0.11	0.42	-0.04	1.42	1.59	139019
Garmisch-P.	0.78	0.26	0.82	0.17	1.47	1.63	35669
Park Falls	-0.06	0.33	0.33	0.11	1.70	1.63	213033
Rikubetsu	0.27	0.32	0.42	-0.11	1.68	1.61	16586
Xianghe	0.65	0.52	0.83	0.35	2.18	1.60	85338
Lamont	0.32	0.27	0.41	0.02	1.58	1.59	485926
Tsukuba_tk	-0.35	0.23	0.41	0.05	1.60	1.64	91780
Edwards	0.13	0.17	0.21	0.06	1.61	1.58	490288
Nicosia	0.51	0.18	0.54	-0.06	1.43	1.61	224109
Pasadena	-1.18	0.13	1.18	0.06	1.80	1.60	321112
Saga	-0.05	0.10	0.12	0.31	1.58	1.62	220064
Hefei	0.96	0.22	0.99	-0.02	1.98	1.61	68093
Burgos	-0.07	0.24	0.25	-0.10	1.14	1.62	100729
Darwin	-0.44	0.12	0.46	-0.20	1.44	1.58	395590
Reunion Isl.	0.23	0.13	0.26	-0.23	1.24	1.64	138082
Wollongong	-0.04	0.18	0.18	-0.03	1.38	1.62	185145
Lauder_lr	-0.47	0.20	0.51	-0.15	1.36	1.62	19186
Lauder_ll	-0.07	0.24	0.25	0.04	1.35	1.59	19369
Summary	**0.08±0.45**	**0.24**	**0.51**	**0.04±0.19**	**1.57**	**1.61**	**3741027**

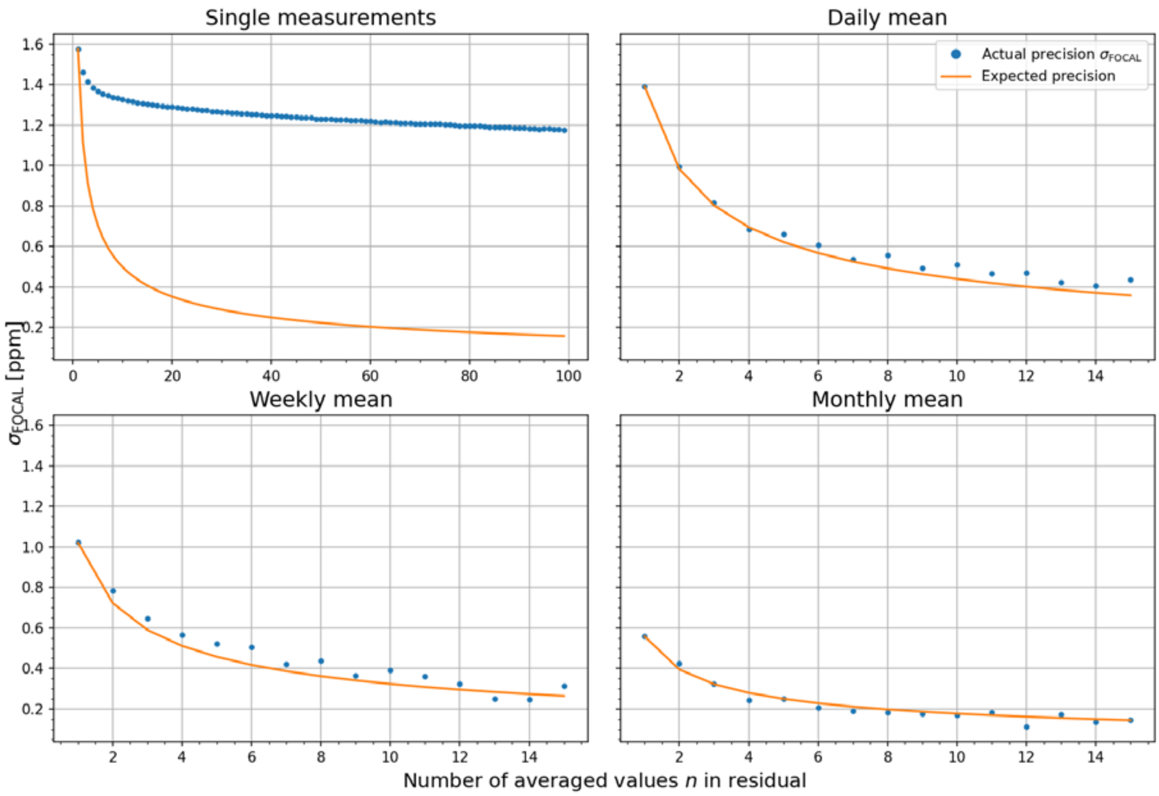

Figure 5.6: Actual and expected retrieval precision of FOCAL computed from residuals with increasing bin size for the TCCON site Lamont for single measurements (top/left), daily (top/right), weekly (bottom/left), and monthly averages (bottom/right).

The validation results for the individual soundings (**Table 5.1**, **Figure 5.5**) show that there is only a small overall average bias of 0.08ppm. Regional biases estimated from the site-to-site bias variability amount to 0.45ppm and are strongly influenced by the relatively large negative bias of -1.18ppm at the TCCON site Pasadena. The average seasonal and spatiotemporal bias amounts to 0.24ppm and 0.51ppm, respectively. The overall linear drift of 0.04ppm/a is much smaller than its site-to-site variability of 0.19ppm and, therefore, considered not significant.

Additionally, a measure for the year-to-year stability is computed as follows. For each TCCON site, the residual ε of the bias fit (**Eq. 5-1**) is smoothed by a running average of 365 days. Only days where more than 10 co-locations contribute to the running average of at least 5 TCCON sites are further considered. At these days, the station-to-station average is calculated (**Figure 5.7**, black line).

The corresponding expected uncertainty is computed from the standard error of the mean (derived from the station-to-station standard deviation and the number of stations) and by error propagation of the reported single sounding uncertainties (**Figure 5.7**, red line). For FOCAL, the average is always between about -0.3ppm and 0.3ppm with an uncertainty of typically about 0.15ppm. Most of the time, the average is not significantly different from zero, i.e., its two sigma uncertainty is larger than its absolute value.

Due to the relatively large uncertainty, we decided to compute not the maximum minus minimum as a measure for the year-to-year stability because this quantity can be expected to increase with length of the time series simply due to statistics. Therefore, we estimate the year-to-year stability by randomly selecting pairs of dates with a time difference of at least 365 days. For each selection we computed the difference modified by a random component corresponding to the estimated uncertainty. From 1000 of such pairs, we compute the standard deviation as estimate for the year-to-year stability. We repeat this experiment 1000 times and compute the average (0.19ppm) and standard deviation (0.01ppm). From this, we conclude that the year-to-year stability is 0.19ppm/a (**Figure 5.7**).

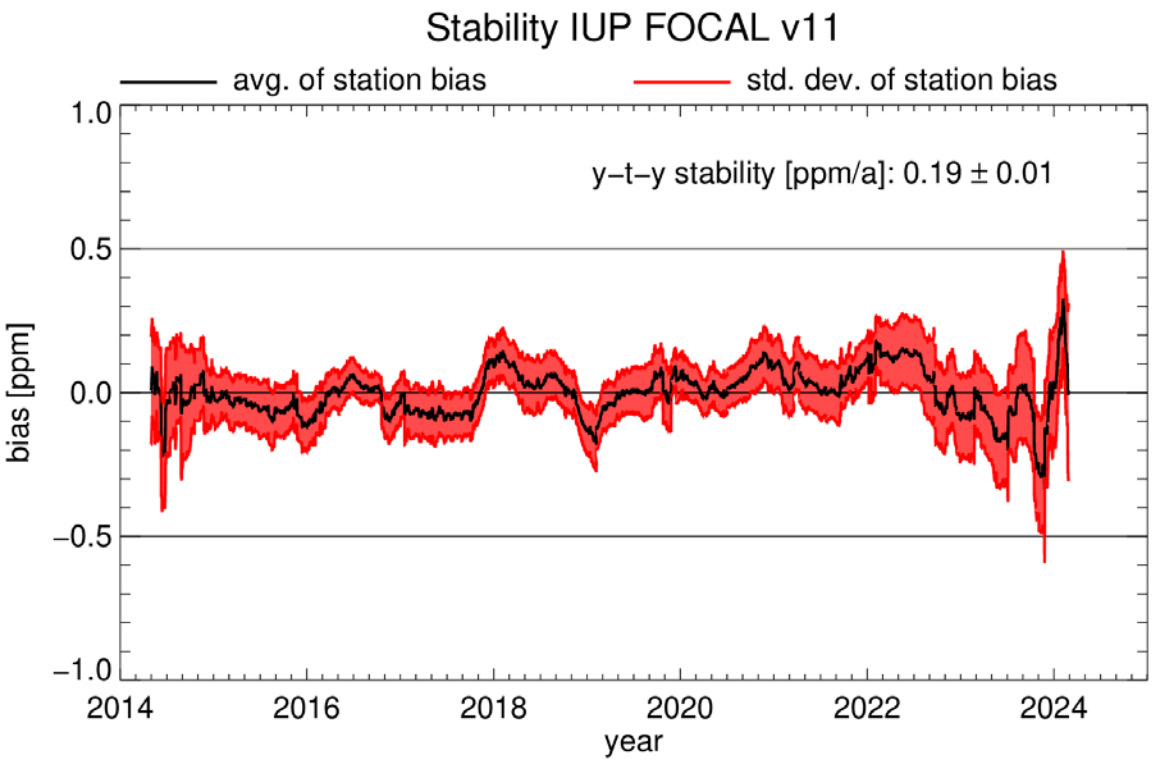

Figure 5.7: Stability analyses for FOCAL. The black curve shows the average station bias and the red curves its uncertainty represented by the station-to-station standard deviation.

5.1.6 Summary

We validated the FOCAL v11 XCO_2 data product with TCCON GGG2020 data of the years 2014 – 2023. The validation has been performed for daily, weekly, and monthly averages as well as for single soundings. Analyzing the single soundings without temporal averaging, we find that the overall bias of the FOCAL data amounts to 0.08ppm. Regional biases vary from site to site by 0.45ppm. Seasonal and spatiotemporal biases amount on average to 0.24ppm and 0.51ppm, respectively. We found no significant linear drift (0.04±0.19ppm). In the context of the systematic error characteristics, it shall be noted that **/Wunch et al., 2010, 2011/** specifies the accuracy (1σ) of TCCON to be about 0.4ppm. This means, e.g., that it cannot be expected to find regional biases considerably less than 0.4ppm using TCCON as reference. We find that the inferred systematic errors, i.e., regional, seasonal, and spatiotemporal biases as well as linear drift, do not critically depend on averaging. The year-to-year stability has been estimated to be 0.19ppm/a. The overall precision of the individual soundings is 1.57ppm which agrees well with the corresponding reported uncertainty of 1.61ppm. This is no surprise, because FOCAL's uncertainty estimates have been empirically corrected **/ATBDv5, 2024/**. The overall precision improves for daily (1.30ppm), weekly (1.06ppm), and monthly (0.76ppm) averages. We find indications that the estimated precision of the individual soundings does actually comprise not only purely stochastic but also residual unknown systematic components. No such indications were found for the daily, weekly, and monthly averages.

Table 5.2 presents an overview of the estimated data quality as obtained from comparisons with TCCON ground-based reference observations.

Table 5.2: Summary validation of product CO2_OC2_FOCA.

Product Quality Summary Table for Product: CO2_OC2_FOCA Level: 2, Version: v11, Time period covered: 9.2014 – 02.2024 Assessment: Data Provider (DP)			
Parameter [unit]	**Achieved performance**	**Requirement**	**Comments**
Single measurement precision (1-sigma) in [ppm]	1.57	< 8 (T) < 3 (B) < 1 (G)	Computed as standard deviation of the difference to TCCON
Uncertainty ratio [-]: Ratio reported uncertainty to standard deviation of satellite-TCCON difference	1.03	-	No requirement but value close to unity expected for a high quality data product with reliable reported uncertainty.
Mean bias (global offset) [ppm]	0.09	-	No requirement but value close to zero expected for a high quality data product.
Accuracy: Relative systematic error [ppm]	Spatial: 0.45 Spatiotemporal: 0.51	< 0.5	Spatial: Computed as standard deviation of the biases at the various TCCON sites. Spatio-temporal: As "Spatial" but also considering seasonal biases.
Stability: Drift [ppm/year]	0.04±0.19 (1-sigma)	< 0.5	Linear drift

5.2 Validation and intercomparison results for product CO2_TAN_OCFP

Development of this product ended at the end of Phase 1 with CRDP7. Please see the relevant CRDP7 CO2_TAN_OCFP documents available from https://climate.esa.int/en/projects/ghgs/key-documents/.

5.3 Validation and intercomparison results for product CO2_GO2_SRFP

The CO2_GO2_SRFP product is retrieved from GOSAT-2 TANSO-FTS SWIR spectra using the RemoTeC algorithm that has been jointly developed by SRON and KIT **/Butz et al., 2011; Schepers et al., 2012/**. The retrievals are performed globally for the time period between February 2019 and December 2023 and are evaluated against ground based TCCON observations.

5.3.1 Detailed results

To assess the quality of SRFP retrieval XCO_2 observations against TCCON values, SRFP soundings are matched to TCCON observations spatially and temporally. GOSAT-2 observations are co-located with TCCON sites based on a square latitude and longitude region around each TCCON site (in ±2.5º latitude/longitude box). For the temporal co-location we select only the TCCON measurements whose observation time falls within ±2 hour of each GOSAT-2 observation time. The TCCON observations that match these criteria are averaged for each individual GOSAT-2 observation.

We co-located GOSAT-2 and TCCON measurements with a maximum time difference of 2.5h, a maximum distance of 300 km in both longitudinal and latitudinal directions. In cases of multiple TCCON measurements of the same site collocating with a GOSAT-2 sounding, we averaged the TCCON measurements. In total we achieve 17,203 collocations for land soundings and 349 collocations over ocean.

The comparions for each TCCON site is shown in **Figure 5.3-1**. The statistics (mean bias, standard deviation) for each site are given in **Table 5.3-1**. The overall correlation between the GOSAT-2 and TCCON retrievals is given in **Figure 5.3-2**. The mean bias (global offset) amounts to -0.15 ppm. The standard deviation of the site biases (spatial accuracy or station-to-station variability) is 0.57 ppm. The single measurement precision of GOSAT-2 compared to TCCON amounts to 2.14 ppm.

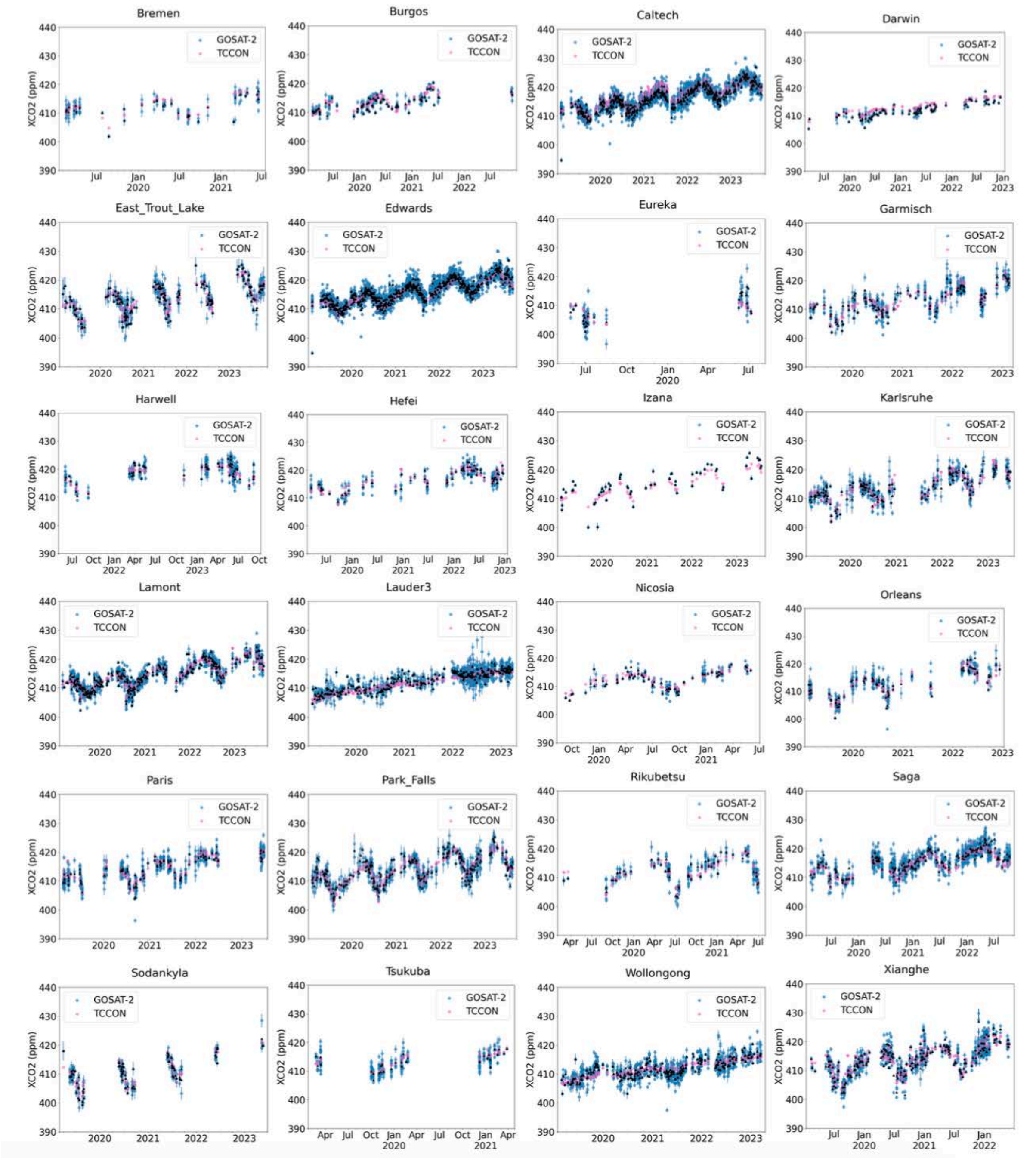

Figure 5-3-1: Comparison of land single soundings of XCO_2 from the full physics retrieval (blue circles) with co-located TCCON (pink triangles) measurements at all TCCON sites.

Table 5.3-1: Overview of the SRFP/RemoTeC XCO_2 validation with TCCON (after bias correction).

TCCON site [Land mode]	Δreg (ppm)	Δseas (ppm)	Δdri (ppm yr^{-1})	Δspt (ppm)	N
Bremen	-0.76	0.57	-0.76	0.95	139
Burgos	-0.74	0.55	-0.43	0.92	187
Caltech	-1.07	0.66	0.69	1.26	2744
Darwin	-0.79	0.68	-0.76	1.04	138
East Trout Lake	-0.74	0.04	-0.17	0.75	477
Edwards	-0.23	2.45	2.17	2.46	3066
Eureka	0.89	0.83	6.73	1.22	96
Garmisch	-0.1	0.55	0.47	0.56	580
Harwell	0.18	0.58	-0.30	0.60	344
Hefei	-0.16	0.81	-0.50	0.83	337
Izana	0.42	0.65	-0.48	0.77	61
Karlsruhe	-0.49	1.29	0.33	1.38	556
Lamont	0.12	0.21	0.01	0.25	1327
Lauder3	0.88	0.53	-0.39	1.02	1175
Nicosia	-0.26	0.03	0.58	0.26	156
Orleans	-0.39	1.59	0.89	1.64	389
Paris	0.18	0.22	0.11	0.29	624
Park Falls	0.55	0.12	-0.36	0.56	807
Rikubetsu	-0.27	0.54	1.37	0.60	276
Saga	0.67	0.19	0.36	0.70	1161
Sodankyla	-0.54	0.95	0.38	1.09	201
Tsukuba	-1.08	0.31	0.63	1.12	264
Wollongong	0.31	0.43	-0.24	0.53	1173
Xianghe	-0.12	0.65	1.13	0.66	915

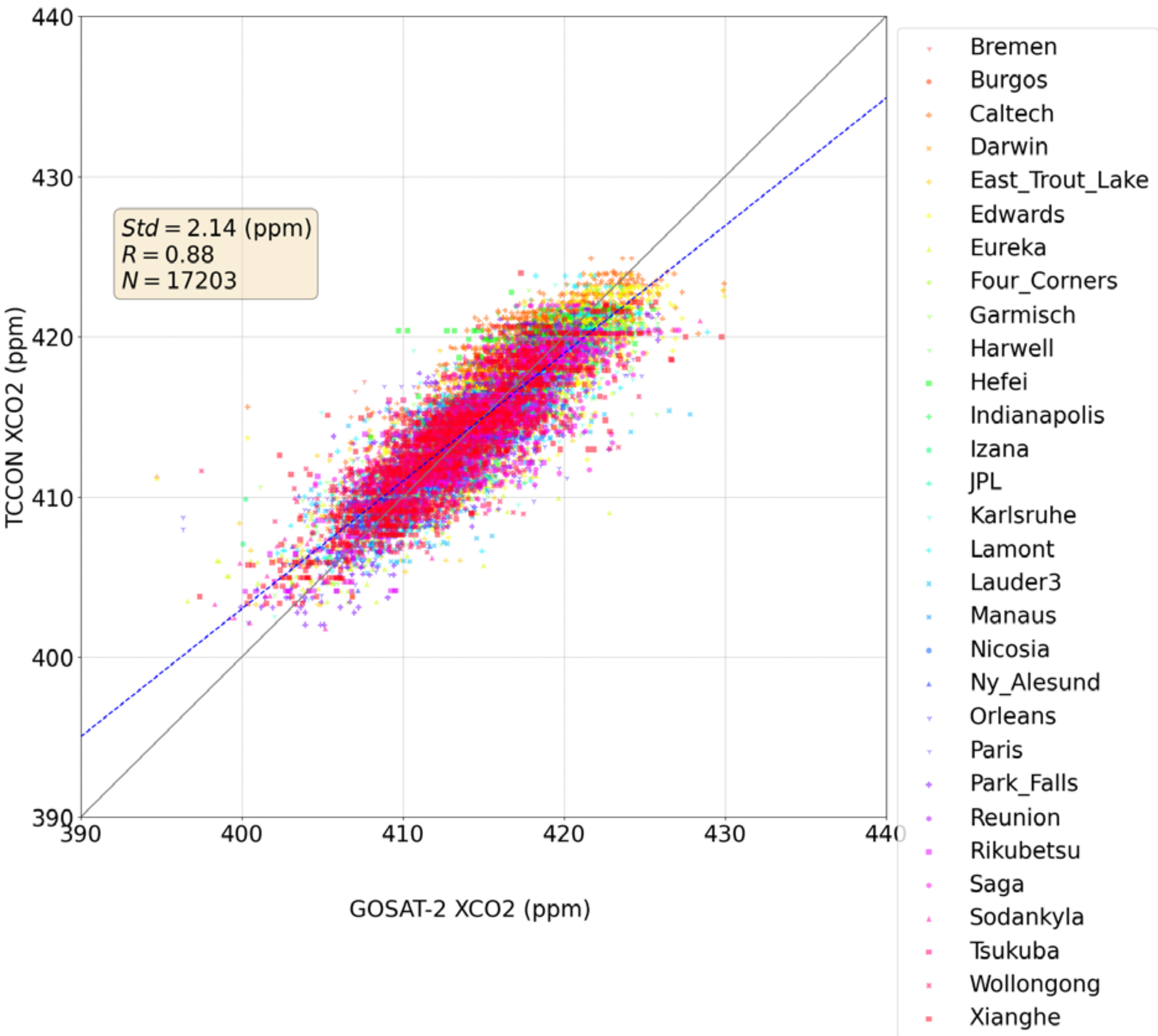

Figure 5-3-2: GOSAT-2 XCO_2 for soundings over land plotted against TCCON, for the RemoTeC Full Physics product. Data are compared only if they are fully colocated in space and time. The standard deviation of the population, Pearson's correlation coefficient and number of retrievals are given in the inset. The legend plots the different TCCON stations where markers are as follows. Stations that are along the coast and also sensitive to glint mode (ocean) measurements are indicated as circles. Those that have high latitudes in the northern and southern hemispheres are upward triangles and crosses, respectively. Stations in Asia, North America and Europe are indicated by squares, pluses and downward triangles respectively.

The error that comes out of the RemoTeC retrieval is just a purely statistical error on the radiance that has been propagated through the entire retrieval chain.

In order to more accurately estimate the actual random error on the GOSAT-2 sounding, we applied the following procedure to obtain a scaling factor with which to scale our statistical error. We take the absolute difference of every co-located sounding and divide it by the retrieved statistical error corresponding to that sounding. We then average these values to obtain the average scaling factor by which to scale the retrieved statistical error to obtain a more correct estimate of the random error.

Based on the analysis, we obtain the following scaling factors for the SRFP XCO_2 product, 2.12 for land retrievals and 2.86 for ocean retrievals and an uncertainty ratio of 0.83 and 0.77 for land and ocean, respectively.

5.3.2 Summary

The result of the validation of the CO2_GO2_SRFP dataset is given in **Table 5.3-2** and compared to the requirement. The mean estimate of the single-measurement precision is 2.14 ppm which exceeds the goal requirement but is within the breakthrough requirement of 3 ppm. The uncertainties provided by RemoTeC agree on average with the observed scatter of the data when compared to TCCON. The mean (global bias) of the GOSAT-2 XCO_2 retrieval is -0.15 ppm with a relative accuracy of 0.57 ppm slightly exceeding the requirement of 0.5 ppm.

Table 5.3-2: Summary validation of product CO2_GO2_SRFP by the data provider using TCCON ground-based reference data.

Product Quality Summary Table for Product: CO2_GO2_SRFP Level: 2, Version: v2.0.3, Time period covered: 2.2019 – 12.2023 Assessment: Data Provider (DP)			
Parameter [unit]	**Achieved performance**	**Requirement**	**Comments**
Single measurement precision (1-sigma) in [ppm]	2.14	< 8 (T) < 3 (B) < 1 (G)	Computed as standard deviation of the difference to TCCON
Uncertainty ratio [-]: Ratio reported uncertainty to standard deviation of satellite-TCCON difference	0.83 (0.77 sunglint)	-	No requirement but value close to unity expected for a high quality data product with reliable reported uncertainty.
Mean bias (global offset) [ppm]	-0.15	-	No requirement but value close to zero expected for a high quality data product.
Accuracy: Relative systematic error [ppm]	Spatial: 0.57 Spatio-temporal: 0.89	< 0.5	Spatial: Computed as standard deviation of the biases at the various TCCON sites. Spatio-temporal: As "Spatial" but also considering seasonal biases.
Stability: Drift [ppm/year]	0.48	< 0.5	Linear drift

5.4 Validation and intercomparison results for product CH4_S5P_WFMD

Validation results for XCH_4 retrieved from TROPOMI with the WFMDv1.8 algorithm **/Schneising et al., 2023/** are summarised in this section. The validation data set is the GGG2020 collection of the Total Carbon Column Observing Network (TCCON) (available from https://tccondata.org/). To ensure comparability, all TCCON sites use similar instrumentation (Bruker IFS 125HR) and a common retrieval algorithm. The TCCON data are tied to the WMO trace gas scale using airborne in situ measurements applying individual scaling factors for each species. The estimated TCCON accuracy (1σ) is about 3.5 ppb for XCH_4. From the validation with TCCON data at 25 TCCON sites, realistic error estimates of the satellite data are provided.

To compare the satellite data with TCCON quantitatively, it has to be taken into account that the sensitivities of the instruments differ from each other and that individual apriori profiles are used to determine the best estimate of the true atmospheric state, respectively. The first step is to correct for the apriori contribution to the smoothing equation by adjusting the measurements for a common apriori. Here we use the TCCON prior as the common apriori profile for all measurements:

$$\hat{c}_{adj} = \hat{c} + \frac{1}{m_0}\sum_l m_l\,(1 - A_l)(x_{a,T}^l - x_a^l)$$

In this equation, $\hat{c}$ represents the originally retrieved TROPOMI column-averaged dry air mole fraction, l is the index of the vertical layer, A_l the corresponding column averaging kernel of the TROPOMI algorithm, $\boldsymbol{x}_a$ and $\boldsymbol{x}_{a,T}$ the TROPOMI and TCCON apriori dry air mole fraction profiles. m_l is the mass of dry air determined from the dry air pressure difference between the upper and lower boundary of layer l and $m_0 = \sum_l m_l$ is the total mass of dry air. To minimise the smoothing error introduced by the averaging kernels we do not compare $\hat{c}_{adj}$ directly with the retrieved TCCON mole fractions $\hat{c}_T$ but rather with the adjusted expression

$$\hat{c}_{T,adj} = c_{a,T} + \left(\frac{\hat{c}_T}{c_{a,T}} - 1\right)\frac{1}{m_0}\sum_l m_l A_l x_{a,T}^l$$

Thereby, $c_{a,T}$ represents the TCCON apriori column-averaged dry air mole fraction associated with the apriori profile $\boldsymbol{x}_{a,T}$.

5.4.1 Detailed results

For the comparison a set of collocation criteria has been specified. The representativity is maximised by as strict as possible criteria while concurrently ensuring sufficient data for a sound and stable comparison. This trade-off is resolved by the following selection. The spatial collocation criterion requires the satellite measurements to lie within a radius of 100 km around the TCCON site and that the altitude difference is smaller than 250 m. The temporal collocation criterion is set to ±2 hours. For each satellite measurement within the collocation radius, all TCCON data meeting the temporal collocation criterion are averaged to obtain a unique satellite-TCCON data pair. This approach is consistent with the well-established methods used in previous GHG-CCI PVIRs.

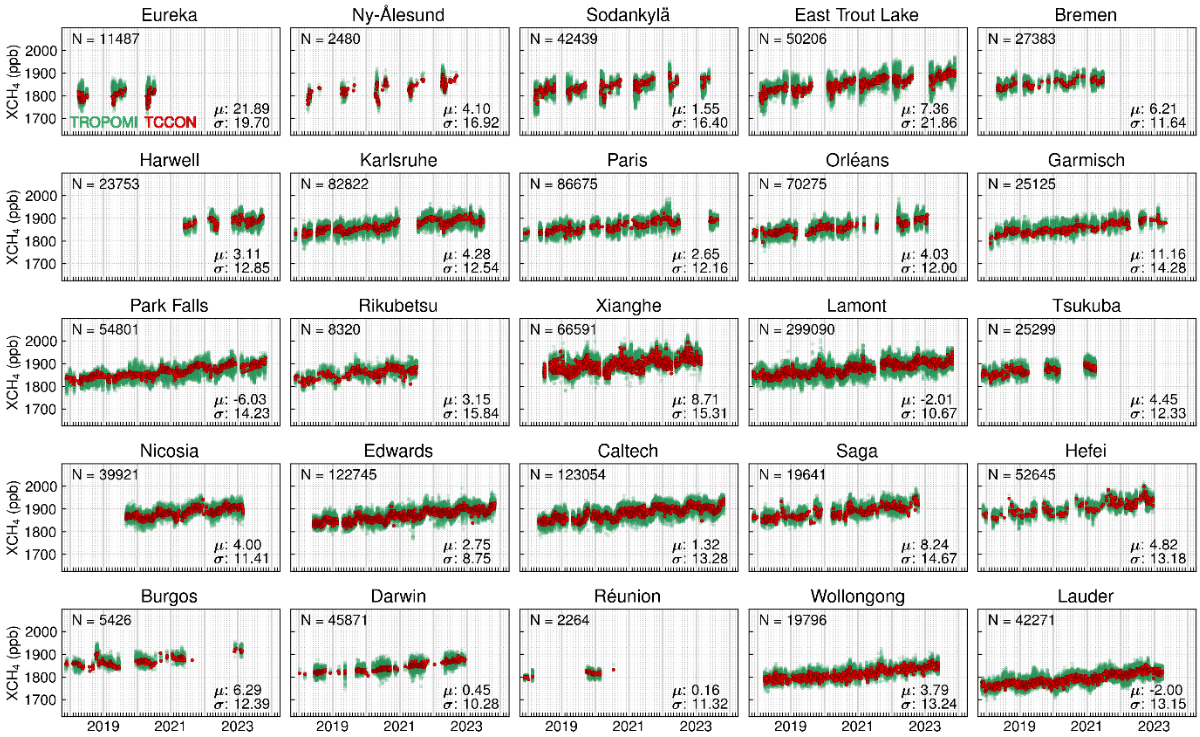

Figure 5.4-1: Comparison of the TROPOMI/WFMD v1.8 XCH_4 time series (green) with ground-based measurements from the TCCON (red). For each site, ***N*** is the number of collocations, ***μ*** corresponds to the mean bias and ***σ*** to the scatter of the satellite data relative to TCCON in ppb.

The validation results are summarised in **Figure 5.4-1** including the mean bias μ and the scatter σ relative to TCCON for each site. As a consequence of the altitude representativity criterion, there are not enough collocations for a robust comparison at the mountain site Izaña. The parameter σ is estimated from Huber's Proposal-2 M-estimator, which is a well-established estimator of location and scale being robust against outliers of a normal distribution. This is an appropriate choice and preferred over the standard deviation, because one is interested in the actual single measurement precision without distortion of the results by a few outliers, which are rather attributed to systematic errors, e.g. due to residual clouds. As a consequence, outliers are fully included in the computation of the systematic error but get lower weight in the robust determination of the random error, which is interpreted as a measure of the repeatability of measurements.

It is also checked whether the respective site biases are sensitive to the selection of the spatial collocation radius, which is an indication of sources within the satellite collocation area with only marginal influence on the TCCON measurements itself. A considerable sensitivity was found for XCH_4 at Edwards. The collocation region intersects oil production areas in California’s Central Valley (in contrast to Caltech, see **/Schneising et al., 2019/**) as well as the South Coast Air Basin (SoCAB), which has a well-known methane enhancement. As such nearby sources limit the representativity of affected satellite measurements, the collocation radius is reduced to 50 km for Edwards. A corresponding reduction of the collocation radius was also applied for the Chinese TCCON site Xianghe.

The results for the individual sites are condensed to the following parameters for the overall quality assessment of the satellite data: the global offset is defined as the mean of the local biases at the individual sites, the random error is the global scatter of the differences to TCCON after subtraction of the respective regional biases, and the spatial systematic error is the standard deviation of the local offsets relative to TCCON at the individual sites as a measure of the station-to-station biases. For XCH_4 the global offset amounts to 4.18 ppb, the random error is 12.35 ppb (13.66 ppb when using the standard deviation instead of Huber’s Proposal-2 M-estimator), and the spatial systematic error is given by 5.10 ppb. The seasonal systematic error is defined as the standard deviation of the four overall seasonal offsets (using all sites combined after subtraction of the respective local offsets) relative to TCCON and amounts to 1.19 ppb. The spatio-temporal systematic error (defined as the the root-sum-square of the spatial and seasonal systematic errors) amounts to 5.24 ppb, which is on the order of the estimated (station-to-station) accuracy of the TCCON of about 3.5 ppb.

The local offsets have considerably changed at some sites between the previous GGG2014 collection of the TCCON and GGG2020, e.g. there is an increased offset at Eureka, without resulting in an obvious improvement in agreement with TROPOMI/WFMD.

To further analyse how well the real temporal and spatial variations are captured by the TROPOMI data, **Figure 5.4-2** shows a comparison to TCCON based on daily means for days with more than three collocations. The obvious linear relationship with a high correlation of $R = 0.95$ underlines the typical good agreement of the satellite and validation data.

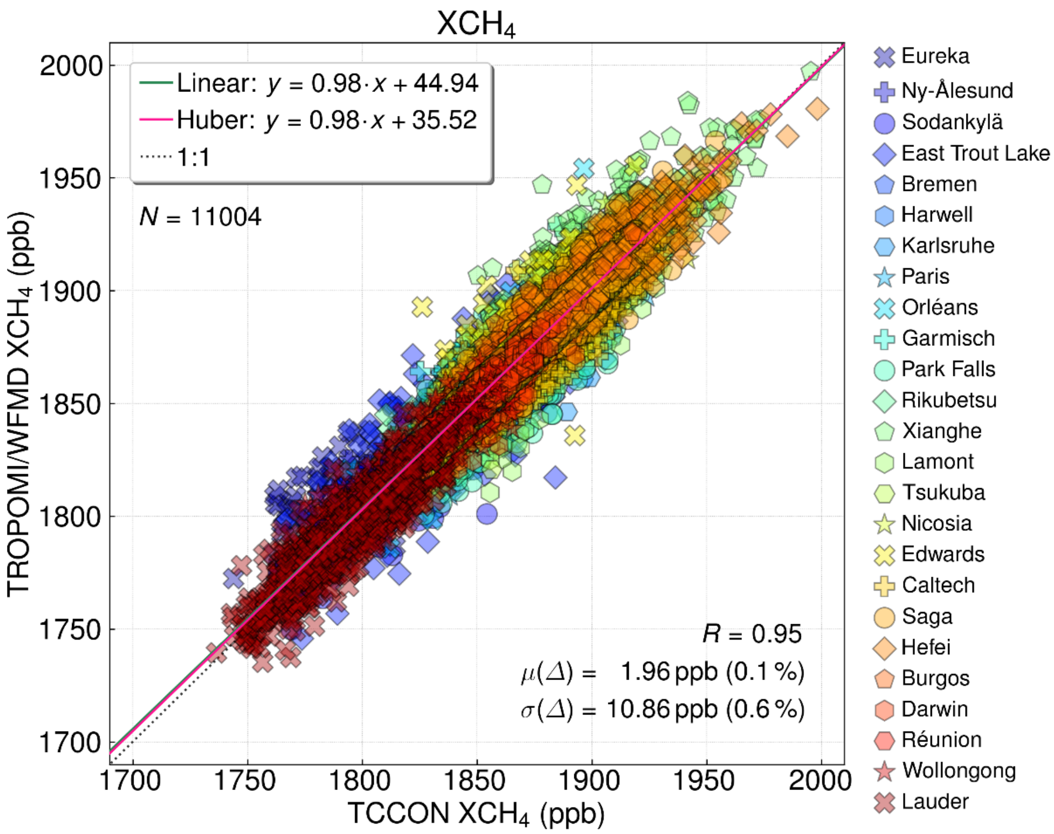

Figure 5.4-2: Comparison of the TROPOMI/WFMD data to the TCCON based on daily means. Specified are the linear regression results and the correlation of the data sets, as well as the mean and standard deviation of the difference. To analyse the impact of outliers, the regression is also performed for the Huber linear regression model, which is robust to outliers.

There are a few outliers where the satellite values are considerably lower than the TCCON values. These occasional instances are not site specific and can probably be ascribed to days with residual or partial cloud cover interfering with the satellite retrievals. Outliers at high latitude sites may be attributable to Arctic polar vortex air potentially causing the following related issues: associated fronts of different air masses may complicate the identification of collocations near the vortex edge and/or the stratospheric part of the methane profiles may be largely affected by the polar vortex leading to a considerable deviation from the assumed apriori profile shapes. It is verified that the impact of outliers on the regression is marginal by repeating the fit with the Huber linear regression model, which is robust to outliers and provides similar results to the standard linear regression here.

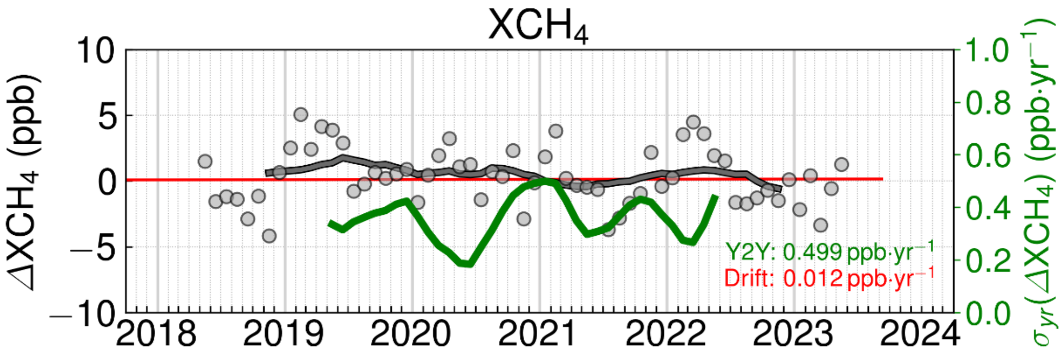

Figure 5.4-3: Long-term drift and year-to-year stability of TROPOMI/WFMD at TCCON sites.

To analyse the stability, we use comparisons with the TCCON since the start of the routine operations phase of Sentinel-5P to have sufficient data coverage. To assess the long-term drift stability, a robust Huber regression of the monthly mean differences relative to the reference (using all data combined after subtraction of the respective regional offsets) with time is used. The resulting stability estimate is 0.01 ppb/year (see red straight line in **Figure 5.4-3**).

The year-to-year stability allowing to detect potential jumps in the time series is defined in the following way: The one-year moving average of the differences relative to the reference (grey curve in **Figure 5.4-3**) is generated. For a given point in time t, let $\sigma_{yr}(t)$ be defined as the standard deviation of this deseasonalised difference within a one-year window around t (green curve in **Figure 5.4-3**). The year-to-year stability is then defined as the maximum of $\sigma_{yr}(t)$ over time, which amounts to 0.50 ppb/year here. Due to the moving average and the one-year moving standard deviation procedure, the green curve loses one year of data at the beginning and end of the time series.

The reported uncertainty of TROPOMI/WFMD v1.8 XCH_4 is validated based on a comparison to the measured scatter relative to the TCCON. After dividing up the reported uncertainties in equal sized bins of about 20000 measurements each, a robust regression provides the results shown in **Figure 5.4-4** (neglecting the random and systematic errors of the TCCON measurements) confirming that the reported estimates are realistic: The uncertainty ratio (reported uncertainty to measured scatter) is about 1.06, indicating a reliable estimation of the measurement uncertainties with a slight overestimation of the reported values.

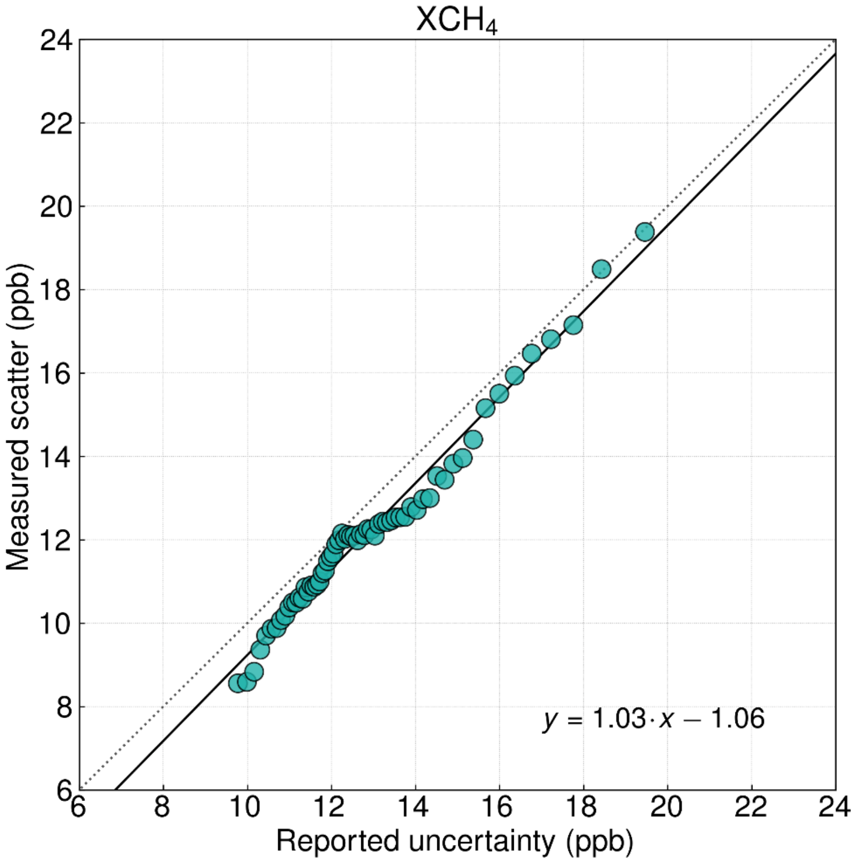

Figure 5.4-4: Comparison of the reported uncertainty of TROPOMI/WFMD v1.8 XCH_4 with the measured scatter relative to the TCCON after dividing up the reported uncertainties in equal sized bins.

5.4.2 Summary

In summary, the natural XCH_4 variations are well captured by the satellite data. We find a single measurement precision of the TROPOMI data of about 0.7%, while the station-to-station accuracy of the satellite data (0.3%) is comparable to the TCCON.

The single measurement precision is below the breakthrough requirement and the uncertainty ratio is close to 1. The accuracy also complies with the requirements and the stability is well below the required value. **Table 5.4-1** presents an overview of the estimated data quality as obtained from comparisons with TCCON ground-based reference observations.

Table 5.4-1: Summary validation of product CH4_S5P_WFMD by the data provider using TCCON GGG2020 ground-based reference data.

Product Quality Summary Table for Product: CH4_S5P_WFMD Level: 2, Version: v1.8, Time period covered: 11.2017 – 12.2022 Assessment: Data Provider (DP)			
Parameter [unit]	**Achieved performance**	**Requirement**	**Comments**
Single measurement precision (1-sigma) in [ppb]	12.35	< 34 (T) < 17 (B) < 9 (G)	Computed as standard deviation of the difference to TCCON
Uncertainty ratio [-]: Ratio reported uncertainty to standard deviation of satellite-TCCON difference	1.06	-	No requirement but value close to unity expected for a high quality data product with reliable reported uncertainty.
Mean bias (global offset) [ppb]	4.18	-	No requirement but value close to zero expected for a high quality data product.
Accuracy: Relative systematic error [ppb]	Spatial: 5.10 Spatio-temporal: 5.24	< 10	Spatial: Computed as standard deviation of the biases at the various TCCON sites. Spatio-temporal: As "Spatial" but also considering seasonal biases.
Stability: Drift [ppb/year]	0.01	< 3	Linear drift

5.5 Validation and intercomparison results for product CH4_GO2_SRFP

The CH4_GO2_SRFP product is retrieved from GOSAT-2 TANSO-FTS SWIR spectra using the RemoTeC algorithm that has been jointly developed by SRON and KIT **/Butz et al., 2011; Schepers et al., 2012/**. The retrievals are performed globally for the time period between February 2019 and December 2023 and are evaluated against ground based TCCON observations.

5.5.1 Detailed results

To assess the quality of SRFP retrieval XCH_4 observations against ground based TCCON values, SRFP soundings are matched to TCCON observations spatially and temporally. GOSAT-2 observations are co-located with TCCON sites based on a square latitude and longitude region around each TCCON site (in ±2.5º latitude/longitude box). For the temporal co-location we select only the TCCON measurements whose observation time falls within ±2 hour of each GOSAT-2 observation time. The TCCON observations that match these criteria are averaged for each individual GOSAT-2 observation.

We co-located GOSAT-2 and TCCON measurements with a maximum time difference of 2.5h, a maximum distance of 300 km in both longitudinal and latitudinal directions. In cases of multiple TCCON measurements of the same site collocating with a GOSAT-2 sounding, we averaged the TCCON measurements. In total we achieve 17,319 collocations for land soundings and 349 collocations over ocean.

The comparison for each TCCON site is shown in **Figure 5.5-1**. The statistics (mean bias, standard deviation) for each site are given in **Table 5.5-1**. The overall correlation between the GOSAT-2 and TCCON retrievals is given in **Figure 5.5-2**. The mean bias (global offset) amounts to 0.41 ppb. The standard deviation of the site biases (spatial accuracy or station-to-station variability) is 4.78 ppb. The single measurement precision of GOSAT-2 compared to TCCON amounts to 15.2 ppb.

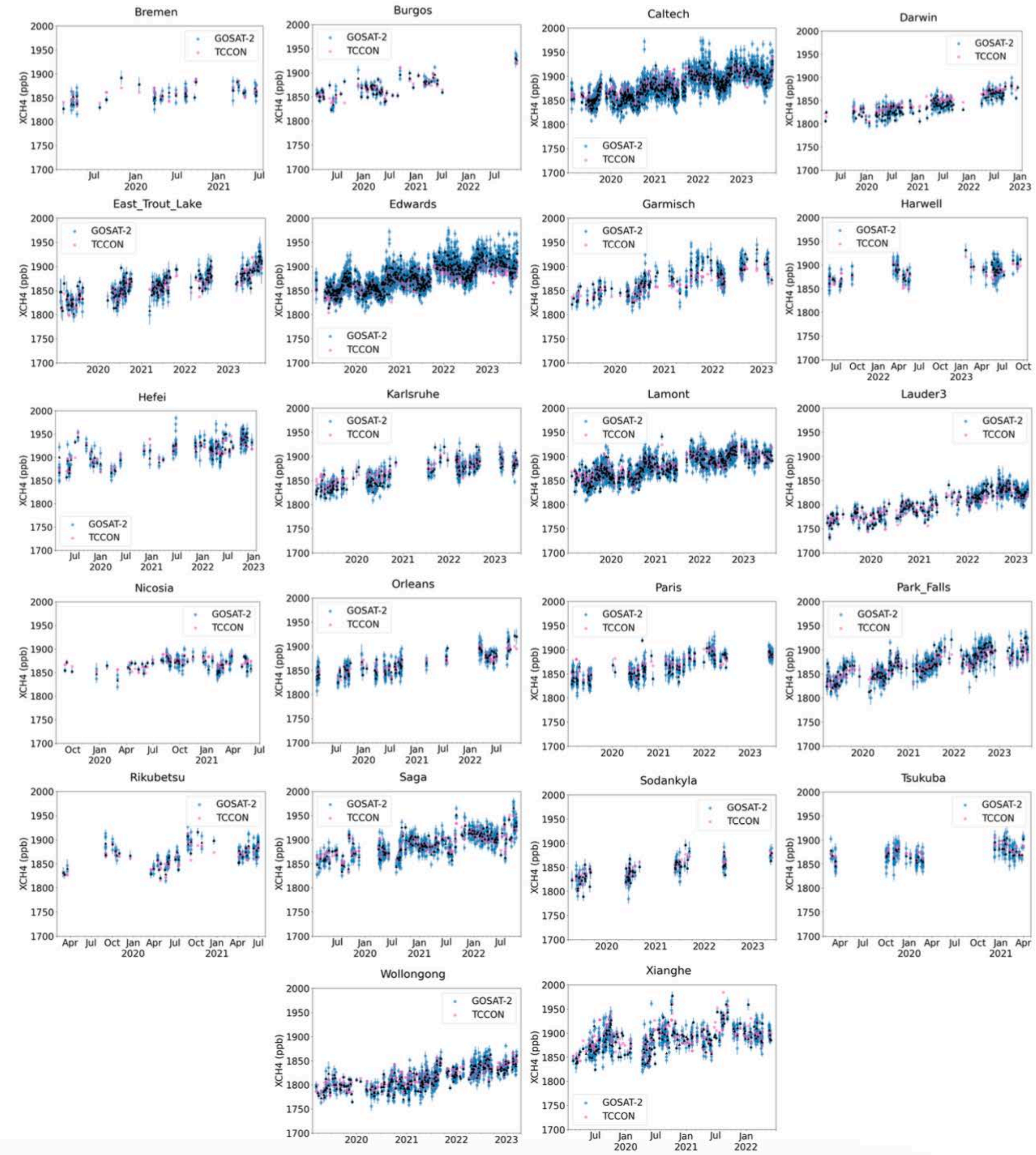

Figure 5.5-1: Comparison of land single soundings of XCH_4 from the full physics retrieval (blue circles) with co-located TCCON (pink triangles) measurements at all TCCON sites.

Table 5.5-1: Overview of the SRFP/RemoTeC XCH_4 validation with TCCON (after bias correction) for land retrievals.

TCCON site [Land mode]	Δreg (ppb)	Δseas (ppb)	Δdri (ppb yr^{-1})	Δspt (ppb)	N
Bremen	0.04	6.63	6.14	6.63	99
Burgos	0.87	7.68	1.78	7.73	124
Caltech	-2.77	3.28	1.64	4.29	3161
Darwin	-7.56	6.03	-3.80	9.67	312
East Trout Lake	1.74	1.23	-2.56	2.13	472
Edwards	8.98	2.06	2.31	9.21	3563
Garmisch	11.49	0.49	4.51	11.5	527
Harwell	3.18	2.49	-0.31	4.04	283
Hefei	1.29	3.31	1.27	3.56	394
Karlsruhe	-0.91	4.08	3.27	4.18	505
Lamont	-2.67	0.59	0.48	2.73	1890
Lauder3	1.37	2.14	0.36	2.54	716
Nicosia	-3.44	2.27	5.39	4.12	198
Orleans	3.73	6.73	0.32	7.70	414
Paris	-4.09	6.72	0.11	7.86	591
Park Falls	3.86	5.08	-0.60	6.38	715
Rikubetsu	9.26	5.51	-4.27	10.78	200
Saga	-1.88	1.44	1.07	2.37	896
Sodankyla	-0.98	7.61	-3.96	7.67	151
Tsukuba	-5.58	2.66	1.67	6.18	300
Wollongong	-3.89	2.96	-1.17	4.89	1079
Xianghe	-3.13	3.93	3.34	5.03	718

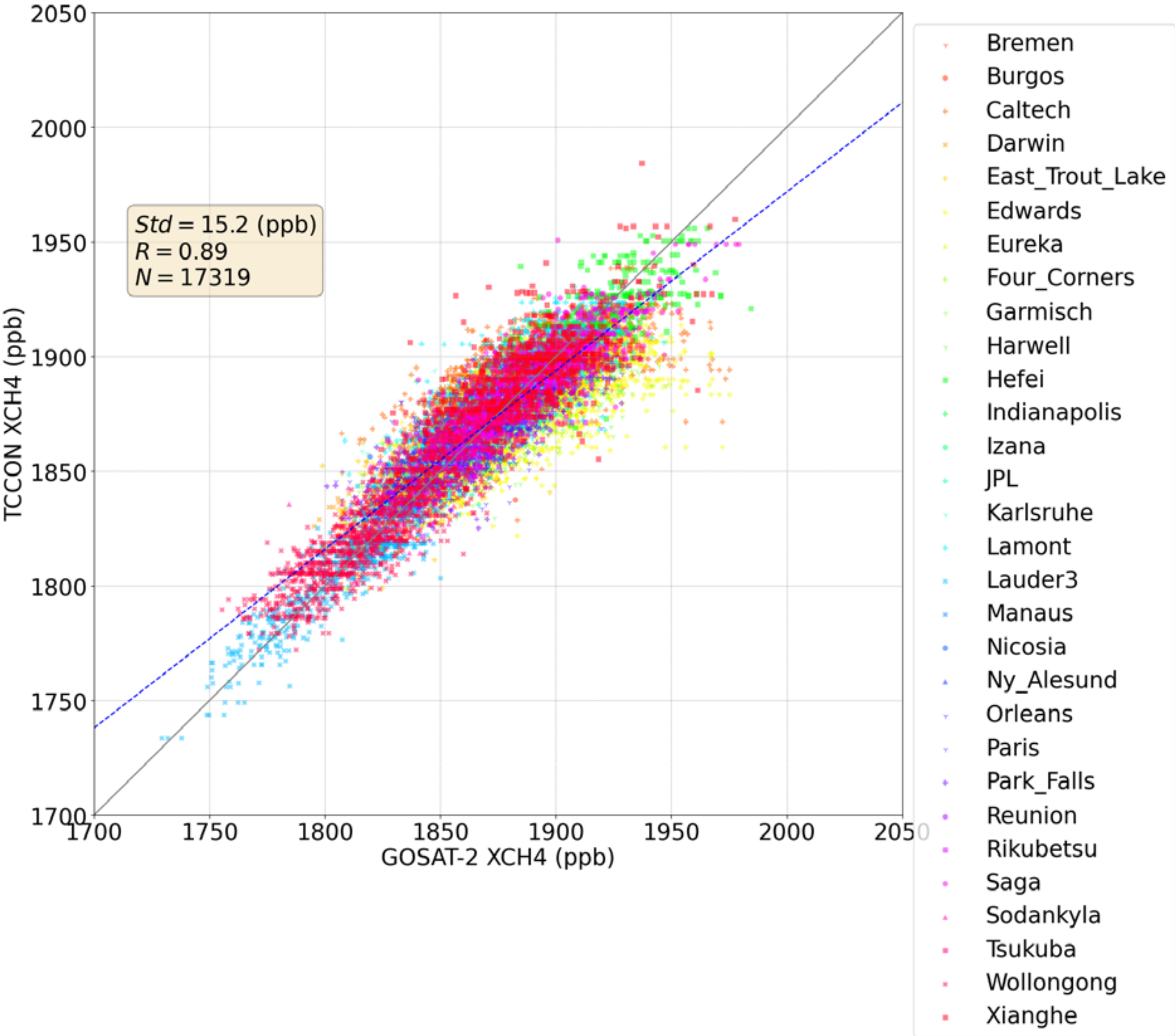

Figure 5.5-2: GOSAT-2 XCH_4 for soundings over land plotted against TCCON, for the RemoTeC Full Physics product. Data are compared only if they are fully colocated in space and time. The standard deviation of the population, Pearson's correlation coefficient and number of retrievals are given in the inset. The legend plots the different TCCON stations where markers are as follows. Stations that are along the coast and also sensitive to glint mode (ocean) measurements are indicated as circles. Those that have high latitudes in the northern and southern hemispheres are upward triangles and crosses, respectively. Stations in Asia, North America and Europe are indicated by squares, pluses and downward triangles respectively.

The error that comes out of the RemoTeC retrieval is just a purely statistical error on the radiance that has been propagated through the entire retrieval chain. In order to more accurately estimate the actual random error on the GOSAT-2 sounding, we applied the following procedure to obtain a scaling factor with which to scale our statistical error. We take the absolute difference of every co-located sounding and divide it by the retrieved statistical error corresponding to that sounding. We then average these values to obtain the average scaling factor by which to scale the retrieved statistical error to obtain a more correct estimate of the random error.

Based on the analysis, we obtain the following scaling factors for the SRFP XCH_4 product, 1.69 for the normal mode and 1.80 for the sunglint mode. Subsequently, we calculate the uncertainty ratio which is defined as the ratio of the mean value of the reported uncertainty and the standard deviation of the difference to TCCON. We obtain uncertainty ratios of 0.89 for the normal mode and 0.89 for the sunglint mode.

5.5.2 Summary

The result of the validation of the CH4_GO2_SRFP dataset is given in **Table 5.5-2** and compared to the requirement. The mean estimate of the single-measurement precision is 15.2 ppb which exceeds the goal requirement but is within the breakthrough requirement of 17 ppb. The uncertainties provided by RemoTeC agree on average with the observed scatter of the data when compared to TCCON. The mean, global bias of the GOSAT-2 XCH_4 retrieval is 0.41 ppb with a relative accuracy of 4.78 ppb which is smaller than the requirement of 10 ppb.

Table 5.5-2: Summary validation of product CH4_GO2_SRFP by the data provider using TCCON ground-based reference data.

Product Quality Summary Table for Product: CH4_GO2_SRFP Level: 2, Version: v2.0.3, Time period covered: 2.2019 – 12.2023 Assessment: Data Provider (DP)			
Parameter [unit]	**Achieved performance**	**Requirement**	**Comments**
Single measurement precision (1-sigma) in [ppb]	15.2	< 34 (T) < 17 (B) < 9 (G)	Computed as standard deviation of the difference to TCCON
Uncertainty ratio [-]: Ratio reported uncertainty to standard deviation of satellite-TCCON difference	0.89 (0.89 glint)	-	No requirement but value close to unity expected for a high quality data product with reliable reported uncertainty.
Mean bias (global offset) [ppb]	-0.41	-	No requirement but value close to zero expected for a high quality data product.
Accuracy: Relative systematic error [ppb]	Spatial: 4.78 Spatio-temporal: 5.96	< 10	Spatial: Computed as standard deviation of the biases at the various TCCON sites. Spatio-temporal: As "Spatial" but also considering seasonal biases.
Stability: Drift [ppb/year]	0.77 (1-sigma)	< 3	Linear drift

5.6 Validation and intercomparison results for product CH4_GO2_SRPR

The CH4_GO2_SRPR product is retrieved from GOSAT-2 TANSO-FTS SWIR spectra using the RemoTeC algorithm that has been jointly developed by SRON and KIT **/Butz et al., 2011; Schepers et al., 2012/**. The retrievals are performed globally for the time period between February 2019 and December 2023 and are evaluated against ground based TCCON observations.

5.6.1 Detailed results

To assess the quality of SRPR retrieval XCH_4 observations against ground based TCCON values, SRPR soundings are matched to TCCON observations spatially and temporally. GOSAT-2 observations are co-located with TCCON sites based on a square latitude and longitude region around each TCCON site (in ±2.5º latitude/longitude box). For the temporal co-location we select only the TCCON measurements whose observation time falls within ±2 hour of each GOSAT-2 observation time. The TCCON observations that match these criteria are averaged for each individual GOSAT-2 observation.

We co-located GOSAT-2 and TCCON measurements with a maximum time difference of 2.5h, a maximum distance of 300 km in both longitudinal and latitudinal directions. In cases of multiple TCCON measurements of the same site collocating with a GOSAT-2 sounding, we averaged the TCCON measurements. In total we achieve 56,022 collocations for land soundings and 798 collocations over ocean.

The comparison for each TCCON site is shown in **Figure 5.6-1**. The statistics (mean bias, standard deviation) for each site are given in **Table 5.6-1**. The overall correlation between the GOSAT-2 and TCCON retrievals is given in **Figure 5.6-2**. The mean bias (global offset) amounts to -0.23 ppb. The standard deviation of the site biases (spatial accuracy or station-to-station variability) is 5.2 ppb. The single measurement precision of GOSAT-2 compared to TCCON amounts to 15.69 ppb.

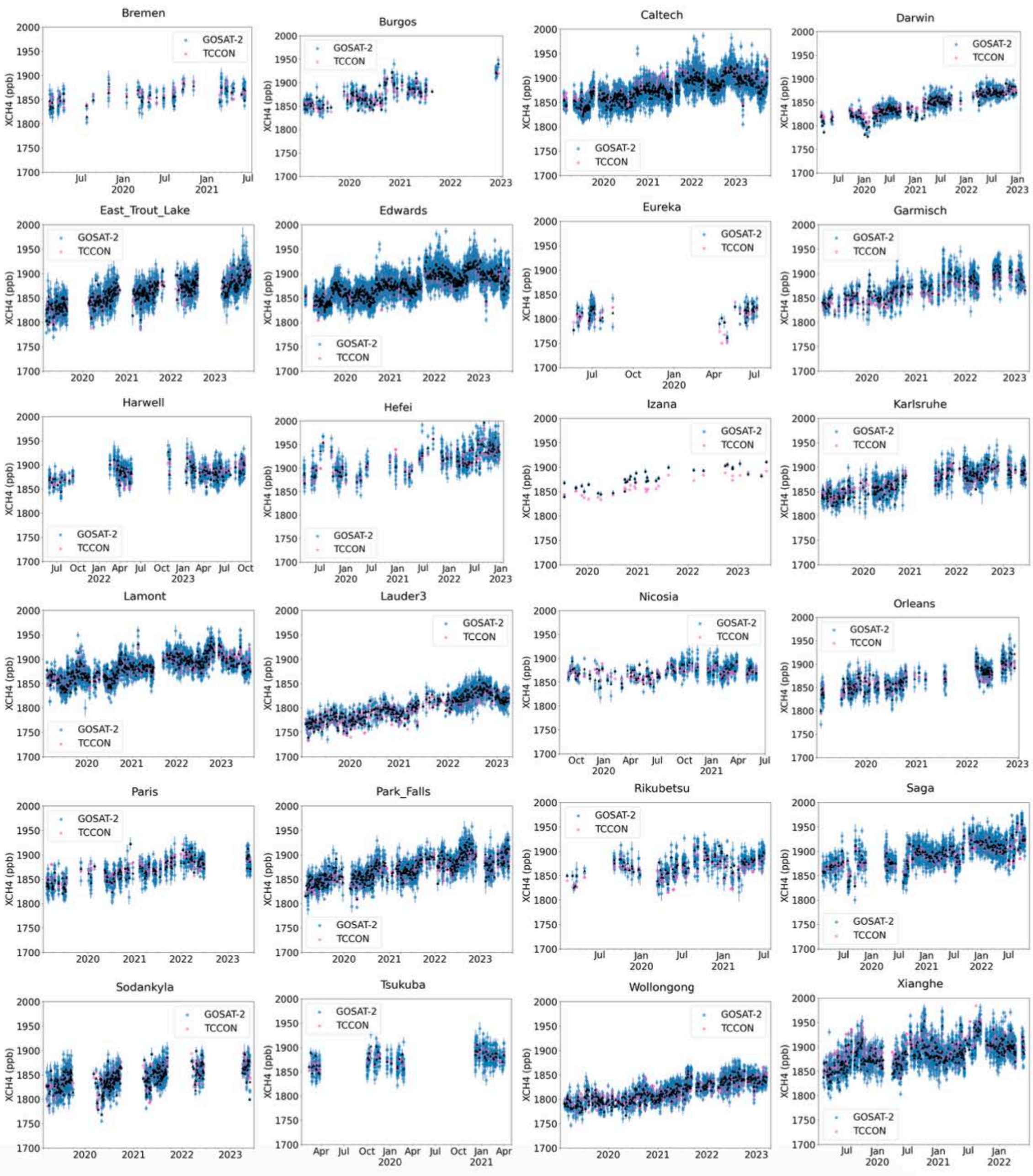

Figure 5.6-1: Comparison of land single soundings of XCH_4 from the Proxy retrieval (blue circles) with co-located TCCON (pink triangles) measurements at all TCCON sites.

Table 5.6-1: Overview of TCCON validation of XCH_4 from the GOSAT-2 Proxy product.

TCCON site [Land mode]	Δreg (ppb)	Δseas (ppb)	Δdri (ppb yr^{-1})	Δspt (ppb)	N
Bremen	-0.29	5.94	5.6	5.95	276
Burgos	3.53	1.54	-1.51	3.85	535
Caltech	-6.96	0.66	1.24	6.99	9551
Darwin	-2.62	3.0	1.8	3.99	1073
East Trout Lake	0.19	1.94	-0.65	1.95	2991
Edwards	5.82	3.55	-1.26	6.82	10642
Eureka	-4.42	6.7	0.65	8.02	165
Garmisch	9.61	1.8	0.14	9.78	1523
Harwell	0.55	3.39	-1.5	3.43	1239
Hefei	2.51	3.0	0.73	3.91	1183
Karlsruhe	-1.46	4.3	0.66	4.54	1500
Lamont	0.99	5.42	-3.5	5.51	3910
Lauder3	2.82	1.79	-0.17	3.34	2163
Nicosia	1.53	1.31	3.86	2.02	864
Ny Alesund	-16.0	6.75	1.63	17.37	115
Orleans	-1.48	5.3	6.96	5.5	1268
Paris	-0.17	5.49	5.62	5.49	1322
Park Falls	2.72	2.93	-1.83	4.0	2573
Rikubetsu	7.75	2.08	0.71	8.02	858
Saga	2.63	0.6	0.86	2.7	3065
Sodankyla	-2.08	5.63	-2.2	6.0	1527
Tsukuba	-3.38	4.14	5.54	5.34	798
Wollongong	0.87	1.62	0.25	1.84	3032
Xianghe	-8.26	1.88	4.89	8.47	3813

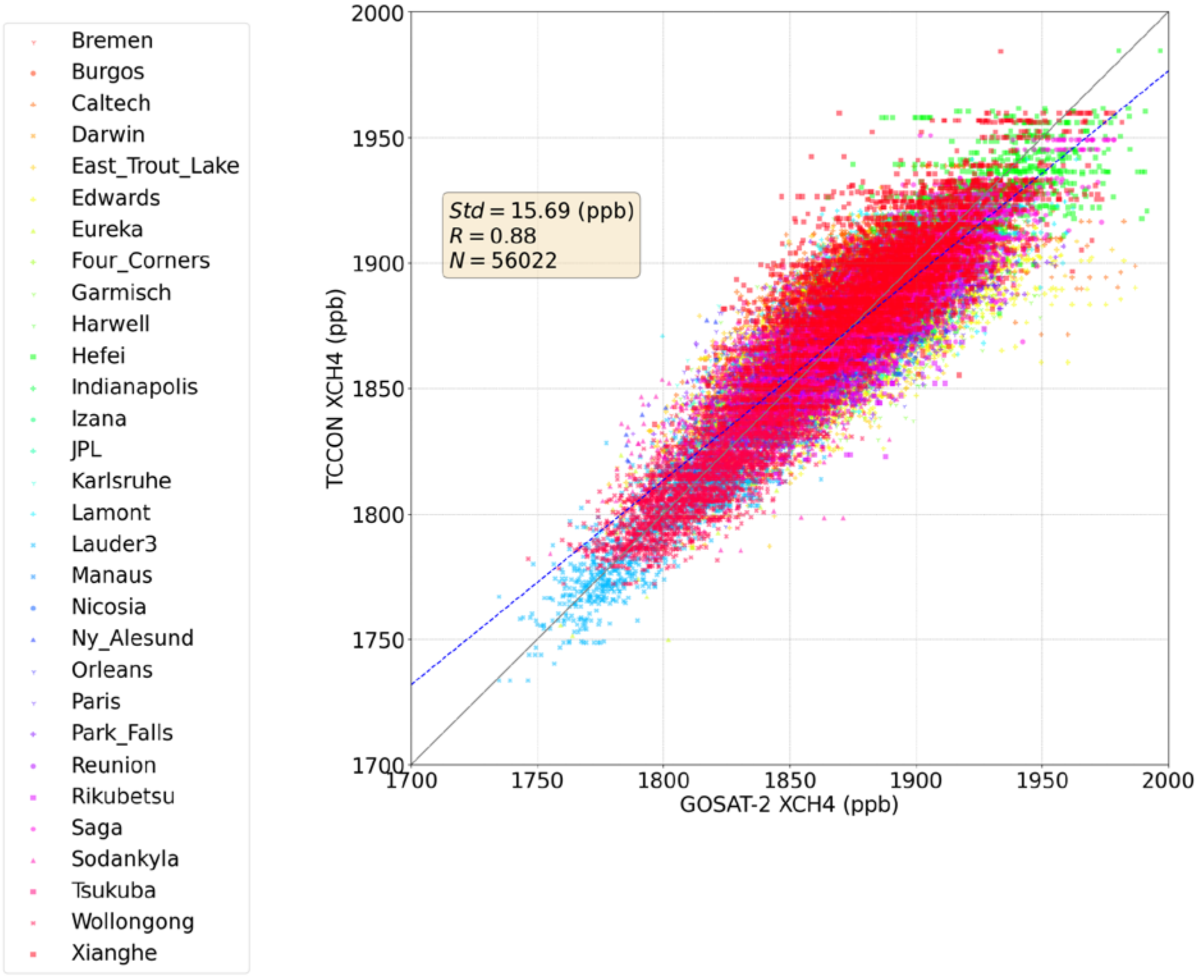

Figure 5.6-2: GOSAT-2 XCH_4 for soundings over land plotted against TCCON, for the RemoTeC Proxy product. Data are compared only if they are fully colocated in space and time. The standard deviation of the population, Pearson's correlation coefficient and number of retrievals are given in the inset. The legend plots the different TCCON stations where markers are as follows. Stations that are along the coast and also sensitive to glint mode (ocean) measurements are indicated as circles. Those that have high latitudes in the northern and southern hemispheres are upward triangles and crosses, respectively. Stations in Asia, North America and Europe are indicated by squares, pluses and downward triangles respectively.

The error that comes out of the RemoTeC retrieval is just a purely statistical error on the radiance that has been propagated through the entire retrieval chain. In order to more accurately estimate the actual random error on the GOSAT-2 sounding, we applied the following procedure to obtain a scaling factor with which to scale our statistical error. We take the absolute difference of every co-located sounding and divide it by the retrieved statistical error corresponding to that sounding. We then average these values to obtain the average scaling factor by which to scale the retrieved statistical error to obtain a more correct estimate of the random error.

Based on the analysis, we obtain the following scaling factors for the SRPR XCH_4 product, 1.84 for the normal mode and 1.58 for the sunglint mode. Subsequently, we calculate the uncertainty ratio which is defined as the ratio of the mean value of the reported uncertainty and the standard deviation of the difference to TCCON. We obtain uncertainty ratios of 0.81 for the normal mode and 0.77 for the sunglint mode.

5.6.2 Summary

The result of the validation of the CH4_GO2_SRPR dataset is given in **Table 5.6-2** and compared to the requirement. The mean estimate of the single-measurement precision is 15.69 ppb which exceeds the goal requirement but is within the breakthrough requirement of 17 ppb. The uncertainties provided by RemoTeC agree on average with the observed scatter of the data when compared to TCCON. The mean, global bias of the GOSAT-2 XCH_4 retrieval is -0.23 ppb with a relative accuracy of 5.2 ppb which is smaller than the requirement of 10 ppb.

Table 5.6-2: Summary validation of product CH4_GO2_SRPR by the data provider using TCCON ground-based reference data.

Product Quality Summary Table for Product: CH4_GO2_SRPR Level: 2, Version: v2.0.3, Time period covered: 2.2019 – 12.2023 Assessment: Data Provider (DP)			
Parameter [unit]	**Achieved performance**	**Requirement**	**Comments**
Single measurement precision (1-sigma) in [ppb]	15.69	< 34 (T) < 17 (B) < 9 (G)	Computed as standard deviation of the difference to TCCON
Uncertainty ratio [-]: Ratio reported uncertainty to standard deviation of satellite-TCCON difference	0.81	-	No requirement but value close to unity expected for a high quality data product with reliable reported uncertainty.
Mean bias (global offset) [ppb]	-0.23	-	No requirement but value close to zero expected for a high quality data product.
Accuracy: Relative systematic error [ppb]	Spatial: 5.2 Spatio-temporal: 5.62	< 10	Spatial: Computed as standard deviation of the biases at the various TCCON sites. Spatio-temporal: As "Spatial" but also considering seasonal biases.
Stability: Drift [ppb/year]	1.18 (1-sigma)	< 3	Linear drift

6 References

/Aben et al., 2019/ Aben, I., L. Wu, O. Hasekamp, M. Buchwitz, M. Reuter, O. Schneising, H. Boesch, D. Yang, ESA Climate Change Initiative "Plus" (CCI+) System Specification Document (SSD) for the Essential Climate Variable (ECV) Greenhouse Gases (GHG): XCO_2 and/or XCH_4 from OCO-2, TanSat, Sentinel-5-Precursor and GOSAT-2, Version 1.0, 26-August-2019, pp. 33, 2019.

/Ackermann et al., 2010/ Ackerman, S.; Frey, R.; Strabala, K.; Liu, Y.; Gumley, L.; Baum, B.; Menzel, P. Discriminating Clear-Sky from Cloud with MODIS—Algorithm Theoretical Basis Document (MOD35); Version 6.1; Cooperative Institute for Meteorological Satellite Studies, University ofWisconsin—Madison: Madison, WI, USA, 2010.

/ATBDv1 FOCAL, 2019/ Reuter et al.: Algorithm Theoretical Basis Document Version 1 (ATBDv1) - Retrieval of XCO_2 from the OCO-2 satellite using the Fast Atmospheric Trace Gas Retrieval (FOCAL), ESA GHG-CCI project, 2019.

/ATBDv3, 2021/ M. Reuter, M. Hilker, S. Noël, M. Buchwitz, O. Schneising, H. Bovensmann, and J. P. Burrows: Algorithm Theoretical Basis Document Version 3 (ATBDv3) - Retrieval of XCO2 from the OCO-2 satellite using the Fast Atmospheric Trace Gas Retrieval (FOCAL), ESA Climate Change Initiative "Plus" (CCI+) for the Essential Climate Variable (ECV) Greenhouse Gases (GHG), ESA GHG CCI+, 2021.

/ATBDv5, 2024/ M. Reuter, M. Hilker, S. Noël, M. Buchwitz, O. Schneising, H. Bovensmann, and J. P. Burrows: Algorithm Theoretical Basis Document Version 5 (ATBDv5) for the FOCAL XCO2 OCO-2 Data Product CO2_OC2_FOCA (v11), ESA Climate Change Initiative "Plus" (CCI+) for the Essential Climate Variable (ECV) Greenhouse Gases (GHG), ESA GHG CCI+, 2024

/Batchelor at al., 2009/ Batchelor, R. L., Strong, K., Lindenmaier, R., Mittermeier, R. L.,Fast, H., Drummond, J. R., and Fogal, P. F.: A New Bruker IFS 125HR FTIR Spectrometer for the Polar Environment Atmospheric Research Laboratory at Eureka, Nunavut, Canada: Measurements and Comparison with the Existing Bomem DA8 Spectrometer, J. Atmos. Ocean. Tech., 26, 1328–1340,https://doi.org/10.1175/2009JTECHA1215.1, 2009.

/Blumenstock et al., 2020/ Blumenstock T., Raffalski U., and Matsumi Y., NDACC Metadata File for Eureka FTIR and references cited therein, https://www-air.larc.nasa.gov/pub/NDACC/PUBLIC/meta/ftir/Kiruna_ftir_tb_2020.pdf

/Boesch et al., 2011/ Boesch, H., Baker, D., Connor, B., Crisp, D., and Miller, C.: Global characterization of CO_2 column retrievals from shortwave-infrared satellite observations of the Orbiting Carbon Observatory-2 mission, Remote Sens., 3, 270–304, doi:10.3390/rs3020270, 2011.

/Bovensmann et al., 2010/ Bovensmann, H., Buchwitz, M., Burrows, J. P., Reuter, M., Krings, T., Gerilowski, K., Schneising, O., Heymann, J., Tretner, A., and Erzinger, J.: A remote sensing technique for global monitoring of power plant CO2 emissions from space and related applications, Atmospheric Measurement Techniques, 3, 781–811, doi:10.5194/amt-3-781-2010, URL http: //www.atmos-meas-tech.net/3/781/2010/, 2010.

/Buschmann et al. 2022/ Buschmann, M., Petri, C., Palm, M., Warneke, T., & Notholt, J. (2022). TCCON data from Ny-Ålesund, Svalbard (NO), Release GGG2020.R0 (Version R0) [Data set]. CaltechDATA. https://doi.org/10.14291/tccon.ggg2020.nyalesund01.R0.

/Butz et al., 2009/ Butz, André, Otto P. Hasekamp, Christian Frankenberg, and Ilse Aben, "Retrievals of atmospheric CO_2 from simulated space-borne measurements of backscattered near-infrared sunlight: accounting for aerosol effects," Appl. Opt. 48, 3322-3336 (2009)

/Butz et al., 2010/ Butz, André, Otto P. Hasekamp, Christian Frankenberg, Jerome Vidot, and Ilse Aben, ",CH4 retrievals from space-based solar backscatter measurements: Performance evaluation against simulated aerosol and cirrus loaded scenes" , J. Geophys. Res., 115, 24,302, doi:10.1029/2010JD014514, 2010.

/Butz et al., 2011/ Butz, A., S. Guerlet, O. Hasekamp, et al., Toward accurate CO_2 and CH_4 observations from GOSAT, Geophys. Res. Lett., Geophys. Res. Lett., doi:10.1029/2011GL047888, 2011.

/CECRv3, 2017/ M. Reuter, O. Schneising, M. Buchwitz, J. Heymann: Comprehensive Error Characterisation Report: BESD full-physics retrieval algorithm for XCO2 for the Essential Climate Variable (ECV) Greenhouse Gases (GHG), ESA GHG-CCI project, 2017.

/De Mazière et al., 2017/ De Mazière, M., Sha, M. K., Desmet, F., Hermans, C., Scolas, F., Kumps, N., Metzger, J.-M., Duflot, V., and Cammas, J.-P.: TCCON data from Réunion Island (RE), Release GGG2014.R1, https://doi.org/10.14291/TCCON.GGG2014.REUNION01.R1, https://data.caltech.edu/records/322, 2017.

/De Mazière et al., 2018/ De Mazière, M., Thompson, A. M., Kurylo, M. J., Wild, J. D., Bernhard, G., Blumenstock, T., Braathen, G. O., Hannigan, J. W., Lambert, J.-C., Leblanc, T., McGee, T. J., Nedoluha, G., Petropavlovskikh, I., Seckmeyer, G., Simon, P. C., Steinbrecht, W., and Strahan, S. E.: The Network for the Detection of Atmospheric Composition Change (NDACC): history, status and perspectives, Atmos. Chem. Phys., 18, 4935–4964, https://doi.org/10.5194/acp-18-4935-2018, 2018.

/De Mazière et al., 2022/ De Mazière, M., Sha, M. K., Desmet, F., Hermans, C., Scolas, F., Kumps, N., Zhou, M., Metzger, J.-M., Duflot, V., & Cammas, J.-P. : TCCON data from Réunion Island (RE), Release GGG2020.R0 (Version R0) [Data set]. CaltechDATA. https://doi.org/10.14291/tccon.ggg2020.reunion01.R0, 2022.

/Deutcher et al, 2010/ Deutscher, N. M., Griffith, D. W. T., Bryant, G. W., Wennberg, P.O., Toon, G. C., Washenfelder, R. A., Keppel-Aleks, G., Wunch,D., Yavin, Y., Allen, N. T., Blavier, J.-F., Jiménez, R., Daube,B. C., Bright, A. V., Matross, D. M., Wofsy, S. C., and Park,S.: Total column CO2 measurements at Darwin, Australia – site description and calibration against in situ aircraft profiles, Atmos. Meas. Tech., 3, 947–958, https://doi.org/10.5194/amt-3-947-2010, 2010

/Deutscher et al., 2019/ Deutscher, N. M., Notholt, J., Messerschmidt, J., Weinzierl, C., Warneke, T., Petri, C., and Grupe, P.: TCCON data from Bialystok (PL), Release

GGG2014.R2, https://doi.org/10.14291/TCCON.GGG2014.BIALYSTOK01.R2, https://data.caltech.edu/records/1300, 2019.

/Deutscher et al., 2023/ Deutscher, N. M., Griffith, D. W. T., Paton-Walsh, C., Jones, N. B., Velazco, V. A., Wilson, S. R., Macatangay, R. C., Kettlewell, G. C., Buchholz, R. R., Riggenbach, M. O., Bukosa, B., John, S. S., Walker, B. T., & Nawaz, H. (2023). TCCON data from Wollongong (AU), Release GGG2020.R0 (Version R0) [Data set]. CaltechDATA. https://doi.org/10.14291/tccon.ggg2020.wollongong01.R0

/E3UBv3, 2022/ M.Reuter, M.Hilker, M. Ingendahl, and M.Buchwitz: End-to-End ECV Uncertainty Budget Version 3 (E3UBv3) for the FOCAL XCO_2 OCO-2 Data Product CO2_OC2_FOCA (v10) for the Essential Climate Variable (ECV) Greenhouse Gases (GHG) ESA Climate Change Initiative "Plus" (CCI+), 2022

/Eldering et al., 2015/ Eldering, A.; Pollock, R.; Lee, R.; Rosenberg, R.; Oyafuso, F.; Crisp, D.; Chapsky, L.; Granat, R. Orbiting Carbon Observatory-2 (OCO-2) - LEVEL 1B - Algorithm Theoretical Basis; Version 1.2 Rev 1; National Aeronautics and Space Administration, Jet Propulsion Laboratory, California Institute of Technology: Pasadena, CA, USA, 2015.

/Feist et al.,2014/ Feist, D. G., Arnold, S. G., John, N., and Geibel, M. C.: TCCON data from Ascension Island (SH), Release GGG2014.R0, https://doi.org/10.14291/TCCON.GGG2014.ASCENSION01.R0/1149285, https://data.caltech.edu/records/210, 2014.

/Frankenberg et al., 2005/ Frankenberg, C., Meirink, J.F., van Weele, M., Platt, U., Wagner, T. (2005), Assessing methane emissions from global space-borne obseravtions, Science, ., doi:10.1126/science.1106644

/Frankenberg et al., 2011/ Frankenberg, C., Aben, I., Bergamaschi, P., et al. (2011), Global column-averaged methane mixing ratios from 2003 to 2009 as derived from SCIAMACHY: Trends and variability, J. Geophys. Res., doi:10.1029/2010JD014849.

/Garcia et al., 2022/ García, O. E., Schneider, M., Herkommer, B., Gross, J., Hase, F., Blumenstock, T., & Sepúlveda, E. (2022). TCCON data from Izana (ES), Release GGG2020.R1 (Version R1) [Data set]. CaltechDATA. https://doi.org/10.14291/tccon.ggg2020.izana01.R1.

/GCOS-154/ Global Climate Observing System (GCOS), SYSTEMATIC OBSERVATION REQUIREMENTS FOR SATELLITE-BASED PRODUCTS FOR CLIMATE, Supplemental details to the satellite-based component of the "Implementation Plan for the Global Observing System for Climate in Support of the UNFCCC (2010 update)", Prepared by World Meteorological Organization (WMO), Intergovernmental Oceanographic Commission, United Nations Environment Programme (UNEP), International Council for Science, Doc.: GCOS 154, link: http://cci.esa.int/sites/default/files/gcos-154.pdf, 2011.

/GCOS-195/ Status of the Global Observing System for Climate. GCOS-195. Link: https://library.wmo.int/pmb_ged/gcos_195_en.pdf, 2015.

/GCOS-200/ The Global Observing System for Climate: Implementation Needs, GCOS 2016 Implementation Plan, World Meteorological Organization (WMO), GCOS-200 (GOOS-214), pp. 325, link: https://library.wmo.int/opac/doc_num.php?explnum_id=3417, 2016.

/GCOS-245/ The 2022 GCOS ECVs Requirements, https://library.wmo.int/doc_num.php?explnum_id=11318, pp. 244, 2022.

/Goo et al., 2014/ Goo, T.-Y., Oh, Y.-S., & Velazco, V. A. (2014). *TCCON data from Anmeyondo (KR), Release GGG2014.R0* (Version GGG2014.R0) [Data set]. CaltechDATA. https://doi.org/10.14291/TCCON.GGG2014.ANMEYONDO01.R0/1149284, https://data.caltech.edu/records/266

/Griffith et al. 2014a/ Griffith, D. W., Deutscher, N. M., Velazco, V. A., Wennberg, P. O., Yavin, Y., Keppel-Aleks, G., Washenfelder, R. A., Toon, G. C., Blavier, J.-F., Paton-Walsh, C., Jones, N. B., Kettlewell, G. C., Connor, B. J., Macatangay, R. C., Roehl, C., Ryczek, M., Glowacki, J., Culgan, T., and Bryant, G. W.: TCCON data from Darwin (AU), Release GGG2014.R0, https://doi.org/10.14291/TCCON.GGG2014.DARWIN01.R0/1149290, https://data.caltech.edu/records/269, 2014a.

/Griffith et al. 2014b/ Griffith, D. W., Velazco, V. A., Deutscher, N. M., Paton-Walsh, C., Jones, N. B., Wilson, S. R., Macatangay, R. C., Kettlewell, G. C., Buchholz, R. R., and Riggenbach, M. O.: TCCON data from Wollongong (AU), Release GGG2014.R0, https://doi.org/10.14291/TCCON.GGG2014.WOLLONGONG01.R0/1149291, https://data.caltech.edu/records/291, 2014b.

/Hannigan et al., 2021/ Hannigan J. W., Ortega I. and Coffey M.: NDACC Metadata File for Thule FTIR and references cited therein, https://www-air.larc.nasa.gov/pub/NDACC/PUBLIC/meta/ftir/Thule_ftir_jh_2021.pdf

/Hase et al., 2015/ Hase, F., Blumenstock, T., Dohe, S., Groß, J., and Kiel, M.: TCCON data from Karlsruhe (DE), Release GGG2014.R1, https://doi.org/10.14291/TCCON.GGG2014.KARLSRUHE01.R1/1182416, https://data.caltech.edu/records/278, 2015.

/Hase et al., 2023/ Hase, F., Herkommer, B., Groß, J., Blumenstock, T., Kiel, M. ä ., & Dohe, S. (2023). TCCON data from Karlsruhe (DE), Release GGG2020.R1 (Version R1) [Data set]. CaltechDATA. https://doi.org/10.14291/tccon.ggg2020.karlsruhe01.R1

/HITRAN2016/ Gordon et al., The HITRAN2016 molecular spectroscopic database, J. Quant. Spectrosc. Radiat. Transfer, 203, 3-69, 2017.

/Iraci et al. 2016/ Iraci, L. T., Podolske, J. R., Hillyard, P. W., Roehl, C., Wennberg, P. O., Blavier, J.-F., Landeros, J., Allen, N., Wunch, D., Zavaleta, J., Quigley, E., Osterman, G. B., Albertson, R., Dunwoody, K., and Boyden, H.: TCCON data from Edwards (US), Release GGG2014.R1, https://doi.org/10.14291/TCCON.GGG2014.EDWARDS01.R1/1255068, https://data.caltech.edu/records/270, 2016.

/Iraci et al. 2022/ Iraci, L. T., Podolske, J. R., Roehl, C., Wennberg, P. O., Blavier, J.-F., Allen, N., Wunch, D., & Osterman, G. B. (2022). TCCON data from Edwards (US), Release GGG2020.R0 (Version R0) [Data set]. CaltechDATA. https://doi.org/10.14291/tccon.ggg2020.edwards01.R0.

/Kawakami et al. 2014/ Kawakami, S., Ohyama, H., Arai, K., Okumura, H., Taura, C., Fukamachi, T., and Sakashita, M.: TCCON data from Saga (JP), Release GGG2014.R0, https://doi.org/10.14291/TCCON.GGG2014.SAGA01.R0/1149283, https://data.caltech.edu/records/288, 2014.

/Kiel et al., 2019/ Kiel, M., O'Dell, C. W., Fisher, B., Eldering, A., Nassar, R., MacDonald, C. G., and Wennberg, P. O.: How bias correction goes wrong: measurement of XCO2 affected by erroneous surface pressure estimates, Atmos. Meas. Tech., 12, 2241–2259, https://doi.org/10.5194/amt-12-2241-2019, 2019.

/Kivi et al., 2014/ Kivi, R., Heikkinen, P., and Kyrö, E.: TCCON data from Sodankylä (FI), Release GGG2014.R0, https://doi.org/10.14291/TCCON.GGG2014.SODANKYLA01.R0/1149280, https://data.caltech.edu/records/289, 2014.

/Kivi et al., 2022/ Kivi, R., Heikkinen, P., & Kyrö, E. (2022). TCCON data from Sodankylä (FI), Release GGG2020.R0 (Version R0) [Data set]. CaltechDATA. https://doi.org/10.14291/tccon.ggg2020.sodankyla01.R0.

/Kuruz, 1994/ Kurucz, H.L. The Solar Spectrum: Atlases and Line Identifications, Workshop on Laboratory and Astronomical High Resolution Spectra. Astronomical Society of the Pacific Conference Series. In Proceedings of the ASP Conference, Brussels, Belgium, 29 August–2 September 1994; pp. 17–31.

/Langerock et al., 2015/ Langerock, B., De Mazière, M., Hendrick, F., Vigouroux, C., Desmet, F., Dils, B., and Niemeijer, S.: Description of algorithms for co-locating and comparing gridded model data with remote-sensing observations, Geosci. Model Dev., 8, 911–921, https://doi.org/10.5194/gmd-8-911-2015, 2015.

/Laughner et al., 2022/ J. L. Laughner, G. C. Toon, D. Wunch, S. Roche, J. Mendonca, M. Kiel, C. M. Roehl, C. Petri, and P. O. Wennberg (2022). “The Total Carbon Column Observing Network's GGG2020 Data Version”. Earth Sys. Sci. Data (in prep)

/Laughner et al., 2023/ Laughner, J. L., Roche, S., Kiel, M., Toon, G. C., Wunch, D., Baier, B. C., Biraud, S., Chen, H., Kivi, R., Laemmel, T., McKain, K., Quéhé, P.-Y., Rousogenous, C., Stephens, B. B., Walker, K., and Wennberg, P. O.: A new algorithm to generate a priori trace gas profiles for the GGG2020 retrieval algorithm, Atmos. Meas. Tech., 16, 1121–1146, https://doi.org/10.5194/amt-16-1121-2023, 2023.

/Liu et al. 2018/ Liu, C, Wang, W., Sun, Y., TCCON data from Hefei(PRC), Release GGG2014.R0, (Version GGG2014.R0) [Data set]. CaltechDATA. https://doi.org/10.14291/TCCON.GGG2014.HEFEI01.R0, https://data.caltech.edu/records/1092.

/Liu et al. 2022/Liu, C., Wang, W., Sun, Y., & Shan, C. (2022). TCCON data from Hefei (PRC), Release GGG2020.R0 (Version R0) [Data set]. CaltechDATA. https://doi.org/10.14291/tccon.ggg2020.hefei01.R0.

/Lunneborg, 2020/ Lunneborg, C. E. Data analysis by resampling: Concepts and applications. PacificGrove, CA: Duxbury, 2000.

/Mahieu 2017/ Mahieu, M. NDACC Metadata File for Jungraujoch FTIR and references cited therein https://www-air.larc.nasa.gov/pub/NDACC/PUBLIC/meta/ftir/Jungfraujoch_ftir_em_2017.pdf

/Makarova et al. 2017/, Marakova M.V., Virolainen Y., Polyakov A.: NDACC Metadata File for St. Petersburg FTIR and references cited therein https://www-air.larc.nasa.gov/pub/NDACC/PUBLIC/meta/ftir/StPetersburg_ftir_mm_2017.pdf

/Mellqvist et al., 2021/ Mellqvist J., Persson G., NDACC Metadata File for Harestua FTIR and references cited therein, https://www-air.larc.nasa.gov/pub/NDACC/PUBLIC/meta/ftir/Harestua_ftir_hrt_jm_2021.pdf

/Morino et al. 2018a/ Morino, I., Matsuzaki, T., and Horikawa, M.: TCCON data from Tsukuba (JP), 125HR, Release GGG2014.R2, https://doi.org/10.14291/TCCON.GGG2014.TSUKUBA02.R2, https://data.caltech.edu/records/958, 2018a.

/Morino et al. 2018b/ Morino, I., Yokozeki, N., Matsuzaki, T., and Horikawa, M.: TCCON data from Rikubetsu (JP), Release GGG2014.R2, https://doi.org/10.14291/TCCON.GGG2014.RIKUBETSU01.R2, https://data.caltech.edu/records/957, 2018b.

/Morino et al., 2018c/ Morino, I., Velazco, V. A., Hori, A., Uchino, O., & Griffith, D. W. T. (2018). *TCCON data from Burgos, Ilocos Norte (PH), Release GGG2014.R0* (Version GGG2014.R0) [Data set]. CaltechDATA. https://doi.org/10.14291/TCCON.GGG2014.BURGOS01.R0, https://data.caltech.edu/records/1090.

/Morino et al., 2022c/ Morino, I., Velazco, V. A., Hori, A., Uchino, O., & Griffith, D. W. T. (2022). TCCON data from Burgos, Ilocos Norte (PH), Release GGG2020.R0 (Version R0) [Data set]. CaltechDATA. https://doi.org/10.14291/tccon.ggg2020.burgos01.R0.

/Notholt et al., 2019/ Notholt, J., Petri, C., Warneke, T., Deutscher, N. M., Palm, M., Buschmann, M., Weinzierl, C., Macatangay, R. C., and Grupe, P.: TCCON data from Bremen (DE), Release GGG2014.R1, https://doi.org/10.14291/TCCON.GGG2014.BREMEN01.R1, https://data.caltech.edu/records/1290, 2019.

/Notholt et al., 2021a/ Notholt, J., Palm, M., NDACC Metadata File for Ny Alesund FTIR and references cited therein https://www-air.larc.nasa.gov/pub/NDACC/PUBLIC/meta/ftir/NyAlesund_ftir_jn_2021.pdf

/Notholt et al., 2021b/ Notholt, J., Palm, M., NDACC Metadata File for Bremen FTIR and references cited therein https://www-air.larc.nasa.gov/pub/NDACC/PUBLIC/meta/ftir/Bremen_ftir_jn_2021.pdf.

/Notholt et al., 2022/ Notholt, J., Petri, C., Warneke, T., & Buschmann, M. (2022). TCCON data from Bremen (DE), Release GGG2020.R0 (Version R0) [Data set]. CaltechDATA. https://doi.org/10.14291/tccon.ggg2020.bremen01.R0.

/O'Dell et al., 2012/ O'Dell, C.W.; Connor, B.; Bösch, H.; O'Brien, D.; Frankenberg, C.; Castano, R.; Christi, M.; Eldering, D.; Fisher, B.; Gunson, M.; et al. The ACOS CO_2 retrieval algorithm - Part 1: Description and validation against synthetic observations. Atmos. Meas. Tech. 2012, 5, 99–121.

/O'Dell et al., 2018/ O'Dell, C. W., Eldering, A., Wennberg, P. O., Crisp, D., Gunson, M. R., Fisher, B., Frankenberg, C., Kiel, M., Lindqvist, H., Mandrake, L., Merrelli, A., Natraj, V., Nelson, R. R., Osterman, G. B., Payne, V. H., Taylor, T. E., Wunch, D., Drouin, B. J., Oyafuso, F., Chang, A., McDuffie, J., Smyth, M., Baker, D. F., Basu, S., Chevallier, F., Crowell, S. M. R., Feng, L., Palmer, P. I., Dubey, M., García, O. E., Griffith, D. W. T., Hase, F., Iraci, L. T., Kivi, R., Morino, I., Notholt, J., Ohyama, H., Petri, C., Roehl, C. M., Sha, M. K., Strong, K., Sussmann, R., Te, Y., Uchino, O., and Velazco, V. A.: Improved retrievals of carbon dioxide from Orbiting Carbon Observatory-2 with the version 8 ACOS algorithm, Atmos. Meas. Tech., 11, 6539–6576, https://doi.org/10.5194/amt-11-6539-2018, 2018.

/Ortega et al., 2019/ Ortega, I., Buchholz, R. R., Hall, E. G., Hurst, D. F., Jordan, A. F.,and Hannigan, J. W.: Tropospheric water vapor profiles obtained with FTIR: comparison with balloon-borne frost point hygrometers and influence on trace gas retrievals, Atmos. Meas. Tech.,12, 873–890, https://doi.org/10.5194/amt-12-873-2019, 2019.

/Ostler et al., 2014/ Ostler, A., Sussmann, R., Rettinger, M., Deutscher, N. M., Dohe, S., Hase, F., Jones, N., and Palm, M.: Multistation intercomparison of column-averaged methane from NDACC and TCCON: Impact of dynamical variability, Atmos. Meas. Tech., 7, 4081–4101, https://doi.org/10.5194/amt-7-4081-2014, 2014.

/Parker et al., 2011/ Parker, R., Boesch, H, Cogan, A., et al. (2011), Methane Observations from the Greenhouse gases Observing SATellite: Comparison to ground-based TCCON data and Model Calculations, Geophys. Res. Lett., doi:10.1029/2011GL047871.

/Petri et al., 2020/ Petri, C., Vrekoussis M., Rousogenous, C., Warneke, T., Sciare, J., Notholt, J., TCCON data from Nicosia, Cyprus (CY), Release GGG2014.R0, https://doi.org/10.14291/TCCON.GGG2014.NICOSIA01.R0/, https://data.caltech.edu/records/1690.

/Petri et al., 2022/ Petri, C., Vrekoussis, M., Rousogenous, C., Warneke, T., Sciare, J., & Notholt, J. (2022). TCCON data from Nicosia (CY), Release GGG2020.R0 (Version R0) [Data set]. CaltechDATA. https://doi.org/10.14291/tccon.ggg2020.nicosia01.R0.

/PUGS, 2019/ Buchwitz, M., Aben, I., J., Armante, R., Boesch, H., Crevoisier, C., Di Noia, A., Hasekamp, O. P., Reuter, M., Schneising-Weigel, O., Wu, L.., Product User Guide and Specification (PUGS) – Main document for Greenhouse Gas (GHG: CO_2 & CH_4) data set CDR 3 (2003-2018), C3S project C3S_312b_Lot2_DLR, v3.1, 97 pages, https://www.iup.uni-bremen.de/carbon_ghg/docs/C3S/CDR3_2003-2018/PUGS/C3S_D312b_Lot2.3.2.3-v1.0_PUGS-GHG_MAIN_v3.1.pdf, 2019.

/PUGv4.1, 2023/ Reuter. M., M.Hilker, and M.Buchwitz: Product User Guide Version 4 (PUGv4.1) for the FOCAL XCO2 OCO-2 Data Product CO2_OC2_FOCA (v10.1) for the Essential Climate Variable (ECV) Greenhouse Gases (GHG) ESA Climate Change Initiative "Plus" (CCI+), 2023.

/PUGv5, 2024/ M.Reuter, M.Hilker, and M.Buchwitz: Product User Guide Version 5 (PUGv5) for the FOCAL XCO2 OCO-2 Data Product CO2_OC2_FOCA (v11) for the Essential Climate Variable (ECV) Greenhouse Gases (GHG) ESA Climate Change Initiative "Plus" (CCI+), 2024

/PVIRv5, 2017/ Buchwitz et al., Product Validation and Intercomparison Report (PVIR), version 5, ESA GHG-CCI project, 2017

/PVIR v5, 2017/ Product Validation and Intercomparison Report" (PVIR), ESA Climate Change Initiative (CCI) GHG-CCI project, Version 5, 9 Feb 2017, 2017.

/PVIR GHG-CCI+ v1.1, 2020/ ESA Climate Change Initiative "Plus" (CCI+) Product Validation and Intercomparison Report (PVIR) for the Essential Climate Variable (ECV) Greenhouse Gases (GHG): XCO2 and/or XCH4 from OCO-2, TanSat, Sentinel-5-Precursor and GOSAT-2,13 Mar 2020, version 1.1, pp. 74, 2020.

/PVIR GHG-CCI+ v2.1, 2021/ ESA Climate Change Initiative "Plus" (CCI+) Product Validation and Intercomparison Report (PVIR) for the Essential Climate Variable (ECV) Greenhouse Gases (GHG): XCO2 and/or XCH4 from OCO-2, TanSat, Sentinel-5-Precursor and GOSAT-2,19 Mar 2021, version 2.1, pp. 118, 2021.

/PVIR GHG-CCI+ v3.0, 2022/ ESA Climate Change Initiative "Plus" (CCI+) Product Validation and Intercomparison Report (PVIR) for the Essential Climate Variable (ECV) Greenhouse Gases (GHG): XCO2 and/or XCH4 from OCO-2, TanSat, Sentinel-5-Precursor and GOSAT-2,16 Feb 2022, version 3.0, pp. 148, 2022.

/PVIR GHG-CCI+ v4.0, 2023/ ESA Climate Change Initiative "Plus" (CCI+) Product Validation and Intercomparison Report (PVIR) for data set CRDP8 for the Essential Climate Variable (ECV) Greenhouse Gases (GHG): XCO2 and/or XCH4 from OCO-2, Sentinel-5-Precursor and GOSAT-2,29 Aug 2023, version 4.0, pp. 158, 2023.

/Reuter et al., 2011/ Reuter, M., Bovensmann, H., Buchwitz, M., Burrows, J. P., Connor, B. J., Deutscher, N. M., Griffith, D.W. T., Heymann, J., Keppel-Aleks, G., Messerschmidt, J., and et al.: Retrieval of atmospheric CO_2 with enhanced accuracy and precision from SCIAMACHY: Validation with FTS measurements and comparison with model results., Journal of Geophysical Research, 116, doi:10.1029/2010JD015047, URL http://dx.doi.org/10.1029/2010JD015047, 2011.

/Reuter et al., 2012/ M. Reuter, M. Buchwitz, O. Schneising, F. Hase, J. Heymann, S. Guerlet, A.J. Cogan, H. Bovensmann, J.P. Burrows: A simple empirical model estimating atmospheric CO_2 background concentrations, Atmospheric Measurement Techniques, 5, 1349-1357, 2012.

/Reuter et al., 2013/ Reuter, M., H. Boesch, H. Bovensmann, A. Bril, M. Buchwitz, A. Butz, J. P. Burrows, C. W. O'Dell, S. Guerlet, O. Hasekamp, J. Heymann, N. Kikuchi, S. Oshchepkov, R. Parker, S. Pfeifer, O. Schneising, T. Yokota, and Y. Yoshida, A joint effort to deliver satellite retrieved atmospheric CO_2 concentrations for surface flux inversions: the ensemble median algorithm EMMA, Atmos. Chem. Phys., 13, 1771-1780, 2013.

/Reuter et al., 2017a/ M.Reuter, M.Buchwitz, O.Schneising, S.Noël, V.Rozanov, H.Bovensmann and J.P.Burrows: A Fast Atmospheric Trace Gas Retrieval for Hyperspectral Instruments Approximating Multiple Scattering - Part 1: Radiative Transfer and a Potential OCO-2 XCO_2 Retrieval Setup, Remote Sensing, 9(11), 1159; doi:10.3390/rs9111159, 2017.

/Reuter et al., 2017b/ M.Reuter, M.Buchwitz, O.Schneising, S.Noël, H.Bovensmann and J.P.Burrows: A Fast Atmospheric Trace Gas Retrieval for Hyperspectral Instruments Approximating Multiple Scattering - Part 2: Application to XCO_2 Retrievals from OCO-2, Remote Sensing, 9(11), 1102; doi:10.3390/rs9111102, 2017.

/Reuter et al., 2020/ M. Reuter, M. Buchwitz, O. Schneising, S. Noël, H. Bovensmann, J.P. Burrows, H. Boesch, A. Di Noia, J. Anand, R.J. Parker, P. Somkuti, L. Wu, O.P. Hasekamp, I. Aben, A. Kuze, H. Suto, K. Shiomi, Y. Yoshida, I. Morino, D. Crisp, C.W. O'Dell, J. Notholt, C. Petri, T. Warneke, V.A. Velazco, N.M. Deutscher, D.W.T. Griffith, R. Kivi, D.F. Pollard, F. Hase, R. Sussmann, Y.V. Té, K. Strong, S. Roche, M.K. Sha, M. De Mazière, D.G. Feist, L.T. Iraci, C.M. Roehl, C. Retscher, and D. Schepers: Ensemble-based satellite-derived carbon dioxide and methane column-averaged dry-air mole fraction data sets (2003-2018) for carbon and climate applications, Atmos. Meas. Tech., https://www.atmos-meas-tech.net/13/789/2020, 2020

/Rodgers, 2000/ Rodgers, C. D.: Inverse Methods for Atmospheric Sounding: Theory and Practice, World Scientific Publishing, 2000.

/Rozanov et al., 2014/ Rozanov, V., Rozanov, A., Kokhanovsky, A., and Burrows, J.: Radiative transfer through terrestrial atmosphere and ocean: Software package SCIATRAN, Journal of Quantitative Spectroscopy and Radiative Transfer, 133, 13 – 71, doi:https://doi.org/10.1016/j.jqsrt.2013.07.004,
URL http://www. sciencedirect.com/science/article/pii/S0022407313002872, 2014

/**Schepers et al., 2012/** Schepers, D., Guerlet, S., Butz, A., et al. (2012), Methane retrievals from Greenhouse Gases Observing Satellite (GOSAT) shortwave infrared measurements: Performance comparison of proxy and physics retrieval algorithms, *J. Geophys. Res*., 117, D10307, doi:10.1029/2012JD017549.

/Schneising et al., 2011/ Schneising, O., Buchwitz, M., Reuter, M., et al., Long-term analysis of carbon dioxide and methane column-averaged mole fractions retrieved from SCIAMACHY, Atmos. Chem. Phys., 11, 2881-2892, 2011.

/Schneising et al., 2012/ Schneising, O., Bergamaschi, P., Bovensmann, H., et al, Atmospheric greenhouse gases retrieved from SCIAMACHY: comparison to ground-based FTS measurements and model results, Atmos. Chem. Phys., 12, 1527-1540, 2012.

/Schneising et al., 2019/ Schneising, O., Buchwitz, M., Reuter, M., Bovensmann, H., Burrows, J. P., Borsdorff, T., Deutscher, N. M., Feist, D. G., Griffith, D. W. T., Hase, F., Hermans, C., Iraci, L. T., Kivi, R., Landgraf, J., Morino, I., Notholt, J., Petri, C., Pollard, D. F., Roche, S., Shiomi, K., Strong, K., Sussmann, R., Velazco, V. A., Warneke, T., and Wunch, D.: A scientific algorithm to simultaneously retrieve carbon monoxide and methane from

TROPOMI onboard Sentinel-5 Precursor, Atmos. Meas. Tech., 12, 6771-6802, https://doi.org/10.5194/amt-12-6771-2019, 2019.

/Schneising et al., 2023/ Schneising, O., Buchwitz, M., Hachmeister, J., Vanselow, S., Reuter, M., Buschmann, M., Bovensmann, H., and Burrows, J. P.: Advances in retrieving XCH4 and XCO from Sentinel-5 Precursor: improvements in the scientific TROPOMI/WFMD algorithm, Atmos. Meas. Tech., 16, 669–694, https://doi.org/10.5194/amt-16-669-2023, 2023.

/Sherlock et al., 2014/ Sherlock, V., Connor, B., Robinson, J., Shiona, H., Smale, D., and Pollard, D. F.: TCCON data from Lauder (NZ), 125HR, Release GGG2014.R0, https://doi.org/10.14291/TCCON.GGG2014.LAUDER02.R0/1149298, https://data.caltech.edu/records/281, 2014.

/Sherlock et al., 2022/ Sherlock, V., Connor, B., Robinson, J., Shiona, H., Smale, D., & Pollard, D. F. (2022). TCCON data from Lauder (NZ), 120HR, Release GGG2020.R0 (Version R0) [Data set]. CaltechDATA. https://doi.org/10.14291/tccon.ggg2020.lauder01.R0.

/Shiomi et al., 2022/ Shiomi, K., Kawakami, S., Ohyama, H., Arai, K., Okumura, H., Ikegami, H., & Usami, M. (2022). TCCON data from Saga (JP), Release GGG2020.R0 (Version R0) [Data set]. CaltechDATA. https://doi.org/10.14291/tccon.ggg2020.saga01.R0.

/Stammes, 2002/ Stammes, P. OMI Algorithm Theoretical Basis Document, Volume III, Clouds, Aerosols, and Surface UV Irradiance (ATBD-OMI-03); Royal Netherlands Meteorological Institute (KNMI): De Bilt, The Netherlands, 2002.

/Strong et al., 2019/ Strong, K., Roche, S., Franklin, J. E., Mendonca, J., Lutsch, E., Weaver, D., Fogal, P. F., Drummond, J. R., Batchelor, R., and Lindenmaier, R.: TCCON data from Eureka (CA), Release GGG2014.R3, https://doi.org/10.14291/TCCON.GGG2014.EUREKA01.R3, https://data. caltech.edu/records/1171, 2019.

/Strong, 2021/ Strong K., NDACC Metadata File for Eureka FTIR and references cited therein, https://www-air.larc.nasa.gov/pub/NDACC/PUBLIC/meta/ftir/Eureka_ftir_ks_2021.pdf.

/Strong et al., 2022/ Strong, K., Roche, S., Franklin, J. E., Mendonca, J., Lutsch, E., Weaver, D., Fogal, P. F., Drummond, J. R., Batchelor, R., Lindenmaier, R., & McGee, E. (2022). TCCON data from Eureka (CA), Release GGG2020.R0 (Version R0) [Data set]. CaltechDATA. https://doi.org/10.14291/tccon.ggg2020.eureka01.R0.

/Sussmann et al., 2018a/ Sussmann, R. and Rettinger, M.: TCCON data from Garmisch (DE), Release GGG2014.R2, https://doi.org/10.14291/TCCON.GGG2014.GARMISCH01.R2, https://data.caltech.edu/records/956, 2018.

/Sussmann et al., 2018b/ Sussmann, R. and Rettinger, M.: NDACC Metadata File for Zugspitze FTIR and references cited therein M.: https://www-air.larc.nasa.gov/pub/NDACC/PUBLIC/meta/ftir/Zugspitze_ftir_rs_2018.pdf.

/Sussmann et al., 2023/ Sussmann, R., & Rettinger, M. (2023). TCCON data from Garmisch (DE), Release GGG2020.R0 (Version R0) [Data set]. CaltechDATA. https://doi.org/10.14291/tccon.ggg2020.garmisch01.R0

/TCCON GGG2020/ Total Carbon Column Observing Network (TCCON) Team. (2022). 2020 TCCON Data Release (Version GGG2020) [Data set]. CaltechDATA. https://doi.org/10.14291/TCCON.GGG2020

/Té et al., 2014/ Té, Y., Jeseck, P., & Janssen, C. (2014). *TCCON data from Paris (FR), Release GGG2014.R0* (Version GGG2014.R0) [Data set]. CaltechDATA. https://doi.org/10.14291/TCCON.GGG2014.PARIS01.R0/1149279, https://data.caltech.edu/records/284.

/Té et al., 2022/ Té, Y., Jeseck, P., & Janssen, C. (2022). TCCON data from Paris (FR), Release GGG2020.R0 (Version R0) [Data set]. CaltechDATA. https://doi.org/10.14291/tccon.ggg2020.paris01.R0.

/Thompson et al., 2012/ Thompson, D.R.; Chris Benner, D.; Brown, L.R.; Crisp, D.; Malathy Devi, V.; Jiang, Y.; Natraj, V.; Oyafuso, F.; Sung, K.; Wunch, D.; et al. Atmospheric validation of high accuracy CO_2 absorption coefficients for the OCO-2 mission. J. Quant. Spectrosc. Radiat. Transf. 2012, 113, 2265–2276.

/URDv2.1/ User Requirements Document (URD), ESA Climate Change Initiative (CCI) GHG-CCI project, Version 2.1, 38 pages, 19-Oct-2016, http://cci.esa.int/sites/default/files/URDv2.1_GHG-CCI_Final.pdf, 2016.

/URDv3.0/ Chevallier et al., GHG-CCI: User Requirements Document for the GHG-CCI+ project of ESA's Climate Change Initiative, pp. 42, version 3.0, 17-February-2020, https://www.iup.uni-bremen.de/carbon_ghg/docs/GHG-CCIplus/URD/URDv3.0_GHG-CCIp_Final.pdf, 2020.

/URDv4.0/ Chevallier et al., GHG-CCI: User Requirements Document for the GHG-CCI+ project of ESA's Climate Change Initiative, pp. 40, version 4.0, 16-May-2024, https://www.iup.uni-bremen.de/carbon_ghg/docs/GHG-CCIplus/URDv4/URDv4.0_GHG-CCI+.pdf, 2024.

/Warneke et al., 2019/ Warneke, T., Messerschmidt, J., Notholt, J., Weinzierl, C., Deutscher, N. M., Petri, C., and Grupe, P.: TCCON data from Orléans (FR), Release GGG2014.R1, https://doi.org/10.14291/TCCON.GGG2014.ORLEANS01.R1, https://data.caltech.edu/records/1301, 2019.

/Warneke et al., 2022/ Warneke, T., Petri, C., Notholt, J., & Buschmann, M. (2022). TCCON data from Orléans (FR), Release GGG2020.R0 (Version R0) [Data set]. CaltechDATA. https://doi.org/10.14291/tccon.ggg2020.orleans01.R0.

/Wennberg et al., 2015/ Wennberg, P. O., Wunch, D., Roehl, C. M., Blavier, J.-F., Toon, G. C., and Allen, N. T.: TCCON data from Caltech (US), Release GGG2014.R1, https://doi.org/10.14291/TCCON.GGG2014.PASADENA01.R1/1182415, https://data.caltech.edu/records/285, 2015.

/Wennberg et al., 2016a/ Wennberg, P. O., Roehl, C. M., Blavier, J.-F.,Wunch, D., and Allen, N. T.: TCCON data from Jet Propulsion Laboratory (US), 2011, Release GGG2014.R1, https://doi.org/10.14291/TCCON.GGG2014.JPL02.R1/1330096, https://data.caltech.edu/records/277, 2016a.

/Wennberg et al., 2016b/ Wennberg, P. O., Wunch, D., Roehl, C. M., Blavier, J.-F., Toon, G. C., and Allen, N. T.: TCCON data from Lamont (US), Release GGG2014.R1, https://doi.org/10.14291/TCCON.GGG2014.LAMONT01.R1/1255070, https://data.caltech.edu/records/279, 2016b.

/Wennberg et al., 2017/ Wennberg, P. O., Roehl, C. M., Wunch, D., Toon, G. C., Blavier, J.-F., Washenfelder, R., Keppel-Aleks, G., Allen, N. T., and Ayers, J.: TCCON data from Park Falls (US), Release GGG2014.R1, https://doi.org/10.14291/TCCON.GGG2014.PARKFALLS01.R1, https://data.caltech.edu/records/295, 2017.

/Wennberg et al., 2022/ Wennberg, P. O., Roehl, C. M., Wunch, D., Toon, G. C., Blavier, J.-F., Washenfelder, R., Keppel-Aleks, G., & Allen, N. T. (2022). TCCON data from Park Falls (US), Release GGG2020.R1 (Version R1) [Data set]. CaltechDATA. https://doi.org/10.14291/tccon.ggg2020.parkfalls01.R1.

/Wennberg et al., 2022b/Wennberg, P. O., Wunch, D., Yavin, Y., Toon, G. C., Blavier, J.-F., Allen, N. T., Keppel-Aleks, G., & Roehl, C. M. (2022). TCCON data from Jet Propulsion Laboratory (US), 2007, Release GGG2020.R0 (Version R0) [Data set]. CaltechDATA. https://doi.org/10.14291/tccon.ggg2020.jpl01.R0

/Wennberg et al., 2022c/ Wennberg, P. O., Roehl, C. M., Wunch, D., Blavier, J.-F., Toon, G. C., Allen, N. T., Treffers, R., & Laughner, J. (2022). TCCON data from Caltech (US), Release GGG2020.R0 (Version R0) [Data set]. CaltechDATA. https://doi.org/10.14291/tccon.ggg2020.pasadena01.R0.

/Wiacek et al., 2007/ Wiacek, A., Taylor, J. R., Strong, K., Saari, R., Kerzenmacher, T. E., Jones, N. B., and Griffith, D. W. T.: Ground-Based Solar Absorption FTIR Spectroscopy: Characterization of Retrievals and First Results from a Novel Optical Design Instrument at a New NDACC Complementary Station, J. Atmos. Ocean. Tech., 24,432–448, https://doi.org/10.1175/JTECH1962.1, 2007.

/Wiedmann et al. 2023/ Weidmann, D., Brownsword, R., & Doniki, S. (2023). TCCON data from Harwell, Oxfordshire (UK), Release GGG2020.R0 (Version R0) [Data set]. CaltechDATA. https://doi.org/10.14291/tccon.ggg2020.harwell01.R0.

/Wunch et al., 2010/ Wunch, D., Toon, G. C., Wennberg, P. O., Wofsy, S. C., Stephens, B. B., Fischer, M. L., Uchino, O., Abshire, J. B., Bernath, P., Biraud, S. C., Blavier, J.-F. L., Boone, C., Bowman, K. P., Browell, E. V., Campos, T., Connor, B. J., Daube, B. C., Deutscher, N. M., Diao, M., Elkins, J. W., Gerbig, C., Gottlieb, E., Griffith, D. W. T., Hurst, D. F., Jiménez, R., Keppel-Aleks, G., Kort, E. A., Macatangay, R., Machida, T., Matsueda, H., Moore, F., Morino, I., Park, S., Robinson, J., Roehl, C. M., Sawa, Y., Sherlock, V., Sweeney, C., Tanaka, T., and Zondlo, M. A.: Calibration of the Total Carbon Column Observing Network using aircraft profile data, Atmospheric Measurement Techniques, 3, 1351–1362, doi:10.5194/amt-3-1351-2010, URL http://www.atmos-meas-tech.net/3/1351/2010/, 2010.

/Wunch et al., 2011/ Wunch, D., Toon, G. C., Blavier, J.-F. L., Washenfelder, R. A., Notholt, J., Connor, B. J., Griffith, D. W. T., Sherlock, V., and Wennberg, P. O.: The Total Carbon Column Observing Network (TCCON), Philosophical Transactions of the Royal Society of London, Series A: Mathematical, Physical and Engineering Sciences, 369, 2087–2112, doi:10.1098/rsta.2010.0240, 2011.

/Wunch et al., 2015/ Wunch, D., Toon, G. C., Sherlock, V., Deutscher, N. M., Liu, C., Feist, D. G., & Wennberg, P. O. (2015). Documentation for the 2014 TCCON Data Release. CaltechDATA. https://doi.org/10.14291/TCCON.GGG2014.DOCUMENTATION.R0/1221662, https://data.caltech.edu/records/249.

/Wunch et al., 2017/ Wunch, D., Mendonca, J., Colebatch, O., Allen, N. T., Blavier, J.-F., Springett, S., Neufeld, G., Strong, K., Kessler, R., & Worthy, D. (2017). *TCCON data from East Trout Lake, SK (CA), Release GGG2014.R0* (Version GGG2014.R0) [Data set]. CaltechDATA. https://doi.org/10.14291/TCCON.GGG2014.EASTTROUTLAKE01.R0/1348207, https://data.caltech.edu/records/296.

/Wunch et al., 2022/ Wunch, D., Mendonca, J., Colebatch, O., Allen, N. T., Blavier, J.-F., Kunz, K., Roche, S., Hedelius, J., Neufeld, G., Springett, S., Worthy, D., Kessler, R., & Strong, K. (2022). TCCON data from East Trout Lake, SK (CA), Release GGG2020.R0 (Version R0) [Data set]. CaltechDATA. https://doi.org/10.14291/tccon.ggg2020.easttroutlake01.R0.

/Yang et al., 2020/ Yang, D., H. Boesch, Y. Liu, P. Somkuti, Z. Cai, X. Chen, A. Di Noia, C. Lin, N. Lu, D. Lyu, R. J. Parker, L. Tian, M. Wang, A. Webb, L. Yao, Z. Yin, Y. Zheng, N. M. Deutscher, D. W. T. Griffith, F. Hase, R. Kivi, I. Morino, J. Notholt, H. Ohyama, D. F. Pollard, K. Shiomi, R. Sussmann, Y. Te, V. A. Velazco, T. Warneke, D. Wunch: Toward high precision XCO_2 retrievals from TanSat observations: Retrieval improvement and validation against TCCON measurements, Journal of Geophysical Research: Atmospheres, 125, e2020JD032794, https://doi.org/10.1029/2020JD032794, 2020.

/Zhou et al., 2022/ Zhou, M., Wang, P., Kumps, N., Hermans, C., & Nan, W. (2022). TCCON data from Xianghe, China, Release GGG2020.R0 (Version R0) [Data set]. CaltechDATA. https://doi.org/10.14291/tccon.ggg2020.xianghe01.R0.

7 List of Acronyms and Abbreviations

Abbreviation	Meaning
AAI	Absorbing Aerosol Index
ACA	Additional Constraints Algorithm
AOD	Aerosol Optical Depth
AOT	Aerosol Optical Thickness
ATBD	Algorithm Theoretical Basis Document
BIRA-IASB	Royal Belgian Institute for Space Aeronomy
CCI	Climate Change Initiative
CDR	Climate Data Record
CMUG	Climate Modelling User Group (of ESA's CCI)
COD	Cloud Optical Depth
CRG	Climate Research Group
D/B	Data base
DOAS	Differential Optical Absorption Spectroscopy
DPM	Detailed Processing Model
EC	European Commission
ECA	ECV Core Algorithm
ECMWF	European Centre for Medium Range Weather Forecasting
ECV	Essential Climate Variable
EO	Earth Observation
ESA	European Space Agency
ESM	Earth System Model
FCDR	Fundamental Climate Data Record
FOCAL	Fast atmOspheric traCe gAs retrievaL
FoM	Figure of Merit
FP	Full Physics

FTIR	Fourier Transform InfraRed
FTS	Fourier Transform Spectrometer
GCOS	Global Climate Observing System
GEO	Group on Earth Observation
GEOSS	Global Earth Observation System of Systems
GHG	GreenHouse Gas
GMES	Global Monitoring for Environment and Security
GOSAT	Greenhouse Gas Observing Satellite
IDL	Interactive Data Language
ITT	Invitation To Tender
IODD	Input Output Data Definition
IPCC	International Panel in Climate Change
IPR	Intellectual Property Right
IUP	Institute of Environmental Physics (IUP) of the University of Bremen, Germany
JCGM	Joint Committee for Guides in Metrology
LMD	Laboratoire de Météorologie Dynamique
LUT	Look-up table
MACC	Monitoring Atmospheric Composition and Climate, EU GMES project
MERIS	Medium Resolution Imaging Spectrometer
MIPAS	Michelson Interferometer for Passive Atmospheric Sounding
MODIS	Moderate Resolution Imaging Spectrometer
N/A	Not applicable
NDACC	Network for the Detection of Atmospheric Composition Change
NASA	National Aeronautics and Space Administration
NIES	National Institute for Environmental Studies
NIWA	National Institute Of Water & Atmospheric Research
NOAA	National Oceanic and Atmospheric Administration

OCO	Orbiting Carbon Observatory
OD	Optical Depth
OE	Optimal Estimation
PBL	Planetary Boundary Layer
PMD	Polarization Measurement Device
PR	Proxy (retrieval method)
PVP	Product Validation Plan
PVR	Product Validation Report
RA	Relative Accuracy
RD	Reference Document
RMS	Root-Mean-Square
RTM	Radiative transfer model
S5P	Sentinel-5 Precursor
SoW	Statement of work
SQWG	SCIAMACHY Quality Working Group
SRA	Seasonal Relative Accuracy
SRD	Software Requirements Document
SRON	Netherlands Institute for Space Research
SUM	Software User Manual
SVR	Software Verification Report
TANSAT	CarbonSat
TANSO	Thermal And Near infrared Sensor for carbon Observation
TBC	To be confirmed
TCCON	Total Carbon Column Observing Network
TBD	To be defined / to be determined
TROPOMI	TROPOspheric Monitoring instrument
UNAM	Universidad Nacional Autónoma de México
WFM-DOAS (or WFMD)	Weighting Function Modified DOAS
WG	Working Group

***** End of Document *****